CPT-55 Applied Research Associates 07/18/00

Depth = 96.3 ft Max Pressure = 37.55 psi Pn = 7.98 psi

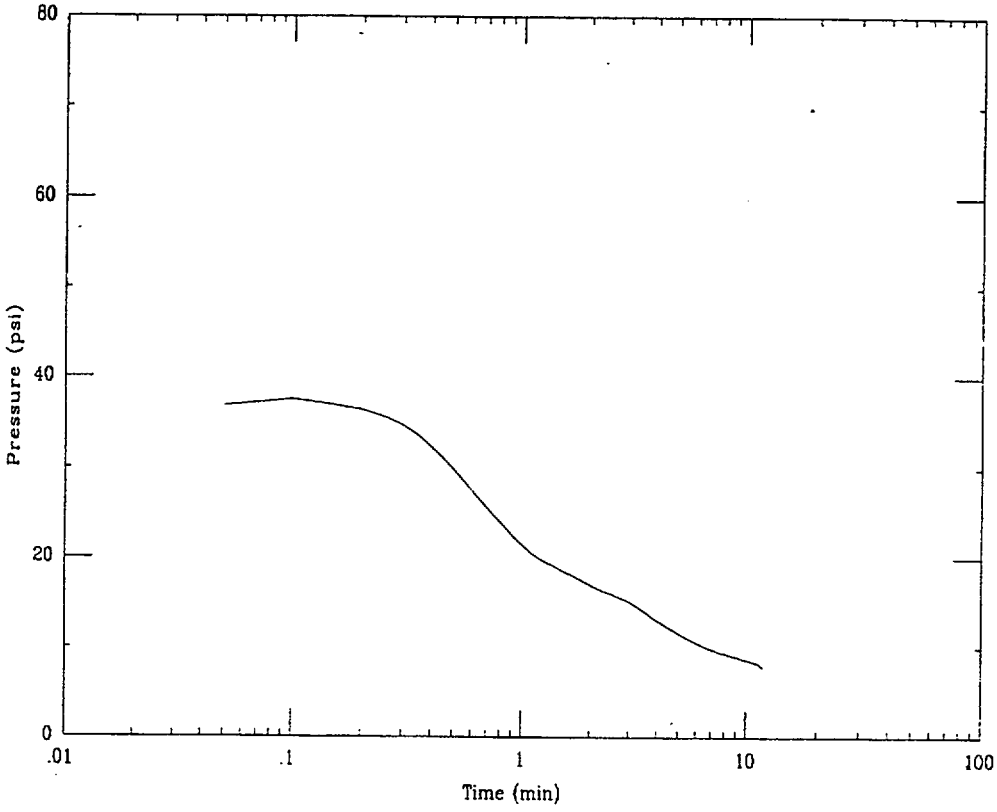

CPT-55 Applied Research Associates 07/18/00

Depth = 113.0 ft Max Pressure = 8.10 psi Pn = 8.09 psi

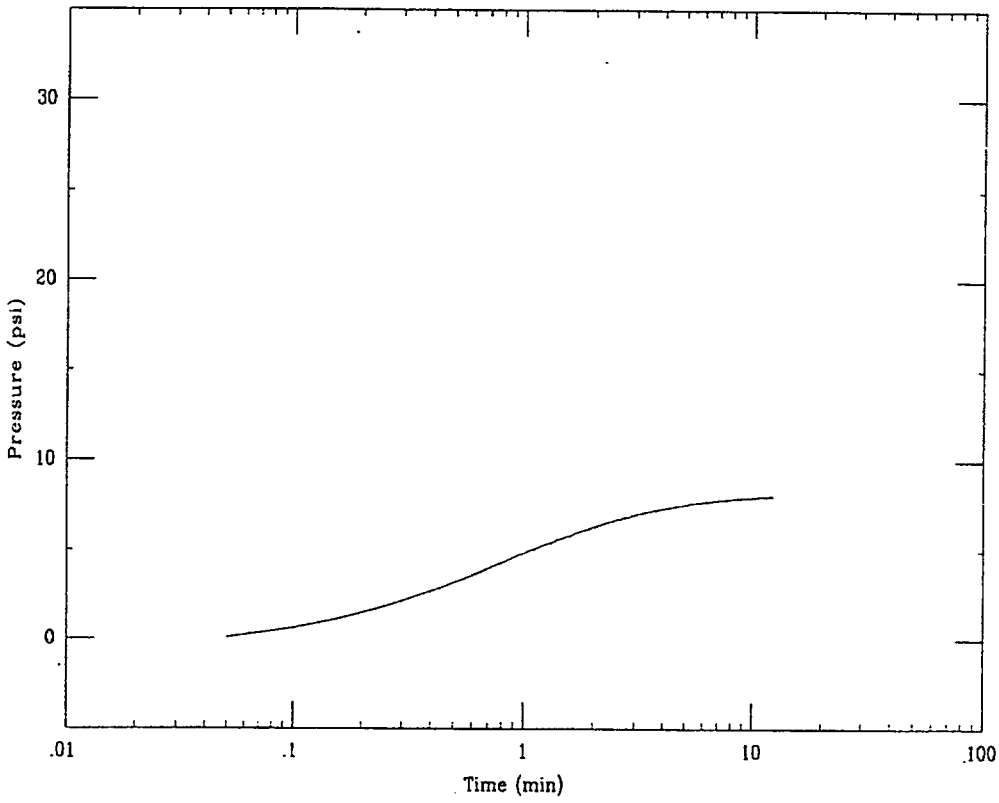

Project : Duke Cogema Stone & Webster

Test Id : CPT-55
Test Date : 7/18/00

Northing : 80259.6 (ft)
Easting : 55141.9 (ft)
Surface Elevation : 294.4 (ft)
Water Table Elevation : 200.3 (ft)

Probe Diameter : 1.75 (in)

Notes	Test Depth (ft)	Test Elev (ft)	Static Pressure (psi)	Maximum Pressure (psi)	50 % Pressure (psi)	Tip Stress (psi)	Alpha	Constrained Modulus (psi)	Time 50 % (min)	Coefficient Lateral Consolidation (in2/s)	Coefficient Lateral Consolidation (cm2/sec)	Coefficient Lateral Permeability (cm/s)
	96.3	198.1	1.0	37.55	19.25	193.1	3.0	579.17	1.35	5.20E-02	3.35E-01	8.23E-06
Soil Dilation	113.0	181.4	8.2	8.11								

CPT-56 Applied Research Associates 07/18/00

Depth = 103.5 ft Max Pressure = 4.83 psi Pn = 4.80 psi

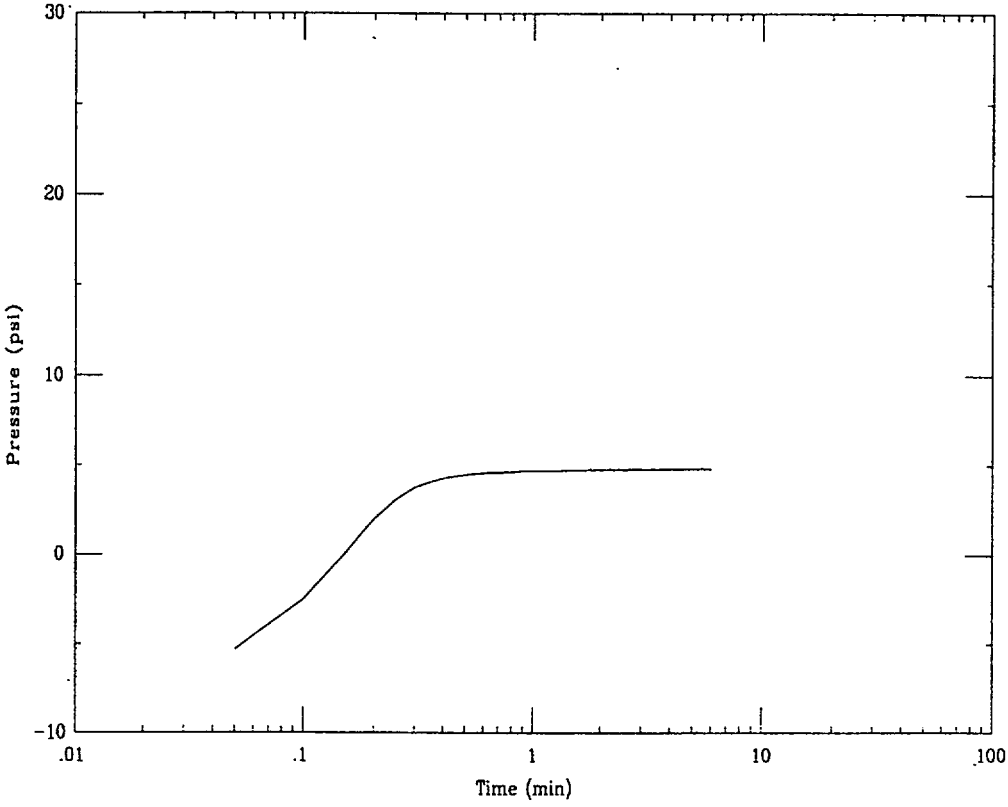

Project : Duke Cogema Stone & Webster

Test Id : CPT-56
Test Date : 7/18/00

Northing : 80207.0 (ft)
Easting : 54866.7 (ft)
Surface Elevation : 294.2 (ft)
Water Table Elevation : 201.7 (ft)

Probe Diameter : 1.75 (in)

Notes	Test Depth (ft)	Test Elev (ft)	Static Pressure (psi)	Maximum Pressure (psi)	50 % Pressure (psi)	Tip Stress (psi)	Alpha	Constrained Modulus (psi)	Time 50 % (min)	Coefficient Lateral Consolidation (in2/s)	Coefficient Lateral Consolidation (cm2/sec)	Coefficient Lateral Permeability (cm/s)
Soil Dilation	103.5	190.7	4.8	4.83								

DCS, MFFF Project No. 08716

CPT-57 Applied Research Associates 07/18/00

Depth = 101.2 ft Max Pressure = 4.09 psi Pn = 4.07 psi

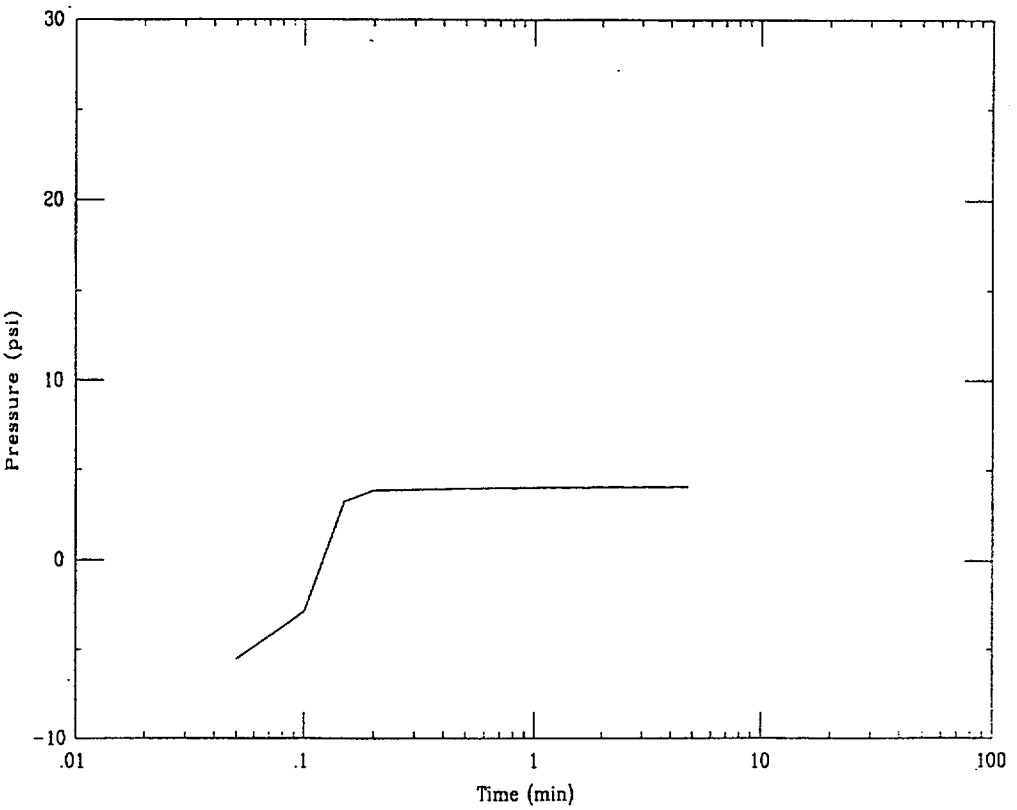

CPT-57 Applied Research Associates 07/18/00

Depth = 115.1 ft Max Pressure = 111.64 psi Pn = 18.80 psi

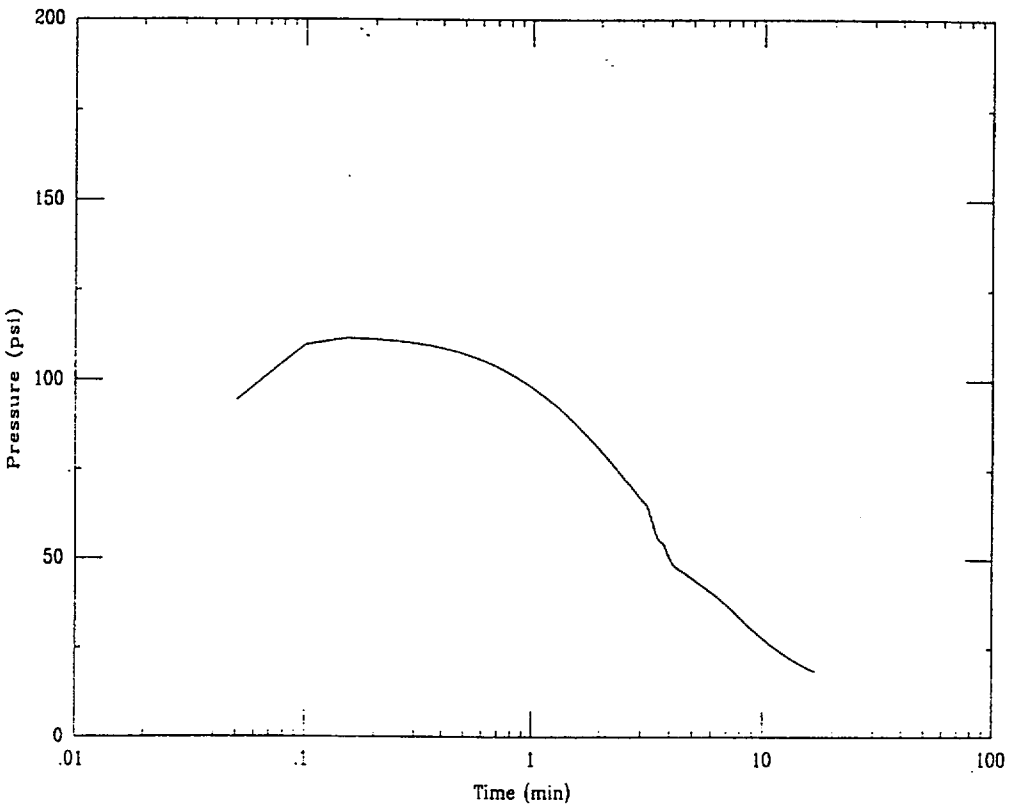

Project : Duke Cogema Stone & Webster

Test Id : CPT-57
Test Date : 7/18/00

Northing : 80229.2 (ft)
Easting : 55058.2 (ft)
Surface Elevation : 293.6 (ft)
Water Table Elevation : 201.8 (ft)

Probe Diameter : 1.75 (in)

Notes	Test Depth (ft)	Test Elev (ft)	Static Pressure (psi)	Maximum Pressure (psi)	50 % Pressure (psi)	Tip Stress (psi)	Alpha	Constrained Modulus (psi)	Time 50 % (min)	Coefficient Lateral Consolidation (in2/s)	Coefficient Lateral Consolidation (cm2/sec)	Coefficient Lateral Permeability (cm/s)
Soil Dilation	101.2	192.4	4.1	4.09								
	115.1	178.5	10.1	111.64	60.87	327.8	2.5	819.44	3.35	2.09E-02	1.35E-01	2.34E-06

CPT-58 Applied Research Associates 07/17/00

Depth = 103.0 ft Max Pressure = 6.60 psi Pn = 6.51 psi

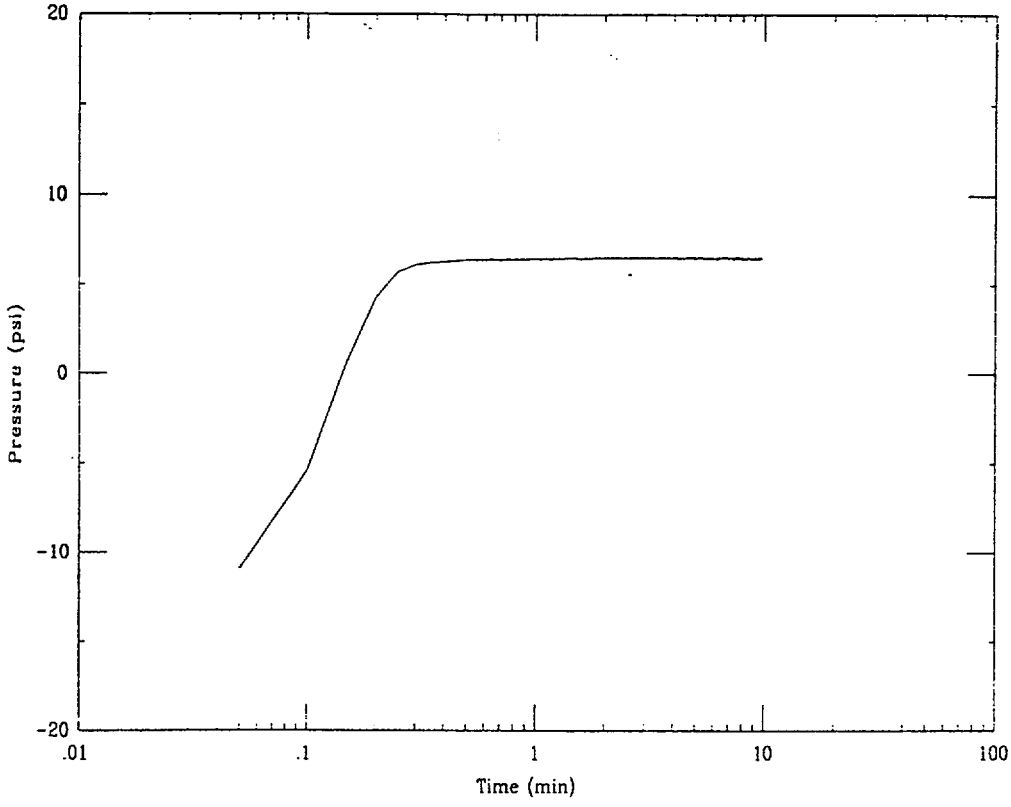

CPT-58 Applied Research Associates 07/17/00

Depth = 114.1 ft Max Pressure = 17.17 psi Pn = 17.17 psi

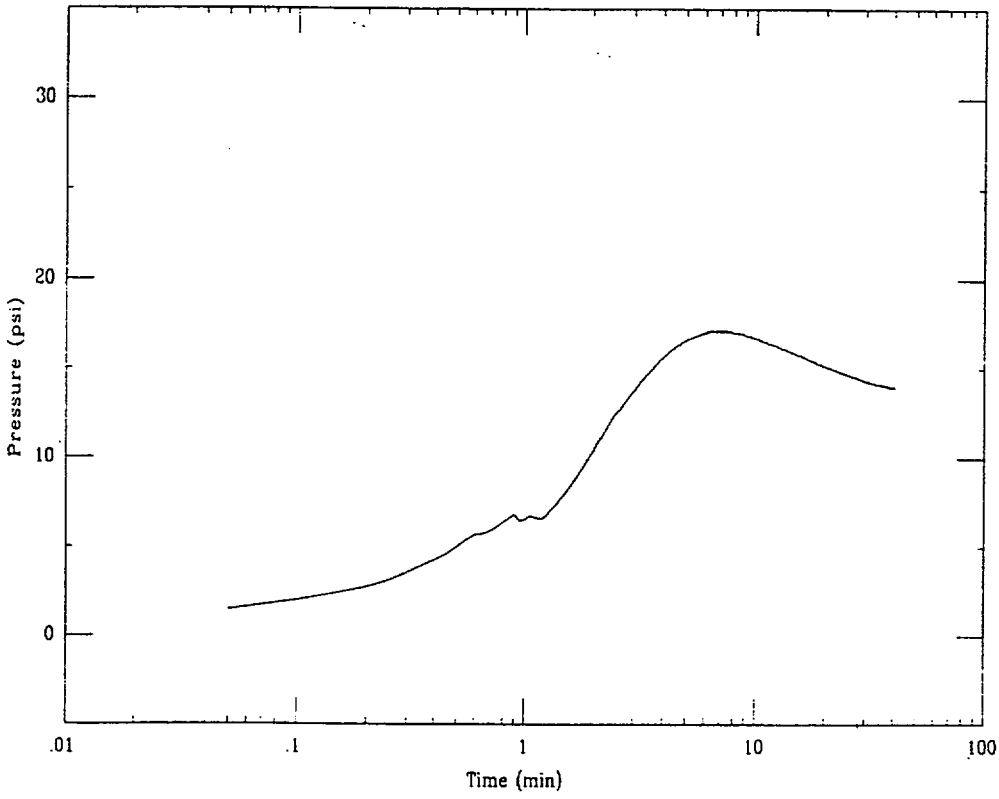

Project : Duke Cogema Stone & Webster

Test Id : CPT-58
Test Date : 7/17/00

Northing : 80135.1 (ft)
Easting : 54866.9 (ft)
Surface Elevation : 295.1 (ft)
Water Table Elevation : 207.1 (ft)

Probe Diameter : 1.75 (in)

Notes	Test Depth (ft)	Test Elev (ft)	Static Pressure (psi)	Maximum Pressure (psi)	50 % Pressure (psi)	Tip Stress (psi)	Alpha	Constrained Modulus (psi)	Time 50 % (min)	Coefficient Lateral Consolidation (in2/s)	Coefficient Lateral Consolidation (cm2/sec)	Coefficient Lateral Permeability (cm/s)
Soil Dilation	103.0	192.1	6.5	6.60								
	114.1	181.0	11.3	17.17	14.24	81.9	4.0	327.78	27.00	2.60E-03	1.68E-02	7.27E-07

CPT-59 Applied Research Associates 07/15/00

Depth = 99.1 ft Max Pressure = 10.33 psi Pn = 10.17 psi

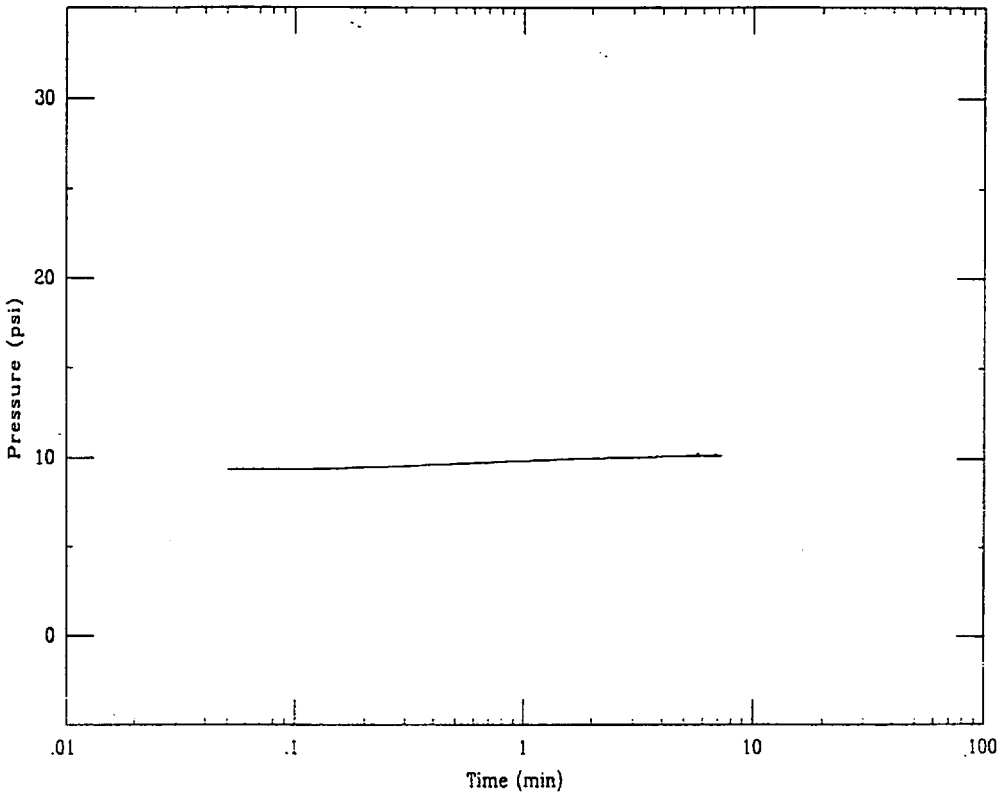

Project : Duke Cogema Stone & Webster

Test Id : CPT-59
Test Date : 7/15/00

Northing : 80152.7 (ft)
Easting : 54956.9 (ft)
Surface Elevation : 295.5 (ft)
Water Table Elevation : 219.8 (ft)

Probe Diameter : 1.75 (in)

Notes	Test Depth (ft)	Test Elev (ft)	Static Pressure (psi)	Maximum Pressure (psi)	50 % Pressure (psi)	Tip Stress (psi)	Alpha	Constrained Modulus (psi)	Time 50 % (min)	Coefficient Lateral Consolidation (in2/s)	Coefficient Lateral Consolidation (cm2/sec)	Coefficient Lateral Permeability (cm/s)
Immediate dissip.	99.1	196.4	10.1	10.33								

CPT-60 Applied Research Associates 07/15/00

Depth = 99.4 ft Max Pressure = 14.27 psi Pn = 14.23 psi

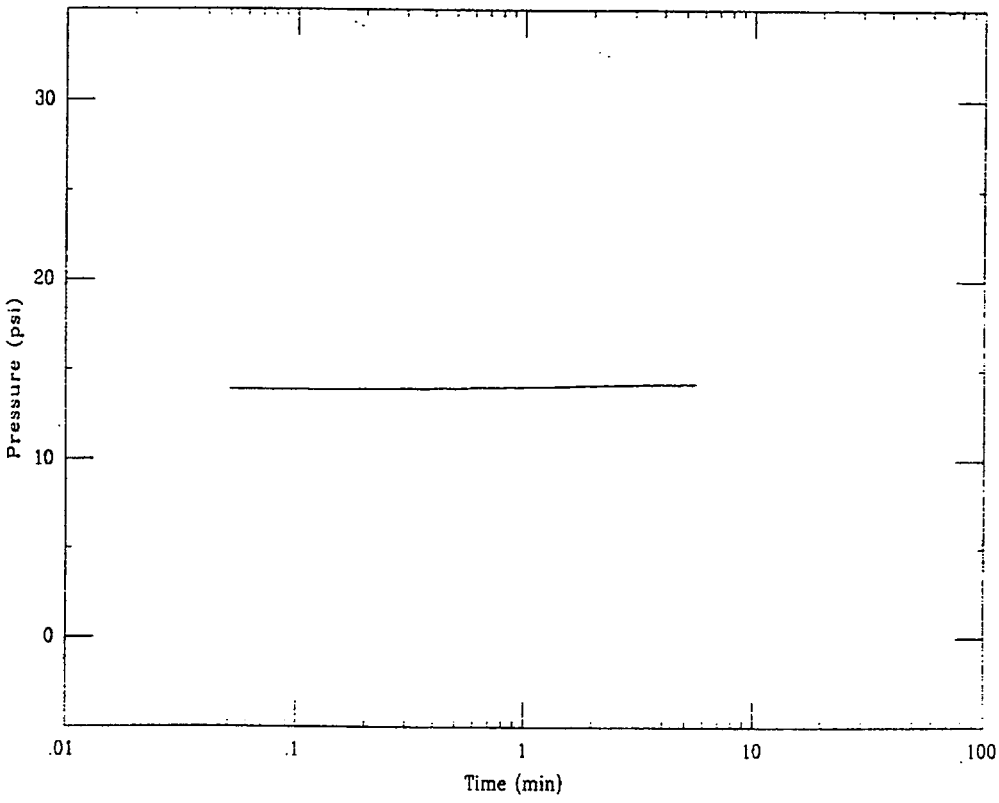

Project : Duke Cogema Stone & Webster

Test Id : CPT-60
Test Date : 7/15/00

Northing : 80142.2 (ft)
Easting : 55140.6 (ft)
Surface Elevation : 295.7 (ft)
Water Table Elevation : 229.1 (ft)

Probe Diameter : 1.75 (in)

Notes	Test Depth (ft)	Test Elev (ft)	Static Pressure (psi)	Maximum Pressure (psi)	50 % Pressure (psi)	Tip Stress (psi)	Alpha	Constrained Modulus (psi)	Time 50 % (min)	Coefficient Lateral Consolidation (in2/s)	Coefficient Lateral Consolidation (cm2/sec)	Coefficient Lateral Permeability (cm/s)
Immediate dissip.	99.4	196.3	14.2	14.27								

CPT-61 Applied Research Associates 07/21/00

Depth = 90.5 ft Max Pressure = 6.25 psi Pn = 6.19 psi

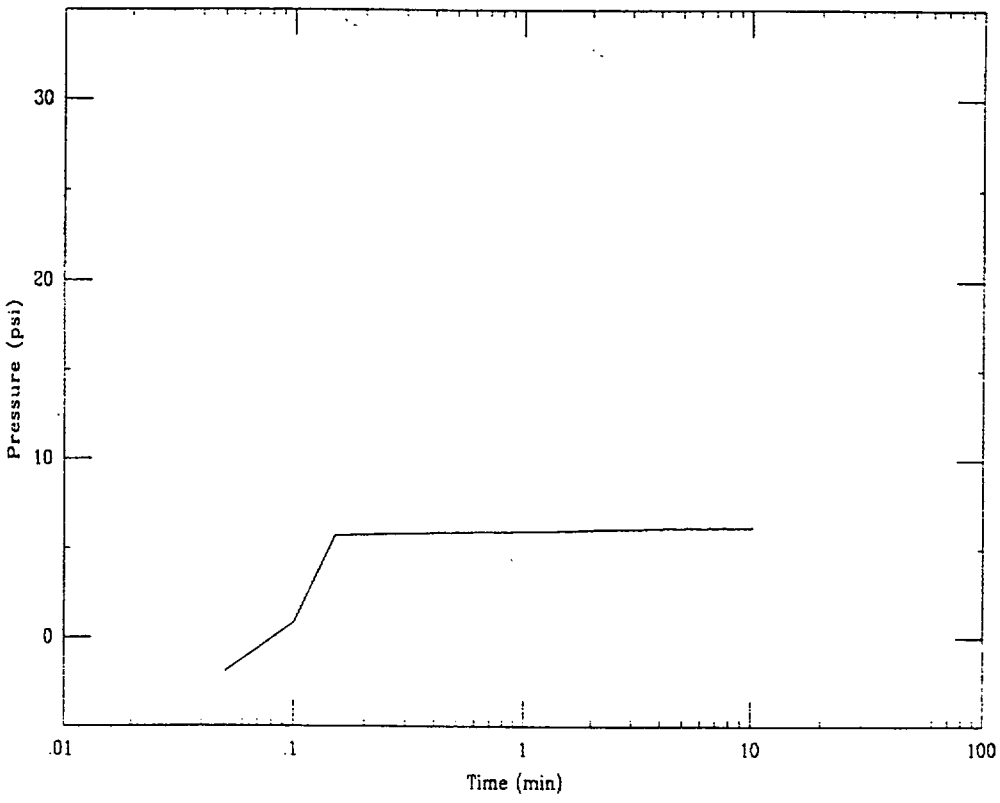

CPT-61 Applied Research Associates 07/21/00

Depth = 97.1 ft Max Pressure = 43.27 psi Pn = 17.78 psi

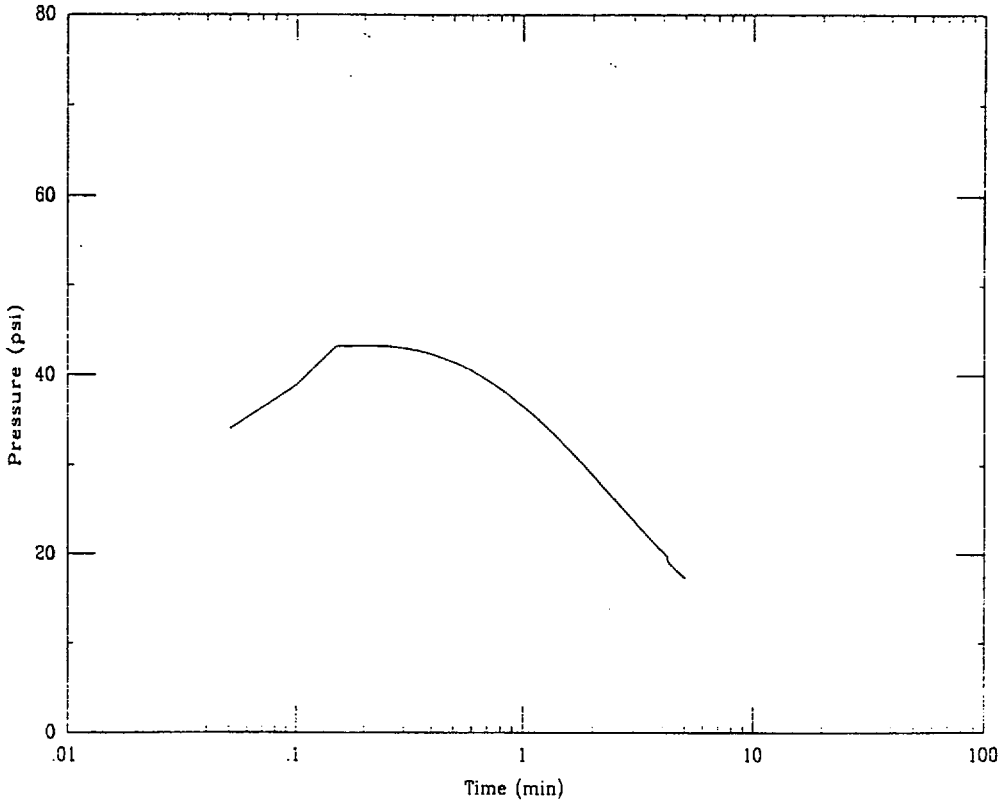

Project : Duke Cogema Stone & Webster

Test Id : CPT-61
Test Date : 7/21/00

Northing : 80037.6 (ft)
Easting : 54869.6 (ft)
Surface Elevation : 279.3 (ft)
Water Table Elevation : 203.0 (ft)

Probe Diameter : 1.75 (in)

Notes	Test Depth (ft)	Test Elev (ft)	Static Pressure (psi)	Maximum Pressure (psi)	50 % Pressure (psi)	Tip Stress (psi)	Alpha	Constrained Modulus (psi)	Time 50 % (min)	Coefficient Lateral Consolidation (in2/s)	Coefficient Lateral Consolidation (cm2/sec)	Coefficient Lateral Permeability (cm/s)
Soil Dilation	90.5	188.8	6.2	6.25								
	97.1	182.2	9.0	43.27	26.14	131.9	3.0	395.83	2.50	2.81E-02	1.81E-01	6.51E-06

CPT-62 Applied Research Associates 07/22/00

Depth = 70.8 ft Max Pressure = 58.94 psi Pn = 23.50 psi

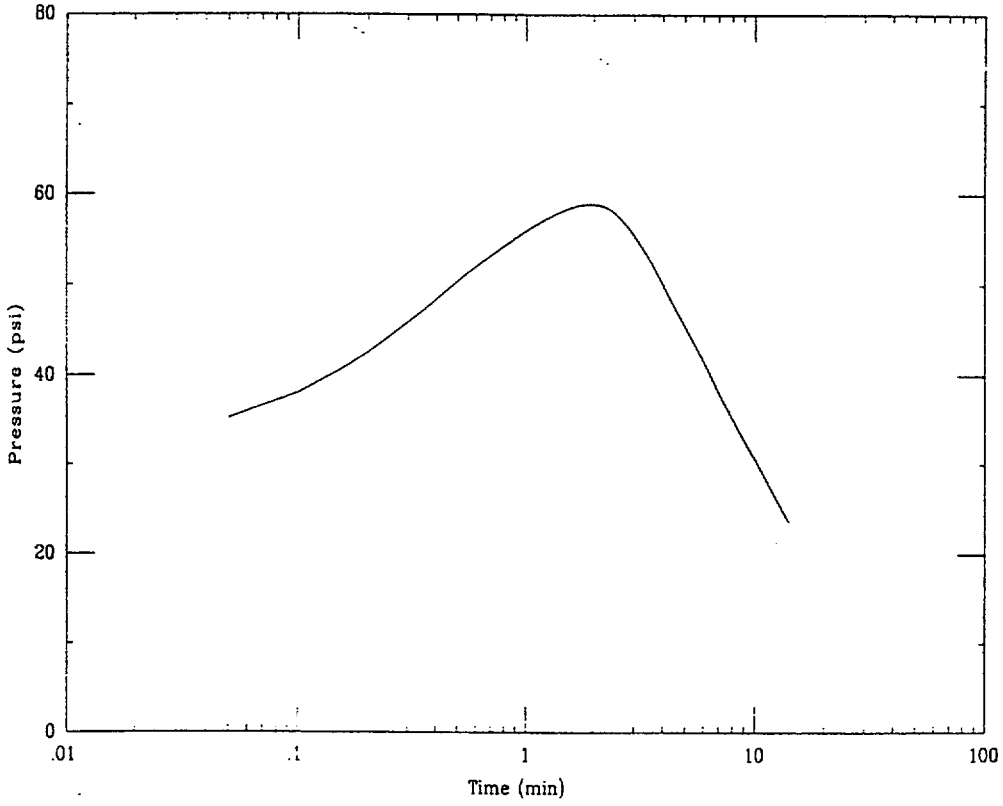

CPT-62 Applied Research Associates 07/22/00

Depth = 95.6 ft Max Pressure = 51.30 psi Pn = 8.57 psi

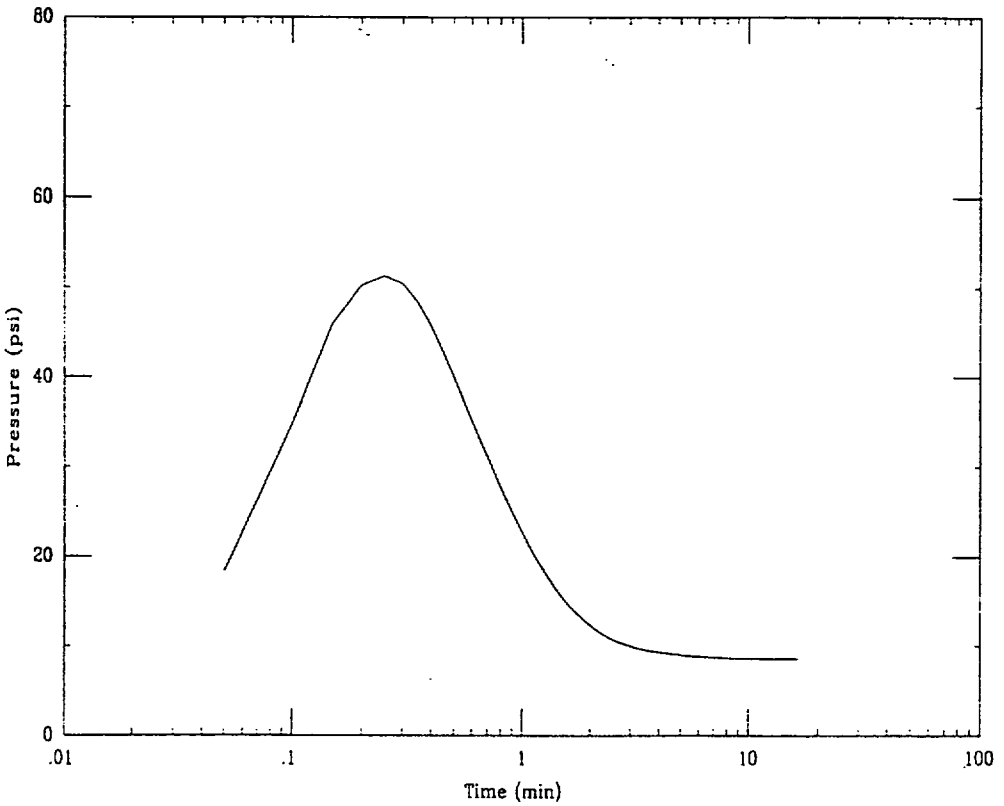

Project : Duke Cogema Stone & Webster

Test Id : CPT-62
Test Date : 7/22/00

Northing : 80055.6 (ft)
Easting : 54956.3 (ft)
Surface Elevation : 278.5 (ft)
Water Table Elevation : 202.6 (ft)

Probe Diameter : 1.75 (in)

Notes	Test Depth (ft)	Test Elev (ft)	Static Pressure (psi)	Maximum Pressure (psi)	50 % Pressure (psi)	Tip Stress (psi)	Alpha	Constrained Modulus (psi)	Time 50 % (min)	Coefficient Lateral Consolidation (in2/s)	Coefficient Lateral Consolidation (cm2/sec)	Coefficient Lateral Permeability (cm/s)
Above GWT	70.8	207.7	-2.2									
	95.6	182.9	8.5	51.30	29.92	205.6	3.0	616.67	0.75	9.36E-02	6.04E-01	1.39E-05

CPT-63 Applied Research Associates 07/22/00

Depth = 104.5 ft Max Pressure = 79.23 psi Pn = 38.21 psi

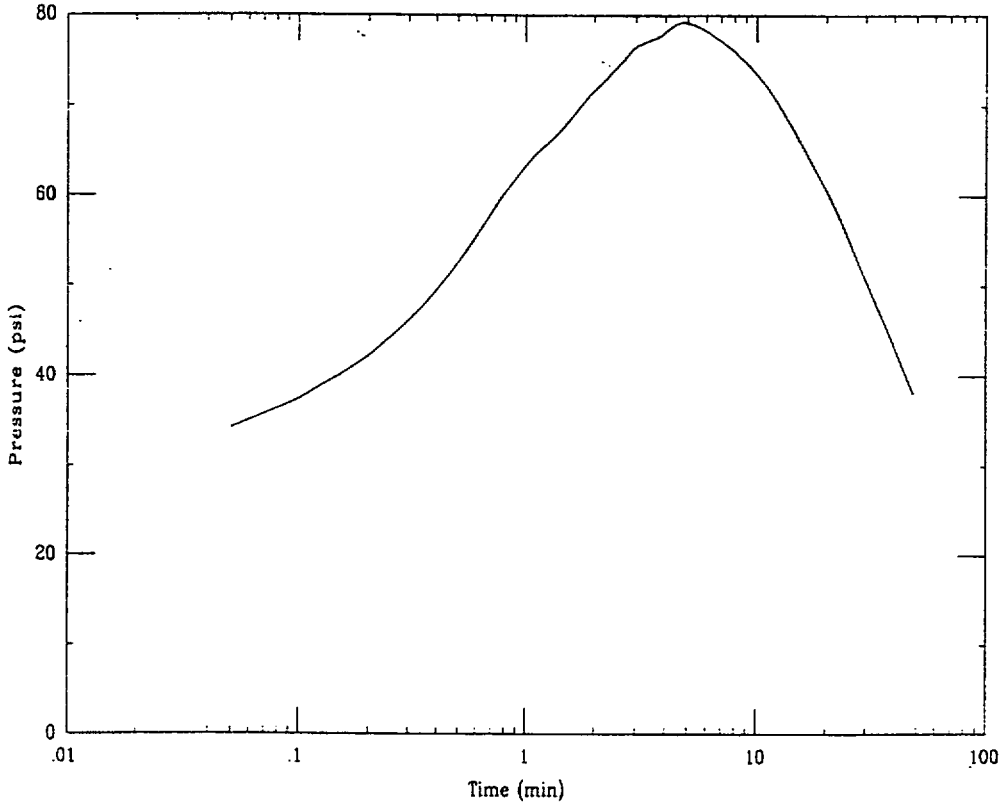

Project : Duke Cogema Stone & Webster

Test Id : CPT-63
Test Date : 7/22/00

Northing : 80066.0 (ft)
Easting : 55055.5 (ft)
Surface Elevation : 279.4 (ft)
Water Table Elevation : 189.4 (ft)

Probe Diameter : 1.75 (in)

Notes	Test Depth (ft)	Test Elev (ft)	Static Pressure (psi)	Maximum Pressure (psi)	50 % Pressure (psi)	Tip Stress (psi)	Alpha	Constrained Modulus (psi)	Time 50 % (min)	Coefficient Lateral Consolidation (in2/s)	Coefficient Lateral Consolidation (cm2/sec)	Coefficient Lateral Permeability (cm/s)
	104.5	174.9	6.3	79.23	42.76	273.6	3.0	820.83	40.74	1.72E-03	1.11E-02	1.92E-07

Dilatometer SDG. No.	GB-115			Client	DCS
Location	DMT-10	A avg (bars)	0.05	DMT Operator	DGC
Gage Zero LR (bars)	0.00	B avg (bars)	0.80	Rig Operator	JDB
Gage Zero HR (bars)	0.20			Rig Type	MACK 1
GWT Depth (ft)	63.00			Rod Type	1.75
Casing Depth (ft)				Membrane Type	H
Predrill Depth (ft)				Date:	07-Jul-00

Depth (Ft)	Thrust (psi)	A bars	B bars	C bars	Depth (Ft)	Thrust (psi)	A bars	B bars	C bars
1					51	550	3.15	14.40	NR
2					52	600	4.40	17.40	NR
3					53	600	1.25	16.70	NR
4					54	550	1.85	8.40	NR
5					55	550	4.05	14.70	NR
6					56	400	3.80	14.20	NR
7					57	300	4.00	14.60	NR
8					58	400	4.40	14.00	NR
9					59	400	4.00	15.60	NR
10	BROKE MEMBRANE. PULLING RODS.				60	450	4.15	16.30	NR
11	800	14.20	>20	3.35	61	400	3.30	13.50	NR
12	750	20.00	>20	15.50	62	400	2.75	13.00	NR
13	1100	13.80	>20	2.35	63	400	5.25	10.00	NR
14	1200	9.40	>20	0.00	64	200	4.20	11.60	NR
15	700	10.10	>20	0.00	65	500	2.00	10.80	NR
16	600	9.00	>20	NR	66	500	2.40	11.80	NR
17	500	5.85	16.80	NR	67	500	2.25	8.60	NR
18	500	5.25	17.20	NR	68	450	5.05	17.80	NR
19	400	4.00	15.60	NR	69	500	2.35	10.20	NR
20	400	3.20	13.60	NR	70	400	3.30	13.70	NR
21	600	4.90	19.40	NR	71	500	5.50	13.20	NR
22	700	5.20	>20	NR	72	600	1.65	8.80	NR
23	650	3.55	>20	NR	73	450	1.35	5.55	0.00
24	650	4.70	19.40	NR	74	350	2.65	11.40	0.00
25	700	3.75	18.80	NR	75	200	3.50	11.40	0.00
26	500	4.15	16.60	NR	76	200	5.85	13.40	0.00
27	550	4.30	15.20	NR	77	250	5.85	10.80	0.00
28	NO READINGS FOR THIS DEPTH.				78	250	7.45	13.00	0.10
29	500	4.40	15.80	NR	79	250	12.80	13.60	2.45
30	500	4.05	14.80	NR	80	300	12.60	19.80	2.45
31	500	4.55	15.20	NR	81	600	13.20	>20	3.85
32	400	2.00	10.80	NR	82	400	7.15	8.10	4.95
33	450	1.70	16.80	NR	83	400	15.20	>20	4.75
34	500	1.65	11.40	NR	84	400	11.20	>20	0.35
35	500	2.10	11.60	NR	85	450	11.00	16.20	2.45
36	600	4.15	>20	NR	86	NR	5.55	18.80	0.00
37	550	4.65	17.30	NR	87	800	5.85	>20	0.00
38	750	4.45	>20	NR	88	1150	4.35	18.40	0.00
39	750	8.15	>20	0.00	89	REFUSAL			
40	700	3.70	19.60	NR	90				
41	600	1.85	>20	NR	91				
42	500	3.15	17.40	NR	92				
43	450	8.10	>20	NR	93				
44	500	4.00	17.20	NR	94				
45	500	7.55	>20	NR	95				
46	400	7.75	>20	0.00	96				
47	350	4.35	17.00	NR	97				
48	300	6.65	14.60	0.00	98				
49	500	4.10	19.20	NR	99				
50	600	1.95	12.80	NR	100				

NR = NO READING

Post Calibration :

A avg (bars)	0.10
B avg (bars)	0.27

Dilatometer SDG. No.	GB-133			Client	DCS
Location	DMT-15	A avg (bars)	0.10	DMT Operator	DGC
Gage Zero LR (bars)	0.00	B avg (bars)	0.60	Rig Operator	JDB
Gage Zero HR (bars)	0.20			Rig Type	MACK1
GWT Depth (ft)	68.00			Rod Type	1.75
Casing Depth (ft)				Membrane Type	H
Predrill Depth (ft)				Date:	30-Jun-00

Depth (Ft)	Thrust (psi)	A bars	B bars	C bars	Depth (Ft)	Thrust (psi)	A bars	B bars	C bars
1					51	300	4.00	11.00	NR
2					52	250	3.10	12.00	NR
3					53	300	4.05	9.80	NR
4					54	200	1.90	10.70	NR
5					55	200	5.35	7.85	1.20
6					56	350	1.65	12.80	NR
7					57	600	1.65	10.40	NR
8					58	650	ERROR	17.40	NR
9					59	600	2.35	14.40	NR
10	700	10.80	NR	NR	60	400	2.35	6.65	NR
11	700	10.80	28.20	NR	61	250	10.00	15.00	1.85
12	600	9.80	NR	9.40	62	200	5.47	9.60	0.75
13	650	6.65	24.20	NR	63	200	5.95	10.20	0.20
14	650	6.30	NR	17.00	64	550	2.90	15.60	NR
15	600	6.65	22.80	NR	65	600	4.30	14.80	NR
16	600	5.75	21.20	NR	66	800	5.70	>20.00	NR
17	650	6.25	27.80	NR	67	800	4.75	>20.00	NR
18	650	5.05	19.20	NR	68	700	2.80	13.60	NR
19	600	4.65	17.60	NR	69	700	3.25	14.80	NR
20	500	5.65	17.60	NR	70	700	3.95	17.20	NR
21	500	5.35	16.80	NR	71	700	3.35	15.30	NR
22	600	4.30	15.60	NR	72	600	2.85	14.70	NR
23	600	4.45	17.60	NR	73	550	6.55	15.60	NR
24	700	4.70	19.20	NR	74	650	3.75	20.60	NR
25	500	6.55	19.40	NR	75	800	4.15	>20.00	NR
26	400	4.55	16.20	NR	76	750	3.45	17.20	NR
27	400	6.50	20.40	NR	77	750	3.25	17.80	NR
28	400	5.95	26.20	NR	78	650	2.45	11.80	0.00
29	400	2.30	10.00	NR	79	750	2.50	13.20	0.00
30	500	4.25	16.40	NR	80	650	2.30	11.80	0.00
31	600	3.45	14.80	NR	81	800	2.65	14.20	0.00
32	600	3.20	14.20	NR	82	800	3.10	14.80	0.00
33*	550	3.00	NR	2.15	83	800	3.40	16.50	0.00
34	see below				84	600	4.95	16.60	0.05
35	600	4.90	18.80	NR	85	400	4.50	14.00	0.00
36	550	1.55	8.80	NR	86	200	3.30	5.35	0.10
37	3500	1.45	7.75	NR	87	200	5.95	9.20	2.60
38	450	1.25	7.00	NR	88	200	6.65	12.60	1.65
39**	450	1.25		NR	89	250	7.40	13.20	3.30
40	500	1.75		NR	90	200	7.40	10.80	4.05
41	600	1.70	9.40	NR	91	250	7.15	11.60	2.65
42	500	1.60	9.20	NR	92	300	7.20	14.60	0.45
43	500	1.75	8.40	NR	93	400	8.80	11.20	5.30
44	500	1.70	9.80	NR	94	250	4.45	8.60	0.35
45	550	2.95	15.60	NR	95	350	7.90	16.20	0.00
46	600	2.55	13.80	NR	96	550	7.75	16.20	0.00
47	500	4.00	17.00	NR	97	600	4.00	15.00	0.15
48	650	5.45	>20.00	NR	98	650	5.75	19.60	0.25
49	650	2.65	14.00	NR	99	500	5.85	12.60	0.00
50	550	1.40	8.80	NR	100	900	11.20	>20.00	2.35
					101	800	5.35	>20.00	0.30
					102	700	6.15	>20.00	0.30
					103	1100	7.25	>20.00	0.65

NR = NO READING

Notes :

* Pulling DMT. Same cal. Factors as earlier calibration. New max. pressure 400 psi. 33 ft data is suspect.

** New Diaphram. New Max = 20 bars. A avg. - 0.10 bars. B ave = 0.55 bars.

Post Calibration :

A avg (bars)	0.30
B avg (bars)	0.10

APPENDIX E

DILATOMETER DATA

Dilatometer SDG. No.	GB-115			Client	DCS
Location	DMT-10	A avg (bars)	0.05	DMT Operator	DGC
Gage Zero LR (bars)	0.00	B avg (bars)	0.80	Rig Operator	JDB
Gage Zero HR (bars)	0.20			Rig Type	MACK 1
GWT Depth (ft)	63.00			Rod Type	1.75
Casing Depth (ft)				Membrane Type	H
Predrill Depth (ft)				Date:	07-Jul-00

Depth (Ft)	Thrust (psi)	A bars	B bars	C bars	Depth (Ft)	Thrust (psi)	A bars	B bars	C bars
1					51	550	3.15	14.40	NR
2					52	600	4.40	17.40	NR
3					53	600	1.25	16.70	NR
4					54	550	1.85	8.40	NR
5					55	550	4.05	14.70	NR
6					56	400	3.80	14.20	NR
7					57	300	4.00	14.60	NR
8					58	400	4.40	14.00	NR
9					59	400	4.00	15.60	NR
10	BROKE MEMBRANE. PULLING RODS.				60	450	4.15	16.30	NR
11	800	14.20	>20	3.35	61	400	3.30	13.50	NR
12	750	20.00	>20	15.50	62	400	2.75	13.00	NR
13	1100	13.80	>20	2.35	63	400	5.25	10.00	NR
14	1200	9.40	>20	0.00	64	200	4.20	11.60	NR
15	700	10.10	>20	0.00	65	500	2.00	10.80	NR
16	600	9.00	>20	NR	66	500	2.40	11.80	NR
17	500	5.85	16.80	NR	67	500	2.25	8.60	NR
18	500	5.25	17.20	NR	68	450	5.05	17.80	NR
19	400	4.00	15.60	NR	69	500	2.35	10.20	NR
20	400	3.20	13.60	NR	70	400	3.30	13.70	NR
21	600	4.90	19.40	NR	71	500	5.50	13.20	NR
22	700	5.20	>20	NR	72	600	1.65	8.80	NR
23	650	3.55	>20	NR	73	450	1.35	5.55	0.00
24	650	4.70	19.40	NR	74	350	2.65	11.40	0.00
25	700	3.75	18.80	NR	75	200	3.50	11.40	0.00
26	500	4.15	16.60	NR	76	200	5.85	13.40	0.00
27	550	4.30	15.20	NR	77	250	5.85	10.80	0.00
28	NO READINGS FOR THIS DEPTH.				78	250	7.45	13.00	0.10
29	500	4.40	15.80	NR	79	250	12.80	13.60	2.45
30	500	4.05	14.80	NR	80	300	12.60	19.80	2.45
31	500	4.55	15.20	NR	81	600	13.20	>20	3.85
32	400	2.00	10.80	NR	82	400	7.15	8.10	4.95
33	450	1.70	16.80	NR	83	400	15.20	>20	4.75
34	500	1.65	11.40	NR	84	400	11.20	>20	0.35
35	500	2.10	11.60	NR	85	450	11.00	16.20	2.45
36	600	4.15	>20	NR	86	NR	5.55	18.80	0.00
37	550	4.65	17.30	NR	87	800	5.85	>20	0.00
38	750	4.45	>20	NR	88	1150	4.35	18.40	0.00
39	750	8.15	>20	0.00	89	REFUSAL			
40	700	3.70	19.60	NR	90				
41	600	1.85	>20	NR	91				
42	500	3.15	17.40	NR	92				
43	450	8.10	>20	NR	93				
44	500	4.00	17.20	NR	94				
45	500	7.55	>20	NR	95				
46	400	7.75	>20	0.00	96				
47	350	4.35	17.00	NR	97				
48	300	6.65	14.60	0.00	98				
49	500	4.10	19.20	NR	99				
50	600	1.95	12.80	NR	100				

NR = NO READING

Post Calibration :

A avg (bars)	0.10
B avg (bars)	0.27

Dilatometer SDG. No.	GB-133			A avg (bars)	0.10	Client	DCS		
Location	DMT-15			B avg (bars)	0.60	DMT Operator	DGC		
Gage Zero LR (bars)	0.00					Rig Operator	JDB		
Gage Zero HR (bars)	0.20					Rig Type	MACK1		
GWT Depth (ft)	68.00					Rod Type	1.75		
Casing Depth (ft)						Membrane Type	H		
Predrill Depth (ft)						Date:	30-Jun-00		

Depth (Ft)	Thrust (psi)	A bars	B bars	C bars	Depth (Ft)	Thrust (psi)	A bars	B bars	C bars
1					51	300	4.00	11.00	NR
2					52	250	3.10	12.00	NR
3					53	300	4.05	9.80	NR
4					54	200	1.90	10.70	NR
5					55	200	5.35	7.85	1.20
6					56	350	1.65	12.80	NR
7					57	600	1.65	10.40	NR
8					58	650	ERROR	17.40	NR
9					59	600	2.35	14.40	NR
10	700	10.80	NR	NR	60	400	2.35	6.65	NR
11	700	10.80	28.20	NR	61	250	10.00	15.00	1.85
12	600	9.80	NR	9.40	62	200	5.47	9.60	0.75
13	650	6.65	24.20	NR	63	200	5.95	10.20	0.20
14	650	6.30	NR	17.00	64	550	2.90	15.60	NR
15	600	6.65	22.80	NR	65	600	4.30	14.80	NR
16	600	5.75	21.20	NR	66	800	5.70	>20.00	NR
17	650	6.25	27.80	NR	67	800	4.75	>20.00	NR
18	650	5.05	19.20	NR	68	700	2.80	13.60	NR
19	600	4.65	17.60	NR	69	700	3.25	14.80	NR
20	500	5.65	17.60	NR	70	700	3.95	17.20	NR
21	500	5.35	16.80	NR	71	700	3.35	15.30	NR
22	600	4.30	15.60	NR	72	600	2.85	14.70	NR
23	600	4.45	17.60	NR	73	550	6.55	15.60	NR
24	700	4.70	19.20	NR	74	650	3.75	20.60	NR
25	500	6.55	19.40	NR	75	800	4.15	>20.00	NR
26	400	4.55	16.20	NR	76	750	3.45	17.20	NR
27	400	6.50	20.40	NR	77	750	3.25	17.80	NR
28	400	5.95	26.20	NR	78	650	2.45	11.80	0.00
29	400	2.30	10.00	NR	79	750	2.50	13.20	0.00
30	500	4.25	16.40	NR	80	650	2.30	11.80	0.00
31	600	3.45	14.80	NR	81	800	2.65	14.20	0.00
32	600	3.20	14.20	NR	82	800	3.10	14.80	0.00
33*	550	3.00	NR	2.15	83	800	3.40	16.50	0.00
34	see below				84	600	4.95	16.60	0.05
35	600	4.90	18.80	NR	85	400	4.50	14.00	0.00
36	550	1.55	8.80	NR	86	200	3.30	5.35	0.10
37	3500	1.45	7.75	NR	87	200	5.95	9.20	2.60
38	450	1.25	7.00	NR	88	200	6.65	12.60	1.65
39**	450	1.25		NR	89	250	7.40	13.20	3.30
40	500	1.75		NR	90	200	7.40	10.80	4.05
41	600	1.70	9.40	NR	91	250	7.15	11.60	2.65
42	500	1.60	9.20	NR	92	300	7.20	14.60	0.45
43	500	1.75	8.40	NR	93	400	8.80	11.20	5.30
44	500	1.70	9.80	NR	94	250	4.45	8.60	0.35
45	550	2.95	15.60	NR	95	350	7.90	16.20	0.00
46	600	2.55	13.80	NR	96	550	7.75	16.20	0.00
47	600	4.00	17.00	NR	97	600	4.00	15.00	0.15
48	650	5.45	>20.00	NR	98	650	5.75	19.60	0.25
49	650	2.65	14.00	NR	99	500	5.85	12.60	0.00
50	550	1.40	8.80	NR	100	900	11.20	>20.00	2.35
					101	800	5.35	>20.00	0.30
					102	700	6.15	>20.00	0.30
					103	1100	7.25	>20.00	0.65

NR = NO READING

Notes :

* Pulling DMT. Same cal. Factors as earlier calibration. New max. pressure 400 psi. 33 ft data is suspect.

** New Diaphram. New Max = 20 bars. A avg. - 0.10 bars. B ave = 0.55 bars.

Post Calibration :

A avg (bars)	0.30
B avg (bars)	0.10

Dilatometer SDG. No.	GB-133			Client	DCS
Location	DMT-25	A avg (bars)	0.15	DMT Operator	DGC
Gage Zero LR (bars)	0.00	B avg (bars)	0.25	Rig Operator	JDB
Gage Zero HR (bars)	0.20			Rig Type	MACK 1
GWT Depth (ft)	68.00			Rod Type	1.75
Casing Depth (ft)				Membrane Type	H
Predrill Depth (ft)				Date:	01-Jul-00

Depth (Ft)	Thrust (psi)	A bars	B bars	C bars	Depth (Ft)	Thrust (psi)	A bars	B bars	C bars
1					51	350	5.35	11.00	0.00
2					52	200	6.10	11.80	0.15
3					53	400	5.95	10.40	0.30
4					54	400	1.15	10.00	NR
5					55	400	2.50	10.40	NR
6					56	300	3.55	9.60	NR
7					57	300	4.45	11.20	0.00
8					58	400	4.35	16.00	NR
9					59	450	1.35	6.35	NR
10	600	12.00	>20	1.90	60	550	4.45	16.80	NR
11	550	12.40	>20	1.95	61	600	2.55	12.20	NR
12	450	11.80	>20	1.65	62	550	2.00	10.20	NR
13	500	10.00	>20	0.80	63	550	1.25	6.75	NR
14	500	10.20	>20	1.05	64	500	3.25	13.60	NR
15	700	5.35	>20	NR	65	500	3.35	13.30	NR
16	800	12.40	>20	2.75	66	550	3.45	14.30	NR
17	550	12.40	>20	2.40	67	450	1.85	8.00	NR
18	700	10.20	>20	1.55	68	400	3.40	12.90	NR
19	750	12.60	>20	2.15	69	550	1.45	6.55	NR
20	1000	11.60	>20	2.05	70	500	2.80	12.00	NR
21	1200	13.20	>20	3.65	71	600	2.20	9.80	NR
22	1100	8.80	>20	NR	72	700	1.45	6.70	NR
23	700	11.60	>20	1.55	73	650	1.40	7.25	NR
24	550	2.75	13.20	2.85	74	500	1.35	7.25	NR
25	550	5.55	19.80	NR	75	600	1.75	10.50	NR
26	600	4.65	18.00	NR	76	500	1.70	10.00	NR
27	600	4.10	15.80	NR	77	500	1.30	6.25	0.00
28	600	2.05	11.40	NR	78	500	1.75	7.45	0.00
29	600	1.45	7.85	NR	79	600	1.95	10.50	0.00
30	600	2.45	13.20	NR	80	700	1.75	10.30	0.00
31	650	3.65	15.20	NR	81	750	2.00	10.80	0.00
32	600	3.80	15.60	NR	82	1000	5.25	>20	0.00
33	600	3.35	15.00	NR	83	1200	5.65	>20	0.00
34	600	3.35	14.60	NR	84				
35	600	4.15	15.70	NR	85				
36	500	4.15	15.40	NR	86				
37	500	1.55	7.30	NR	87				
38	500	3.60	14.20	NR	88				
39	500	3.30	14.50	NR	89				
40.4	450	2.94	12.60	NR	90				
41	500	2.45	11.80	NR	91				
42	700	4.75	18.30	NR	92				
43	700	3.55	15.20	NR	93				
44	700	6.55	>20	NR	94				
45	700	10.00	>20	0.85	95				
46	700	3.35	15.60	NR	96				
47	550	2.00	9.50	NR	97				
48	500	3.55	14.00	NR	98				
49	450	6.45	19.30	NR	99				
50	400	4.55	15.20	NR	100				

NR = NO READING

Post Calibration :

A avg (bars)	0.10
B avg (bars)	0.20

Dilatometer SDG. No.	GB-133			Client	DCS
Location	DMT-23	A avg (bars)	0.10	DMT Operator	DGC
Gage Zero LR (bars)	0.00	B avg (bars)	0.70	Rig Operator	JDB
Gage Zero HR (bars)	0.20			Rig Type	MACK 1
GWT Depth (ft)	70.00			Rod Type	1.75
Casing Depth (ft)				Membrane Type	H
Predrill Depth (ft)				Date:	06-Jul-00

Depth (Ft)	Thrust (psi)	A bars	B bars	C bars	Depth (Ft)	Thrust (psi)	A bars	B bars	C bars
1					51	650	3.35	16.20	NR
2					52	750	3.10	15.50	NR
3					53	900	3.00	15.30	NR
4					54	1000	5.15	>20	NR
5					55	800	3.55	15.60	NR
6					56	800	3.45	14.20	NR
7					57	500	2.70	12.50	NR
8					58	650	4.55	17.10	NR
9					59	550	2.75	12.80	NR
10	500	13.80	>20	3.65	60	550	3.35	15.00	NR
11	500	12.70	>20	1.60	61	700	1.80	9.80	NR
12	500	5.05	15.60	NR	62	600	4.45	17.80	NR
13	500	4.55	13.70	NR	63	850	3.15	15.60	NR
14	400	5.40	16.80	NR	64	600	3.35	14.40	NR
15	300	3.25	11.20	NR	65	600	4.25	14.30	NR
16	350	2.75	11.60	NR	66	750	3.35	15.70	NR
17	500	2.45	11.50	NR	67	900	6.00	>20	NR
18	400	3.80	14.10	NR	68	600	3.35	15.60	NR
19	400	3.85	13.90	NR	69	500	3.65	14.60	NR
20	400	4.65	15.80	NR	70	500	2.55	11.40	NR
21	400	5.20	17.00	NR	71	400	9.80	13.80	4.25
22	400	3.55	13.30	NR	72	200	15.00	>20	9.00
23	400	4.95	15.50	NR	73	300	18.80	>20	12.80
24	500	4.60	15.70	NR	74	300	6.85	19.80	0.00
25	400	4.35	14.80	NR	75	300	11.00	15.60	3.55
26	400	4.55	14.80	NR	76	250	8.80	13.80	0.00
27	400	4.80	16.20	NR	77	500	5.45	19.60	NR
28	400	4.60	15.30	NR	78	400	7.35	13.80	0.00
29	600	5.35	16.40	NR	79	300	7.25	16.80	NR
30	500	2.15	10.40	NR	80	450	2.35	11.00	NR
31	500	3.65	14.20	NR	81	400	4.25	13.20	0.00
32	500	4.80	16.20	NR	82	350	4.75	16.00	0.00
33	500	2.25	11.20	NR	83	300	5.75	10.00	0.00
34	600	4.55	16.80	NR	84	350	5.15	9.40	NR
35	650	3.00	14.00	NR	85	400	5.80	19.90	0.00
36	700	3.15	13.40	NR	86	550	6.75	>20	0.00
37	650	2.25	12.00	NR	87	700	2.85	12.20	0.00
38	600	4.00	16.20	NR	88	600	5.20	12.40	0.00
39	700	1.70	9.40	NR	89	600	4.65	11.60	0.00
40	700	1.55	8.80	NR	90	600	4.05	15.20	0.00
41	550	2.25	12.60	NR	91	600	5.25	19.60	0.00
42	550	7.65	>20	NR	92	650	6.15	>20	0.00
43.4	500	4.85	>20	NR	93	700	5.90	>20	0.00
44	500	1.95	>20	NR	94	550	4.85	16.60	0.00
45	450	5.70	>20	NR	95	850	3.95	14.80	0.00
46	500	2.65	13.00	NR	96	1050	5.15	>20	0.00
47	550	1.35	8.80	NR	97	1300	7.30	>20	0.00
48	600	2.95	14.60	NR	98	1300			
49	600	2.20	12.20	NR	99	1100	5.05	>20	0.00
50	800	2.15	12.50	NR	100.2	600	3.15	12.20	0.00
					101	500	6.80	15.00	0.00
					102	200	8.00	12.50	2.65
					103	200	8.40	13.60	2.60
					104	250	>20	NR	NR
					105	150	>20	NR	NR
					106	150	ERROR		
					107	350	>20	NR	NR
					108	400	>20	NR	NR

NR = NO READING

Post Calibration :

A avg (bars)	0.10
B avg (bars)	0.70

Notes :

* AT 45 FEET, PULLING RODS, GOT 4 READINGS OF >20 FOR B-VALUE
CHANGED DIAPHRAM AND RECALIBRATING AT 45 FEET
DEPTHS 42 TO 45 THE B-VALUE IS QUESTIONABLE

Dilatometer SDG. No.	GB-133			Client	DCS
Location	DMT-29	A avg (bars)	0.10	DMT Operator	DGC
Gage Zero LR (bars)		B avg (bars)	0.60	Rig Operator	JDB
Gage Zero HR (bars)				Rig Type	MACK 1
GWT Depth (ft)	70.00			Rod Type	1.75
Casing Depth (ft)				Membrane Type	H
Predrill Depth (ft)				Date:	29-Jun-00

Depth (Ft)	Thrust (psi)	A bars	B bars	C bars	Depth (Ft)	Thrust (psi)	A bars	B bars	C bars
1	1800	20.80	55.80	NR	51	550	4.00	16.60	NR
2	1700	19.60	52.00	NR	52	600	1.85	8.60	NR
3	1200	13.00	38.00	NR	53	600	2.00	9.20	NR
4	800	8.40	24.20	NR	54	600	1.55	9.00	NR
5	400	3.40	13.00	0.15	55	600	1.75	8.20	NR
6	450	3.50	11.60	NR	56	600	1.95	10.20	NR
7	400	3.60	11.00	NR	57	700	1.85	9.60	NR
8	500	3.60	12.00	NR	58	700	1.75	9.00	NR
9	500	5.30	17.00	NR	59	650	2.00	10.70	NR
10	850	8.30	27.60	NR	60	650	2.25	11.80	NR
11	1300	18.80	50.00	NR	61	700	1.95	11.60	NR
12	1400	14.20	42.00	NR	62	700	3.20	15.00	NR
13	800	11.80	18.80	1.80	63	600	3.40	14.80	NR
14	300	11.80	21.60	0.50	64	600	4.25	17.20	NR
15	500	10.40	24.80	0.15	65	550	2.05	9.70	NR
16	700	6.35	22.60	NR	66	400	4.40	15.00	NR
17	700	7.25	21.60	NR	67	250	7.85	13.20	2.70
18	800	11.40	29.20	NR	68	200	17.00	24.20	6.60
19	800	8.60	23.20	NR	69	250	9.60	13.80	3.65
20	800	7.85	20.80	NR	70	200	11.60	17.80	9.00
21	800	6.15	19.40	NR	71	700	10.20	29.20	NR
22	700	6.60	20.00	NR	72	700	8.80	29.00	NR
23	700	4.80	17.00	NR	73	500	5.35	11.60	2.70
24	750	6.90	22.00	NR	74	400	5.25	11.60	NR
25	750	5.70	20.20	NR	75	450	5.15	17.20	NR
26	NR	NR	NR	NR	76	450	2.20	11.40	NR
27*	NR	NR	NR	NR	77	500	2.15	13.00	NR
28	750	3.75	16.20	NR	78	350	4.30	8.05	NR
29	800	4.25	17.80	NR	79	200	5.45	10.20	NR
30	700	2.80	12.20	NR	80	150	4.85	10.00	NR
31	650	2.60	12.10	NR	81	200	4.65	9.60	NR
32	650	3.05	14.20	NR	82	500	4.35	14.80	NR
33	650	4.95	18.00	NR	83	400	5.80	16.40	NR
34	700	2.45	13.00	NR	84	500	3.60	14.65	NR
35	800	2.05	11.60	NR	85	500	3.60	14.00	NR
36	700	1.40	7.25	NR	86	600	3.65	14.00	NR
37	500	1.10	6.30	NR	87	700	3.75	13.60	0.00
38	500	5.90	15.30	NR	88	600	4.35	13.80	0.00
39	500	2.35	10.80	NR	89	500	4.00	11.40	0.00
40	500	2.65	12.30	NR	90	500	2.55	12.40	0.00
41	450	4.45	17.10	NR	91	650	1.85	9.80	0.00
42	550	1.45	10.60	NR	92	800	3.05	14.20	0.00
43	600	1.15	7.76	NR	93	900	3.15	17.20	0.00
44	550	1.45	9.00	NR	94	1200	4.55	19.80	0.00
45	500	1.95	10.60	NR	95	1600	11.00	47.20	0.00
46	500	1.60	7.75	NR	96				
47	550	1.45	9.00	NR	97				
48	550	1.55	10.60	NR	98				
49	700	1.60	9.80	NR	99				
50	600	1.75	9.80	NR	100				

NR = NO READING

Notes :

* Vane oriented parallel to E-W sides of MOX building.

** Test with diaphram split at 28 ft test depth. Replaced blade , installed H diaphram.

Post Calibration :

A avg (bars)	0.125
B avg (bars)	0.300

GEOMATRIX

FINAL REPORT

Ground Motion Following Selection of SRS Design Basis Earthquake and Associated Deterministic Approach

WSRC Subcontract AA20210S

Prepared for

Westinghouse Savannah River Company
P.O. Box 616
Aiken, South Carolina 29802
E.E. Stephenson, Project Manager

March 1991
Project No. 1724

Geomatrix Consultants

TABLE OF CONTENTS

TABLE OF CONTENTS (cont'd)

LIST OF TABLES

LIST OF FIGURES

Figure
Number Title

TABLE OF CONTENTS (cont'd)

LIST OF FIGURES (cont'd)

LIST OF FIGURES (cont'd)

LIST OF FIGURES (cont'd)

LIST OF FIGURES (cont'd)

LIST OF FIGURES (cont'd)

LIST OF FIGURES (cont'd)

GROUND MOTION FOLLOWING SELECTION OF SRS DESIGN BASIS EARTHQUAKE AND ASSOCIATED DETERMINISTIC APPROACH

1.0 INTRODUCTION

This report summarizes the results of a deterministic assessment of earthquake ground motions at the Savannah River Site (SRS). The purpose of this study is to assist the Environmental Sciences Section of the Savannah River Laboratory in reevaluating the design basis earthquake (DBE) ground motion at SRS using approaches defined in Appendix A to 10 CFR Part 100. This work is in support of the Seismic Engineering Section's Seismic Qualification Program for reactor restart.

The most recent commercial applications of Appendix A in the eastern U.S. occurred in the early 1980's and significant progress has been made since then in the understanding of earthquake ground motions in the eastern U.S. Accordingly, our approach follows the precedents developed in applications of the Appendix in the past, and incorporates new methods for analyzing earthquake potential and ground motions.

Our approach to this study has been to follow deterministic methodologies for the implementation of Appendix A as revealed in recent license applications including that for the Vogtle Electric Generating Plant, and in recent seismic design reviews for commercial plants, including the recently completed deterministic studies for the WNP-3 Satsop, Washington, and Diablo Canyon, California, nuclear plants. These latter projects involved aspects of the analysis that reflect the current level of sophistication in analyzing earthquake sources and evaluating ground motions. For example, both assessments involved assessing ground motions based not only on empirical approaches but also using physical/numerical approaches. We feel that a modern application of the Appendix A approach for the SRS must also include updated, sophisticated approaches.

It is our understanding that the results of this study will serve to update the Safety Analysis Report (SAR) at the SRS. Because we are conducting this study during the time that site-specific geologic and geotechnical data are actively being gathered and interpreted for K-reactor, the results given in this Final Report may be subject to update and revision. We base our assessments on existing geology, seismology, and geotechnical (GSG) data. It is expected that additional GSG data will be gathered as part of the New Production Reactor program and these assessments may have implications to the DBE presented in this report.

We have attempted in presenting our analysis to isolate individual parameters and to show the sensitivity of the final results to these parameters. For example, the relative contribution that individual seismic sources make to the final ground motion response spectra is presented. In doing so, we have sought to identify those aspects of the analysis that are most important and that might be the focus of attention in the future.

2.0 SEISMIC SOURCE CHARACTERIZATION

2.1 INTRODUCTION

The characterization of design basis earthquakes for a deterministic analysis involves the identification of possible earthquake sources, an evaluation of their capability (as defined in Appendix A), a description of their location relative to the site, and an assessment of the maximum earthquake that each source is capable of generating. Taken as a whole, we term these activities "seismic source characterization". Each of these basic steps involves numerous assessments and each involves considerable uncertainty. The history of application of Appendix A by the Nuclear Regulatory Commission (NRC) dictates that not only are the selected deterministic values documented, but also the rationale for arriving at these values are documented. Unlike a probabilistic approach that allows for the explicit incorporation of uncertainty into the analysis, a deterministic assessment is by nature single-valued. In order for the selected values to be evaluated and, thereby the level of conservatism in the final results evaluated, the assessment procedure and decision-making process must be documented. Extended NRC reviews and controversy have centered around the basic seismic source characteristics for deterministic ground motions assessments.

In light of the need to document the basis for our assessments in this study as well as the incomplete level of knowledge of many aspects of the earthquake environment in the eastern US, we present our best interpretation of seismic source characteristics given the available data. We include in this discussion possible alternative interpretations and hypotheses, and provide the support in the data for our selected interpretations.

2.2 SAVANNAH RIVER SITE SEISMIC SOURCE CHARACTERIZATION

The identification and characterization of earthquake sources at the Savannah River Site (SRS) generally follows the methodologies established by precedent in applications of Appendix A for

eastern U.S. commercial reactor sites and as represented in the Standard Review Plan for Chapter 2.5 (NRC,1990). Specifically, the potential causes and geologic structural controls of earthquakes are considered as well as the seismotectonic provinces within which earthquakes occur. The location, size, and, to a lesser extent, rate of occurrence of historical seismicity are important aspects in characterizing the seismic environment. If the seismicity record is to provide a basis for assessing the location of seismic sources, an explicit judgement must be forwarded regarding the temporal and spatial stationarity of earthquake activity in the region that might affect ground motions at the site. Typically, in the eastern U.S., the final seismic source characterization assessment involves a combination of both seismicity and tectonic considerations. Uncertainties in the assessment, which usually are large, are documented.

2.2.1 Charleston Source

Location. The first earthquake source identified that may affect ground motions at the SRS is the source that gave rise to the 1886 Charleston, South Carolina earthquake. This earthquake was the largest historical earthquake in the Coastal Plain tectonic province (maximum intensity of MMI X; Fig. 1) and is one of the largest earthquakes that has occurred in the eastern U.S. during the historical period.

The causal geologic structure (fault) that generated the 1886 earthquake is not known. Geologic studies in the meizoseismal region have not located evidence for coseismic surface fault rupture, which would allow an unequivocal association with a particular geological structure. Because of the importance of this earthquake to the understanding of the seismotectonics of the southeastern U.S., an extensive ten-year program of investigation of the Charleston region was carried out by the U.S. Geological Survey (Gohn, 1983). The program, together with other efforts in the area, did not result in the identification of a single geological structure that can unequivocally be identified as the cause of the 1886 earthquake. Rather, the program, and the subsequent studies that continue up to the present time, resulted in the identification of several candidate faults and geologic structures that could have generated the Charleston earthquake. For example, offshore seismic reflection profiling by the U.S.G.S.

identified several small faults that appear to displace lower to mid-Tertiary units (Dillon et al., 1983). Talwani (1982) has proposed that the Charleston earthquake was the result of stress concentration at the intersection of two inferred faults, the Ashley River fault and the Woodstock fault, and subsequent subsurface rupture along one or both of the faults (Fig. 2). Other hypotheses for the causal structure for the earthquake include slip on the Appalachian detachment beneath the Coastal Plain (Seeber and Armbruster, 1981) and stress concentrations at the intersection of a Mesozoic basin with an inferred meteorite impact crater (Phillips, 1988).

In the face of the uncertainties regarding the causal structure of Charleston earthquake, licensing of nuclear power plants has been carried out based on the hypothesis that the source of the Charleston earthquake, whatever the geologic cause, is located in the meizoseismal area of the 1886 earthquake and in the region of the ongoing zone of microseismicity. In other words, spatial stationarity has generally been assumed. In 1982, the U.S.G.S. issued to the Nuclear Regulatory Commission a clarification of their position of the cause of the Charleston earthquake and the potential for the occurrence of similar earthquakes elsewhere in the eastern U.S. Their conclusion was that their geologic studies of the Charleston area had resulted in the identification of several geologic structures that could have been the causal structure for the 1886 event. However, they were unable to unequivocally associate the event with any one of these candidate structures. Further, they asserted that similar geological structures could be found at other locations throughout the eastern U.S., raising the possibility that Charleston-type earthquakes could occur at locations other than Charleston. They suggested that the probability of occurrence of such events might be very low, but they recommended that probabilistic and deterministic seismic hazard studies be carried out to assess how likely such occurrences might be.

In response to the clarification of position by the U.S.G.S., probabilistic seismic hazard studies involving a large number of experts were carried out by the NRC (through LLNL) and by the electric utilities (through the Electric Power Research Institute). In general, the results of these studies show that most experts considered the probability of the occurrence of a Charleston-type

earthquake (e.g., a M~7 earthquake) outside of the recognized Charleston seismic zone to be very unlikely. A strong piece of evidence for this assessment made by many of the experts is that when the spatial pattern of historical seismicity over the past 100-200 years is compared with the pattern of seismicity during the recent instrumental period, the major seismic zones have generally maintained their present positions. Examples are the Charleston seismic zone, New Madrid, and the Charlevoix zone. Key uncertainties in this assessment are the occasional occurrence of moderate-magnitude earthquakes outside of clear seismic zones, such as the 1982 New Brunswick earthquake, and the recognition that the 100-200 year historical period is probably far shorter than the recurrence intervals for large earthquakes at particular locations in the eastern U.S.

In our assessment of the location of the Charleston source relative to the SRS site, we considered the pattern of historical and instrumental seismicity as described above. We also considered the location all of the candidate geologic structures for the 1886 event, such as the Ashley River and Woodstock faults. Note that essentially all of them are located within the meizoseismal area (Fig. 2).

Fortunately, we are also able to draw on the results of recent and ongoing geologic studies that are designed to assess the location of prehistoric Charleston earthquakes over time periods of several thousand years. Over the past several years, investigators from the U.S.G.S. and other groups have identified evidence for liquefaction that accompanied the 1886 earthquake (Fig. 3), as well as evidence for pre-1886 liquefaction. The geologic features are in most cases sand blows that represent the surface manifestation of the liquefaction of sand layers at depth. Observations following several historical earthquakes worldwide have shown that these features are diagnostic of earthquake shaking-induced liquefaction associated with moderate to large earthquakes. In general, it is observed that the occurrence of liquefaction over an extensive region requires the occurrence of moderate to large magnitude earthquakes, although other characteristics such as liquefaction susceptibility of the soils also plays an important role.

By calibrating geologic observations of sandblows in the Charleston region with those features associated with the 1886 event, the investigators have been able to identify pre-1886 sandblows and to date them (e.g., Obermeir et al., 1987; Talwani and Cox, 1985; Amick et al., 1989). In general, the results of these studies have shown evidence for at least five pre-1886 earthquakes in the Charleston seismic zone. Over the past two thousand years, the average recurrence interval for these events in coastal South Carolina is estimated to be about 500 to 600 years (Amick and Gelinas, in press). These recurrence rates are somewhat surprising in that they are comparable to those for the more active faults in the western U.S. such as the Calaveras fault. For this assessment, we conclude that the identification of pre-1886 liquefaction features lends considerable credibility to the hypothesis that the 1886 Charleston source has remained where it is presently observed over the past several thousand years (i.e., spatial stationarity). The relatively high rate of recurrence implies that the earthquake process is similar in temporal stability to that of western U.S. active faults, rather than being a episodic or random process (Coppersmith, 1988).

Recent and ongoing geologic studies have moved away from the Charleston meizoseismal area with the particular purpose of attempting to identify evidence for prehistoric liquefaction away from Charleston. Thus far the most significant conclusion of these studies is that it appears that Charleston-type earthquakes have not occurred at other locations within the Coastal Plain of the southeastern U.S. For example, Obermeir et al. (1987) documented evidence for pre-1886 liquefaction features within carefully chosen beach ridge deposits in the Charleston area. Moving away from Charleston but within deposits having the same liquefaction susceptibility, Obermeir et al., identified a pronounced decrease in the number of sandblows and the size of sandblows as one moves north and south of the 1886 meizoseismal area (Fig. 4). This suggests that an earthquake source has existed in the Charleston region over the period of the geologic observation (several thousand years), and that similar earthquake sources do not exist away from the Charleston region. In a more regionally extensive study, Amick et al. (1990) searched for evidence of liquefaction in a region from the Chesapeake Bay to northern Florida. In general, they found that liquefaction-generating earthquake sources do not appear to be present

within the Coastal Plain except within South Carolina (Figs. 5 and 6). Their studies, which are ongoing, also identify the possibility of another earthquake source to the north of Charleston near the South Carolina-North Carolina border.

Taken as a whole, these geologic studies of the distribution and absence of paleoliquefaction lends considerable credibility to the hypothesis that the Charleston source has remained relatively localized over the past several thousand years. We infer, therefore, that the source will likely remain where it is presently observed.

Although placing constraints on the north-south location of pre-1886 earthquakes (i.e., within the coastal plain), the paleoliquefaction studies have not yet provided information on the possible inland extent of pre-1886 liquefaction features. Such would further constrain the location of the Charleston source relative to the SRS. It is our understanding, however, that studies of the presence or absence of paleoliquefaction within alluvial deposits of the major river systems in the southeast are being commissioned at the present time by the Research Division of the Nuclear Regulatory Commission.

Based on our consideration of the historical and instrumental seismicity data as well as the constraints provided by the evidence for pre-1886 liquefaction, we conclude that the Charleston seismic source should be located in the meizoseismal region of the 1886 earthquake, which is also the approximate location of the ongoing microseismicity (Fig. 2). Assuming that the source lies within the intensity X contour, this places the Charleston source at a distance of about 120 km from the site. The possible fault dimensions for the Charleston source is further discussed below in the context of its maximum earthquake magnitude.

Maximum Earthquake Magnitude. The assessment of maximum earthquake magnitudes for earthquake sources in the eastern United States is difficult because the maximum event for any given source is rare relative to the historical period of observation. Standard practice for sources that can be associated with active faults is to evaluate the expected dimensions of future

ruptures, including such characteristics as rupture length, rupture area, and displacement (e.g., Schwartz et al., 1986). In the eastern U.S. and other stable continental regions, however, the assessment of maximum magnitude is more difficult and usually relies on extrapolations of the historical record (see Coppersmith et al., 1987 for a discussion of methods for assessing maximum magnitudes within stable continental regions).

In the case of the Charleston seismic zone, we have already experienced a large magnitude earthquake in the historical record in 1886, as well as several events in the prehistorical geologic record. Unfortunately, the geologic data on the distribution of liquefaction features are not yet sufficiently well-resolved to provide an indication of the size of the prehistoric events or even to allow an assessment of their size relative to the 1886 event. Future and ongoing geologic activities may allow this assessment to be made.

In past licensing practice, the NRC has dealt with the issue of the size of the Charleston source maximum earthquake by considering the 1886 earthquake to be a reasonable earthquake to consider for the evaluation. As stated in the Operating License Safety Evaluation Report for the Vogtle Electric Generating Plant (USNRC, 1985):

> "The staff's current position, as in the past, is that, in accordance with the tectonic province approach (Appendix A of 10 CFR 100), the effects of a recurrence of an 1886 Charleston earthquake in the Summerville-Charleston area shall be postulated to assess its influence on the Vogtle site."

In this deterministic assessment, we will follow the precedent set by the NRC in the application of Appendix A and assume that an appropriate maximum earthquake for the Charleston source is one that is similar in size to the 1886 earthquake. This raises the issue of what the size of the 1886 earthquake was, particularly in terms of moment magnitude, M.

Several investigators have made assessments of the size of the Charleston earthquake based on the maximum intensity and the distribution of intensities from the event. All published estimates

of the size of the Charleston earthquake are based on correlating intensity data with short-period magnitudes that are equivalent to one-Hertz m_b or m_{bLg}. The standard estimates, upon which all recent published values derive, are from Nuttli et al. (1979), utilizing the method originally developed by Nuttli (1973). Nuttli (1983) expanded the m_b values to include M_S and M_O by use of his empirical source scaling relationships for mid-plate earthquakes. Most recently, (Nuttli et al., 1989; Jost and Herrmann, unpublished) the original Nuttli (1983) estimates of M_S and M_O have been revised but they still depend on the original intensity-based m_b range of 6.6 to 6.9 with 6.7 usually favored. Given these values of mb and source scaling relationships, Nuttli (1983) and Nuttli et al. (unpublished) arrive at a seismic moment for the event of about $M_O = 3 \cdot 10^{26}$ dyne-cm.

As part of the present study, A. Johnston (unpublished consulting report) has reviewed the approaches used by past researchers to estimate the magnitude and seismic moment of the 1886 earthquake. He finds that there are several problems with these analyses that result in underestimating the Charleston earthquake's true size. In general these problems relate to the data bases used to estimate M_S and M_O from the m_b estimates, the choice of the unusually deep 1968 southern Illinois earthquake as a calibration for the intensity-fall off relations of Nuttli (1983), and the use of short period m_b as an estimator of M_O or M_S, which depend mostly on the long-period ($T \geq 15$ sec) contributions to the seismic spectrum. Most of these problems are related to the paucity of the mid-plate data bases available to the researchers during the time that they were developing their relationships.

To alleviate the problems associated with past approaches to estimating seismic moment from intensity, Johnston (in prep.) in the Electric Power Research Institute Stable Continental Regions study (Coppersmith et al., in prep.) directly relates isoseismal areas to seismic moment. As part of that study an extensive earthquake data base was developed for stable continental regions (SCR) that are tectonically similar to the eastern United States. By carefully selecting SCR regions, we are then able to combine isoseismal information from different continental regions into overall regression equations that directly relate isoseismal areas to M_O

(see, for example, Figs. 7 and 8). Johnston (in prep.) shows that there are no systematic differences from continent to continent in the data base and the utilization of the entire SCR data base permits enough data points to be included to make the regressions robust. We therefore conclude that they are well-suited to estimate the size of the 1886 Charleston earthquake in terms of M_o and M.

The map of isoseismals for the 1886 earthquake is particularly well-studied for a pre-instrumental earthquake in the eastern United States (Fig. 1). Based on the smoothed isoseismal map of Bollinger (1977) and assuming symmetry in the isoseismals at the coastline, Johnston (in prep.) arrives at seismic moment estimates based on the isoseismal areas for felt area, and intensities IV, V, and VI. Averaging these moment values and translating them into moment magnitudes using the relationship of Hanks and Kanamori (1979), Johnston arrives at a seismic moment estimate for the 1886 Charleston earthquake of about $M_o = 2.75 \cdot 10^{27}$ dyne-cm and a moment magnitude estimate of $M = 7.56 \pm 0.35$. The uncertainty estimate is a qualitative measure based on the number of magnitude estimates and the quality of the data. Johnston (unpublished consulting report) compares this magnitude estimate to those associated with the 1819 Kutch, India earthquake (M = 7.79) and the 1918 Nanai, China earthquake (M = 7.42) to verify that a moment magnitude of about M = 7.5 is appropriate for the Charleston earthquake.

Because the approach taken by Johnston (in prep.) appears to avoid most of the problems associated with previous studies of the size of the Charleston earthquake, we conclude that the estimate of the seismic moment for the 1886 event of $M_o = 2.75 \cdot 10^{27}$ dyne-cm and moment magnitude of about M = 7.5 is reasonable. We recognize however that there are still remaining uncerainties associated with Johnson's approach and the Charleston estimate: The estimate of seismic moment based on empirical relationships is founded on the assumption that SCR regions are comparable to each other and that the Charleston area is tectonicaly similar to other SCR; the isoseismal areas for the Charleston earthquake are based on the assumption that the total areas should be estimated by doubling the areas observed onland; and the analysis

is highly sensitive to the intensity mapping of Bollinger (1977), any systematic changes in the intensity assignments that would lead to significant changes in the isoseismal map would affect the magnitude estimate.

Following the NRC precedent whereby the size of the 1886 earthquake is assumed to provide an estimate of the maximum magnitude for the Charleston source, we shall use the moment magnitude estimate of 7.5 and a seismic moment of $2.75 \cdot 10^{27}$ dyne-cm in the subsequent analysis of ground motions.

Source Dimensions and Static Stress Drop. Given a seismic moment of about $M_o = 2.75 \cdot 10^{27}$ dyne-cm and a moment magnitude estimate of about M = 7.5, we can examine the implications to the dimensions of the Charleston source and the static stress drop. By definition, seismic moment is directly related to rupture area (length times width), average displacement across the rupture surface, and the rigidity of the fault zone materials (usually taken to be $3.3 \cdot 10^{11}$ dyne/cm^2); moment is also directly related to the rupture area and the static stress drop. Therefore we can evaluate the relative values of these parameters given the above seismic moment estimate.

Because the causitive fault that generated the 1886 earthquake is not known, we are unable to estimate the length and downdip width of the source directly. We can make inferences about the downdip width based on the focal depth distribution of the ongoing instrumental seismicity. Several investigators (e.g., Sibson, 1984) have concluded that the approximate width of the seismogenic crust is represented by the distribution of focal depths of small magnitude earthquakes. A good example of these is the pattern of earthquake hypocenters that occurred in the Loma Prieta rupture zone prior to the 1989 earthquake which displayed focal depths up to about 18 km. The subsequent 1989 rupture as outlined by the pattern of aftershocks extended to these depths.

The distribution of focal depths in the southeastern U.S. is given by Bollinger et al. (in press) and is shown in Figure 9. In general, the average focal depths in the Valley & Ridge and Blue Ridge province are somewhat deeper than the average depths in the Piedmont and Coastal Plain. The maximum focal depths in the Valley & Ridge and Blue Ridge province are about 25 km and about 20 km in the Piedmont and Coastal Plain. Although not indicated in Figure 9, most of the deepest earthquakes within the Coastal Plain province ocurr in the Charleston region. Based on these data, we conclude that the maximum downdip rupture width of the Charleston seismic source is about 20 km.

Envisioning the Charleston earthquake occurring along a 20 km-wide fault, variations in the hypothesized length of the rupture zone imply differences in rupture area and consequent differences in static stress drop. In Figure 10 we present the relationships among these parameters for the 1886 seismic moment estimates made by Nuttli (1983) and by Johnston (in prep.) (The additional line in Figure 10 will be discussed later).

Given the moment magnitude M estimate of 7.5 for the 1886 earthquake, we can assess the expected rupture length and rupture area for the event. We begin by examining empirical relationships between moment magnitude and surface rupture length, subsurface rupture length (measured from the pattern of young aftershocks), and rupture area (also determined from aftershocks). Figures 11, 12, and 13 are empirical regressions between rupture dimension and magnitude (note the regressions of rupture dimension on magnitude is the approporiate regression curve for use here). All of the earthquakes in this data set are those for which instrumental seismic moments have been determined and the magnitudes given are moment magnitudes (Wells and Coppersmith, in review). The data set is dominated by interplate events, but contains some earthquakes from stable continental regions, as will be discussed later.

It is seen from these regressions that the expected rupture length for a M 7.5 earthquake is about 110 km. The subsurface rupture length relationship may be more applicable here given

the apparent lack of surface faulting associated with the 1886 earthquake. The expected rupture area for M 7.5 is about 2,200 km^2. The combination of these two results suggests that the typical rupture width in the data set for a M 7.5 earthquake is about 20 km. Given that the data sets for these regressions contain a high percentage of non-SCR earthquakes, we must assess how the expected rupture lengths and areas might vary for SCR earthquakes.

Because there are far fewer SCR earthquakes for which rupture lengths and rupture areas have been assessed, we are unable to develop robust empirical regressions for SCR earthquakes alone of the type in Figures 11-13. However, comparison of the available SCR data with the data bases as a whole shows no discernable differences (Figs. 14, 15, and 16). There appears to be no compelling evidence for concluding that the expected rupture length or rupture area for a M 7.5 earthquake in SCR should be any different from an interplate earthquake of the same magnitude. As a check, we regress the SCR and interplate rupture length and rupture area separately, and arrive at comparable results (Figs. 17 and 18). We therefore conclude that the expected rupture length for the M 7.5 Charleston earthquake is about 110 km and the expected rupture area is about 2,200 km^2. As discussed above, we estimate the maximum downdip rupture width for the Charleston source to be about 20 km. Accordingly, the rupture length for a 2,200 km^2 rupture area would be about 110 km.

The above analysis is based on an assessment of the expected source dimensions for a M 7.5 earthquake. Are there any source-specific data that would allow us to estimate the source dimensions specifically for the Charleston source? It is our opinion that a primary candidate for the cause of the Charleston earthquake is the northeast-trending Woodstock fault, which is mapped to lie within the meizoseismal region of the 1886 earthquake and to strike in the direction of elongation of the high intensity isoseismals. Talwani (1982) interprets the existence of the fault primarily on the basis of the presence of microseismicity and suggests that both the Woodstock fault and the northwest-trending Ashley River fault may have undergone slip during the 1886 earthquake. Talwani (1982) and Talwani et al. (1990) suggest that the Woodstock fault has a minimum length of about 50 km, which is the length of the ongoing microseismicity

in the area. We would agree that the length of the microseismicity provides a minimum length of the fault, but would not conclude that the length of seismicity defines the maximum length of the 1886 rupture.

This interpretation is based on observations of seismicity along fault zones that are known to have ruptured in historical time. Figure 19 shows the pattern of instrumental seismicity occurring in California. Note that large parts of the the San Andreas fault that ruptured in 1906 and 1857 are not expressed in the pattern of earthquake epicenters. Note that we are not including aftershocks for these ruptures, only the background pattern of earthquakes. In the same way, the ongoing seismicity in the Charleston region is not part of an aftershock sequence. Because we find many cases where the pattern of seismicity does not define the entire length of past ruptures, we conclude that the 50 km-long zone of seismicity in the Charleston region does not definitively constrain the maximum length of the fault that ruptured in 1886.

Recent work by Marple and Talwani (1990) have identified on SPOT satellite imagery a lineament along the surface projection of the Woodstock fault, termed by them the "Woodstock lineament". Thus far the lineament is believed to have a minimum length of 25 km (Marple and Talwani, 1990), and therefore does not provide us with a definitive estimate for the maximum length of the 1886 fault rupture.

Another possible method for estimating the length of the rupture during the 1886 earthquake might be to assume that the rupture was contained within the intensity X (meizoseismal) contour. The maximum length would be about 60 km along a northeasterly direction. However, we have examined several historical surface ruptures worldwide were the rupture was well-mapped and good intensity data exist. The surface rupture pattern and intensity patterns for some of these earthquakes are shown in Figures 20-22. We have found that in over half of the earthquakes that we examined, the surface rupture propagated well beyond the

meizoseismal region. Therefore, we conclude that the isoseismal pattern of the 1886 earthquake does not provide a constraint on the maximum length of the 1886 fault rupture.

After examining the evidence for the Woodstock fault, the pattern of seismicity, and the isoseismal pattern for the 1886 earthquake, we conclude that the available data are not sufficient to uniquely assess the maximum rupture length for the earthquake. The available data provide only a minimum length of about 50 km. Certainly, there are no direct data that would argue for an anomously small rupture area (or short rupture length) for the earthquake. We therefore believe that it is appropriate to assume that the dimensions of the 1886 earthquake were equivalent to those that are expected for a typical M 7.5 earthquake -- namely, a rupture area of about 2,200 km^2 and a rupture length of about 110 km. A rupture length of about 110 km aligned in a northeasterly direction along the axis of the meizoseismal region would imply the existence of rupture beyond the intensity X isoseismal, but still lying within the intensity IX isoseismal (Fig. 1).

Given this assumed rupture length and rupture area for the Charleston earthquake, we can examine the implications of these values to other parameters such as static stress drop and average displacement. In Figure 10 we show that, for a seismic moment of $2.75 \cdot 10^{27}$ dyne-cm, rupture width of 20 km, and rupture length of 110 km, the associated static stress drop is about 65 bars. For comparison, we have calculated static stress drops for worldwide earthquakes (mostly interplate events) based on their observed rupture areas and instrumental seismic moments (Fig. 23). Notice that there is little dependency of static stress drop on magnitude; the average stress drop for the entire data base is about 42 bars. Accordingly, our estimated static stress drop of about 65 bars for the Charleston event appears to be reasonable, if slightly on the high side.

Using the 2,200 km^2 rupture area and the estimated seismic moment for the event, we calculate the average displacement to be about 4 m. Again, we have used the rupture areas and instrumental seismic moments for the worldwide data base to compare average displacement

with M (Fig. 24). This relation suggests that the expected average displacement in this data set for a M 7.5 is about 3 m, which is in reasonable agreement. It is instructive to note that if other assumptions about the source dimensions of the Charleston earthquake are made (say a rupture area that is one-half the 2,200 km^2 that we are assuming), the average displacement would be much higher (about 9 m for a 1,000 km^2 rupture area). The average displacement of 9 meters implied appears to be highly unlikely in that no clear evidence for surface rupture has been identified. Further, because the paleoliquefaction evidence suggests repeated large-magnitude earthquakes have occurred in Holocene time, the cumulative effects of repeated 9 meter displacements would be expected to be dramatically expressed in the geomorphology. Thus far the only documented suggestive evidence of the geomorphic expression for active faulting is the Woodstock Lineament, which is coincident with the surface projection of the Woodstock fault and is associated with a scarp that is up to 2.5 meters high (Marple and Talwani, 1990).

When all of the above interpretations are taken as a whole, we conclude the following: (1) The expected rupture length for a M 7.5 earthquake, whether interplate or SCR, is about 110 km and the rupture area is about 2,200 km^2, (2) The available data on the Woodstock fault, seismicity patterns, and isoseismals do not place constraints on the maximum length of the 1886 rupture, and (3) The dimensions of rupture imply a static stress drop of about 75 bars and an average displacement of about 4 m. As will be discussed in Section 3, these assessments will be used as a starting point for assessing the appropriate stress parameter in the ground motion estimation model.

2.2.2. Bowman Source

Location. A cluster of earthquakes occurred in the vicinity of Bowman, South Carolina that we consider as a possible seismic source (Fig. 2). The Bowman seismicity occurred primarily in the 1970's, shut off in the 1980's, and has shown some recent microseismicity in 1990. The largest earthquakes within this zone are about magnitude 3.5 to 4.0. The Bowman zone is part of a diffuse northwesterly-trending zone of seismicity extending from the Charleston

region to the inner Piedmont and Appalachian tectonic province. This northwest zone would include the M 4.5 (MMI VII) 1913 Union County earthquake (Fig. 2).

The northwesterly trend of this seismic zone is not consistent with the regional structural trends in this region and the causal geologic structure giving rise to the seismicity is not known. However, the episodic nature of the seismicity (during a time when the seismicity near Charleston continued), the paucity of northwesterly-trending structures, as well as the clear separation of the Bowman seismicity from the Charleston seismicity zone leads us to the conclusion that it is not part of the Charleston seismic source. In the absence of geologic data regarding the origin of the Bowman seismic source, we use the pattern of seismicity directly to assess the location of the zone relative to the SRS. The immediate seismic source that would encircle the observed seismicity (Fig. 2) is about 80 km from the site.

Maximum Magnitude. Because the causative geologic structure for the Bowman source is not known, we are unable to use assessments of the source geometry to evaluate the maximum earthquake magnitude. As mentioned, the largest observed earthquakes in the zone have been less than or equal to about magnitude 4.0. Because the Bowman zone is located in an area where the Coastal Plain sediments are less than about one to two kilometers thick and are believed to be underlain by crystalline rocks that are the same as those at the surface in the Piedmont to the west, we consider the source to basically lie within the Piedmont seismotectonic province. In other words, the earthquakes that would occur in the area would lie beneath the thin Coastal Plain sediments and within the Piedmont basement. The largest earthquake in the historical record that has occurred in the southeastern Piedmont tectonic province is the 1913 Union County earthquake (MMI VI-VII, Coffman and von Hake, 1973) The moment magnitude for this earthquake was assessed by Johnston (in prep.) to be M = 4.5, based on the same methodology as previously discussed for the Charleston earthquake using isoseismal areas (Fig. 25). The largest earthquake that has occurred historically in the Appalachian Piedmont province is the 1875 Goochland County, central Virginia earthquake (MMI VII, Oaks and Bollinger, 1986; moment magnitude M = 4.8, Johnston, in prep.)

(Fig. 26). Studies of the instrumental seismicity within the central Virginia seismic zone suggest that the earthquakes are occurring within the rocks above the Appalachian detachment (Bollinger et al., 1985), thus placing them in an analogous position to those occurring at Bowman.

Other earthquakes in the southeastern US are occurring within the eastern Tennessee seismic zone and the Giles County, Virginia zone (Fig. 27). Detailed studies of the focal depths within these zones, however, indicates that the earthquakes within these seismic zones are occurring within the rocks beneath the Appalachian detachment, perhaps along preexisting normal faults whose origin is related to extensional stresses during Eocambrian time (Bollinger et al., 1988). We therefore do not consider the historical earthquakes associated with these seismic zones to be analogous to those that are possible within the Bowman source.

On the basis of our consideration of the largest earthquakes that have occurred within the Piedmont seismotectonic province (M 4.5 Union County and M 4.8 Central Virginia earthquakes), we conclude that the maximum earthquake within the Bowman source should be at least as large as M 5.0. Because the Bowman seismicity zone clearly shows levels of seismicity that are elevated relative to the background levels (the background, random source is discussed below and has a maximum magnitude of M 5.0) and because the zone lies within a diffuse northwesterly-trending zone of seismicity that might represent a larger source volume (Fig. 27), we conclude that a maximum magnitude of moment magnitude M 6.0 is appropriate for the Bowman seismic source.

2.2.3 "Nearby" Source

Following the application of Appendix A as represented in the Standard Review Plan for Chapter 2.5 (USNRC, 1990), we consider the possibility of a nearby source that may generate earthquakes within the local site vicinity. Based on the available data and interpretations, the known faults that exist in the local site vicinity, such as the Pen Branch fault and the border

fault zone of the Dunbarton basin, are not considered to be capable. As summarized in the Vogtle SSER (dated 1989):

> "On the basis of the available information, the staff concludes that the Pen Branch fault is not a capable fault as described by Appendix A to 10 CFR Part 100 and does not represent a hazard to the Vogtle site. However, DOE plans to begin a detailed investigation of the Pen Branch fault on the SRPR in the near future. The investigation is expected to consist of core borings, trench logging, and seismic reflection profiling to determine the upper limit age of last displacement... The licensee will keep the NRC informed of new information when it becomes available. At the end of that time, the staff will determine whether or not any action or additional reporting, such as modification of the FSAR, is necessary."

It is our understanding that no new data have been developed as part of the ongoing Pen Branch fault studies that would alter the position taken by the NRC staff regarding the capability of the Pen Branch fault.

In the absence of an identifiable nearby seismic source, we allow for the possible existence of a random "nearby" source that might exist within the local site vicinity. By convention, the "local site vicinity" is taken to be the region within about 25 km of the site.

Maximum Earthquake Magnitude. The largest earthquakes that have occurred during the historical period within 25 km of the site have been in the magnitude range of about 2.0-3.0, including the 1985 m_{bLg} 2.6 earthquake (Talwani et al., 1985) that occurred within the SRS boundary (Fig. 2). However, we do not consider these events to be representative of the maximum magnitudes possible in the site vicinity. The site is underlain by about 300 meters of Coastal Plain sediments that are, in turn, underlain by crystalline basement rocks equivalent to those of the Piedmont province (Fig. 28). Therefore, we consider the largest earthquakes that have occurred within the Piedmont tectonic province to provide a reasonable constraint on the maximum magnitude within the site vicinity (Fig. 29). As discussed previously, the 1913 Union County earthquake (moment magnitude M 4.5) is the largest historical earthquake within

the southeastern Piedmont province, and the 1875 Central Virginia earthquake (M 4.8) is the largest historical earthquake that has occurred within the Appalachian Piedmont.

Studies of the stress regime within the Piedmont province, based on evaluations of microseismicity data and in-situ stress measurements, have led to the hypothesis that the earthquakes observed within the province are related to a "skin effect" whereby the upper few kilometers of the crust is highly stressed (e.g., Zoback et al., 1986; 1989). Based on studies of reservoir-induced earthquakes within the Piedmont, which appear to differ from naturally-occurring events only in their temporal and spatial association with reservoir impoundment, these events appear to be related to release of stress along existing planes of weakness, such as near-surface fractures. A general model for Piedmont earthquakes has been proposed (Guinn, 1980; Marion and Long, 1980; and Jones et al., 1985) in which the fault area is limited by the depth penetration of joints or other planes of weakness, typically on the order of 4 km. As a result the maximum magnitude earthquakes that might be expected from such limited source areas would be less than about M 5.

On the basis of a consideration of the largest historical earthquakes within the Piedmont and thin Coastal Plain tectonic province, as well as the theoretical models regarding the causes for these events, we conclude that the maximum magnitude for the nearby seismic source is moment magnitude M 5.0.

To compare this moment magnitude to m_{bLg}, a number of relationships have been developed between seismic moment or moment magnitude and m_{bLg} (e.g., Nuttli, 1983; Hasegawa, 1983; Boore and Atkinson, 1987; and Somerville, 1987). Translating seismic moment into moment magnitude using Hanks and Kanamori (1979) and using the above relationahips, it can be concluded that moment magnitude M 5.0 is approximately equivalent to m_{bLg} 5.3 (Fig. 30). For comparison, the maximum magnitude assessed for the nearby source at the Vogtle site was m_{bLg} 5 1/4.

3.0 ASSESSMENT OF STRONG GROUND MOTION

3.1 METHODS USED FOR ASSESSMENT OF STRONG GROUND MOTION

Site-specific strong ground motions resulting from the safety earthquakes defined in Section 2 were assessed using three approaches that have been employed in recent licensing efforts for commercial nuclear power plants. The three methods are: direct estimation of site-specific ground motions using empirical ground motion attenuation relationships for the appropriate tectonic regime and site conditions, statistical analysis of strong motion data from earthquakes within similar tectonic environments recorded on sites with similar subsurface conditions, and direct estimation of site-specific ground motions using physical models. The first two approaches have been the basis for the majority of seismic safety evaluations of commercial nuclear power plants. However, as discussed in Section 1.0, estimates of ground motion obtained from physical and numerical models have played an important role in recent safety reviews. These methods provide both direct estimates of strong ground motion and guidance in extrapolating empirical relationships beyond the range of the available data.

The three approaches used in this analysis are described below. For each postulated event, one or more of the approaches were used, depending on the availability and suitability of data necessary to make the assessment.

3.1.1 Empirical Attenuation Relationships

Given an magnitude and source-to-site distance for a safety evaluation earthquake, published attenuation relationships, usually based on analyses of empirical data, can be used to define the median and 84th-percentile ground motions for the site. The attenuation relationships used in this study were selected on the basis of the appropriateness of the site conditions and tectonic environment for which they were developed. The relationships selected represent recent efforts in modeling strong ground motion in the eastern US on the basis of empirical data and physical/theoretical models of ground motion.

Response spectral ordinates were based either directly on attenuation relationships for spectral ordinates or on appropriate spectral shapes scaled to estimated peak ground accelerations. As most attenuation relationships have been developed for 5 percent damping, spectral ordinates for other damping rations can be obtained using published relationships for the effect of damping on spectral ordinates, such as those developed by Newmark and Hall (1978).

When the safety evaluation earthquake is specified as a random event occurring in the site vicinity, then a single source-to-site distance cannot be used to estimate site ground motions. In this case attenuation relationships were used to estimate median and 84th-percentile ground motions for an event occurring randomly within a specified distance from the site. The mean log ground motion level, $E[\ln(Y)]$, is given by

$$E[\ln(Y)] = \int_M \int_R f(M) \cdot f(R) \cdot E[\ln(Y) \mid m,r] \, dr \, dm \qquad (1)$$

where $f(M)$ is the probability density function for the event magnitude (typically assumed to be uniform over the specified magnitude range), $f(R)$ is the probability density function for the distance to a random event, and $E[\ln(Y \mid m,r)]$ is the mean log ground motion level given by the attenuation relationship for a specific magnitude, m, and distance, r. The 84th-percentile ground motion level is found by solving iteratively for the value, y, that satisfies the equation

$$\int_M \int_R f(M) \cdot f(R) \cdot P(Y > y \mid m,r) \, dr \, dm = 0.8416 \qquad (2)$$

where $P(Y>y \mid m,r)$ is given by the cumulative normal probability function assuming the ground motions are lognormally distributed about the mean log value specified by the attenuation relationship.

3.1.2 Statistical Analysis of Recorded Strong Motion Data

The general approach used for this method is described in Kimball (1983) and the U.S. Nuclear Regulatory Commission's Standard Review Plan (USNRC, 1990). The method consists of collecting a data set of recorded strong motion accelerograms for similar conditions to those that define the safety earthquakes. When insufficient records are available for the appropriate magnitude and distance range, then empirical attenuation relationships may be used to scale the response spectra to the target magnitude and distance. Appropriate scaling relationships may also be used to adjust the recorded motions for differences in tectonic environment. A statistical analysis is then performed of the scaled response spectra to define the median, and 84th-percentile (median-plus-one-sigma) ground motion levels at each spectral period. These estimates are then considered representative of motions that could be expected at the plant site during the safety earthquake.

When the safety evaluation earthquake is specified as a random event occurring in the site vicinity, then magnitude and distance scaling of the records is not performed. Instead, the available near source recordings, typically within 25 km of the recording station from earthquakes within a magnitude band about the target magnitude, typically plus-or-minus one-half magnitude unit, are analyzed statistically to obtain estimates of the median and 84th-percentile site specific spectra.

3.1.3 Numerical Ground Motion Estimation

In recent years a number of methods have been developed to predict strong ground motions on the basis of physical and theoretical models of earthquake source processes and wave propagation effects. These models have proved useful for assessments of ground motions in situations not represented in the empirical data, such as very close source-to-site distances, large

magnitude events, different tectonic environments. The technique selected for use in this study is the band-limited-white-noise/random-vibration-theory (BLWN/RVT) model. This relatively simple model was developed by Hanks (1979), Hanks and McGuire (1981), and Boore (1983) and has been shown to be very useful for estimating of earthquake ground motions for a variety of tectonic environments and ground motion measures (Hanks and McGuire, 1981; Atkinson, 1984; Boore, 1986, Boore and Atkinson, 1987; Toro and McGuire, 1987; Silva et al, 1990). Figure 31 presents a schematic diagram of the model. The model consists of the theoretical estimate of the fourier spectrum of ground motions generated at the source and uses simple body wave attenuation models for geometric spreading and anelastic absorption of energy to estimate the fourier spectrum of ground motions at the site. The effects of near surface crustal velocity structure and energy absorption are accounted for using the crustal amplification factors proposed by Boore (1986) and the Kappa model of Anderson and Hough (1984). Once the fourier spectrum of ground motion has been estimated, then random process theory is used to estimate the appropriate peak ground motion levels.

The BLWN/RVT model used in this analysis has been extended in two ways. First, nonlinear site-specific wave propagation characteristics have be included through the use of an equivalent-linear formulation for one-dimensional wave propagation in a layered medium (Silva, 1989). This allows for direct estimates of ground motions at the surface of deep soil profiles, such as that at the Savannah River K-Reactor site. Second, the crustal wave propagation modeling techniques of Ou and Herrmann (in press) have been included to account for both direct and critically reflected waves within the crust.

3.2 GROUND MOTION ASSESSMENTS FOR SAVANNAH RIVER K-REACTOR SITE

3.2.1 Site Conditions and Dynamic Soil Properties

The K-Reactor site at Savannah River is underlain by approximately 900 ft of coastal plain sediments, consisting of sandy soils with interbedded clays (see Figure 28). Figure 32 shows the average shear wave velocities at the K-Reactor site to a depth of 200 ft (GEI, 1991). The

shear wave velocity profile is similar to that observed at other locations on the Savannah River Plant Site, such as the AFR Spent Fuel site and the Defense Waste Processing site (D'Appolonia, 1980). Also shown in Figure 32 is the preliminary shear wave velocity profile used in the draft report (Geomatrix, 1991).

It was assumed that below a depth of 200 ft the shear wave velocities continue to increase at a smooth rate, reaching values of approximately 2500 fps (760 m/sec) at the baserock interface at a depth of 900 ft (274m), as shown by the solid line in Figure 33. The shear wave velocity gradient with depth was assumed to follow the lower bound generic deep soil site velocity profile developed by the Electric Power Research Institute to analyze ground motions at eastern US nuclear power plants (McGuire et al., 1988). Measured compression wave velocities, V_P, at Savannah River in the depth interval of 200 to 800 feet show a gradual increase from 6,000 fps to 7,000 fps (Chapman and DiStefano, 1989). These values are consistent with the compression wave velocities measured by D'Appolonia (1980) in the 200 to 300-ft depth range. Assuming that the V_P/V_S ratio observed at a depth of 300 ft applies at a depth of 800 ft, the measured compression wave velocities indicate shear wave velocities in the range of 2,300 fps at a depth of 800 ft, in agreement with the estimated velocities shown by the solid line in Figure 33.

One alternative approach for specifying the shear wave velocities at depth would be to assume that the shear modulus of the soils increases with increasing confining pressure according to an empirical relationship, such as that proposed by Hardin and Drnevich (1972). The Hardin and Drnevich (1972) empirical relationship for low strain shear modulus indicates that shear wave velocity is proportional to the fourth root of confining pressure. This would suggest that the measured shear wave velocity of 1,450 fps at a depth of 200 ft would increase to about 2,100 fps at a depth of 900 ft, provided there was not a decrease in soil void ratio accompanying the increased confining stress. The sensitivity of the computed response to the assumed extrapolation of the shear wave velocity profile with depth was examined, as discussed below.

The on the basis of the available data the K-Reactor site would be classified as a deep soil site with shear wave velocities in the lower range of those measured at other deep soil sites where strong motion data have been obtained (mainly in the western US).

Measured compression wave velocities in the crystalline base rock outside of the Triassic basin range from 18,000 to 20,000 fps (Chapman and DiStefano, 1989). Within the basin, the measured compression wave velocities range from 13,000 to 16,000 fps. Assuming a Poisson solid, the average baserock shear wave velocity is approximately 11,000 fps (3.5 k/sec) north of the basin and 8,000 fps (2.5 k/sec) within the basin. The thickness of Triassic sedimentary rocks within the basin is approximately 3 km (D. Stephenson, personal communication).

The strain-compatible soil modulus reduction and damping relationships used in site response analyses are shown in Figure 34. These relationships were developed by GEI (1991) from laboratory tests of soil samples collected from the site. The shear modulus reduction and damping relationships shown in Figure 34 are similar to those developed for other locations at the Savannah River site (GEI, 1983, 1989). The relationships show in increase in stiffness and a decrease in damping as the confining pressure increases. These results are consistent with the findings of other investigations (e.g., Harden and Drnevich, 1972; Iwasaki et al., 1976, GEI, 1983).

The selection of the appropriate modulus reduction and, more importantly, damping relationships for use in site response analyses of the deep soil profile has a major impact on the estimated site ground motions. Figure 35 shows the effect of the use of various modulus reduction and damping curves on the computed surface motions for western US earthquakes. Site response calculations were conducted using soil shear wave velocities similar to those shown in Figure 33, but with a western US base rock velocity (4,000 fps). A western rock motion with a free field peak acceleration of 0.2g was used as an input motion. Two sets of modulus reduction and damping curves were used; a preliminary set of relationships developed from the published literature to analyze the K-Reactor profile (Geomatrix, 1991) that are

generally similar to those shown in Figure 34, and the mid-range shear modulus reduction and damping curves developed by Seed and Idriss (1970). These two sets of modulus reduction and damping curves are compared in Figure 36. The Seed and Idriss (1970) curves exhibit greater reduction in shear modulus and larger damping at a given level of shear strain than specified by the either the preliminary relationships shown in Figure 36 or the site-specific relationships developed by GEI (1991) shown in Figure 34.

As can be seen, there is a significant reduction in the computed high frequency motion when greater modulus reduction and higher damping curves are used. Also shown in Figure 35 are the median response spectra estimated using two western US empirical attenuation relationships for deep soil sites. The spectra were estimated for conditions that would produce 0.2g free field rock motions. These comparisons indicate that the use of modulus reduction and damping curves similar to those originally developed by Seed and Idriss (1970) over the entire 900-ft depth range would tend to under predict the high frequency ground motions observed on western US deep soil sites.

3.2.2 Ground Motions Assessments for the Charleston Source

As defined in Section 2.2.1, the safety evaluation earthquake for the Charleston source is considered to be a M 7.5 (m_{bLg} 7.1) event located at a distance of 120 km from the site with a focal depth of approximately 15 km. Two approaches were used to characterize the potential ground motions from this event, the use of published attenuation relationships and modeling of the event using the BLWN/RVT approach. Because many of the recently developed attenuation relationships for eastern US earthquake ground motions have been developed for rock site conditions, site response analyses were used to translate estimates of ground motion on rock to ground motion at the surface of the deep soil profile at the K-Reactor site. Statistical analysis of recorded strong motion data was not used as there are only a few recordings in this magnitude and distance range and they come from very different tectonic environments.

Empirical/Theoretical Attenuation Relationships. As there are only a limited number of strong ground motion recordings that have been obtained in the eastern US, most attenuation relationships that have been developed for the area rely to a large extent on theoretical scaling laws and/or numerical models to constrain parameters in the attenuation relationships. Figure 37 shows the variation of peak acceleration with distance for a magnitude M 7.5 earthquake predicted by the attenuation relationships examined in this study. Most of these relationships have be used in the analyses of probabilistic seismic hazard at commercial nuclear power plants in the eastern US conducted by the Lawrence Livermore National Laboratory (LLNL) (Bernreuter et al, 1988), and the Seismicity Owners Group (EPRI, 1987). The relationships of Atkinson and Boore (1990), McGuire et al. (1988), and Veneziano (1988) were developed specifically for rock site conditions. Figure 38 compares the median rock site response spectra obtained from these three relationships for a source to site distance of 120 km. The estimates given by the relationships of Atkinson and Boore (1990) and McGuire et al. (1988) are similar. These two relationships use constant stress drop scaling of the earthquake source spectra to constrain the extrapolation of ground motion estimates to large magnitudes. The relationship developed by Veneziano (1988) is based on regression analysis of recorded ground motion and shaking intensity data and the extrapolations to large magnitude are based on the trends observed in the data for smaller magnitude events.

The other three attenuation relationships shown in Figure 37 have been developed by Dr. Nuttli and his co-workers. The two relationships developed by Nuttli (1986a) are based on different models of the scaling of the source spectrum with increasing magnitude. Both of these models assume that the stress drop increases with increasing magnitude, while the relationships developed by Atkinson and Boore (1990) and McGuire et al. (1988) assume that stress drop remains constant with increasing magnitude. The differences between these assumptions will be discussed subsequently in the section describing application of the BLWN/RVT model. The relationship proposed by Nuttli et al. (1984) was developed specifically for the Charleston region. All three of these relationships do not differentiate between soil and rock motions and are assumed to be applicable to deep soil sites.

Site Response Studies. In order to use the rock site attenuation relationships that have been developed for the eastern US to estimate ground motions at the Savannah River K-Reactor site a limited set of site response analyses were conducted using the BLWN/RVT model coupled with an equivalent-linear model for soil response (Silva, 1989). Ground motion estimates were made at the site surface using the shear wave velocity profiles shown in Figure 33 and the strain compatible soil properties shown in Figure 34. The site response analyses were conducted for a range of input rock motion levels. The eastern US rock motions were computed using the BLWN/RVT model with a stress drop of 150 bars for the Charleston event (the basis for this value will be discussed below) and 100 bars for all other events (Boore and Atkinson, 1987), $Q = 190f^{0.94}$ for the Charleston region (Rhea, 1984), and a rock site Kappa of 0.006 seconds (Silva, 1989). A similar set of analyses were conducted for western US conditions to provide a basis for judging the reasonableness of the results. For this analysis, the baserock shear wave velocity was set to 4,000 fps, typical of western US rock, and rock motions were estimated using the BLWN/RVT model with a stress drop of 50 bars (Boore, 1986), $Q = 150f^{0.6}$ (Nuttli, 1986b), and a rock site Kappa of 0.035 sec (Silva, 1989).

Figures 39 and 40 show the procedure used to obtain the soil/rock response spectral ratios for eastern and western US motions, respectively. Shown are the smooth input rock motion spectrum, the computed soil surface motion spectrum, and a smoothed soil spectrum. The smoothed soil spectrum was divided by the input rock motion spectrum to obtain the response spectral ratios, as shown in the lower plot in the two figures.

Figure 41 compares the smoothed response spectral ratios for eastern US and western US conditions for input rock motions of 0.1, 0.2, and 0.3 g. The comparison indicates that there is a greater deamplification at high frequencies and a greater amplification at low frequencies for the eastern US conditions. The larger deamplification at high frequencies for eastern US conditions is primarily do to the greater high frequency content of eastern US rock motions. Figure 42 compares recorded rock motions for M ~ 6 events in eastern and western North America. The response spectra for eastern US records peaks at a much higher frequency than

the western US spectra. This difference in the relative frequency content of eastern and western US records is maintained in the input rock motions as shown in Figures 39 and 40. These high frequency motions tend to be damped out by the soil response, leading to a greater deamplification in this frequency range.

The greater amplification computed at low frequencies for eastern US conditions is largely due to the much larger velocity contrast at the soil profile-baserock interface in the eastern US as compared to the western US. Figure 43 shows the ratio of soil site motions computed using eastern US and western US baserock velocities for eastern US input rock motions. As can be seen, the large velocity contrast for eastern US baserock produces approximately 40 percent higher levels of ground motion. The effect is slightly lower at the K-Reactor site due to the somewhat lower shear wave velocity for the Triassic basin rocks.

Figure 44 shows the effect of earthquake magnitude on the soil/rock response spectral ratios. The larger magnitude event tends to produce lower soil amplification because the larger long period content of the M 7.5 motions produces greater strain in the soil profile for a given level of input acceleration, and thus higher damping.

Figure 45 compares the spectral ratios computed using the properties shown in Figures 33 and 34 with those based on the preliminary site properties (Geomatrix, 1991). The site-specific properties developed by GEI (1991) result in lower amplification of the rock motions, principally do to differences in the shear modulus reduction and damping curves. The relationships developed for the site soils (Fig. 34) show somewhat greater damping at moderate strain levels than the preliminary relationships developed from published literature (Fig. 36).

Figure 46 shows the effect of the alternative extrapolation of shear wave velocity with depth (Fig. 33) on the computed spectral ratios. The lower shear wave velocity profile results in slightly lower soil amplifications. Considering that the stiffer profile is consistent with the

measured compression wave velocities at depth, it is recommended that the stiffer profile shown in Figure 33 be used until shear wave velocities at depth can be measures.

The site response studies indicate that western and eastern US deep soil site ground motions should have different spectral shapes, reflecting the differences in rock motions (e.g. Fig. 42). The limited strong motion data for deep soil sites show similar trends. Figure 47 compares the response spectral shapes for four earthquakes recorded on deep soil sites in the New Madrid seismic zone with the corresponding spectral shapes for western US ground motions predicted using the attenuation relationships developed by Sadigh et al (1986) and spectral shapes for eastern US ground motions predicted using the BLWN/RVT model and the soil/rock spectral ratios shown in Figure 41. The data show a shift of the peak of the response spectra to higher frequencies than would be predicted using western US attenuation relationships. The BLWN/RVT predicted spectral shapes using the Savannah River profile are shown for comparison, although it is not known at the present time how similar the site conditions are to those at the New Madrid recording stations.

Although the site response analyses and the comparisons shown in Figure 39 through 44 indicate significant differences between eastern US and western US deep soil motions, comparison of the soil spectra in these figures with the rock motion comparison shown in Figure 42 suggests that eastern and western US deep soil motions may be more similar in terms of frequency content than rock site motions.

Ground Motion Estimates for Deep Soil Based on Empirical/Theoretical Attenuation Relationships. Figure 48 presents the estimated median 5-percent damped response spectra at the Savannah River K-Reactor site from a M 7.5 Charleston source event at 120 km. The response spectra labeled as scaled were obtained by multiplying the rock site spectrum in Figure 38 by the appropriate soil/rock spectral ratios computed for M 7.5 events. The spectra for Nuttli (1986a) and Nuttli et al (1984) were obtained by multiplying the predicted median peak acceleration, velocity and displacement values given by these relationships by the spectral

amplification factors developed by Newmark and Hall (1978). This approach was used in the EPRI and LLNL seismic hazard studies to generate response spectra for the Nuttli (1986a) relationships. The predicted spectral ordinates are in reasonable agreement, with the exception of the predictions based on Nuttli (1986a) with a slope of 4.0 and by Veneziano (1988). The Nuttli (1986a) slope 4.0 relationship assumes the maximum increase in stress drop with increasing magnitude and, as will be discussed below, appears to over estimate the rate of ground motion scaling with magnitude. As was the case for rock data, the Veneziano (1988) relationship is based on extrapolation of empirical data from smaller magnitudes, and is less well constrained at the larger magnitudes. The corresponding peak ground accelerations are:

Atkinson and Boore (1990) scaled to deep soil	0.05g
McGuire et al. (1988) scaled to deep soil	0.05g
Veneziano (1988)	0.03g
Nuttli (1986a), slope 4.0	0.21g
Nuttli (1986a), slope 3.5	0.11g
Nuttli et al. (1984)	0.09g

Ground Motion Estimates Based on BLWN/RVT Model. The BLWN/RVT model used to conduct the site response studies was also used to directly estimate ground motions at the Savannah River K-Reactor site for the Charleston event. An important aspect of the model is the specification of the appropriate source scaling relationships. Much work has been done in recent years to address the issue of whether or not the earthquake stress drop remains constant with increasing magnitude or increases. These studies have tended to indicate that stress drop remains relatively constant with increasing earthquake size for the larger magnitude earthquakes. Figure 49 shows the results of one such study. Shown is the relationship between source duration (taken to be the inverse of corner frequency) and seismic moment. The data for larger eastern North American earthquakes indicate that source duration scales with the 1/3 power of seismic moment, indicating constant stress drop scaling. The relationship developed by Nuttli that assumes scaling of source duration with the 1/4 power of moment clearly does not fit the data shown in Figure 49. Thus, if constant stress drop scaling is correct, then the Nuttli (1986a) slope 4.0 relationship would be expected to overestimate the ground motions for

large magnitude events, as they are anchored to empirical data in the magnitude range of m_{bLg} 5.0.

The second important parameter is the stress parameter used in the model (or equivalently the relationship required to estimate corner frequency). Figure 50, taken from Somerville et al (1987), shows the data from Figure 49 plotted with earthquakes from other tectonic environments on lines of constant stress drop. Somerville et al (1987) conclude that the median stress drop for eastern North American earthquakes is similar to that for other regions and is approximately 100 bars.

As discussed in Section 2.2.1, the average rupture properties of stable continental region earthquakes (rupture length, rupture area, static stress drop) appear to be similar to those observed for earthquakes in tectonically active areas. The similarity in rupture dimensions is consistent with the similarity in corner frequency and implied stress drop found by Somerville et al. (1987), indicating that 100 bars is a reasonable value for the average stress drop for eastern US earthquakes, although the data in Figure 50 indicate that computed stress drops for individual events can easily vary by a factor of three or more.. In addition, Boore and Atkinson (1987) found that the BLWN/RVT model provided a good overall fit to the empirical eastern US data using a RMS stress drop of 100 bars.

At the present time there exists considerable uncertainty in the appropriate stress drop to use in estimating the amplitude of high frequency ground motion in the eastern US. The data reviewed as part of this study together with the preferred rupture dimensions for the maximum Charleston source earthquake argue in favor of an average stress drop of 100 bars. However, there is only limited data for large magnitude events and higher average values could be possible. Accordingly, a stress parameter of 150 bars was adopted to account for the uncertainty in the appropriate average value for M 7.5 events. The sensitivity of the computed ground motions to the selected stress parameter was evaluated by making additional ground motion estimates using a stress drop of 300 bars.

As discussed in Section 3.1, the BLWN/RVT model was also extended to incorporate direct and critically reflected waves using the formulation of Ou and Herrmann (in press). The critically reflected waves have been suggested as the cause of the lack of significant attenuation in the distance range of 80 to 120 km observed in recent strong motion data in eastern and western North America (Burger et al, 1987; Somerville et al, 1990). One notable example is the data for the 1988 Sagueney earthquake in eastern Canada. Somerville et al. (1990) estimate the seismic moment and source duration for this event to be $0.7 \cdot 10^{25}$ dyne-cm and 1.5 sec, respectively. Examination of Figure 50 suggests that these parameters correspond to a stress drop of approximately 300 bars. Figure 51 compares the rate of attenuation on rock for this event predicted using the BLWN/RVT model with direct waves in a half-space (1/R scaling for $R < 100$ km) with the attenuation predicted using the Ou and Herrmann (in press) extension and with the observed strong motion data. The crustal response model predicts a somewhat greater rate of attenuation within the first 70 km. As can be seen, there is reasonable agreement between the predictions using both methods and the observations. It should be noted that the ground motions for this event would be significantly under predicted if a nominal stress drop of 100 bars was used in the model. However, Atkinson (1990) found that even with the inclusion of the Sagueney earthquake in the eastern North America strong motion data set, the BLWN/RVT model still provides a good overall fit to all of the data using a stress drop of 100 bars.

Figure 52 shows the variation with distance of rock site motions computed using the BLWN/RVT model. The individual curves show the effect of the assumed point source depth on crustal reflections in the distance range of 60 to 120 km. The crustal model used is based upon surface wave analysis for the path from Bowman, South Carolina to Atlanta, Georgia (Herrmann, 1986).

Figure 53 compares the mean and upper limit of the rock site motions for a M 7.5 Charleston event predicted using the BLWN/RVT model with the published relationships shown in Figure 37. The BLWN/RVT model predictions at distances beyond 100 km are comparable to those

of Atkinson and Boore (1990), and McGuire et al. (1988), which are also based primarily on the same model.

Figure 54 shows the variation with distance of site motions computed using the BLWN/RVT model and the K-Reactor site profile. Curves are again shown for point source depths in the range of 10 to 20 km. As was the case for estimates of rock motions, there is a significant effect of critical reflections on the results. Figure 55 compares the mean and upper limit of the soil site motions predicted by the BLWN/RVT model for the K-Reactor site with other attenuation relationships. The predicted motions are somewhat lower than those obtained from the published relationships. Nuttli's (1986a) slope 4.0 relationship predicts much larger ground motions due to assumed rate of increase in stress drop with increasing magnitude.

Also shown in Figure 55 is the variation of peak ground acceleration with distance for the 1886 Charleston earthquake estimated by Martin et al. (1990) on the basis of analysis of liquefaction effects. These results are somewhat lower than those predicted using the methods of this study. This difference may reflect the effect of differences in frequency content between eastern US earthquakes and those that are represented in the empirical correlations between peak ground acceleration and the occurrence of liquefaction used by Martin et al. (1990).

A local peak in the attenuation pattern for both the rock and deep soil ground motion estimates occurs at a distance of 110 km, with a rapid fall off in amplitude on either side. As indicated in Figures 52 and 54, the exact location of such peaks could be easily moved by several km by making small changes in the precise focal depth used for the point source. It is perhaps reasonable to average the ground motions computed over a small distance range to obtain an estimate of the expected level of ground motion. For the results presented in Figures 53 and 55, there is about a 10 percent variation in the ground motion levels in the distance range of 100 to 120 km between the average value and local peaks. In the subsequent comparisons, the computed response at the top of the local peak (at 110 km) was conservatively assumed to apply to a distance of 120 km.

The effect of stress drop on the predicted soil site spectra is illustrated in Figure 56. The predicted peak accelerations are 0.11g and 0.16g for stress drops of 150 and 300 bars, respectively. The rate of increase in peak acceleration on the soil site is less than that for a rock site, indicating the beginning of significant nonlinear soil response at the higher ground motion levels.

Figure 57 compares the horizontal response spectra estimated with the BLWN/RVT model with the median response spectra for the Charleston event shown in Figure 48. Nuttli's (1986a) slope 4.0 relationship gives predictions that envelop the other estimates. As discussed above the slope 4.0 relationship appears to be incompatible with the empirical data shown in Figure 50. The estimates made using this model, as well as those obtained using a stress drop of 300 bars are large in relation to the level of shaking intensity experienced in the site area during the 1886 earthquake, estimated to be intensity VI.

At the present time, no vertical strong ground motion attenuation models have been developed for the eastern US. However, based on western US data, the vertical spectra would be expected to be about one-half or less of the horizontal spectra at this distance from the source.

Effect of Dipping Layer Interface. The interface between the coastal plain sediments and the underlying bed rock is a gently dipping boundary thickening to the southeast (Talwani, 1977). The formulation employed in Ou and Herrmann's extension of the BLWN/RVT model assumes laterally homogeneous crust. A ray tracing analysis was conducted to see if the dipping coastal plane-base rock boundary would result in enhancements of the site ground motions. Figure 58 shows the crustal model used to examine the amplitude at three distances from Charleston of simple wavelets corresponding to different canonical source focal mechanisms (Aki and Richards, 1980). The crustal model used consists of applying the coastal plane structure of Talwani (1977) to the surface layer of Herrmann's (1986) Bowman to Atlanta crustal structure. The bottom plot shows the ratios of the amplitude of various wavelet types for the dipping interface to those for a flat interface. The results indicate that no significant amplification

should be expected at the Savannah River site resulting from the dipping interface. This analysis did not take into account the details of the crustal structure at the Triassic basin boundary, which lies very close to the site. This is considered to be potentially important for local shallow events and will be examined below.

Variance in Ground Motion Estimates. The spectra presented in Figure 57 represent median or average levels of ground motion. A standard error of 0.5 on the natural log of ground motion is judged to be appropriate for estimating the 84th percentile ground motions for the Charleston source event. Recent studies have confirmed that the variance in peak ground motion parameters decreases with increasing magnitude. Estimates of the variance of peak ground motion parameters for eastern US earthquakes have typically been in the ranged of 0.5 to 0.7 (natural log of peak motion parameters). Campbell (1986) estimates a standard error of 0.5 for use in evaluating near-source ground motions for a Charleston sized earthquake and EPRI (1987) used a standard error of 0.5 in their probabilistic assessment of seismic hazard at eastern US nuclear power plants. Given, that the Charleston event is estimated to be a M 7.5 earthquake, a standard error of 0.5 is considered a reasonable value.

3.2.3 Ground Motion Estimates for the Bowman Event

The Bowman event is a M 6.0 (m_{bLg} 6.0) event located 80 km from the site (Section 2.2.2). Figure 59 shows the predicted deep soil response spectra for the Savannah River K-Reactor site for the Bowman event using the attenuation relationships selected to evaluate the Charleston event and using the BLWN/RVT model with a stress drop of 100 bars. The resulting ground motions are significantly lower than those obtained for the Charleston event (Fig. 58).

3.2.4 Ground Motion Estimates for the Local Event

The local event is defined as a magnitude M 5.0$\pm$0.5 event occurring in the site vicinity (within 25 km) (see Section 2.2.3). Ground motions for this event were estimated using the standard site-specific-spectra technique employed for evaluation of commercial nuclear power plants (Kimball, 1983). This involves statistical analysis of response spectra for ground

motions recorded on similar site conditions. The BLWN/RVT model was also employed to examine possible differences between eastern and western US ground motions for a nearby M 5.0 event.

Statistical Analysis of Recorded Strong Motion Data. Table 1 lists available deep soil site recordings for M 4.5 to 5.5 earthquakes recorded within 25 km of the source. All of the recordings were obtained in instrument shelters or small buildings (one to two stories). The depth of the soil column at the recording stations varies from several tens of meters to several kilometers. However, Campbell (1989) found that there is no statistically significant correlation between depth to basement rock and response spectral ordinates recorded on soil sites for ground motions at periods less than 1.5 seconds. Thus the selected data set is considered appropriate for estimating high and intermediate frequency ground motions on soil sites in the western US.

Figure 60 shows the distribution of the data in terms of magnitude and distance. The top plot presents a scattergram of the magnitude and distances of the data set. The bottom plot shows a histogram of the fraction of the data set occurring in 5 km distance intervals. This histogram is compared to the frequencies that would be expected for records uniformly distributed in the area defined by a 25 km radius circle about the site. As can be seen, there is an over representation of the data in the 10 to 15 km distance interval and under representation in several of the other intervals.

To address the differences between the desired and actual distance distribution of the data two statistical analyses were performed. First, statistics of the spectral accelerations of the raw data were performed. Then a weighted statistical analysis was conducted, with weights assigned on the basis of the ratio of desired to the observed fraction of the data set within each distance interval. Examination of the data listed in Table 1 indicates that nearly half comes from the recordings of a single aftershock of the 1979 Imperial Valley earthquake. Accordingly, a second weighted analysis was performed, with the records from this aftershock give reduced

weighted such that their influence on the statistics was similar to recordings from other earthquakes. The results of the three analyses are as follows:

Analysis	Mean Magnitude	Mean Distance (km)	Peak Horizontal Acceleration (g)		Peak Vertical Acceleration (g)	
			Median	84th	Median	84th
Unweighted	5.1	11.6	0.134	0.281	0.071	0.127
Weighted	5.2	15.3	0.109	0.208	0.068	0.110
Adjusted	5.2	15.8	0.098	0.213	0.089	0.146

As can be seen, the distance weighted analysis produces a mean distance close to the desired mean distance to a point in a 25-km radius circle of 16.7 km.

Figures 61 and 62 present the resulting median and 84th-percentile response spectra for horizontal and vertical motions, respectively. As indicated in the figures, the unweighted and weighted analysis produce similar results. In contrast, the down weighting of the recordings from the Imperial Valley aftershock results in an increase in the estimates of the median and 84th-percentile response spectra, especially for the vertical component. However, this result should be viewed with some caution, because the data set has been reduced to essentially 14 recordings.

Also shown in Figures 61 and 61 are the deep soil site specific spectra developed by Bernreuter et al. (1988b) for events in the magnitude range of M_L 4.6 to 5.8 with a target mean magnitude of M_L 5.3 The resulting median and 84th-percentile spectra are very similar to those developed in this study. Although the target mean magnitude of the data set collected for this study is M 5.0, the resulting mean magnitude is 5.2, similar to the target of the Bernreuter et al. (1988b) study.

Estimates Obtained Using Attenuation Relationships - As discussed in Section 3.1.1, attenuation relationships can be used to estimate the median and 84th-percentile ground motions for a random event. Figure 63 compares the median and 84th-percentile ground motions estimated using Equations (1) and (2) and two recently developed attenuation relationships for deep soil site ground motions in the western US with the statistical spectra shown in Figure 45. As can be seen, the response spectra based on statistics of recorded motions are significantly higher that those based on general attenuation relationships.

A likely reason for the differences between the empirical attenuation and statistical spectra shown in Figure 63 is illustrated in Figure 64. The open circles in the figure show the recorded peak accelerations on deep soil sites from earthquakes and recording distances within the specified intervals. The solid circles show those recordings that have been processed to the point of computing response spectra and represent the data set used to compute the statistical spectra (Table 1). The processing agencies (USGS, CDMG) typically tend to process accelerograms from the larger recordings, rather than from all of the accelerograms. The computed median and 84th-percentile peak accelerations of the larger data set are 60% and 70%, respectively of the median and 84th-percentile peak accelerations of the accelerogram data set.

It should be noted that part of the difference between the statistical and attenuation-based spectra arises from differences in the mean magnitudes (M 5.2 for the statistical spectra and M 5.0 specified for the attenuation-based spectra). The 0.2 magnitude units difference in mean magnitude would result in an expected difference of about 15 percent on the basis of the empirical attenuation relationships.

Figure 65 shows "corrected" median and 84th-percentile random earthquake spectra that are 60% and 70%, respectively, of the original spectra under the assumption that the bias in peak acceleration applies throughout the spectrum (at least for frequencies of interest to the evaluation of the K-Reactor site). The "corrected" spectra are likely to be a better

representation of what would be computed if the full data set of accelerograms shown in Figure 64 were available for statistical analysis. These spectra compatible with those developed from empirical attenuation relationships, further suggesting that the "correction" is appropriate. Accordingly, the "corrected" spectra shown in Figure 65 are assumed to be the appropriate representation of ground motions resulting from a M 5.0 random event.

Application of the BLWN/RVT Model. The data set used in the above analysis consists entirely of western US recordings, as there are no eastern US deep soil recordings that fall within the selection criteria. The BLWN/RVT model was used to examine the possible differences between eastern and western ground motions for the local event. These differences were examined by comparing the response spectra predicted by the model for a M 5.0 earthquake occurring 15 km from a deep soil site. In making these comparisons it was noted that the BLWN/RVT model under predicts western US response spectral ordinates for rock sites when using the standard parameters of a Kappa of 0.35 and a stress drop of 50 bars. Boore (1986) found that a stress drop of 50 bars provided a good match between predicted and observed teleseismic P-wave amplitudes. However, he found that the Kappa model results in an under prediction of high frequency ground motion when a stress drop of 50 bars is used. The effect is illustrated in the left hand plot of Figure 66 where response spectra predicted using the BLWN/RVT model with a Kappa of 0.035 and a stress drop of 50 bars are compared to spectra developed from spectral ordinate attenuation relationships developed from recorded rock site data.

A simple way to increase the predictions of the model is to increase the stress drop. As several studies have indicated that the stress drops are similar in the eastern and western US (e.g. Somerville et al., 1987, see Fig. 50) a stress drop of 100 bars was tried. It was found that use of the higher stress drop required increasing the Kappa to 0.04 seconds in order to obtain the proper spectral shape. The resulting predictions of response spectral ordinates are in good agreement with the empirical spectra, as indicated in the right hand plot in Figure 66. These

comparisons indicate that more investigation into the trade of between selection of the various model parameters is needed.

Assuming that the source characteristics of eastern and western US earthquakes are generally similar, as indicated by similar stress drops and source scaling relationships, then the observed differences in recorded rock motions are likely due to travel path effects. To assess these differences predictions of response spectral ordinates were made for eastern Us and western US crustal conditions assuming equal stress drop in both regions. The BLWN/RVT model properties used are as follows:

Parameter	Western US	Eastern US
Stress drop	50 and 100 bars	50 and 100 bars
Shear wave velocity	3.2 k/sec	3.5 k/sec
Density	2.7	2.5
Kappa	0.035 and 0.04 sec	0.006 sec
Q	$150f^{0.6}$	$500f^{0.65}$
Moment Magnitude	1.5 M + 16.1 5.0	1.5 M + 16.1 5.0

Figure 67 compares the estimates of rock site motions from a M 5.0 event at a distance of 15 km for eastern and western US conditions. These motions were transformed into deep soil site motions using the spectral ratios developed for M 5.0 events. The computed spectral ratios between the eastern and western US deep soil spectra is shown in Figure 68. As can be seen, similar ratios were obtained for stress drops of 50 and 100 bars. The corresponding eastern soil site motions are significantly higher than the western deep soil site motions at frequencies greater than 5 Hz, suggesting that the western US statistical response spectra shown in Figures 61 and 62 may under estimate the high frequency ground motions that may occur from a random local event in the eastern US. Also shown are the east/west spectral ratios computed using the preliminary site profile properties. As was the case for direct estimates of site response, the site-specific soil properties give a lower estimate of high frequency amplification.

Using the east/west spectral ratios shown in Figure 68, the "corrected" western US statistical spectra were adjusted for relative frequency content to represent estimated site specific spectra for a random M 5.0 event occurring in the eastern US. The resulting scaled spectra are shown in Figures 69 and 70 for horizontal and vertical motions, respectively. It was assumed that the "correction" and the east/west spectral ratios developed for the horizontal motions also apply to vertical motions. Comparison of the spectra in Figures 69 and 70 indicate that the vertical spectra equal or exceed the horizontal spectra at periods less than about 0.1 seconds. At longer periods, the vertical spectra quickly fall to levels below one-half of the horizontal spectra.

Effect of Triassic Basin Boarder Fault. K-Reactor is located within 1000 ft of the Triassic basin boundary, which consists of a interface dipping between 75° and 85° toward the site. A ray-tracing analysis was conducted to examine the effect of the dipping interface on ground motions originating from local shallow random event. Figure 71 shows a simplified crustal model of the basin and the ray path analyzed. The results of the analysis indicate that the interface tends to reflect energy, resulting in a decrease in the computed motions at the K-Reactor site. Thus the presence of the dipping basin/basement interface is not expected to adversely affect site ground motions.

4.0 SUMMARY

This report presents the results of an assessment of the SRS design basis spectrum. These assessments were developed under the procedures defined in Appendix A to 10 CFR Part 100. The evaluation was performed using approaches that have been employed in recent seismic safety evaluations of commercial nuclear power plants. The assessments where made using currently available information.

The first part of the study consisted of identifying potential sources of future earthquakes and characterizing these sources in terms of the location of potential earthquakes relative to the site and the maximum magnitude earthquakes that could be expected to occur. Three safety evaluation earthquakes were defined: a M 7.5 earthquake occurring at Charleston, 120 km from the site; a M 6 earthquake occurring on the Bowman source, 80 km from the site; and a local event of magnitude M 5.0 occurring near the site (within 25 km).

Ground motion assessments were made using three approaches, published attenuation relationships, statistical analysis of recorded strong motion data, and direct estimation of ground motion values using physical models of the source processes and wave propagation effects. The results of these analyses are summarized in Figures 72 and 73 showing the estimated median horizontal response spectra for the Charleston and local sources, respectively. Ground motions from the Bowman source were well below the ground motion estimates from the other two sources.

The comparisons shown in Figure 72 indicate that the design basis spectrum envelops all of the median estimates of ground motion for the maximum Charleston source event except those based on the Nuttli (1986a) relationship that assumes that the stress drop increases with increasing moment. As discussed in Section 3.2.2, the available data favor the interpretation that stress drop is constant for moderate to large earthquakes. It is our conclusion that the constant stress drop model is appropriate for estimating ground motions for large eastern US

earthquakes. It should also be noted that the design basis spectrum envelops the spectra predicted using alternative models developed by Nuttli (1986a) and Nuttli et al. (1984).

The comparisons in Figure 72 also indicate that the BLWN/RVT spectrum predicted using a stress drop of 300 bars slightly exceeds of the design basis spectrum in the period range of 1.0 to 2.0 seconds. However, as discussed in Section 3.2.2, it is our opinion that a reasonable conservative estimate of the expected stress drop for a large eastern US earthquake is 150 bars. Thus we do not consider ground motion predictions made using 300 bars as representative of median ground motions.

The comparisons shown in Figure 73 indicate that the design basis spectrum is well above the estimated median ground motion levels for a local M 5.0 event.

The major sources of uncertainty identified over the course of this study are: specification of the appropriate stress drop for the Charleston source earthquake, specification of the appropriate levels of soil damping at large depths for site response analyses, and evaluation of the appropriateness of western US recordings for specification of ground motions in the eastern US. The sensitivity of the estimated ground motions to various alternative interpretations are discussed in Section 3. The various estimates of median ground motion levels using reasonable ranges of the various input parameters do not result in significant exceedances of the design basis spectrum.

The evaluations conducted in this study are specific to the K-Reactor site which is located within the Triassic basin. Comparisons with evaluations for other Savannah River Site locations outside of the Triassic basin, such as the proposed NPR site, indicate that ground motion estimates can vary significantly from location to location, and therefore, should be assessed on a site specific basis.

REFERENCES

Aki, K., and P.G. Richards, 1980, Quantitative Seismology, Volume I, W.H. Freeman and Co., San Francisco, 512 p.

Ambraseys, N.N., 1988, Engineering Seismology: Earthquake Engineering and Structural Dynamics, v. 17, p. 1-105.

Amick, D., Gelinas, R., Marauth, G., and Cannon, r., 1989, Paleoliquefaction investigations along the Atlantic seaboard - implications for long-term seismic hazard: in Transactions of the Seventeenth Water Reactor Safety Information Meeting, U.S. Nuclear Regulatory Commission NUREG/CP-1040, 26 p.

Amick, D., Gelinas, R., Maurath,G., Moore, D., Billington, E., and Kemppinen, H., 1990, Paleoliquefaction features along the Atlantic seaboard: U.S. Nuclear Regulatory Commission NUREG/CR-5613, 146p.

Amick, D., and Gelinas, R., in press, The search for evidence of large prehistoric earthquakes along the Atlantic seaboard: Science, in press

Anderson, J.G., and S. E. Hough, 1984, A model for the shape of the fourier amplitude spectrum ao acceleration at high frequencies: Bulletin of the Seismological Society of America, v. 74, p. 1969-1993.

Atkinson, G.M., 1984, Attenuation of strong ground motion in Canada from a random vibrations approach: Bulletin of the Seismological Society of America, vol. 74, no. 6, pp. 2629-2653.

Atkinson, G.M., 1990, A comparison of eastern North American ground motion observations with theoretical predictions: Seismological Research Letters, v. 61, p 171-180.

Atkinson, G.M. and D.M. Boore, 1990, Recent trends in ground motion and spectral response relations for North America, Earthquake Spectra, v. 6, p. 15-36.

Bayer, K.C., Keuckroth, L.E., and Karim, R.A., 1969, An investigation of the Dasht-e Bayaz, Iran, earthquake of August 31, 1968: Bulletin of the Seismological Society of America, v. 59, no. 5, p. 1793-1822.

Bernreuter, D.L., Savy, J.B., Mensing, R.W. and Chen, J.C., 1988, Seismic hazard characterization of 69 nuclear plant sites east of the Rocky Mountains: NUREG/CR-5250, UCID-21517, 8 volumes.

Bernreuter, D.L., J.C. Chen, and J.B. Savy, 1988b, Development of site specific response spectra: U.S. Nuclear Regulatory Commission NUREG/CR-4861.

Bollinger, G.A., Davison, F.C., Jr., and Sibol, M.S., 1989,Magnitude recurrence relations for the southeastern United States and its subdivisions: Journal Geophysical Research, v. 94, p. 2857-2873.

Bollinger, G.A., 1977, Reinterpretation of the intensity data for the 1886 Charleston, South Carolina, earthquake: in Rankin, D.W., ed., Studies Related to the Charleston, South Carolina, earthquake of 1886--A Preliminary Report, U.S.G.S. Prof. Paper 1028, p. 17-32.

Bollinger, G.A., Chapman, M.C., Sibol, M.S., and Costain, J.K., 1985, An analysis of earthquake focal depths in the southeastern U.S.: Geophysical Research Letters, v.12, p. 785-788.

Bollinger, G.A., Sibol, M.S., and Chapman, M.C., in review, Maximum magnitude estimation for an intraplate setting example: the Giles County, Virginia, seismic zone: Bull. Seis. Soc. Am.

Bollinger, G.A., Johnston, A.C., Talwani, P., Long, L.T., Shedlock, K.M., Sibol, M.S., and Chapman, M.C., in press, Seismicity of the southeastern United States: Geol. Soc. Am. DNAG Contribution.

Boore, D.M., 1983, Stochastic simulation of high-frequency ground motions based on seismological models of the radiated spectra: Bulletin of the Seismological Society of America, v. 73, p. 1865-1894.

Boore, D.M., 1986, Short period P- and S-wave radiation from large earthquakes: Implications for spectral scaling relations: Bulletin of the Seismological Society of America, v. 76, p. 43-64.

Boore, D.M, and G.M. Atkinson, 1987, Stochastic prediction of ground motion and spectral response parameters at hard-rock sites in eastern North America: Bulletin of the Seismological Society of America, vol. 77, no. 2, pp. 440-467.

Burger, R.W., Somerville, P.G., Barker, J.S., Herrmann, R.B., and Helmberger, D.V., 1987, The effect of crustal structure on strong ground motion attenuation relations in eastern North America: Bulletin of the Seismological Society of America, v. 77, p. 420-439.

Campbell, K.W., 1986, An empirical estimate of near-source ground motion for a major, m_b = 6.8, earthquake in the eastern United States: Bulletin of the Seismological Society of America, v. 76, p. 1-17.

Campbell, K.W., 1989, Empirical prediction of near-source ground motion for the Diablo Canyon Power Plant Site, San Luis Obispo County, California, U.S. Geological Survey Open-File Report 89-484, 115 p.

Chapman, W.L., and DiStefano, M.P., 1989, Savannah River Plant seismic survey, 1987-1988: Research report no. 1809-005-006-1-89 prepared by Conoco Inc.

Coffman, J., and von Hake, C.A., 1973, Earthquake History of the United States: United States Department of Commerce Publication, revised edition, Pub. 41-1, NOAA, Boulder, CO, 208 p.

Coppersmith, K. J., 1988, Temporal and spatial clustering of earthquake activity in the central and eastern United States: Seismological Research Letters, v. 59, p. 299-304.

Coppersmith, K. J., Johnston, A.C., and Arabasz, W.J., 1987, Estimating maximum earthquakes in the cental and eastern United States: A progress report: Proceedings from the Symposium on Seismic Hazards, Ground Motions, Soil-Liquefaction and Engineering Practice in Eastern North America, Technical Report NCEER-87-0025, p. 217-232.

Coppersmith, K.J., Youngs, R.R., Lapp, D.B., Johnston, A.C., Kanter, L.R., Metzger, A.G., Cornell, A.C., in preparation, Methods for estimating maximum earthquakes within stable continental regions: Report to the Electric Power Research Institute, Project RP2556-12.

D'Appolonia, 1980, Away from reactor spent fuel storage facility: Data report prepared by DePont de Nemours & Company for Savannah River Plant, South Carolina.

Davison, F.C., Jr., and Scholz, C.H., 1985, Frequency-moment distribution of earthquakes in the Aleutian arc: a test of the characteristic earthquake model: Bulletin of the Seismological Society of America, v. 75, p. 1349-1361.

Dillon, W.P., Klitgord, K.D., and Paull, C.K., 1983, Mesozoic development and structure of the continental margin off South Carolina: in Gohn, G.S., ed., Studies related to the Charleston, South Carolina earthquake of 1886--Tectonics and seismicity: U.S. Geological Survey Professional Paper 1313, p. n1-n16.

Dutton, C.E., 1889, The Charleston earthquake of August 31, 1886: in U.S.G.S. Ninth Annual Report of the Director, 1887-1888, p. 203-528.

Electric Power Research Institute (EPRI), 1987, Seismic hazard methodology for the central and eastern United States - Volume 1: Methodology: Report NP-4726, Volume 1, prepared for Seismicity Owners Group and Electric Power Research Institute under research projects P101-38, -45, -46, 2256-14, Revised, February, 1987.

GEI, 1983, Evaluation of dynamic soil properties F-area, sand filter structures (SFT): report by Geotechnical Engineers Inc: to E.I. duPont de Nemours & Co.

GEI, 1989, Geotechnical data report, L-area, seismic risk assessment: report by Geotechnical Engineers Inc. to E.I. duPont de Nemours & Co.

GEI, 1991, K-Reactor area geotechnical investigation for seismic issues - Savannah River Site: draft report by Geotechnical Engineers Inc. to Westinghouse Savannah River Company, February.

Geomatrix, 1991, Ground motion following selection of SRS Design Basis Earthquake and associated deterministic approach: draft final report to Westinghouse Savannah River Company, WSRC - AA20210S, January.

Gohn, G.S., ed., 1983, Studies related to the Charleston, South Carolina earthquake of 1886--Tectonics and seismicity: U.S. Geological Survey Professional Paper 1313, 375 p.

Guinn, S.A., 1980, Earthquake focal mechanisms in the southeastern United States: U.S. Nuclear Reg. Comm. NUREG/CR-1503, 150 p.

Hanks, T.C., 1979, b values and $w^{-\gamma}$ seismic source models: implications for tectonic stress variations along active crustal faults and the estimation of high-frequency strong ground motion: Journal of Geophysical Research, v. 84, 2235-2242.

Hanks, T.C., and Kanamori, H., 1979, A moment magnitude scale: Journal of Geophysical Research, v. 84, p. 2348-2350.

Hanks, T.C., and R.K. McGuire, 1981, The character of high-frequency strong ground motion: Bulletin of the Seismological Society of America, vol. 71, no. 6, pp. 2071-2095.

Hardin, B.O., and V.P. Drnevich, 1972, Shear modulus and damping in soils: design equations and curves: ASCE Journal of the Soil Mechnaics and Foundation Division, v. 98, p. 667-672.

Hasegawa, H.S., 1983, Lg spectra of local earthquakes recorded by the eastern Canada telemetered network and spectral scaling: Seis. soc. Am. Bull., v. 73, p. 1041-1061.

Herrmann, R.B., 1986, Surface-wave studies of some South Carolina earthquakes, Bulletin of the Seismological Society of America, v. 76, no. 1, p. 111-121.

Hill D.P., Eaton, J.P., and Jones, L.M., 199, Chapter 5. Seismicity, 1980-1986, in Wallace, R.E., ed., The San Andreas Fault System, California: U.S. Geological Survey Professional Paper 1515, p. 114-151.

Idriss, I.M., 1985, Evaluating seismic risk in engineering practice: Proceedings of the Eleventh International Conference on Soil Mechanics and Foundation Engineering, San Francisco, August 12-16, p. 255-320.

Iwasaki, T. F. Tatsuoka, and Y. Takagi, 1976, Dynamic shear deformation properties of sand for wide strain range: Report of Civil Engineering Institute No. 1085, Ministry of Construction, Tokyo, Japan.

Johnston, A.C., 1990, The size of the 1886 Charleston Earthquake: unpub. consulting report to Geomatrix Consultants, December 16, 1990, 10 p.

Johnston, A.C., in prep., Chapter 3--The SCR earthquake data base: in Coppersmith et al., in prep., Methods for Estimating Maximum Earthquakes within Stable Continental Regions: Electric Power Research Institute Project RP2556-12.

Jones, R.B., Long, L.T., Chapman, M.C., and Zelt, K.H., 1985, Columbus, Georgia, earthquakes of October 31, 1982: Earthquake Notes, v. 56, p. 55-61.

Jost, M.L., and Herrmann, R.B., unpublished manuscript., On scaling of intra-continental earthquakes.

Joyner, W.B., and D.M. Boore, 1982, Prediction of earthquake response spectra: U.S. Geological Survey Open-File Report 82-997, 16 p.

Joyner, W.B., and D.M. Boore, 1988, Measurement, characterization, and prediction of strong ground motion: in Earthquake Engineering and Soil Dynamics II - Recent Advances in Ground Motion Evaluation, ASCE Geotechnical Special Publication 20, pp. 43-102.

Kimball, J.K., 1983, The use of site dependent spectra: Proceedings of the U.S. Geological Survey Workshop on Site Specific Effects of Soil and Rock on Ground Motions and the Implications for Earthquake-Resistant Design, U.S. Geological Survey Open File Report 83-845, p. 401-422.

Leeds, A., 1983, El-Asnam, Algeria Earthquake October 10, 1980: Earthquake Engineering Research Institute Reconnaissance Report.

Marion, G.E., and Long, L.T., 1980, microearthquake spectra in the southeastern United States: Bull. Seis. Soc. Am., v. 70, p. 1037-1054.

Marple, R.T., and Talwani, P., 1990, Field investigations of the Woodstock lineament: (abs.), Program and Abstracts, 62nd Annual Meeting Eastern Section Seis. Soc. Am., Blacksburg, VA.

Martin, J.R., G.W. Clough, and S.F. Obermeier, 1990, Estimation of seismic loading levels for the 1886 Charleston earthquake form soil liquefaction phenomena and field testing (abs.): Seismological Research Letters, v. 61, p. 156.

McGuire, R.K., G.R. Toro, and W.J. Silva, 1988, Engineering model of earthquake ground motion for eastern North America: prepared by Risk Engineering, Inc. for the Electric Power Research Institute, EPRI Final Report NP-6074.

Newmark, N.H., and W.J. Hall, 1978, Development of criteria for seismic review of selected nuclear power plants: U.S. Nuclear Regulatory Commission Report NUREG/CR-0098.

Nuttli, O.W., 1986a, Letter to Jean Savey, LLNL, concerning ground motion relationships for the eastern United States: published in Bernreuter et al., 1988, v. 7, p. Q10-130-131.

Nuclear Regulatory Commission, 1985, Safety Evaluation Report for the Vogtle Electric Generating Plant Operating License, NUREG-1137.

Nuttli, O.W, R. Rodriguez, and R.B. Herrmann, 1984, Strong ground motion studies for South Carolina Earthquakes: U.S. Nuclear Regulatory Commmission NUREG/CR3755, UCRL-15594, 88 p.

Nuttli, O.W., 1986b, Yield estimates of Nevada Test Site explosions obtained from seismic Lg waves: Journal of Geophysical Research, v. 91, p. 2137-2151.

Nuttli, O.W., 1983, Average seismic source-parameter relatiions for mid-plate earthquakes: Bulletin of the Seismological Society of America, v. 73, p. 519-535.

Nuttli, O.W., 1973, The Mississippi Valley earthquakes of 1811 and 1812: Intensities, ground motion, and magnitudes: Bull. Seis. Soc. Am., v. 63, p. 227-248.

Nuttli, O.W. Bollinger, G.A., and Griffiths, D.W., 1979, On the relations between Modified Mercalli intensity and body-wave magnitude: Bulletin of the Seismological Society of America, v. 69, p. 893-909.

Nuttli, O.W., Jost, M.L., Herrmann, R.B., and Bollinger, G.A., 1989, Numerical models of the rupture mechanics and far-field ground motion of the 1886 South Carolina earthquake: U.S. Geological Survey Bulletin 1586.

Oaks, S.D., and Bollinger, G.A., 1986, The epicenter of the mb 5, December 22, 1875, Virginia earthquake: New findings from documentary sources: Earthquake Notes, v. 57, p. 65-75.

Obermeir, S.F., Weems, R.E., and Jacobson, R.B., 1987, Earthquake induced liquefacton features in the coastal South Carolina region: Proceedings from the Symposium on Seismic Hazards, Ground Motions, Soil-Liquefaction and Engineering Practice in Eastern North America, Technical Report NCEER-87-0025, p. 480-493.

Ou, G.-B., and Herrmann, R.B., in press, A statistical model for ground motion produced by earthquakes at local and regional distances, submitted to the Bulletin of the Seismological Society of America.

Phillips, J.D., 1988, Buried structures at the northern end of the early Mesozoic South Georgia Basin, South Carolina, as interpreted from aeromagnetic data: Studies of the Early Mesozoic Basins of the Eastern United States, U.S.G.S. Bulletin 1776, p. 248-252.

Rhea, S., 1984, Q determined from local earthquakes in the South Carolina coastal plain, Bulletin of the Seismological Society of America, v. 74, no. 6, pp. 2257-2268.

Sadigh, K., J.A. Egan and R.R. Youngs, 1986, Specification of ground motion for seismic design of long period structures: Earthquake Notes, v. 57, no. 1, p. 13., relationships are tabulated in Joyner and Boore (1988) and Youngs et al. (1987)

Sadigh, K., C.-Y. Chang, F. Makdisi, and J.A. Egan, 1989, Attenuation relationships for horizontal peak ground acceleration and response spectral acceleration for rock sites (abs.): Seismological Research Letters, v. 60, n. 1, p. 19.

Schwartz, D.P., Coppersmith, K.J., and Swan, F.H., 1984, Methods for assessing maximum earthquakes: Proceedings of the Eighth World Conference on Earthquake Engineering, San Francisco, CA, v.1, p. 279-285.

Scott, W.E., Pierce, K.L., and Hait, M.H., Jr., 1985, Quaternary tectonic setting of the 1983 Borah Peak earthquake, central Idaho: Bull. Seis. Soc. Am., v. 75, p. 1053-1066.

Seeber, L., and Armbruster, J.G., 1981, The 1886 Charleston, South Carolina earthquake and the Appalachian detachment: Journal of Geophysical Research, v. 86, p. 7874-7894.

Seed, H.B., and I.M. Idriss, 1970, Soil modulii and damping factors for dynamic response analysis: Report No. EERC 70-10, Earthquake Engineering Research Center, University of California, Berkeley.

Sibson, R.J., 1984, Roughness at the base of the seismogenic zone: contributing factors: Journal of Geophysical Research, v.89, no. B7, p. 5791-5799.

Silva, W., 1989, Site dependent specification of strong ground motion; in Dynamic Soil Property and Site Characterization, Proceedings of the Workshop sponsored by the National Science Foundation and the Electric Power Research Institute, Palo Alto, California.

Silva, W.J., and K. Lee, 1987, WES RASCAL code for synthesizing earthquake ground motions: State-of-the-art for assessing earthquake hazards in the United States Report 24, U.S. Army Corps of Engineers Waterways Experiment Station, Vicksberg, Mississippi, Miscellaneous Paper S-73-1.

Silva, W., and Darragh, R.B., 1990, Engineering characterization of strong ground motion recorded at rock sites, Research Project RP2556-48, Draft Report prepared for Electric Power Research Institute: Woodward-Clyde Consultants, Oakland, California.

Silva, W., R.B Darragh, C.L. Stark, I.G. Wong, J.C. Stepp, J. Schneider, and S. Chiou, 1990, A methodology to estimate design response spectra in the near-source region of large earthquakes using the Band-Limited-White-Noise ground motion model: in Proceedings of the Fourth U.S. Conference on Earthquake Engineering, v. 1, p. 487-494.

Somerville, P., J.P, Mclaren, L.V. LeFevre, R.W. Berger, and D.V. Helmberger, 1987, Comparison of source scaling relations of eastern and western North American earthquakes: Bulletin of the Seismological Society of America, v. 77, p. 322- 346.

Somerville, P.G., McLaren, J.P., and Smith, N.F., 1989, Wave propagation modeling of ground motion attenuation of the Saguenay earthquake sequence of November 25, 1988 (abs): Seismological Research Letters, v. 60, n. 1, p. 19.

Somerville, P.G., McLaren, J.P., LeFevre, L.V., Burger, R.W., and Helmberger, D.V., 1987, Bulletin of the Seismological Society of America, v. 77, no. 2, p. 322-346.

Somerville, P.G., McLaren, J.P., Saikia, C.K., and Helmberger, D.V., 1990, The 25 November 1988 Saguenay, Quebec, earthquake: Source parameters and the attenuation of strong ground motion: Bulletin of the Seismological Society of America, v. 80, no. 5, p. 1118-1143.

Talwani, P., 1977, A preliminary shallow crustal model between Columbia and Charleston, South Carolina, determined from quarry blast monitoring and other geophysical data, in Rankin, D.W., ed., Studies Related to the Charleston, South Carolina, Earthquake of 1886-A Preliminary Report, Geological Survey Profession Paper 1028, U.S. Government Printing Office, Washington, D.C.

Talwani, P., 1982, Internally consistent pattern of seismicity near Charleston, South Carolina: Geology, v. 10, p. 654-658.

Talwani, P., and Cox, J., 1985, Paleoseismic evidence for recurrence of earthquakes near Charleston, South Carolina: Science, v. 229, p. 379-381.

Talwani, P., Marple, R.T., and Madabhushi, S., 1990, Further evidence for the presence of the Woodstock fault (abs.): Program and Abstracts, Eastern Section Seismological Society of America, p.50.

Talwani, P., Rawlins, J., and Stephenson,D., 1985, The Savannah River Plant, South Carolina, earthquake of June 9, 1985, and its tectonic setting: Earthquake Notes, v. 56, p. 101-106.

Toro, G.R., and R.K. McGuire, 1987, An investigation into earthquake ground motion characteristics in eastern North America: Bulletin of the Seismological Society of America, vol. 77, no. 2, pp. 468-489.

United States Nuclear Regulatory Commission (USNRC), 1990, Standard Review Plan, Office of Nuclear Reactor Regulation, NUREG - 0800, Rev.2, 2.5.2 Vibratory Ground Motion, 15 p.

Veneziano, D. 1988, Letter to Don Bernreuter, LLNL, concerning ground motion relationships for the eastern United States: published in Bernreuter et al., 1988, v. 7, p. Q10-123-128.

Visvanathan, T.R., 1980, Earthquakes in South Carolina 1698-1975: South Carolina Geological Survey Bull. 40, 61 p.

Wells, D.L., and Coppersmith, K.J., in prep., Updated empirical relationships among magnitude, rupture length, rupture area, and surface displacement: For submittal to Bull. Seis. Soc. Am.

Westinghouse Savannah River Company (WSRC), 1990, Safety Analysis 200-F Area, Savannah River Site, 238 PuO2 Fuel Form Facility (PuFF), v. 2, App. 3A, SRS Site Characteristics, Draft Feb. 1990, 323 p.

Youngs, R.R., F. Makdisi, K. Sadigh, and N.A. Abrahamson, 1990, The case for magnitude dependent dispersion in peak ground acceleration (abs.): Seismological Research Letters, v. 61, n. 1, p. 30.

Youngs, R.R., F.H. Swan, M.S. Power, D.P. Schwartz, and R.K. Green, 1987, Probabilistic analysis of earthquake ground shaking hazard along the Wasatch Front, Utah: Assessment of Regional Earthquake Hazards and Risk Along the Wasatch Front, Utah, U.S. Geological Survey Open File Report 87-585, v. II, pp. M-1-110.

Zoback, M.L., Nishenko. S., Richardson, R., Hasegawa, H., and Zoback, M.D.,1986, Mid-plate stress deformation, and seismicity: in Vogt, P.R., and B. Tucholke, eds., The Geology of North America, v. M., The Western North Atlantic Region, Geol. Soc. Am., p. 297-312.

Zoback, M.L., and Zoback, M.D., 1989, Tectonic stress field of the continental U.S.: Pakiser, L., and W. Mooney, eds., Geophysical Framework of the Continental United States: Geol. Soc. Am. Memoir, 43 p.

Table 1
Available Deep Soil Recordings For Mw 4.5 to 5.5 Earthquakes
Recorded at Distances Less Than 25 km

Earthquake Name	Date	Fault Type	Mw	Station	Dist (km)	Comp	PGA (g)
Port Hueneme	1957 03 18	StrikeSlip	4.7	272	3.0	WEST	0.093
Port Hueneme	1957 03 18	StrikeSlip	4.7	272	3.0	SOUT	0.171
Port Hueneme	1957 03 18	StrikeSlip	4.7	272	3.0	VERT	0.027
Imp.Val., CA (A03)	1979 10 15	StrikeSlip	5.2	5055	7.9	S45W	0.116
Imp.Val., CA (A03)	1979 10 15	StrikeSlip	5.2	5055	7.9	N45W	0.264
Imp.Val., CA (A03)	1979 10 15	StrikeSlip	5.2	5055	7.9	VERT	0.042
Imp.Val., CA (A03)	1979 10 15	StrikeSlip	5.2	5028	9.2	S40E	0.147
Imp.Val., CA (A03)	1979 10 15	StrikeSlip	5.2	5028	9.2	S50W	0.230
Imp.Val., CA (A03)	1979 10 15	StrikeSlip	5.2	5028	9.2	VERT	0.086
Imp.Val., CA (A03)	1979 10 15	StrikeSlip	5.2	942	9.2	S50W	0.263
Imp.Val., CA (A03)	1979 10 15	StrikeSlip	5.2	942	9.2	S40E	0.175
Imp.Val., CA (A03)	1979 10 15	StrikeSlip	5.2	942	9.2	VERT	0.080
Imp.Val., CA (A03)	1979 10 15	StrikeSlip	5.2	5165	9.4	N50E	0.146
Imp.Val., CA (A03)	1979 10 15	StrikeSlip	5.2	5165	9.4	N40W	0.147
Imp.Val., CA (A03)	1979 10 15	StrikeSlip	5.2	5165	9.4	VERT	0.103
Imp.Val., CA (A03)	1979 10 15	StrikeSlip	5.2	958	9.9	S50W	0.157
Imp.Val., CA (A03)	1979 10 15	StrikeSlip	5.2	958	9.9	S40E	0.128
Imp.Val., CA (A03)	1979 10 15	StrikeSlip	5.2	958	9.9	VERT	0.056
Imp.Val., CA (A03)	1979 10 15	StrikeSlip	5.2	952	10.2	S40E	0.235
Imp.Val., CA (A03)	1979 10 15	StrikeSlip	5.2	952	10.2	S50W	0.286
Imp.Val., CA (A03)	1979 10 15	StrikeSlip	5.2	952	10.2	VERT	0.117
Imp.Val., CA (A03)	1979 10 15	StrikeSlip	5.2	955	10.9	S40E	0.237
Imp.Val., CA (A03)	1979 10 15	StrikeSlip	5.2	955	10.9	S50W	0.168
Imp.Val., CA (A03)	1979 10 15	StrikeSlip	5.2	955	10.9	VERT	0.079
Imp.Val., CA (A03)	1979 10 15	StrikeSlip	5.2	5053	11.7	N45W	0.011
Imp.Val., CA (A03)	1979 10 15	StrikeSlip	5.2	5053	11.7	S45W	0.097
Imp.Val., CA (A03)	1979 10 15	StrikeSlip	5.2	5053	11.7	VERT	0.034
Imp.Val., CA (A03)	1979 10 15	StrikeSlip	5.2	5054	12.6	S40E	0.074
Imp.Val., CA (A03)	1979 10 15	StrikeSlip	5.2	5054	12.6	S50W	0.129
Imp.Val., CA (A03)	1979 10 15	StrikeSlip	5.2	5054	12.6	VERT	0.052
Imp.Val., CA (A03)	1979 10 15	StrikeSlip	5.2	5058	14.4	S40E	0.098
Imp.Val., CA (A03)	1979 10 15	StrikeSlip	5.2	5058	14.4	S50W	0.192
Imp.Val., CA (A03)	1979 10 15	StrikeSlip	5.2	5058	14.4	VERT	0.063

Table 1 (cont'd)

Earthquake Name	Date	Fault Type	Mw	Station	Dist (km)	Comp	PGA (g)
Imp.Val., CA (A03)	1979 10 15	StrikeSlip	5.2	5057	15.3	S40E	0.147
Imp.Val., CA (A03)	1979 10 15	StrikeSlip	5.2	5057	15.3	S50W	0.103
Imp.Val., CA (A03)	1979 10 15	StrikeSlip	5.2	5057	15.3	VERT	0.039
Imp.Val., CA (A03)	1979 10 15	StrikeSlip	5.2	5115	18.1	S40W	0.154
Imp.Val., CA (A03)	1979 10 15	StrikeSlip	5.2	5115	18.1	S50W	0.089
Imp.Val., CA (A03)	1979 10 15	StrikeSlip	5.2	5115	18.1	VERT	0.054
Coalinga, CA (A03)	1983 05 08	Reverse	5.1	1162	8.3	135	0.214
Coalinga, CA (A03)	1983 05 08	Reverse	5.1	1162	8.3	045	0.099
Coalinga, CA (A03)	1983 05 08	Reverse	5.1	1162	8.3	VERT	0.102
Coalinga, CA (A03)	1983 05 08	Reverse	5.1	46T04	11.6	N90E	0.124
Coalinga, CA (A03)	1983 05 08	Reverse	5.1	46T04	11.6	N00E	0.134
Coalinga, CA (A03)	1983 05 08	Reverse	5.1	46T04	11.6	VERT	0.070
Coalinga, CA (A03)	1983 05 08	Reverse	5.1	62	13.0	S90W	0.089
Coalinga, CA (A03)	1983 05 08	Reverse	5.1	62	13.0	N00E	0.092
Coalinga, CA (A03)	1983 05 08	Reverse	5.1	62	13.0	VERT	0.074
Coalinga, CA (A03)	1983 05 08	Reverse	5.1	46T07	13.2	N00E	0.073
Coalinga, CA (A03)	1983 05 08	Reverse	5.1	46T07	13.2	N90E	0.144
Coalinga, CA (A03)	1983 05 08	Reverse	5.1	46T07	13.2	VERT	0.073
Coalinga, CA (A08)	1983 06 10	Reverse	5.3	46T04	14.5	N00E	0.057
Coalinga, CA (A08)	1983 06 10	Reverse	5.3	46T04	14.5	N90E	0.061
Coalinga, CA (A08)	1983 06 10	Reverse	5.3	46T04	14.5	VERT	0.031
Coalinga, CA (A10)	1983 07 09	Thrust	5.2	46T04	11.9	N90E	0.164
Coalinga, CA (A10)	1983 07 09	Thrust	5.2	46T04	11.9	N00E	0.184
Coalinga, CA (A10)	1983 07 09	Thrust	5.2	46T04	11.9	VERT	0.081
Coalinga, CA (A13)	1983 07 21	Thrust	4.9	46T04	9.2	N90E	0.217
Coalinga, CA (A13)	1983 07 21	Thrust	4.9	46T04	9.2	N00E	0.130
Coalinga, CA (A13)	1983 07 21	Thrust	4.9	46T04	9.2	VERT	0.108
Coalinga, CA (A14)	1983 07 25	Thrust	5.2	46T04	9.6	N00E	0.479
Coalinga, CA (A14)	1983 07 25	Thrust	5.2	46T04	9.6	N90E	0.715
Coalinga, CA (A14)	1983 07 25	Thrust	5.2	46T04	9.6	VERT	0.325
Coalinga, CA (A16)	1983 09 09	Reverse	5.3	46T04	12.0	N00E	0.024
Coalinga, CA (A16)	1983 09 09	Reverse	5.3	46T04	12.0	N90E	0.033
Coalinga, CA (A16)	1983 09 09	Reverse	5.3	46T04	12.0	VERT	0.029

Table 1 (cont'd)

Earthquake Name	Date	Fault Type	Mw	Station	Dist (km)	Comp	PGA (g)
Coalinga, CA (A17)	1983 09 11	Reverse	4.5	46T04	10.5	N90E	0.474
Coalinga, CA (A17)	1983 09 11	Reverse	4.5	46T04	10.5	N00E	0.313
Coalinga, CA (A17)	1983 09 11	Reverse	4.5	46T04	10.5	VERT	0.209
Whitt.Nar., CA (A)	1987 10 04	StrikeSlip	5.3	5129	15.9	N80W	0.250
Whitt.Nar., CA (A)	1987 10 04	StrikeSlip	5.3	5129	15.9	N10E	0.240
Whitt.Nar., CA (A)	1987 10 04	StrikeSlip	5.3	5129	15.9	VERT	0.080
Whitt.Nar., CA (A)	1987 10 04	StrikeSlip	5.3	634	19.9	N90E	0.050
Whitt.Nar., CA (A)	1987 10 04	StrikeSlip	5.3	634	19.9	N00E	0.060
Whitt.Nar., CA (A)	1987 10 04	StrikeSlip	5.3	634	19.9	VERT	0.100

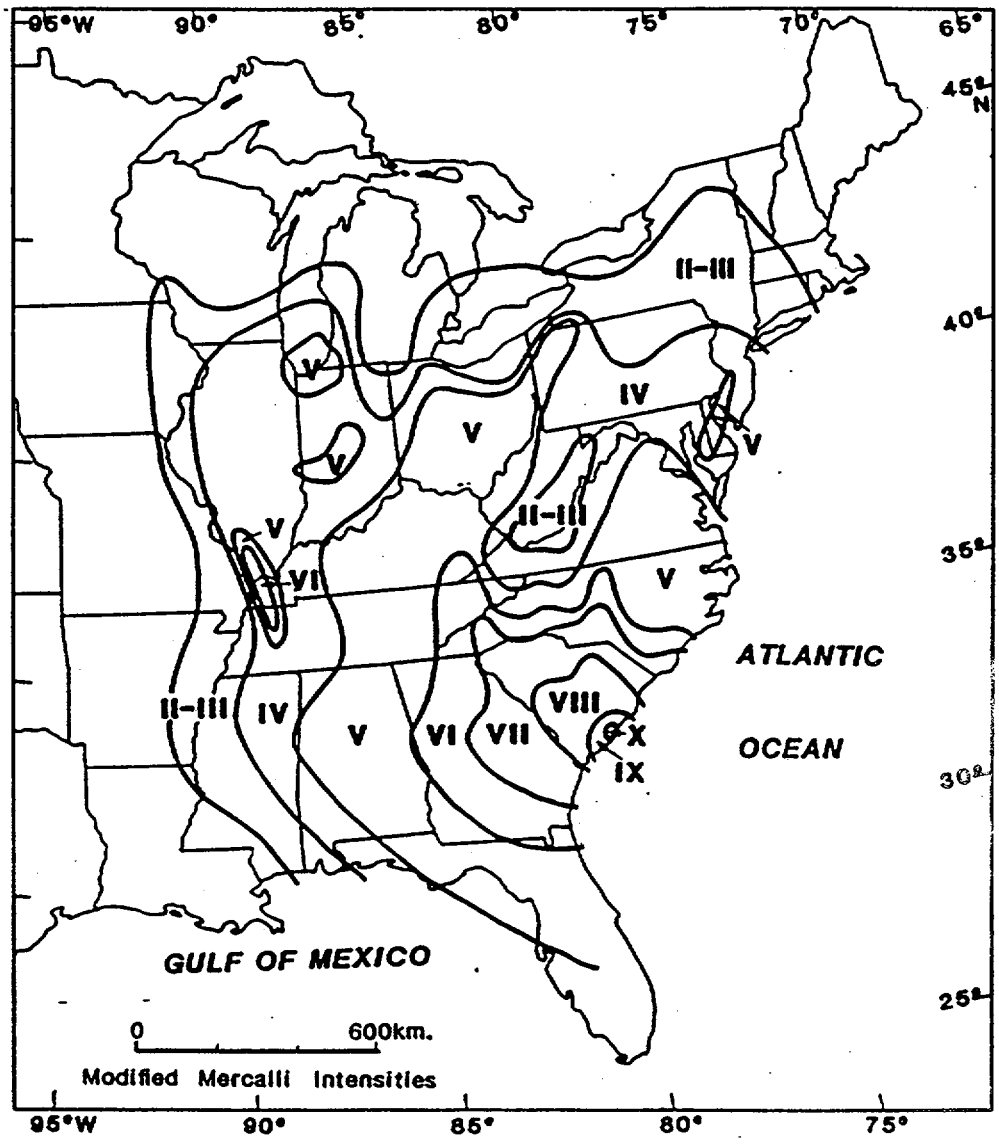

FIGURE 1. Isoseismal map of the Charleston, South Carolina earthquake, September 1, 1886 (after Bollinger, 1977).

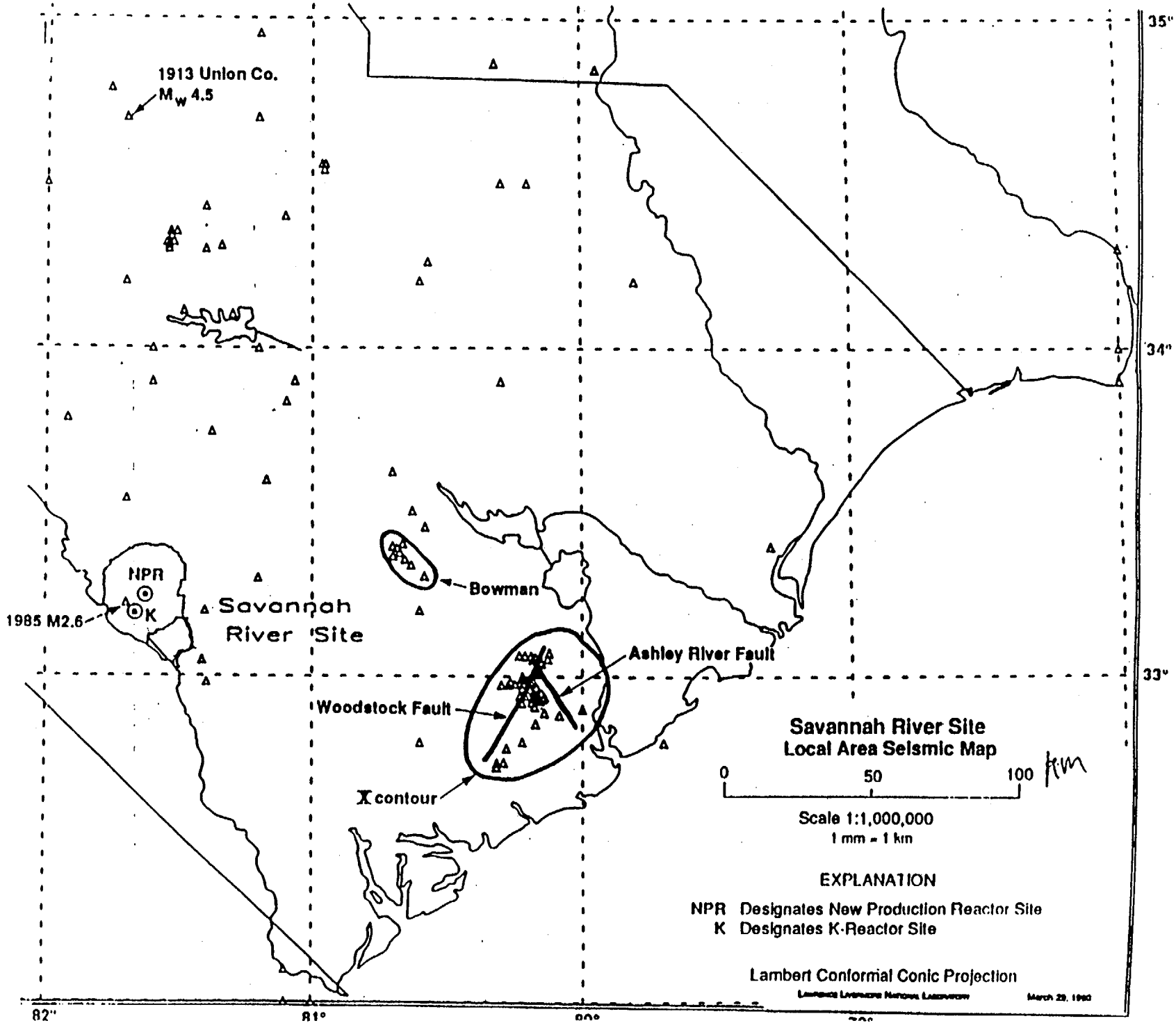

FIGURE 2. Local area seismicity map.

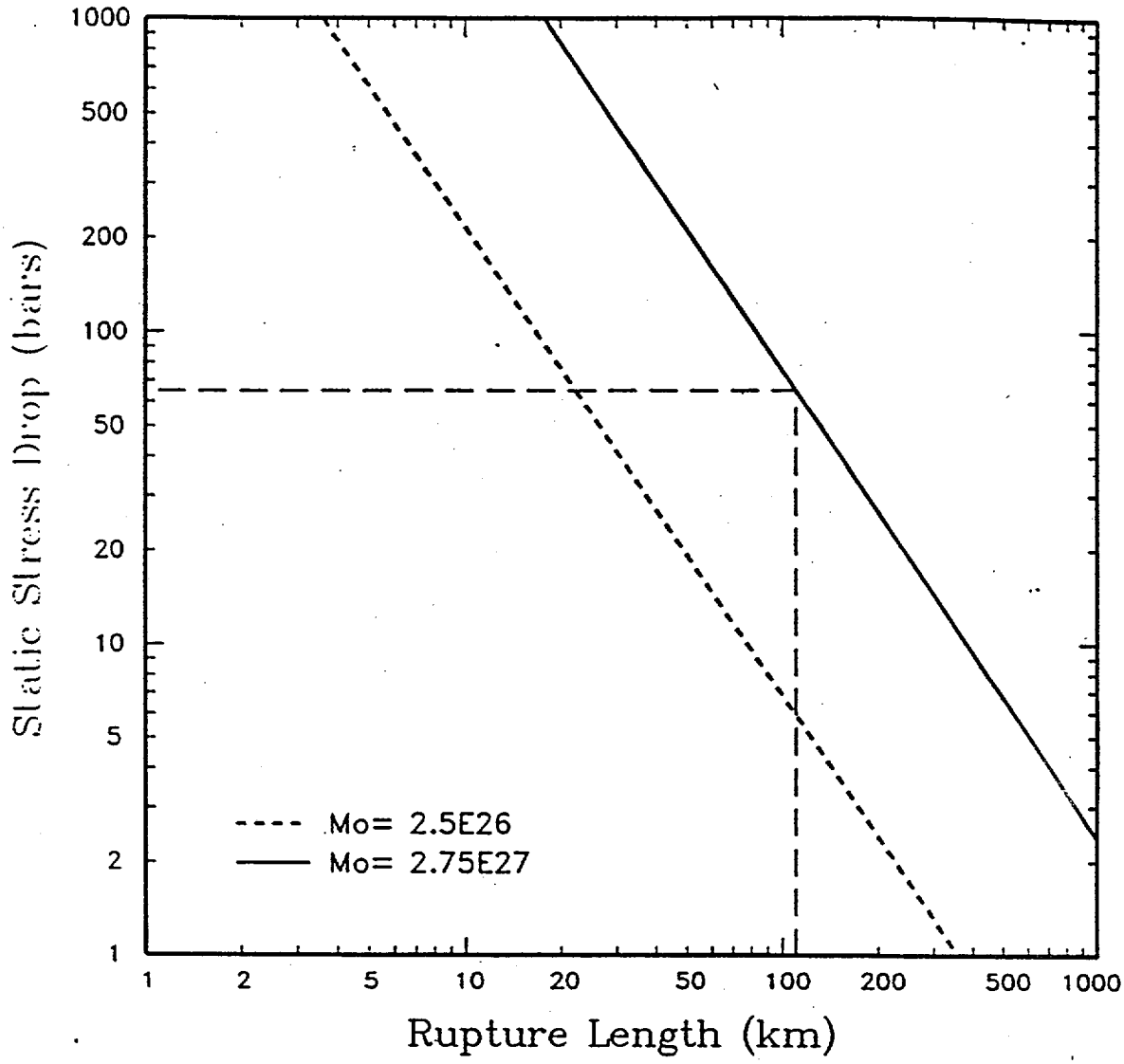

$$\Delta\sigma = \frac{7/16\ Mo}{(LW/\pi)^{3/2}}$$

FIGURE 10. Relationship between rupture length and static stress drop for two proposed seismic moments for the 1886 Charleston earthquake, assuming the downdip rupture width is 20 km and using the formula cited in Nuttli (1983).

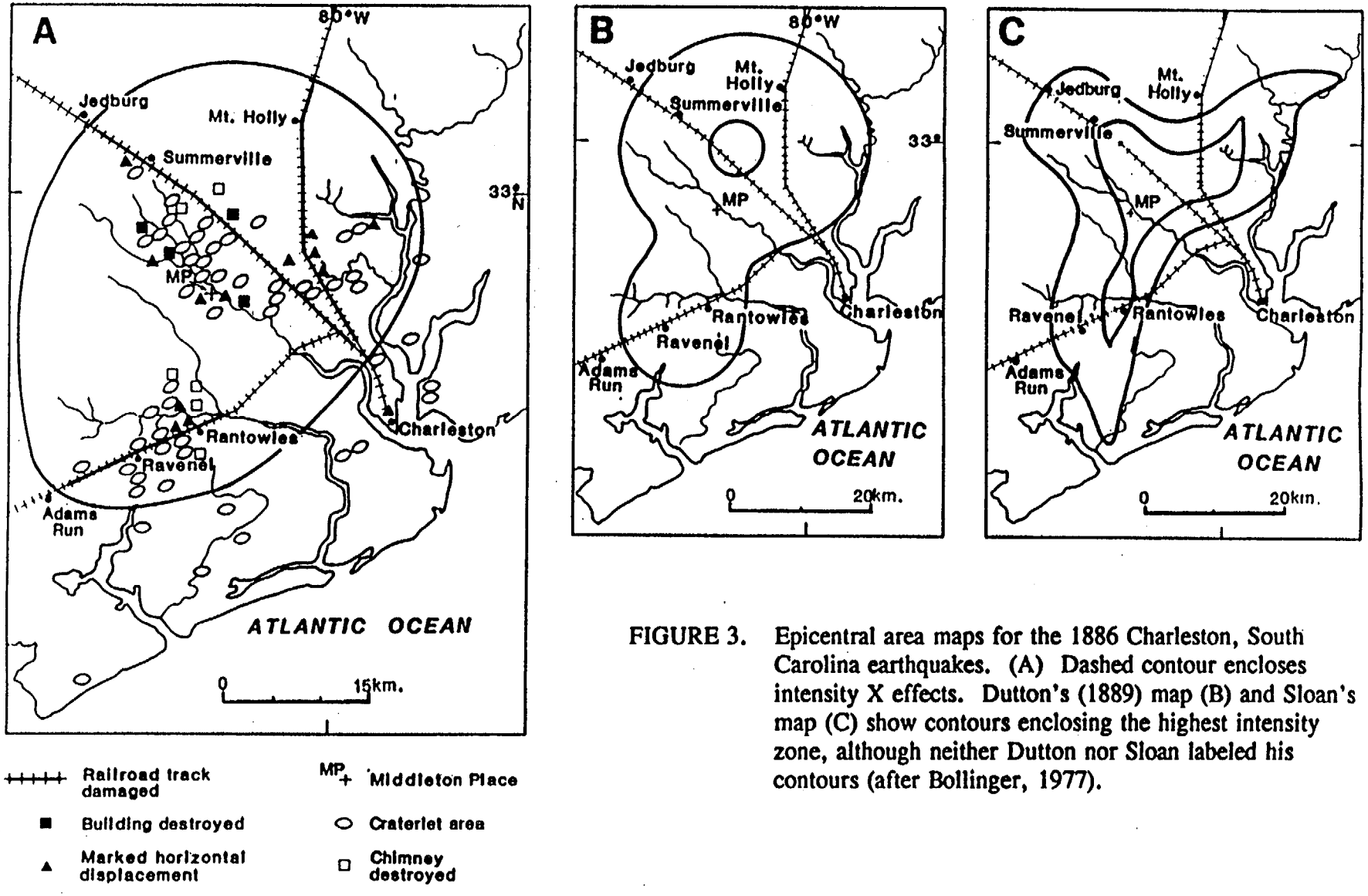

FIGURE 3. Epicentral area maps for the 1886 Charleston, South Carolina earthquakes. (A) Dashed contour encloses intensity X effects. Dutton's (1889) map (B) and Sloan's map (C) show contours enclosing the highest intensity zone, although neither Dutton nor Sloan labeled his contours (after Bollinger, 1977).

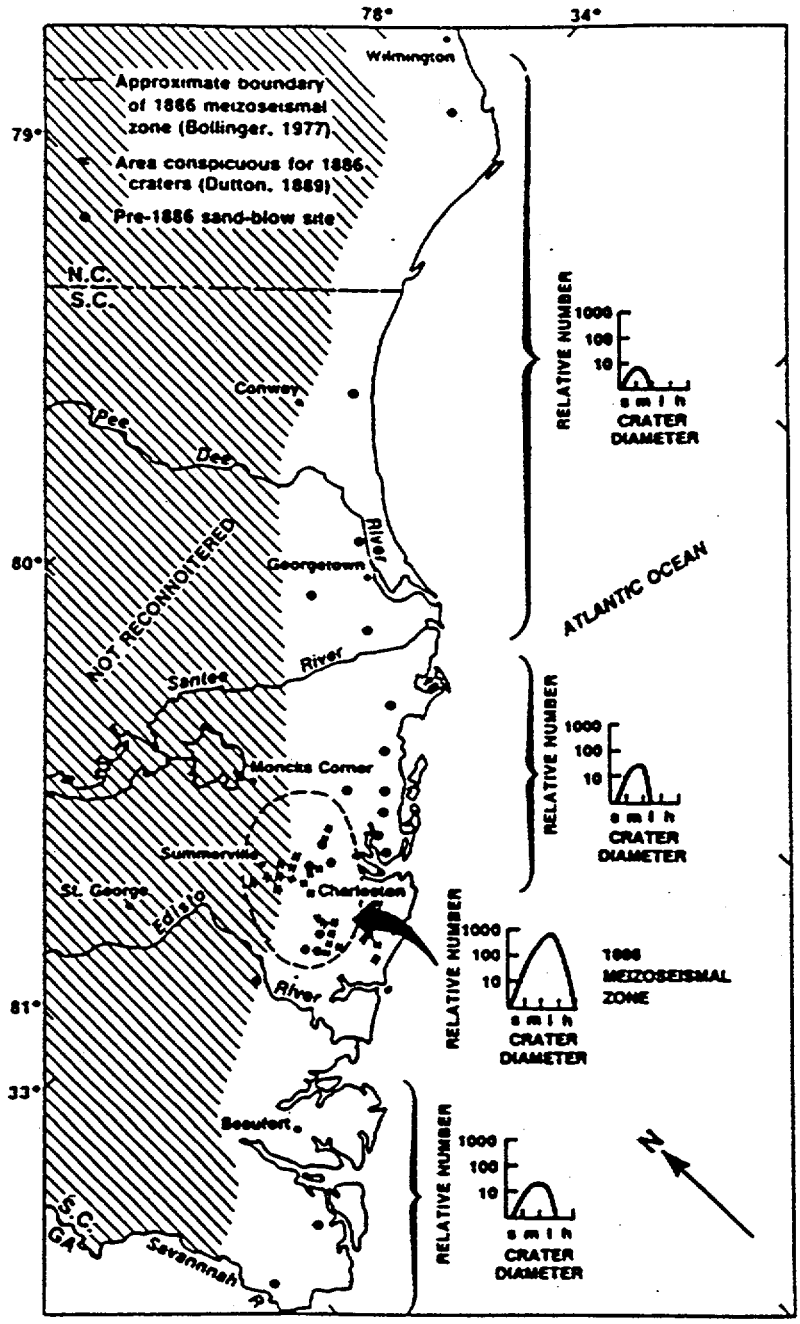

FIGURE 4. Relative number of filled craters and crater diameters for pre-1886 sand blows at sites on marine-related sediments. The relative number is a scaling based on comparison with abundance of craters in the 1886 mesoseismal zone, which has an arbitrary value of 1000. Crater diameters are small (s, less than 1 m), medium (m, 1-2 m), large (l, 2-3 m), and huge (h, greater than 3 m). (From Obermeir et al., 1987.)

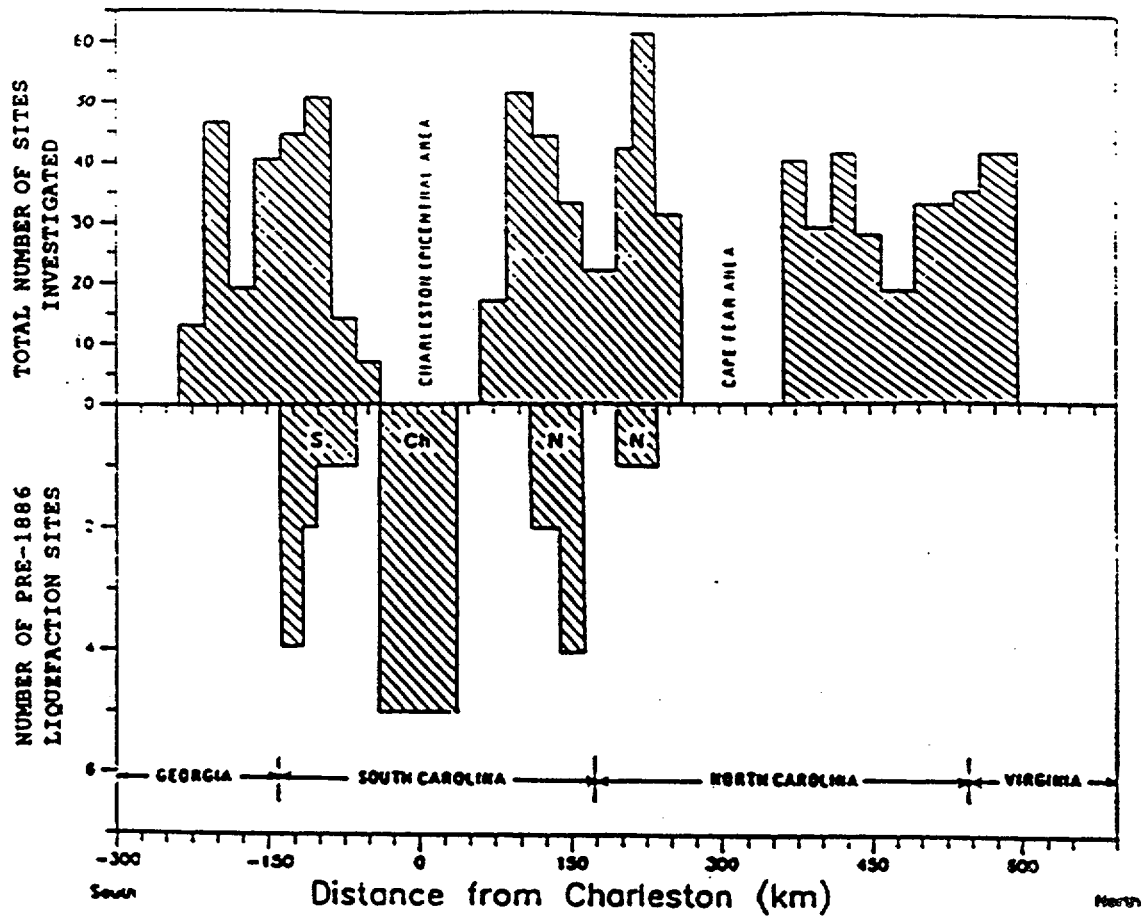

FIGURE 5. Distribution of potential liquefaction sites evaluated along the southeastern Atlantic Seaboard (top) and location of pre-1886 liquefaction sites (bottom) discovered. Sites within the mesoseismal area of the 1886 earthquake are labeled "CH". Outlying liquefaction sites located to the south and north of the 1886 epicentral area are labeled "S" and "N", respectively, (also see insert at right that shows the general location of outlying liquefaction sites with respect to Charleston). The precise number of sites evaluated in the Charleston area has not been shown. However, the total number of sites near Charleston evaluated during our study was significantly less than in other areas. No studies were conducted in the Cape Fear area due to the general absence of suitable deposits over the Cape Fear Arch. (From Amick et al., 1989)

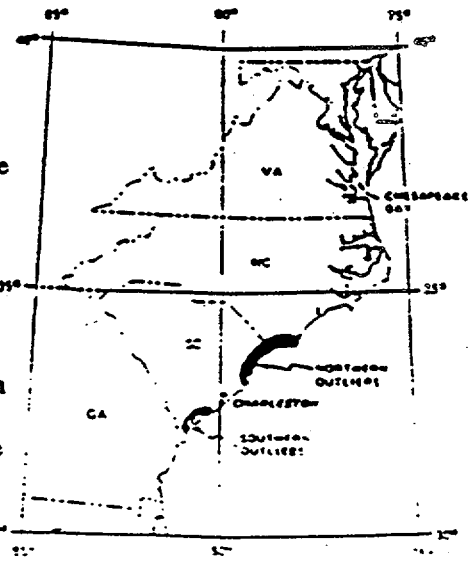

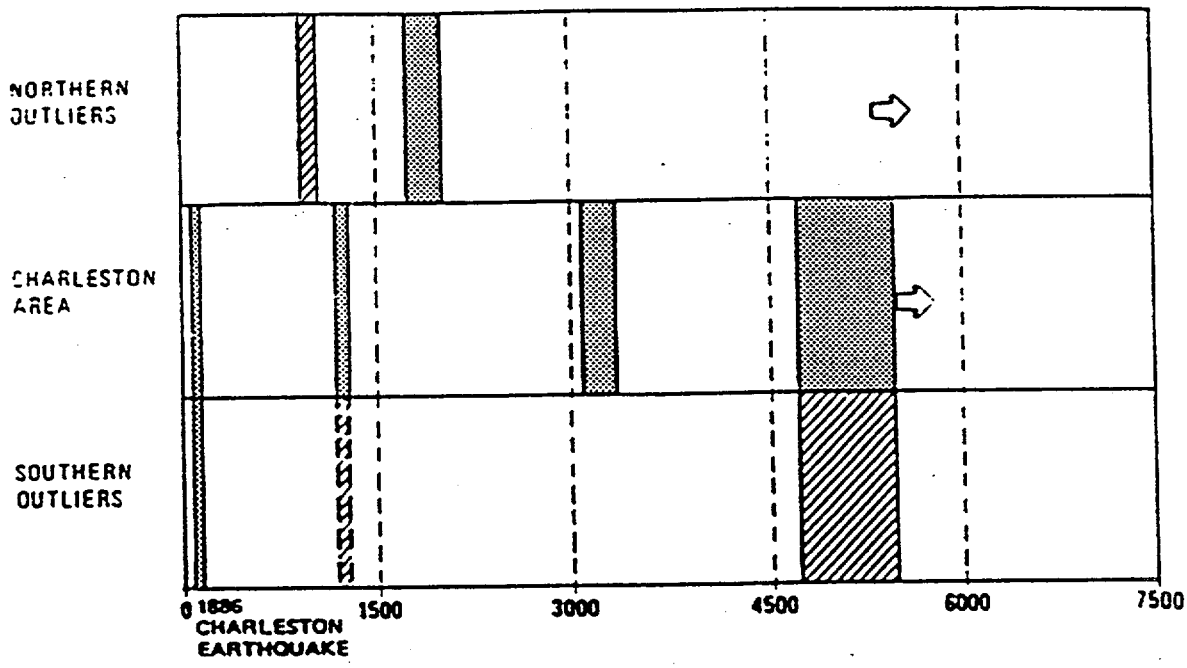

FIGURE 6. Age of liquefaction features. Dates for both southern and northern outliers are shown as well as dates determined for large earthquakes occurring in the Charleston area. Dotted pattern denotes earthquake ages determined from multiple liquefaction sites. Striped pattern denotes earthquake ages based on dates from only one liquefaction site. Arrows indicate the probable occurrence of at least one older liquefaction episode in both the Charleston and northern areas. (From Amick et al., 1989.)

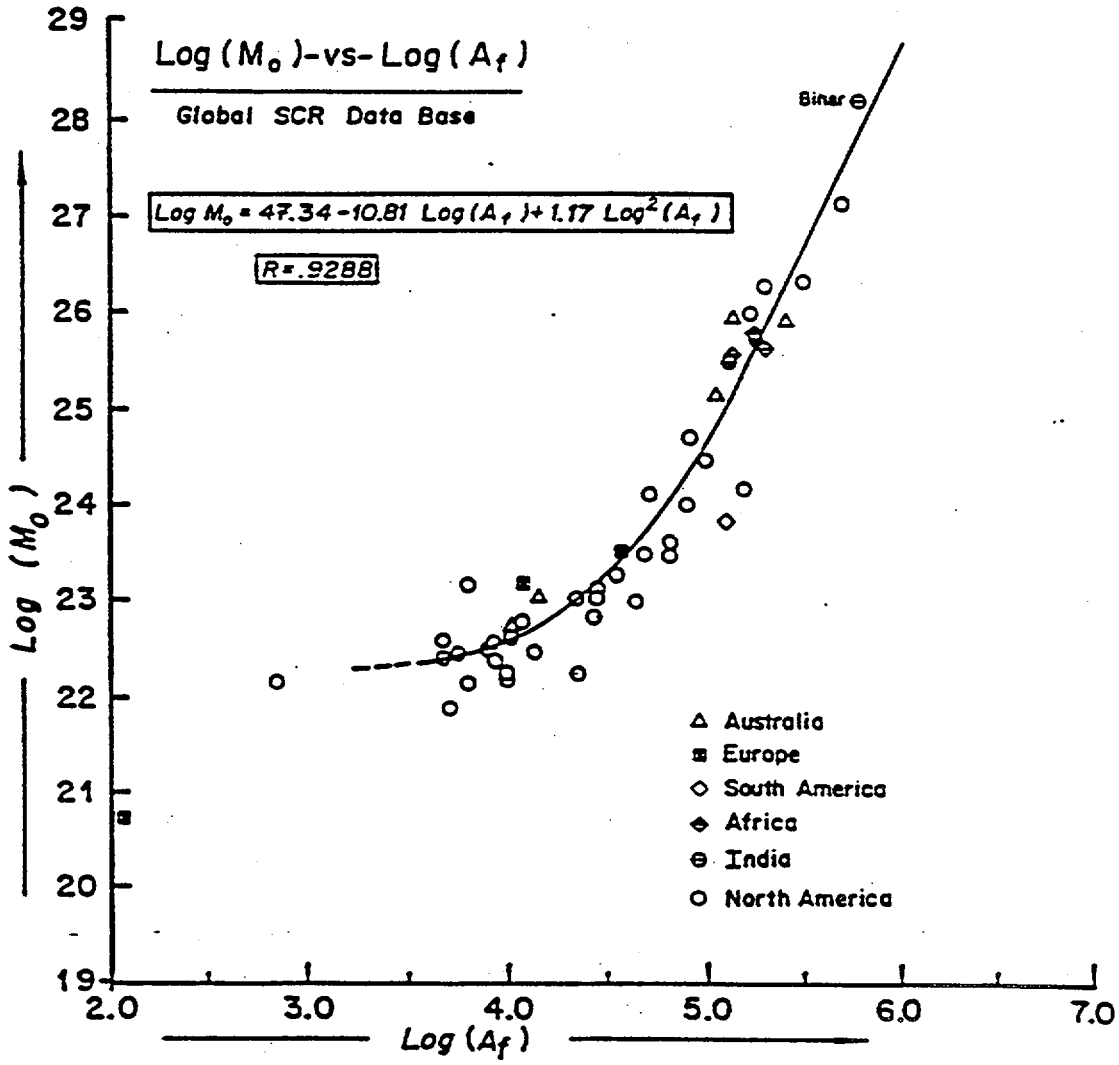

FIGURE 7. Relationship between seismic moment (M_o) and felt area (A_f) for stable continental regions (from Johnston, in prep.).

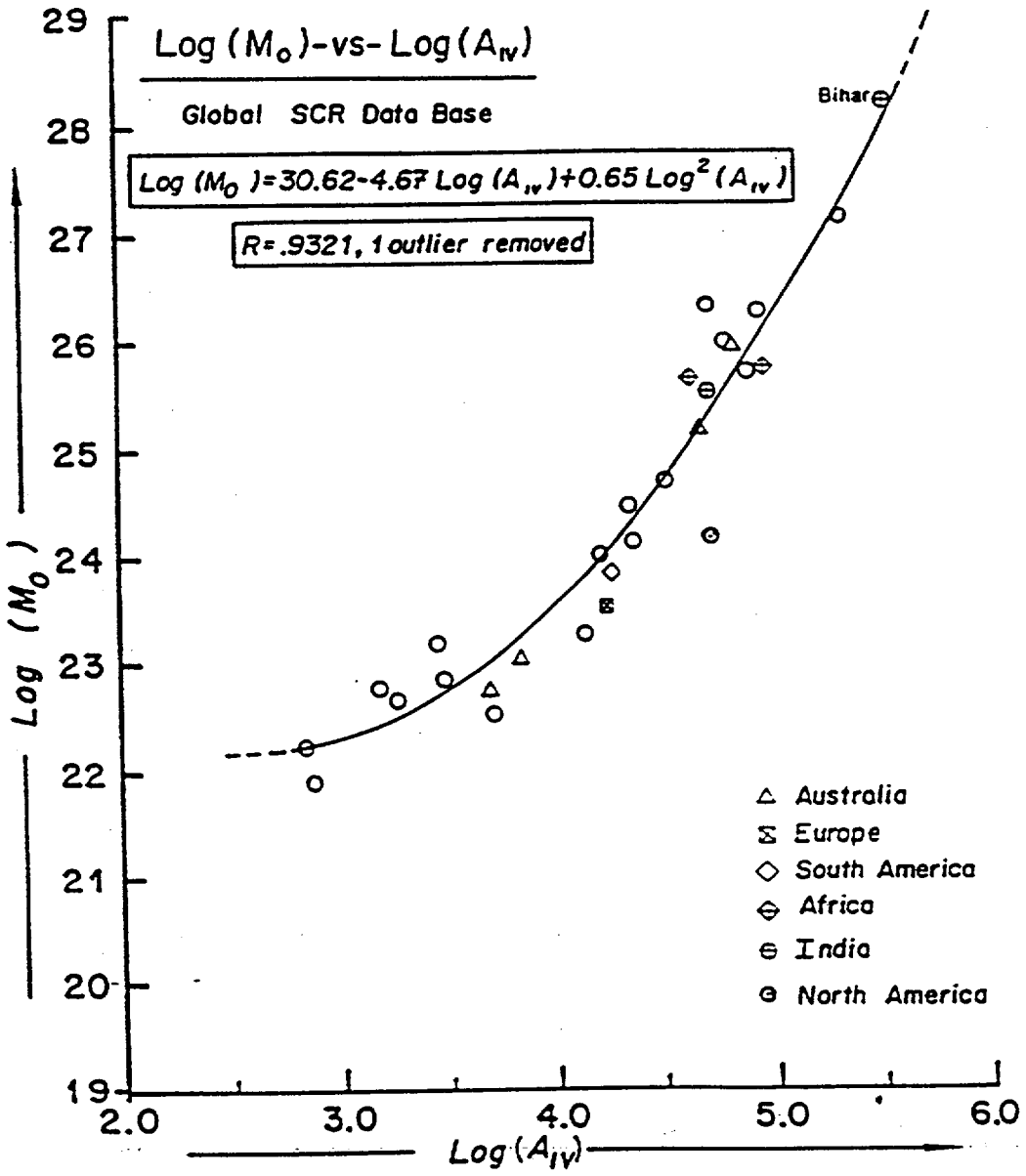

FIGURE 8. Relationship between seismic moment (M_o) and the area contained within the intensity IV isoseismal (A_{IV}) (from Johnston, in prep.).

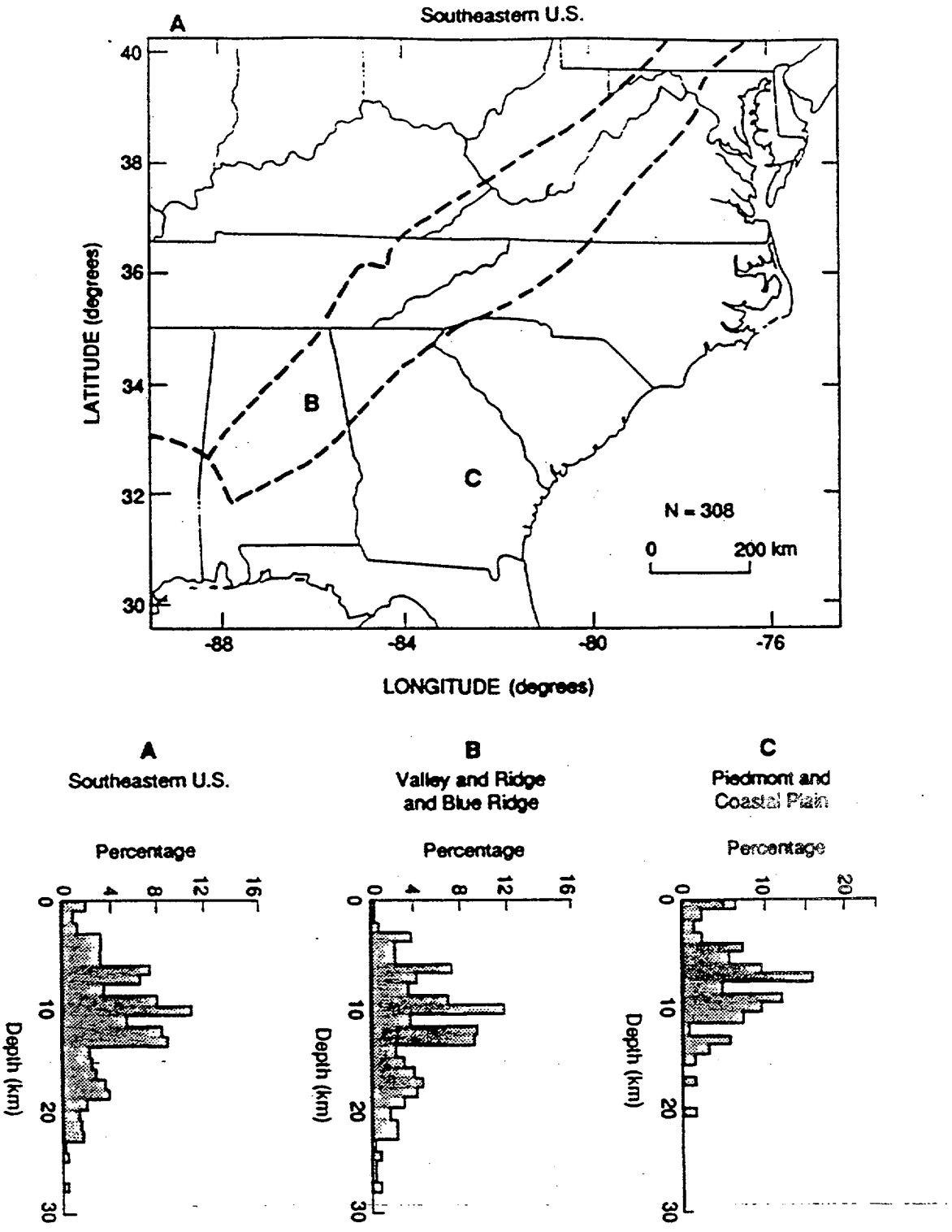

FIGURE 9. Focal depth distribution for instrumental seismicity in the A) Southeastern U.S., B) Valley and Ridge and Blue Ridge province, and C) Piedmont and Coastal Plain (modified from Bollinger et al., in press).

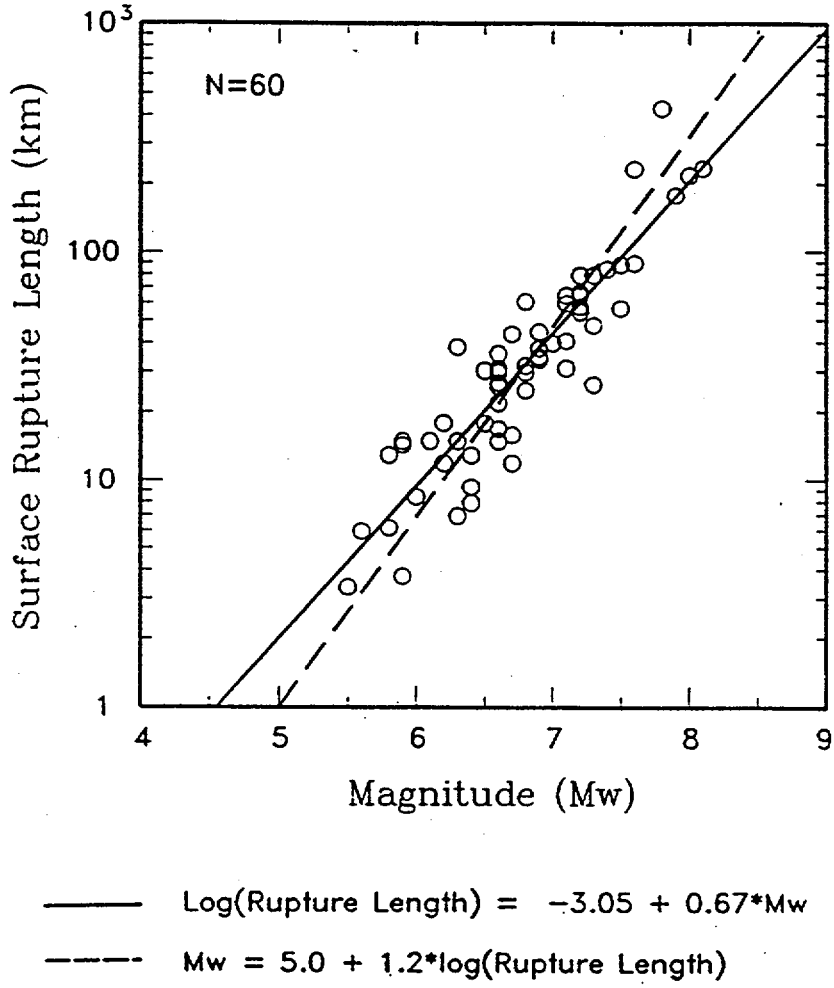

FIGURE 11. Linear regression of surface rupture length on moment magnitude for all slip types (from Wells and Coppersmith, in prep.). The expected surface rupture length for Mw 7.5 is 94 km.

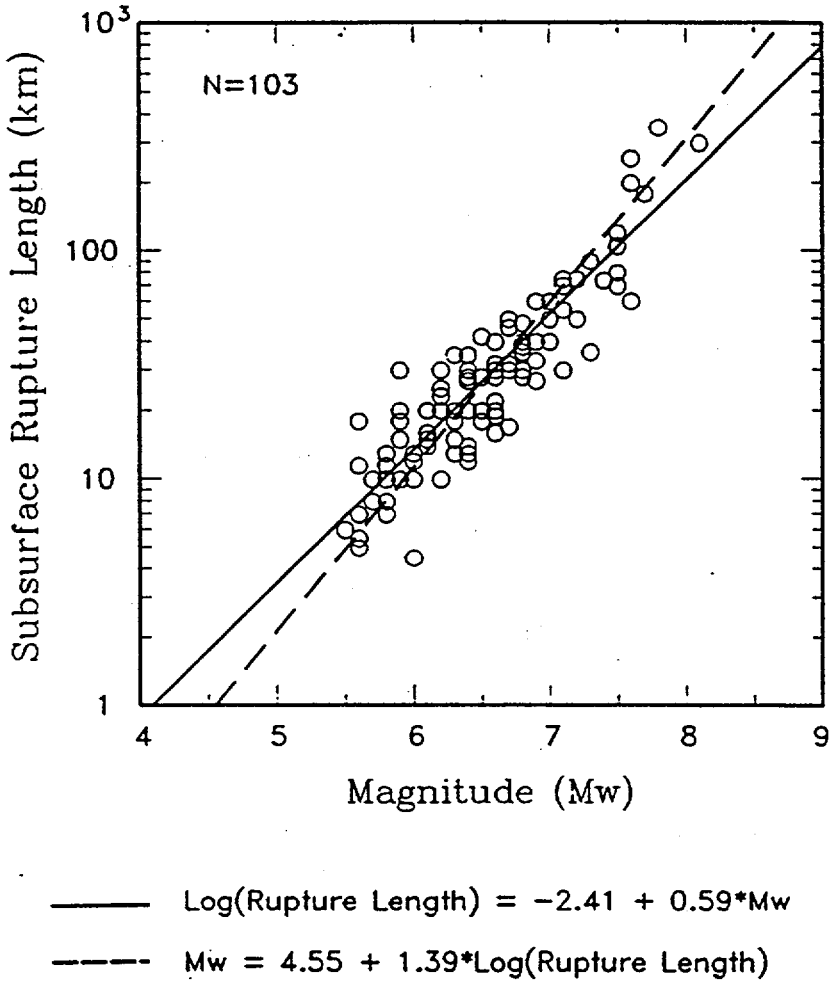

FIGURE 12. Linear regression of subsurface rupture length on moment magnitude for all slip types (from Wells and Coppersmith, in prep.). The expected subsurface rupture length for Mw 7.5 is 104 km.

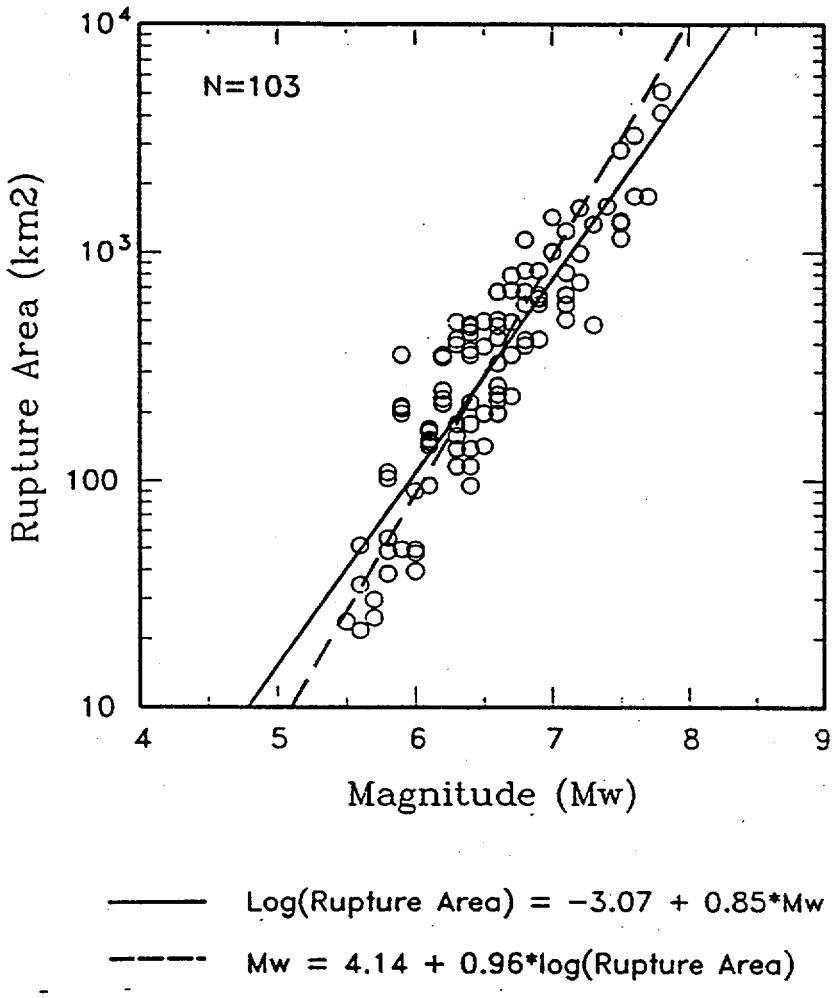

FIGURE 13. Linear regression of rupture area on moment magnitude for all slip types (from Wells and Coppersmith, in prep.). The expected rupture area for Mw 7.5 is 2,018 km2.

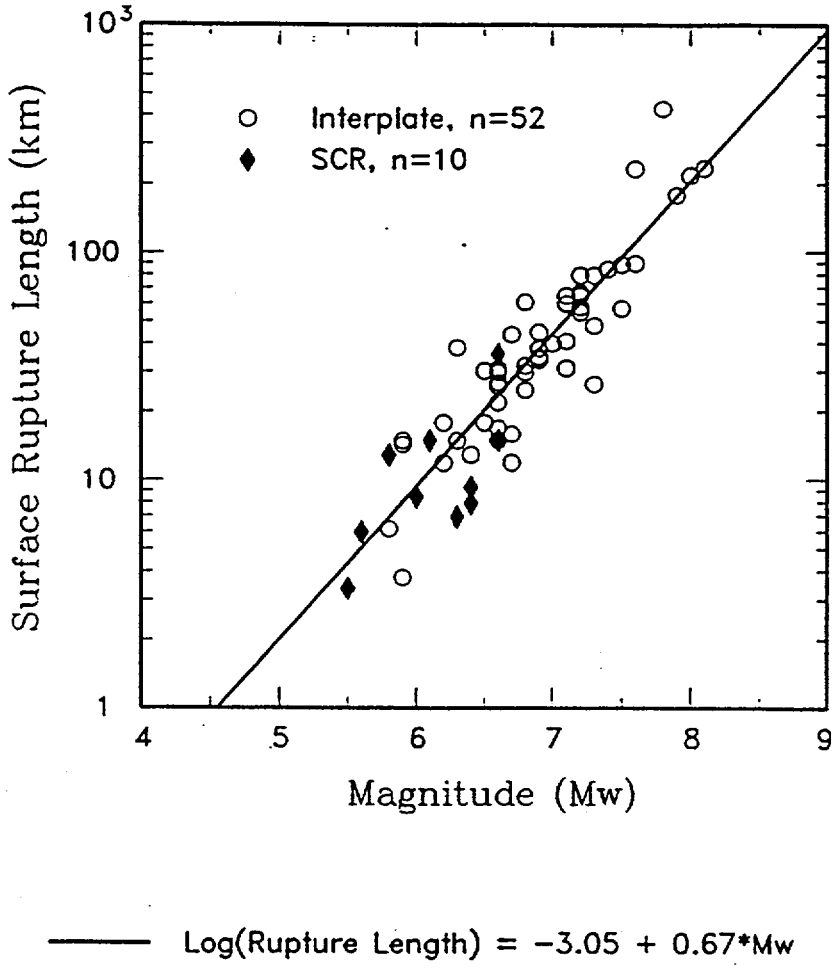

FIGURE 14. Relationship between surface rupture length and moment magnitude for interplate earthquakes and stable continental region (SCR) earthquakes (from Wells and Coppersmith, in prep.).

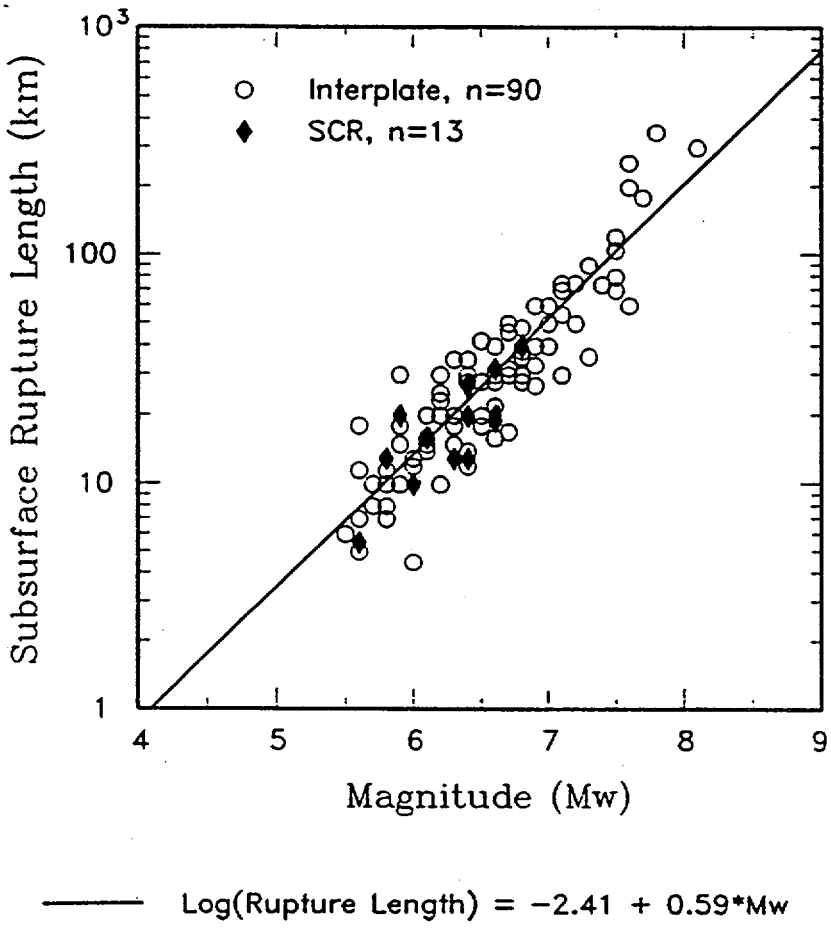

FIGURE 15. Relationship between subsurface rupture length and moment magnitude for interplate earthquakes and stable continental region (SCR) earthquakes (from Wells and Coppersmith, in prep.)

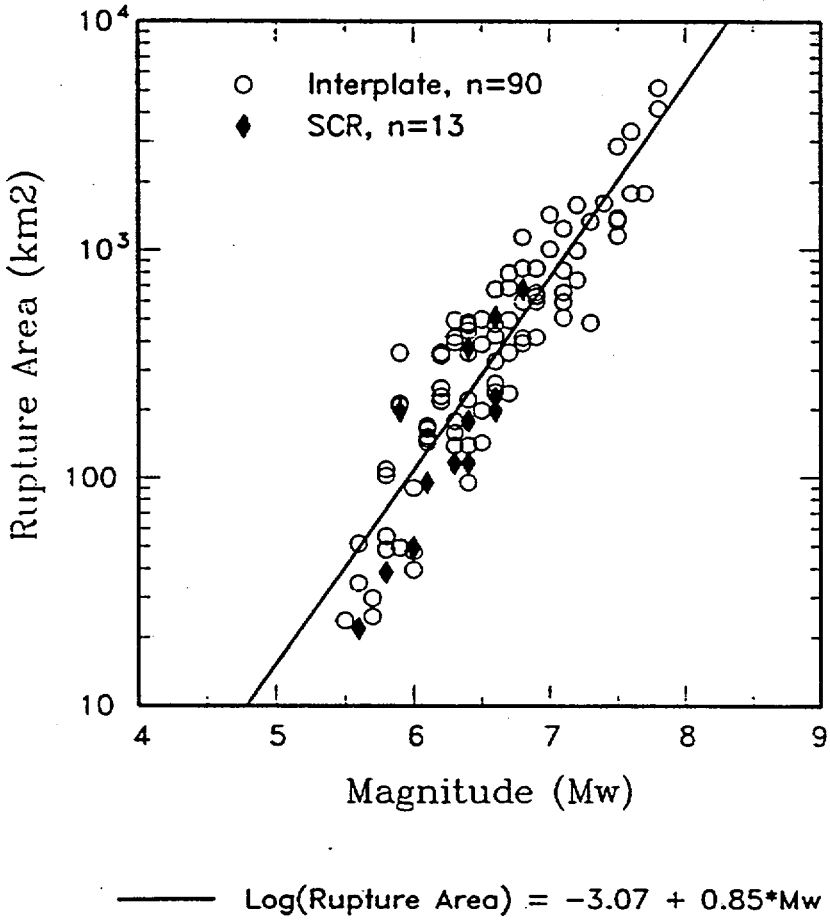

FIGURE 16. Relationship between rupture area and moment magnitude for interplate earthquakes and stable continental region (SCR) earthquakes (from Wells and Coppersmith, in prep.).

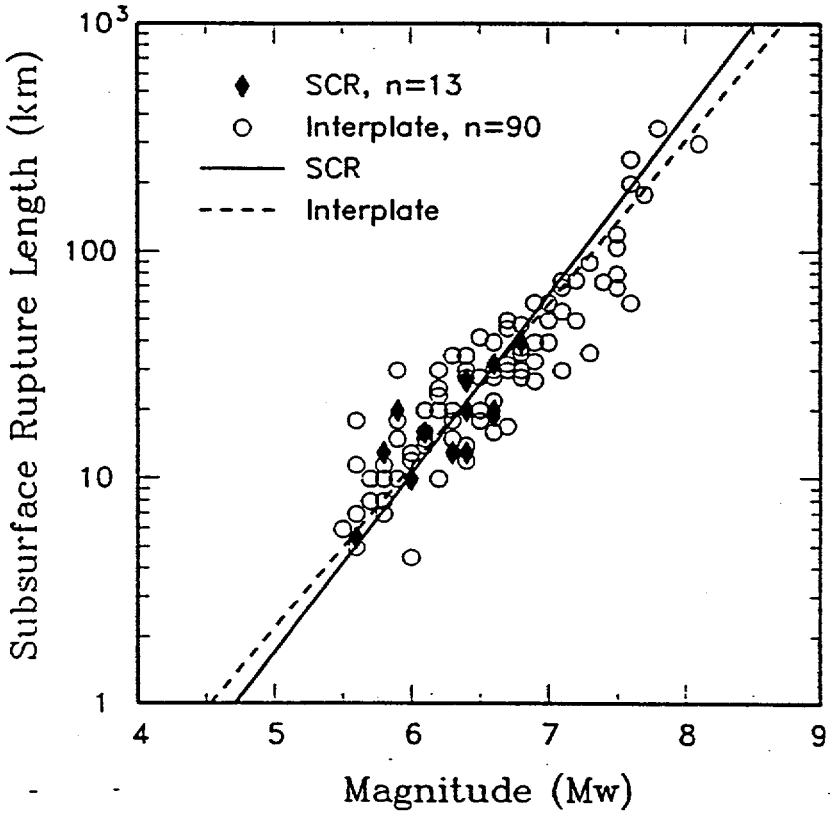

FIGURE 17. Comparison of the regressions of subsurface rupture length on moment magnitude for interplate and SCR earthquakes. Note that there is very little difference in the curves.

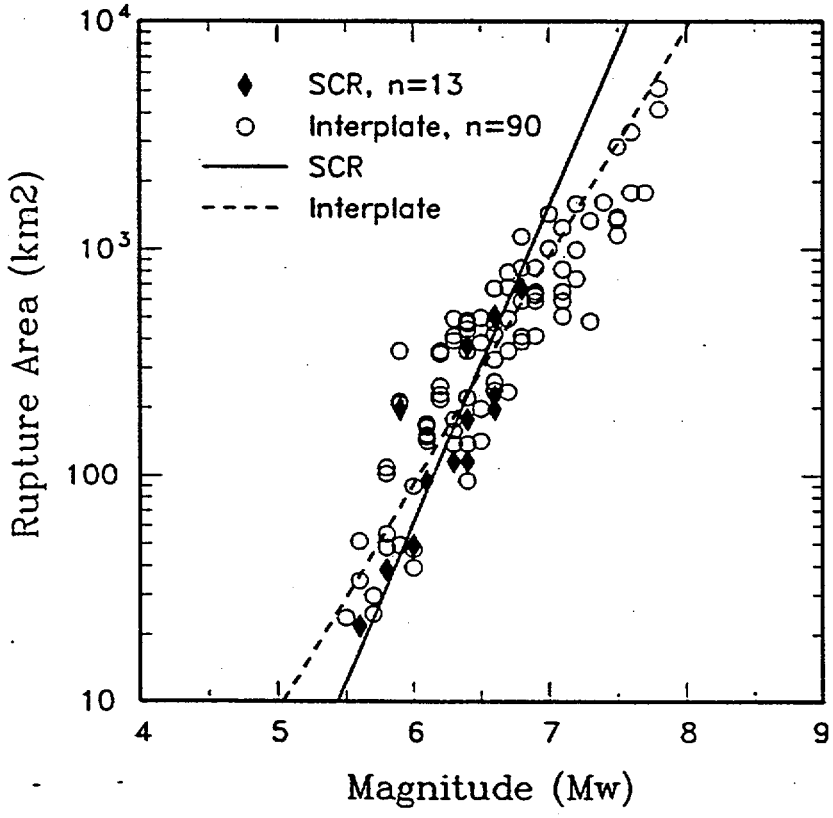

FIGURE 18. Comparison of the regressions of rupture area on moment magnitude for interplate and SCR earthquakes. Note that is very little difference in the curves.

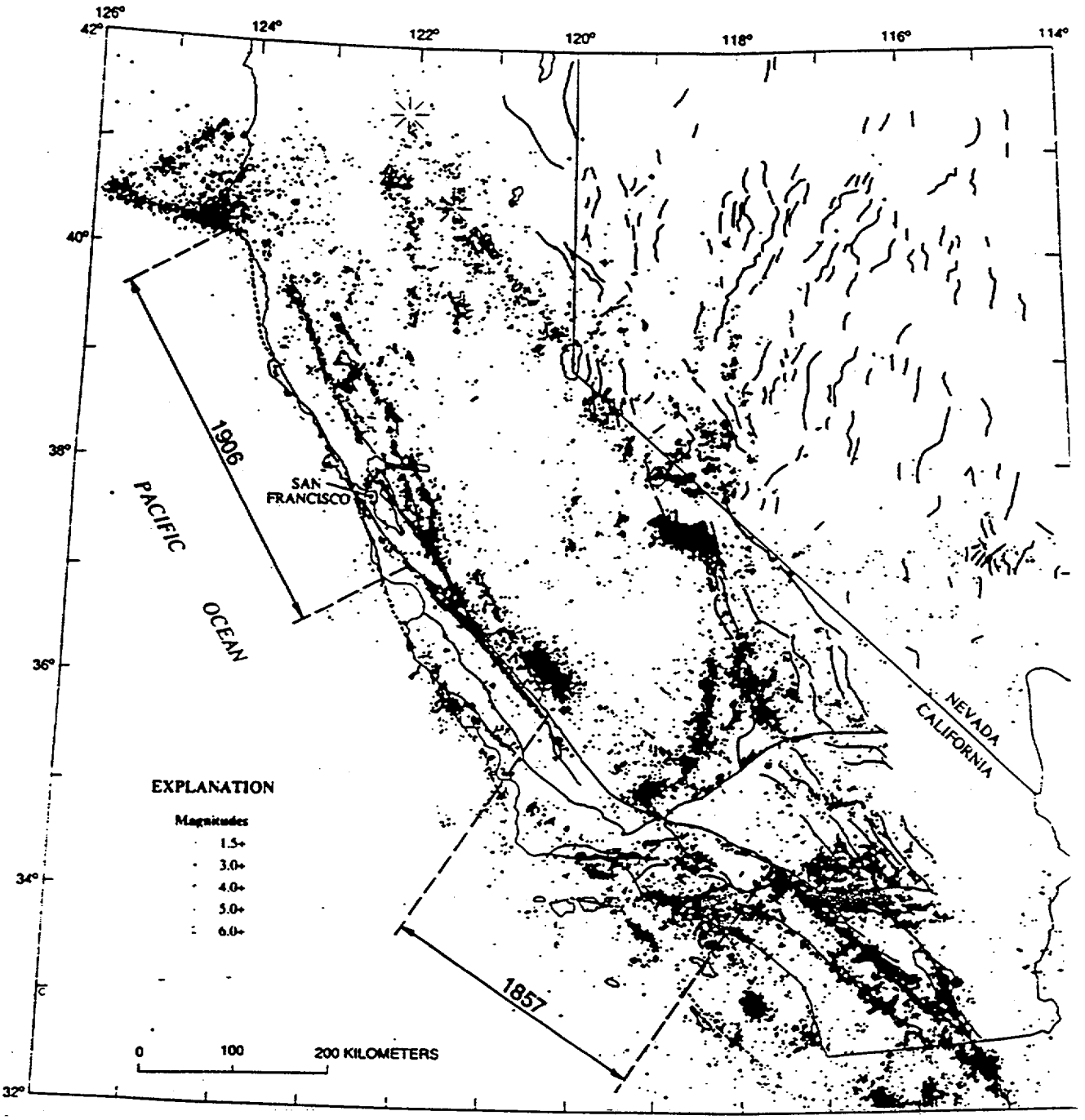

FIGURE 19. Seismicity in California and western Neveda during 1980-1986 including locations of M ≥ 1.5 earthquakes. Also shown are location of 1857 Fort Tejon and 1906 San Francisco surface ruptures, and other mapped Holocene faults (after Hill and others, 1990).

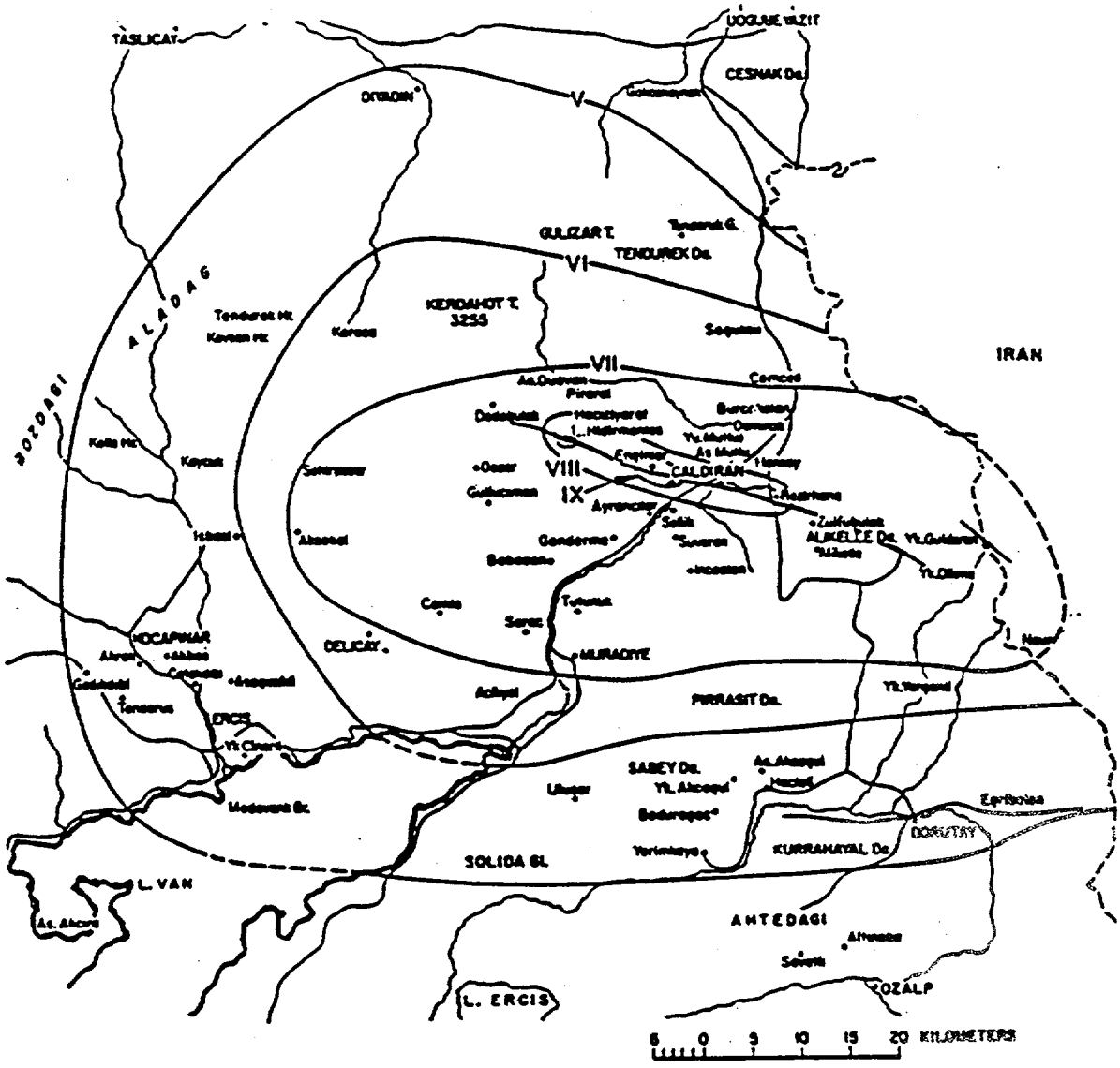

FIGURE 20. Isoseismal map of the M_w 7.2 Caldiran, Turkey, earthquake of November 24, 1976. Intensities assessed in the MSK scale (after Ambraseys, 1988).

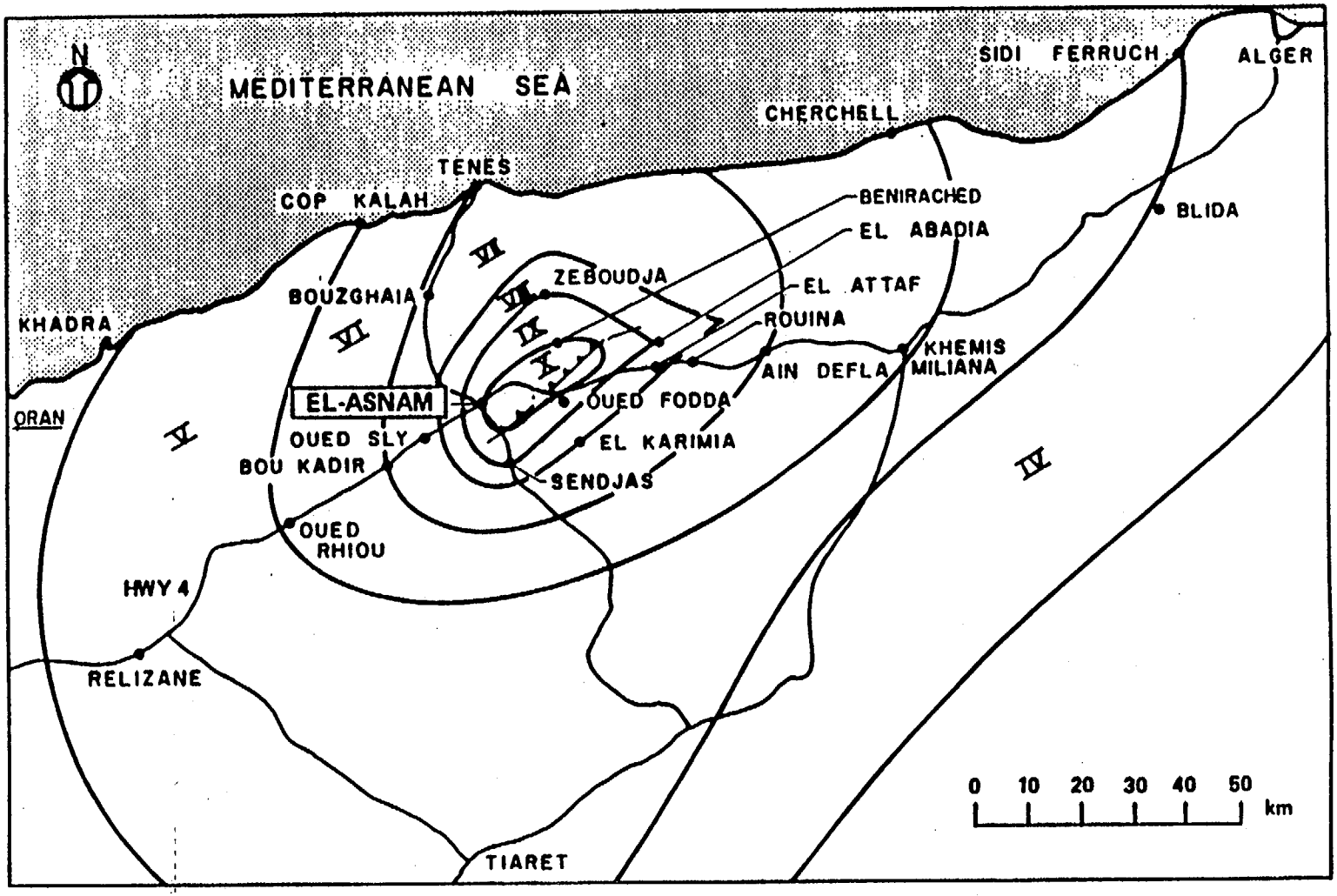

FIGURE 21. Isoseismal map of the M_w 7.1 El-Asnam, Algeria, earthquake of October 10, 1980. Isoseismals based on MMI intensitites (after Leeds, 1983).

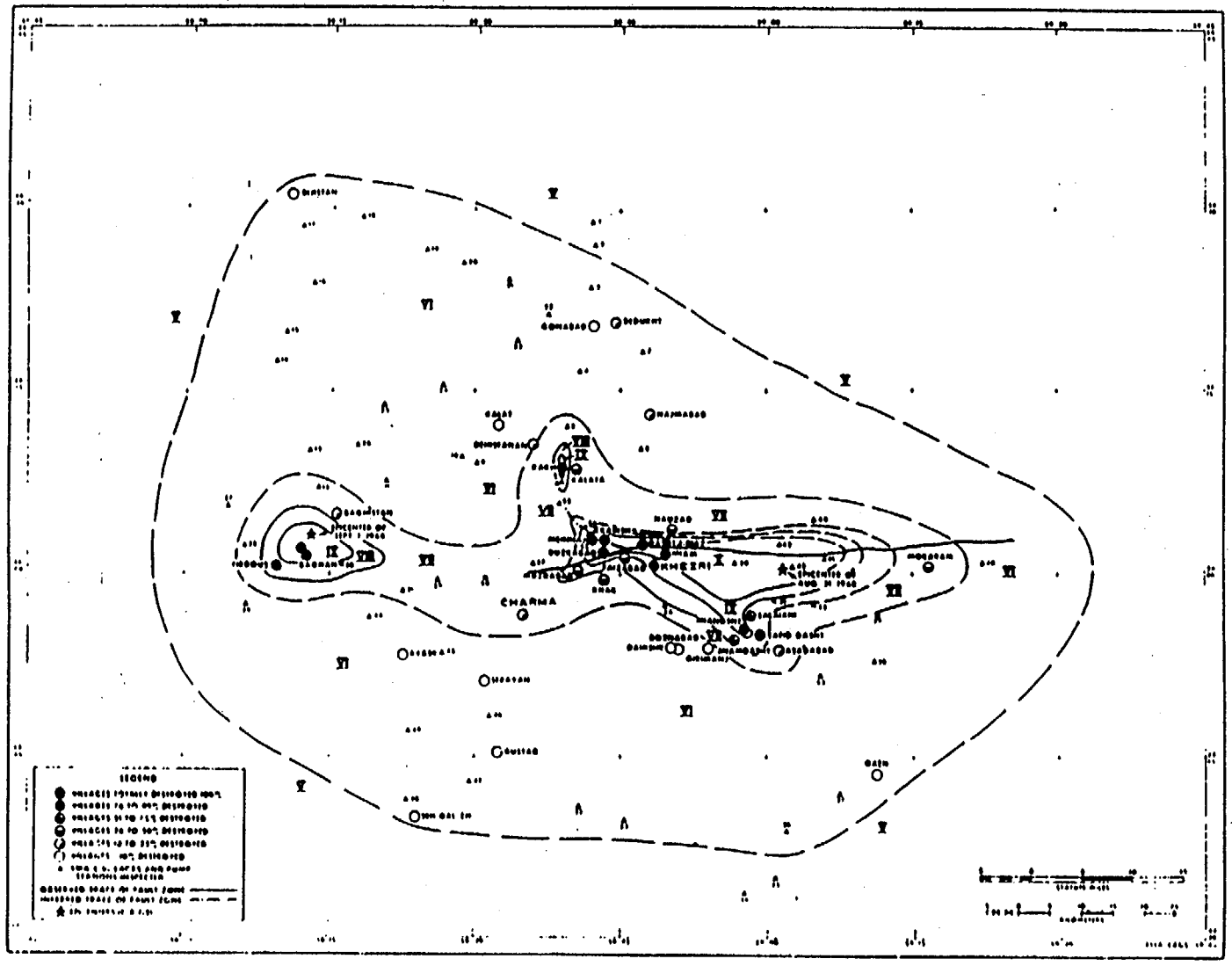

FIGURE 22. Isoseismal map of the M_W 7.2 Dash-e Bayaz, Iran, earthquake of August 31, 1968. Isoseismals based on MMI intensitites (after Bayer and others, 1969).

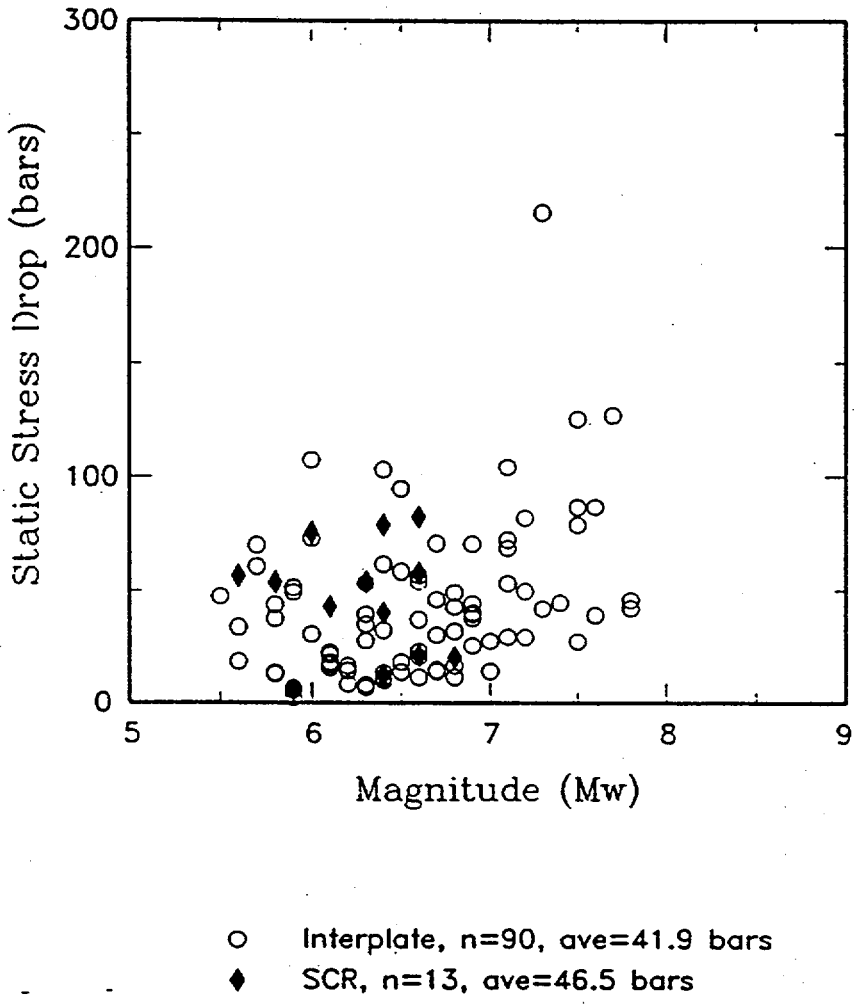

FIGURE 23. Plot of static stress drop as a function of moment magnitude for interplate and SCR earthquakes. Static stress drop was calculated based on observed rupture areas and instrumental seismic moments. The average static drops for interplate and SCR earthquakes are given and are approximately equivalent.

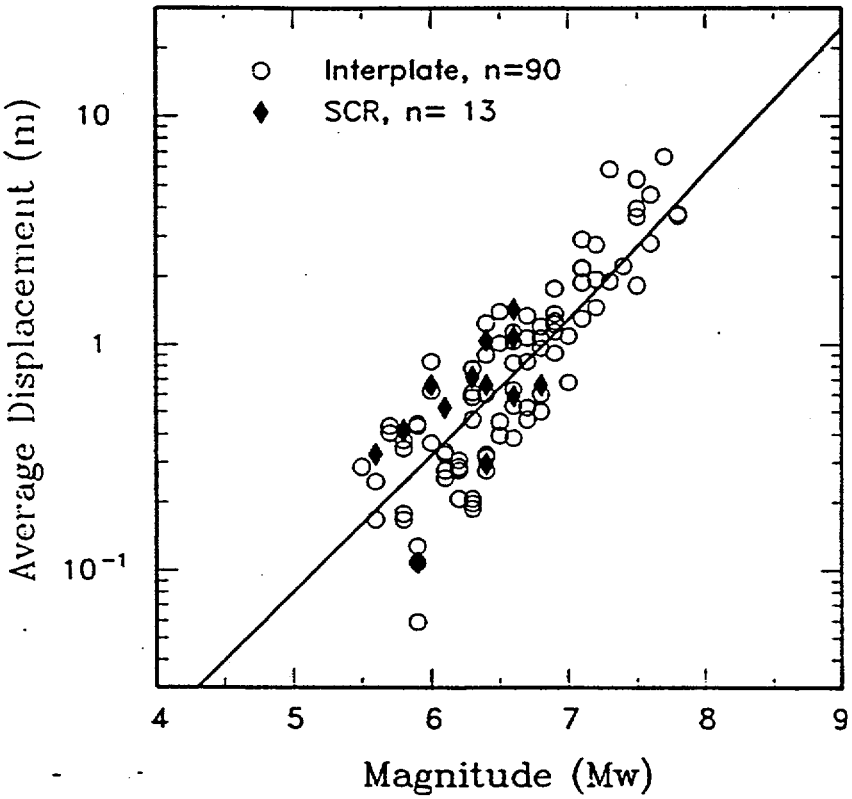

FIGURE 24. Relationship between calculated average displacement and moment magnitude for interplate and SCR earthquakes. Average displacement was calculated based on observed rupture area and instrumental seismic moments. The expected average displacement for Mw 7.5 is about 2.7 m.

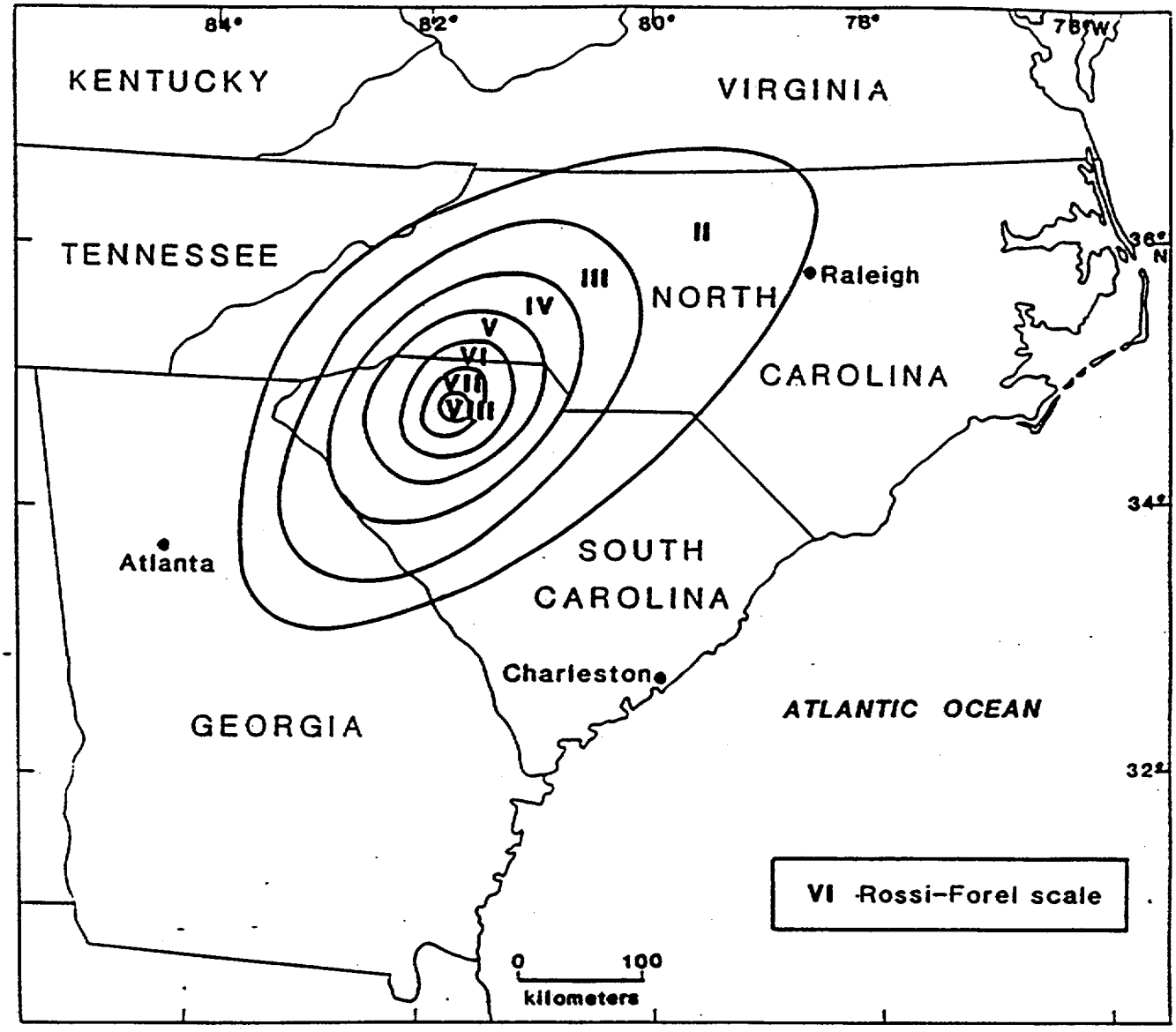

FIGURE 25. Isoseismal map of the Union County earthquake, South Carolina, January 1, 1913 (after Visvanathan, 1980).

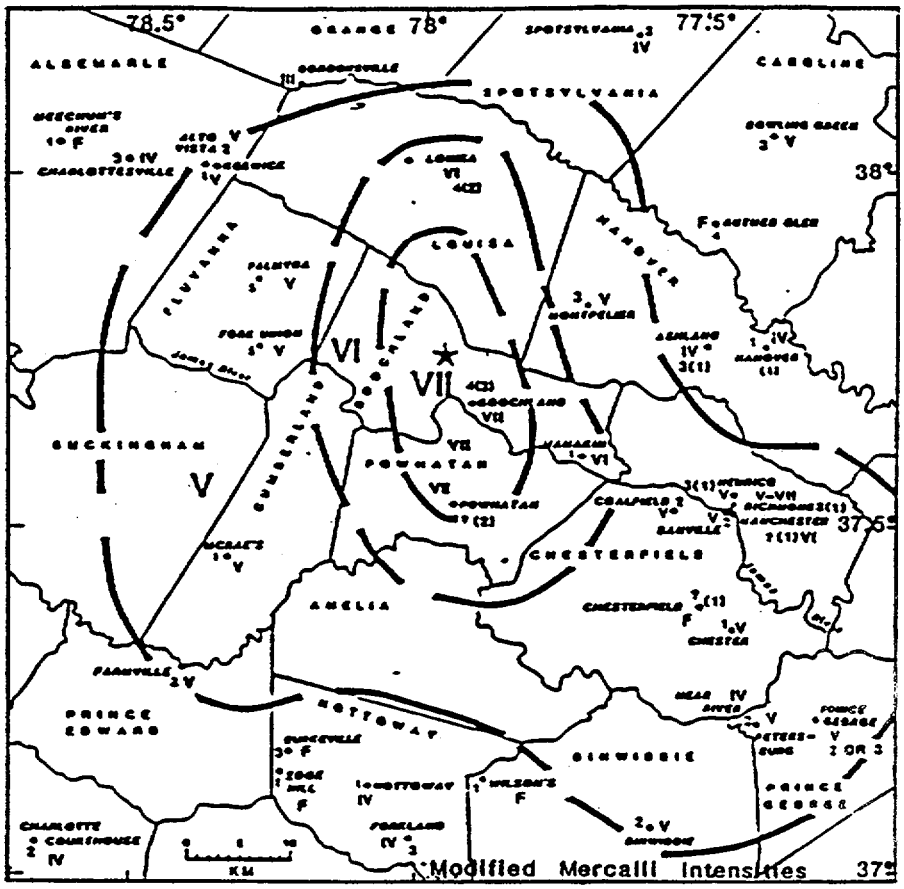

FIGURE 26. Isoseismal map for the Goochland County, central Virginia earthquake, December 22, 1875. Arabic numbers indicate the number of shocks (main shock and aftershocks) felt on the evening of December 22-23, 1875. The Arabic numerals in parentheses indicate later occurring aftershocks. The epicenter is indicated by the star symbol (from Oaks and Bollinger, 1986).

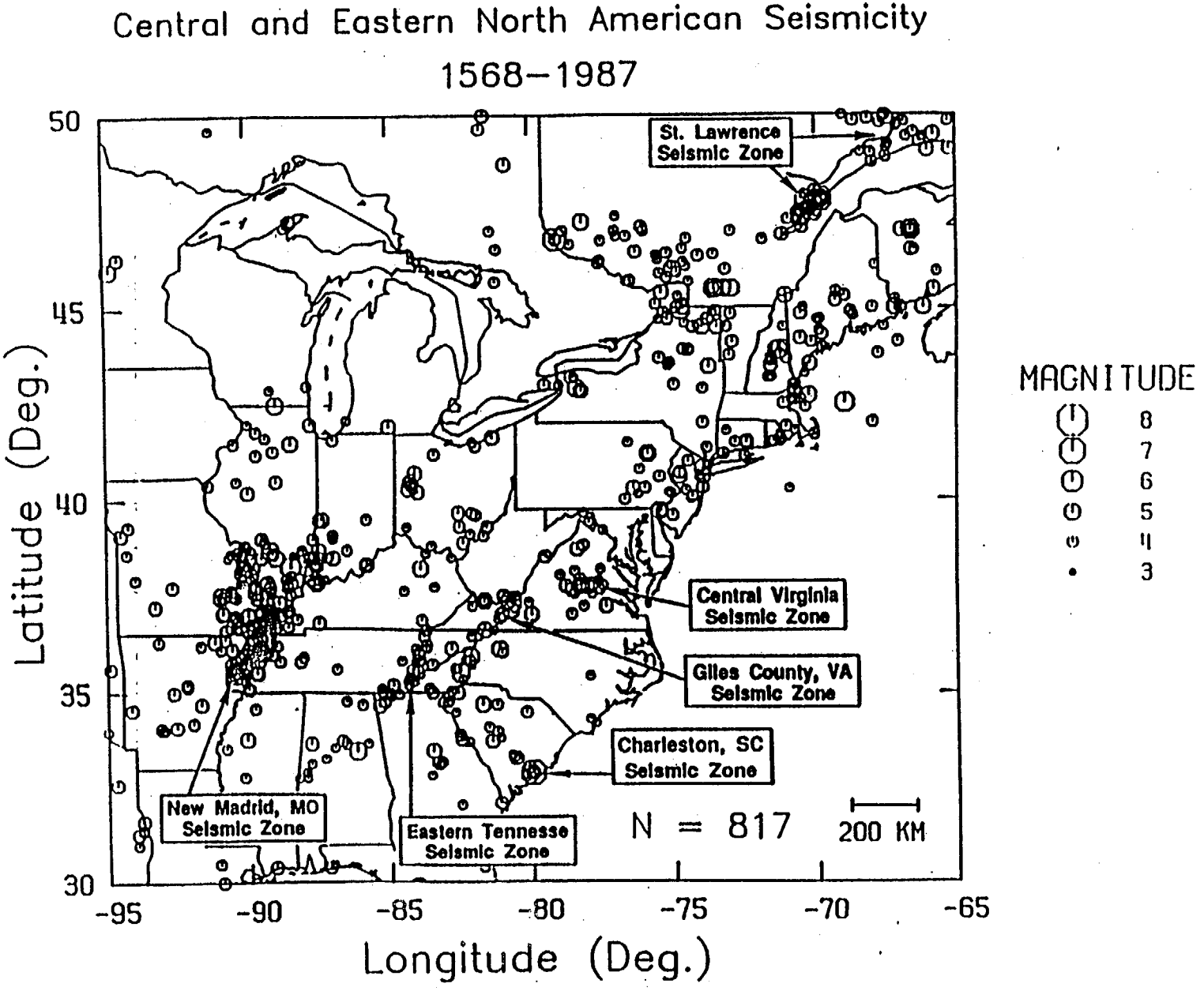
Central and Eastern North American Seismicity
1568–1987
St. Lawrence Seismic Zone
Central Virginia Seismic Zone
Giles County, VA Seismic Zone
Charleston, SC Seismic Zone
New Madrid, MO Seismic Zone
Eastern Tennesse Seismic Zone
N = 817
200 KM
MAGNITUDE
8
7
6
5
4
3
Latitude (Deg.)
Longitude (Deg.)
50
45
40
35
30
-95
-90
-85
-80
-75
-70
-65

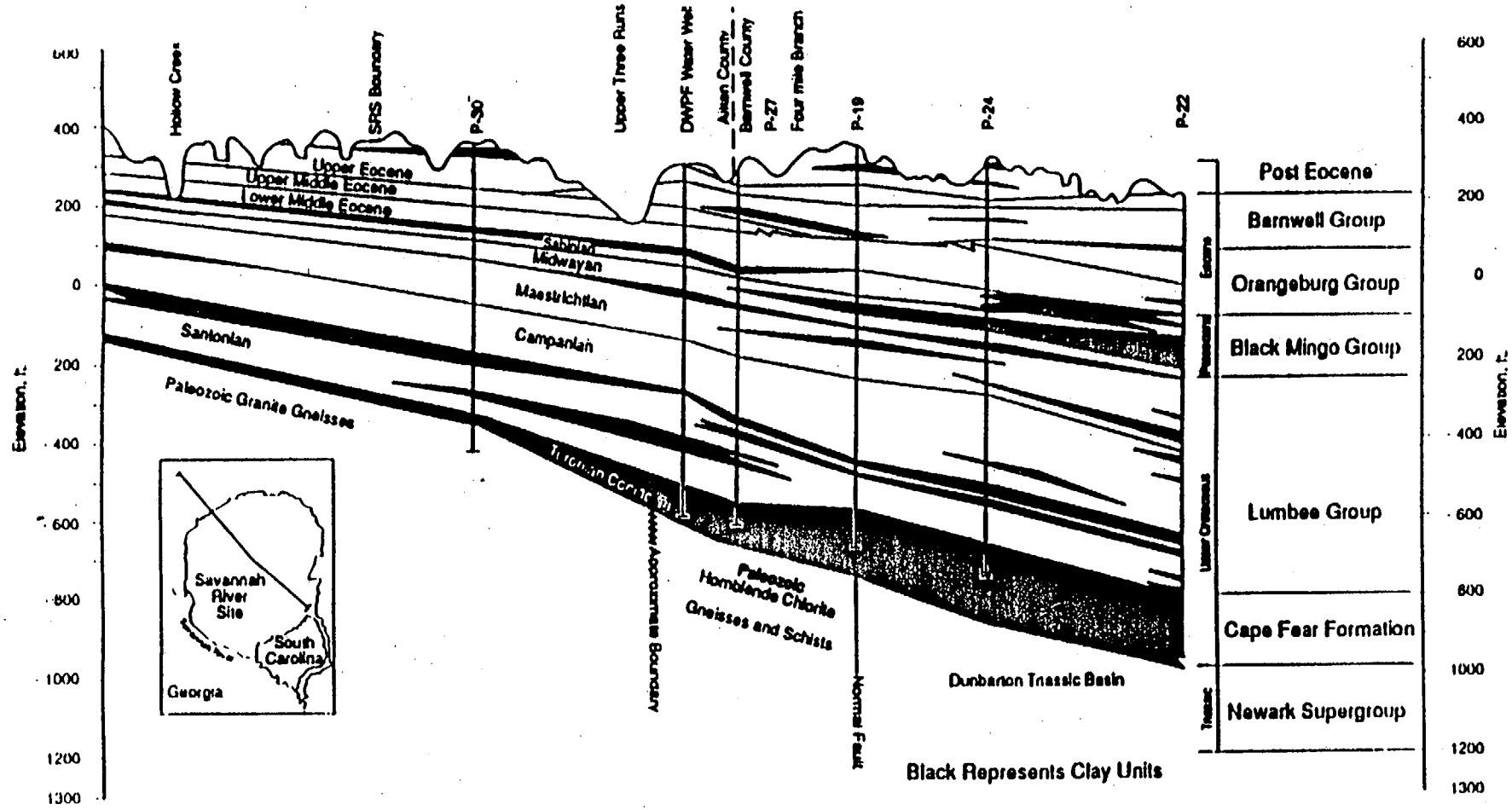

FIGURE 28. Generalized geologic cross section across SRS. (From WSRC, 1990.)

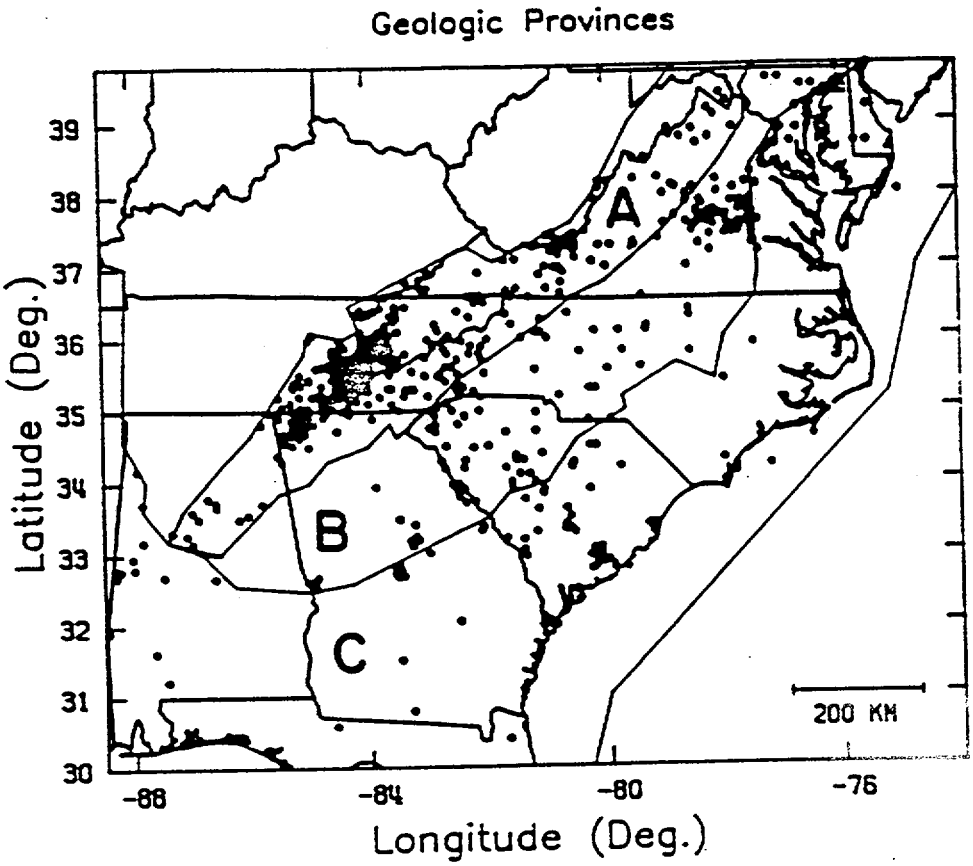

FIGURE 29. Tectonic provinces in the southeastern U.S. A denotes the Valley and Ridge and Blue Ridge, B is the Piedmont, and C is the Coastal Plain (from Bollinger et al., 1989).

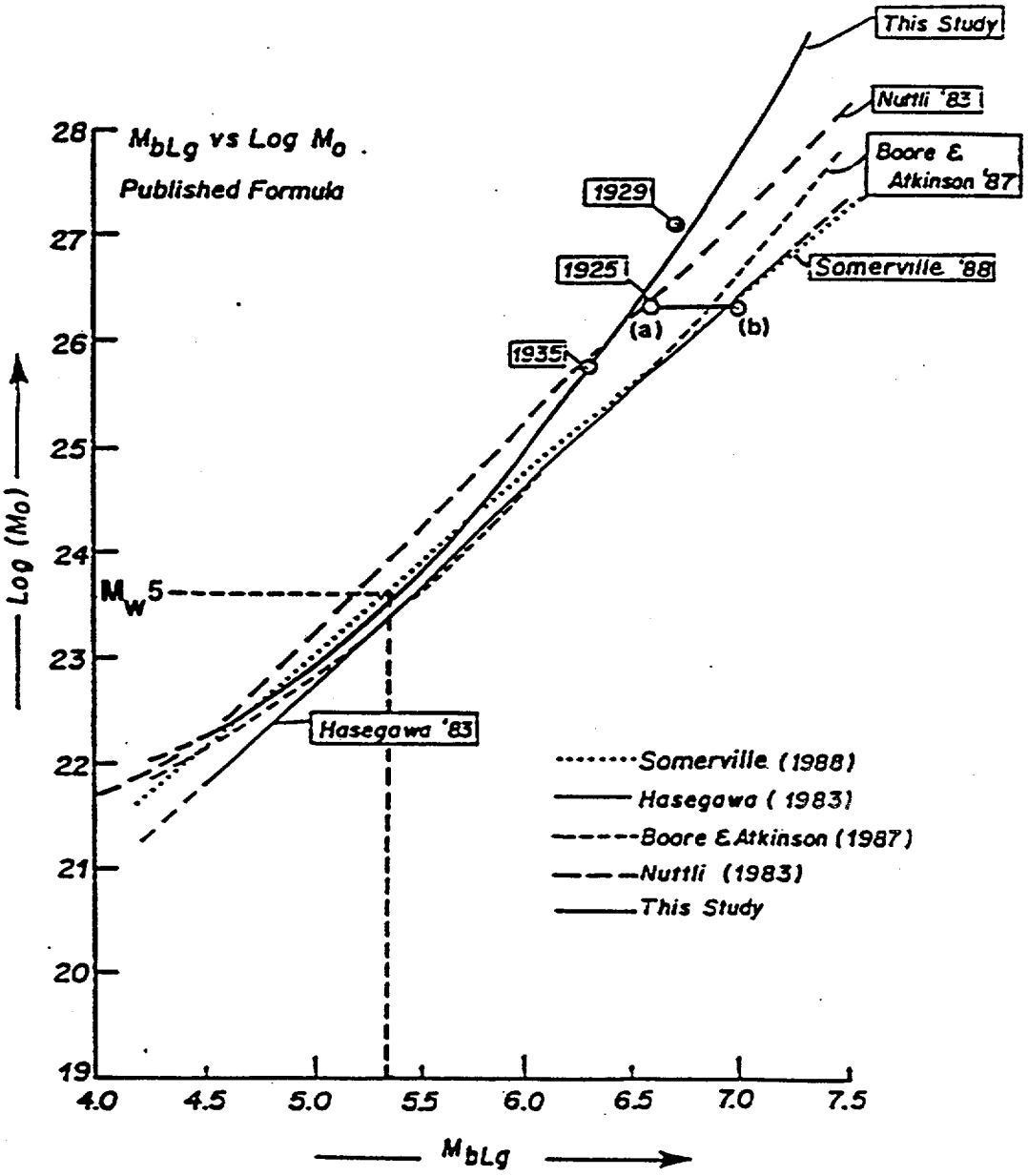

FIGURE 30. A comparison of the T = 1 sec logMo - M_{bLg} formula in Coppersmith and Johnston (in preparation) with other published formulas. Note that a moment magnitude M_w 5 corresponds to approximately an m_{bLg} 5.3. (Modified from Johnston, in preparation.)

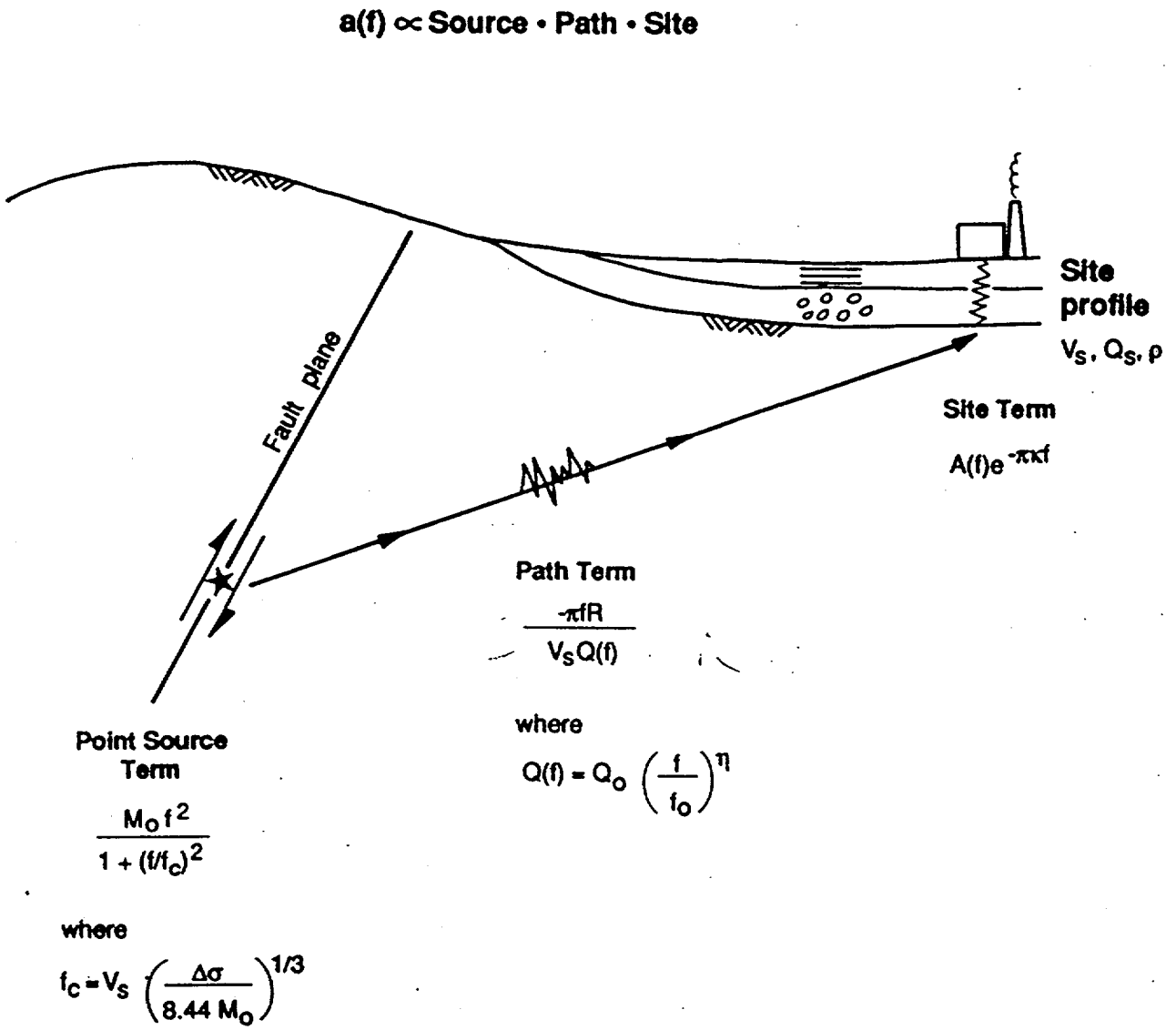

FIGURE 31. Schematic diagram of band-limited-white-noise/random vibration theory (BLWN/RVT) model.

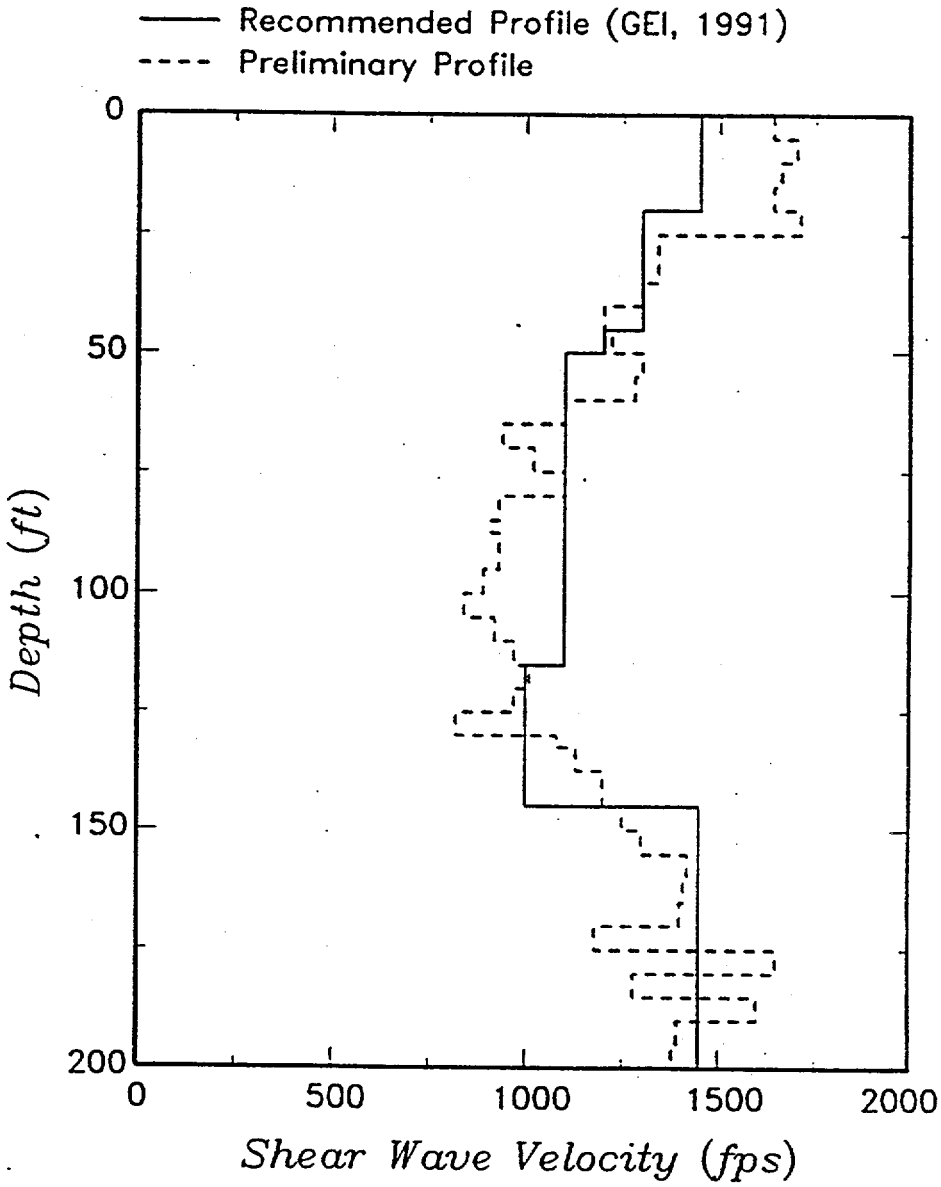

FIGURE 32. Shear wave velocity profile for K-Reactor (GEI, 1991). Dashed line shows velocity profile in 0 to 200 ft depth range used in draft report.

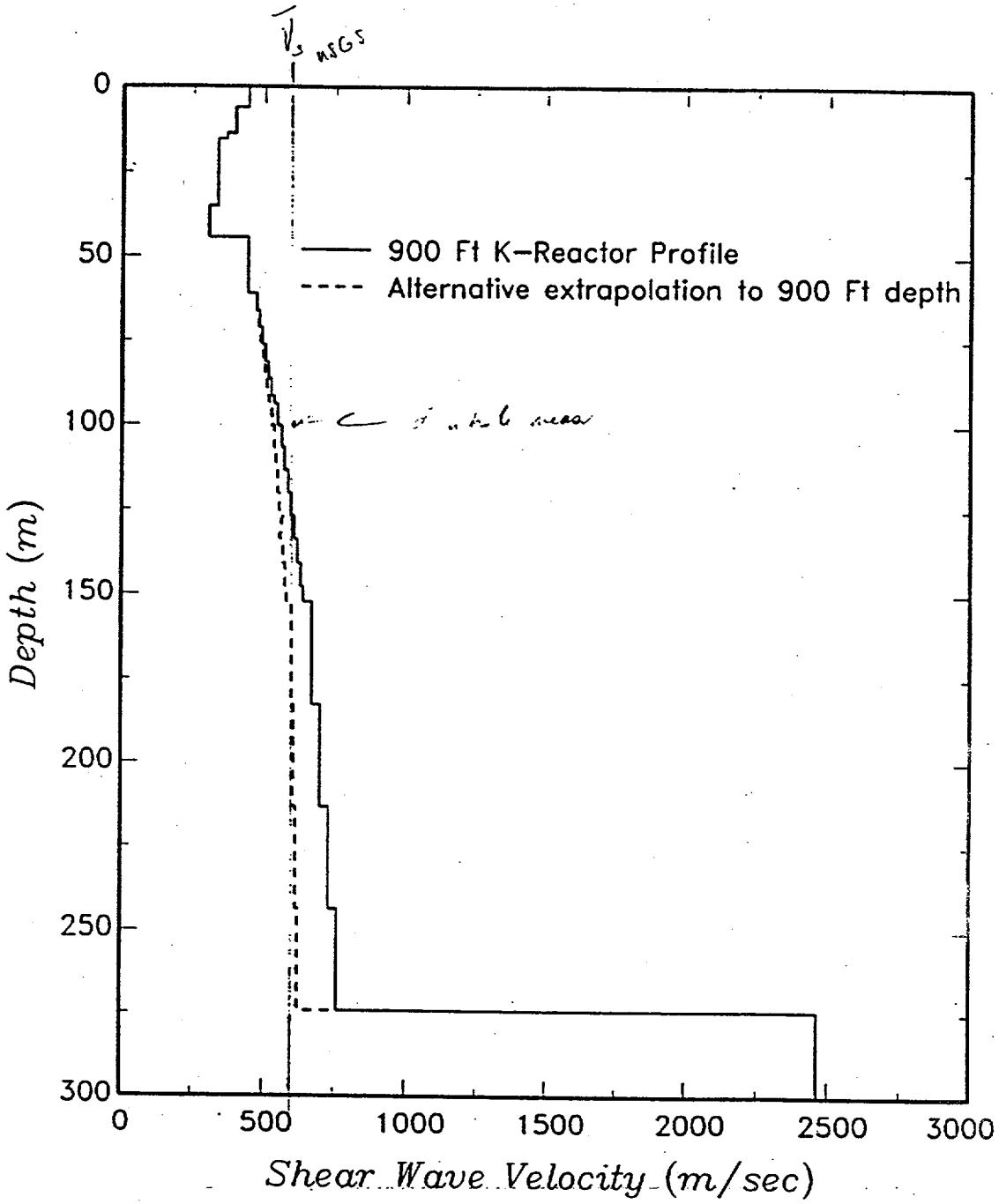

FIGURE 33. Average shear wave velocity profile use for K-Reactor site in depth range of 0 to 900 ft (274m). Dashed curve shows alternative extrapolation of shear wave velocity below measures data.

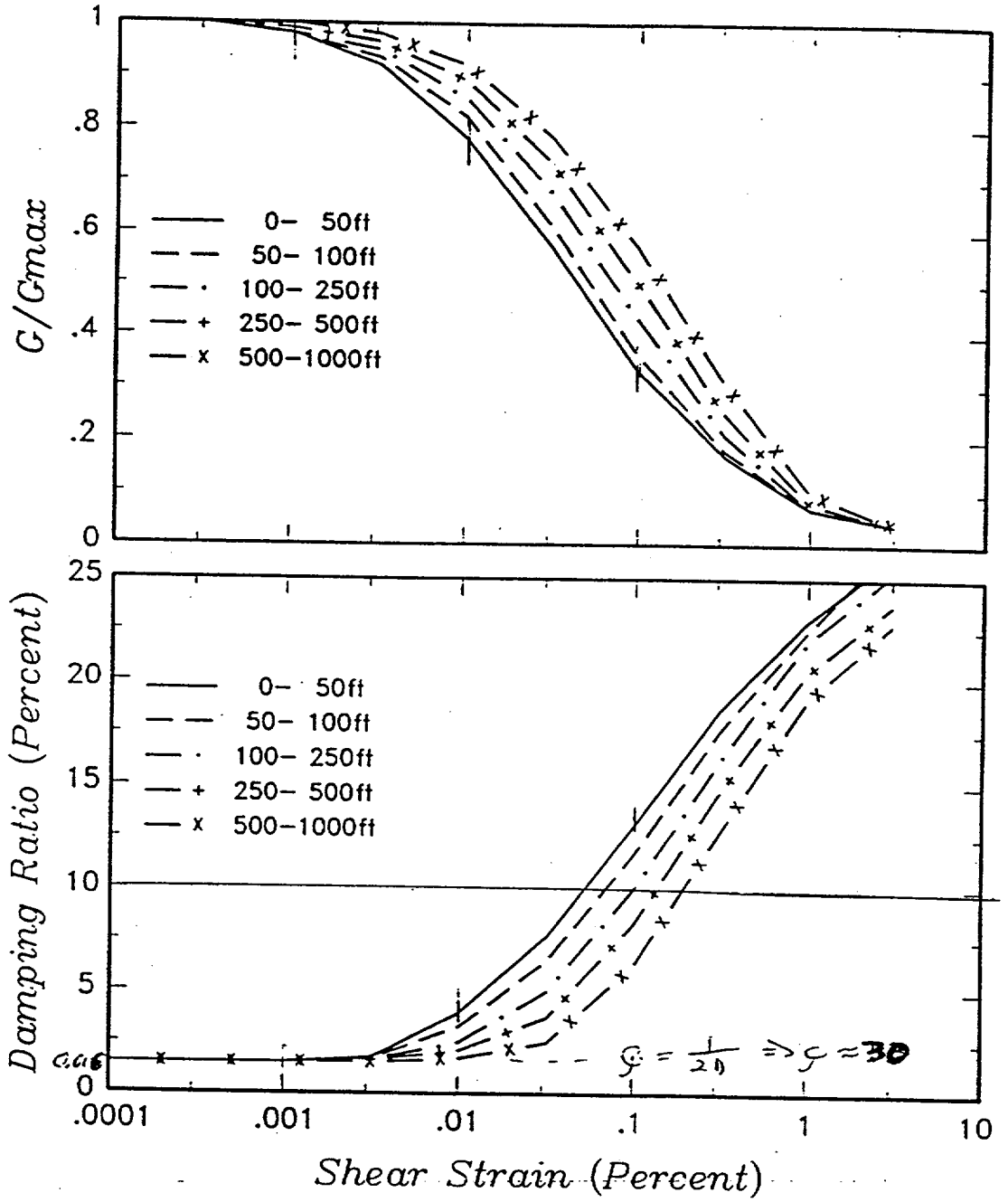

FIGURE 34. Strain-compatible shear modulus and damping ratio relationships used to model the soils at the K-Reactor site (from GEI, 1991).

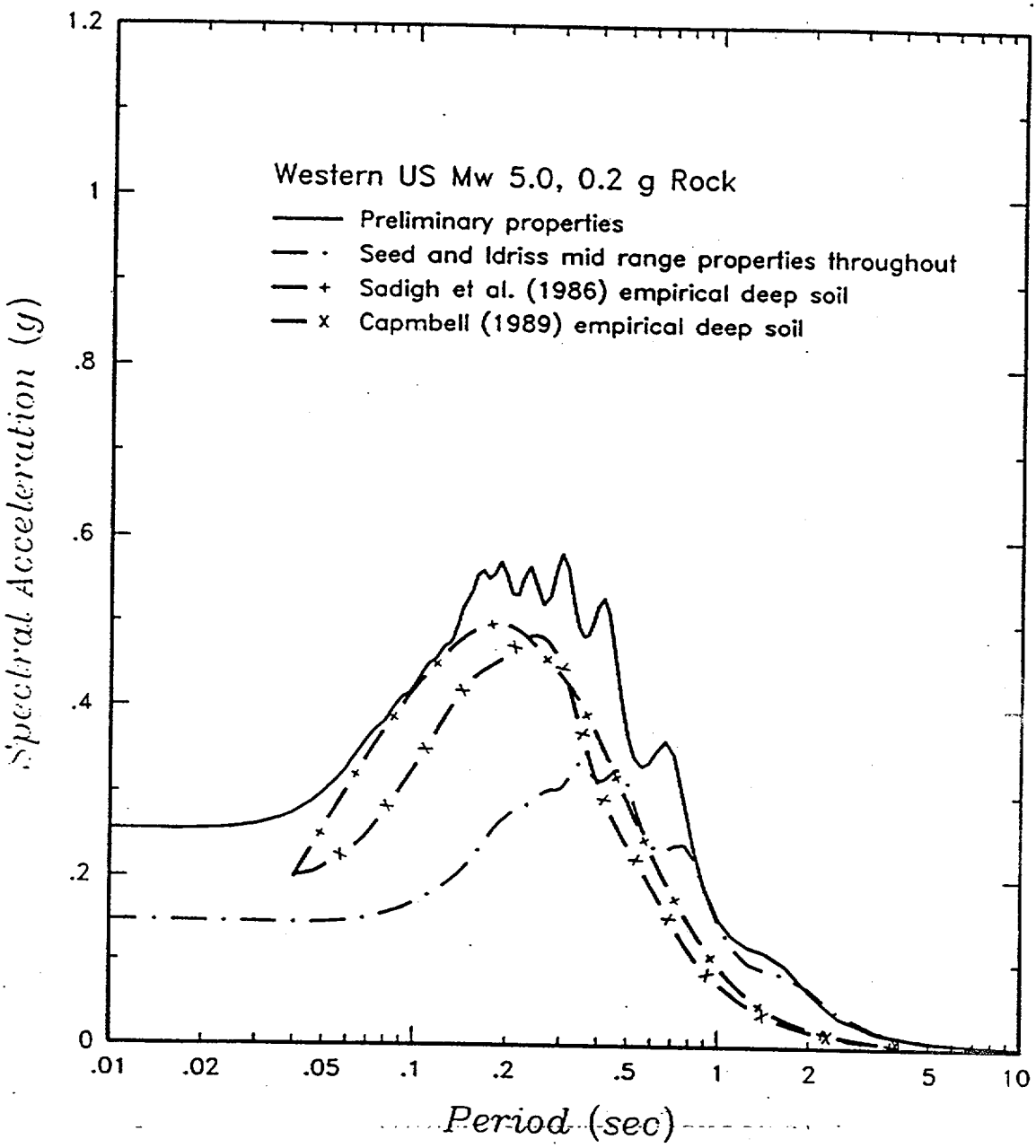

FIGURE 35. Effect of choice of modulus reduction and damping relationships on computed deep soil site ground motions for western US base rock velocity and input rock motion.

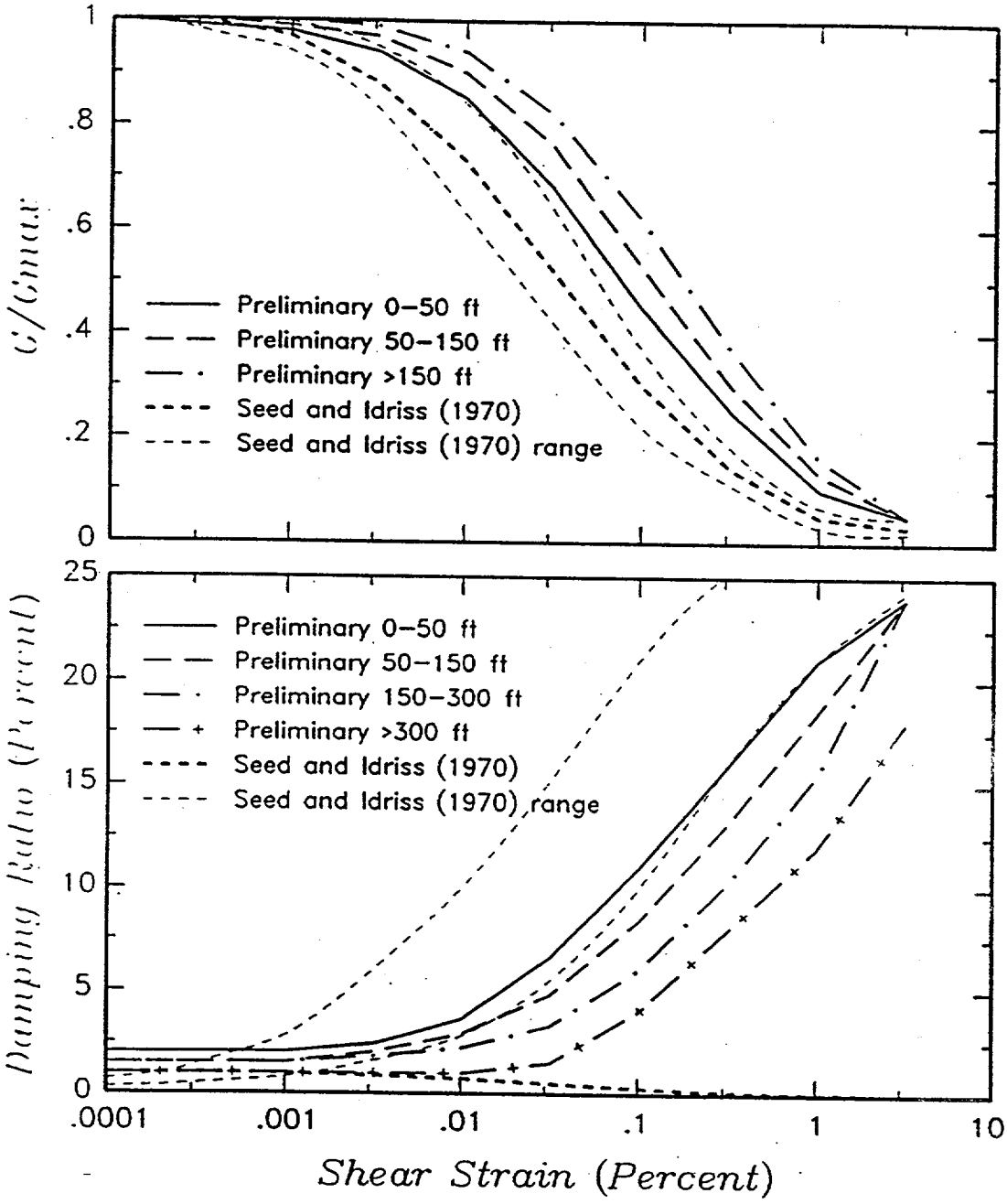

FIGURE 36. Comparison of preliminary shear modulus reduction and damping relationships for K-Reactor (Geomatrix, 1991) with those proposed by Seed and Idriss (1970).

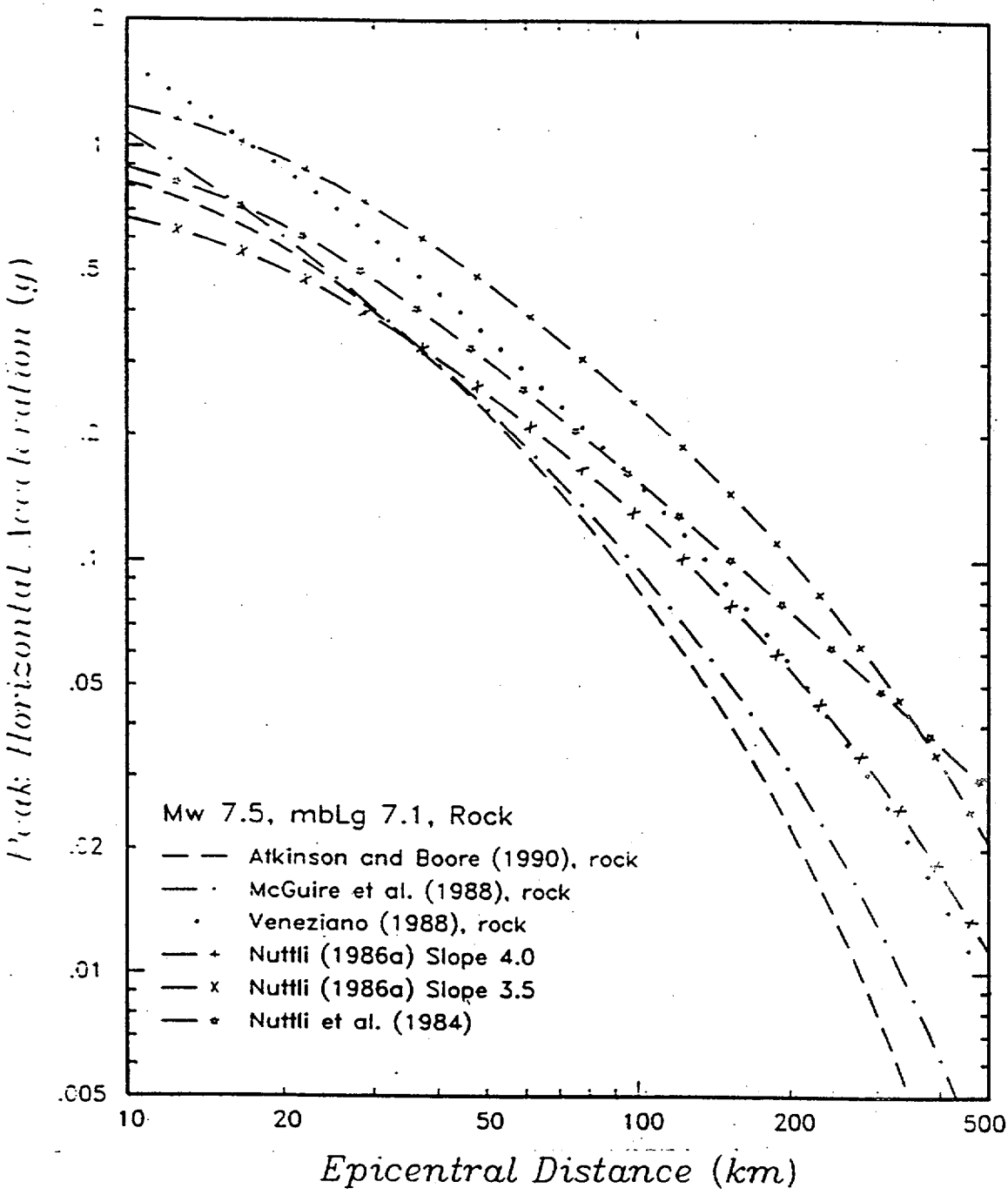

FIGURE 37. Published attenuation relationships for peak acceleration on rock (or undifferentiated sites) for a Charleston source M 7.5 earthquake (m_{bLg} 7.1).

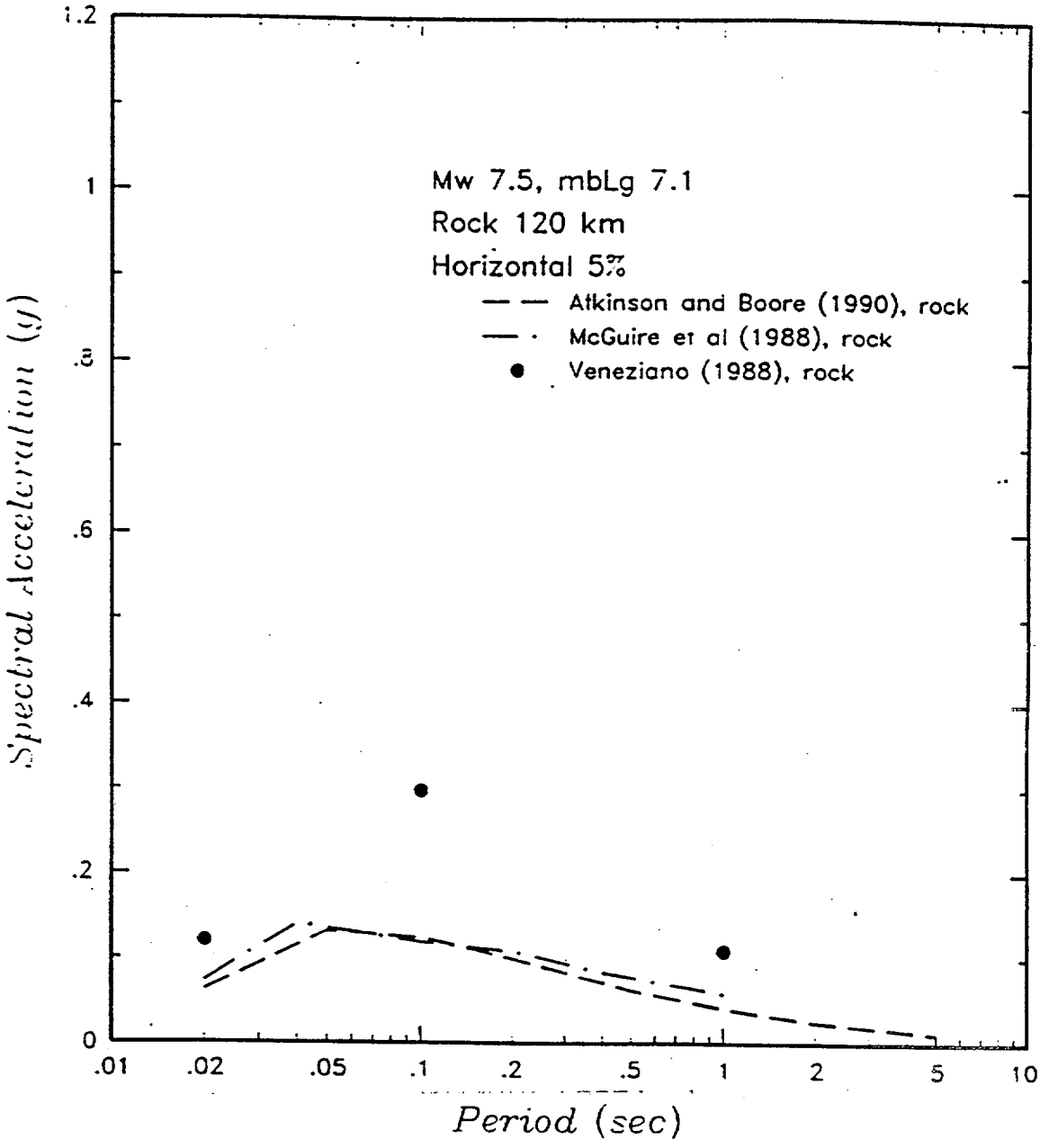

FIGURE 38. Predicted median response spectra on rock for a Charleston source M 7.5 earthquake at a distance of 120 km.

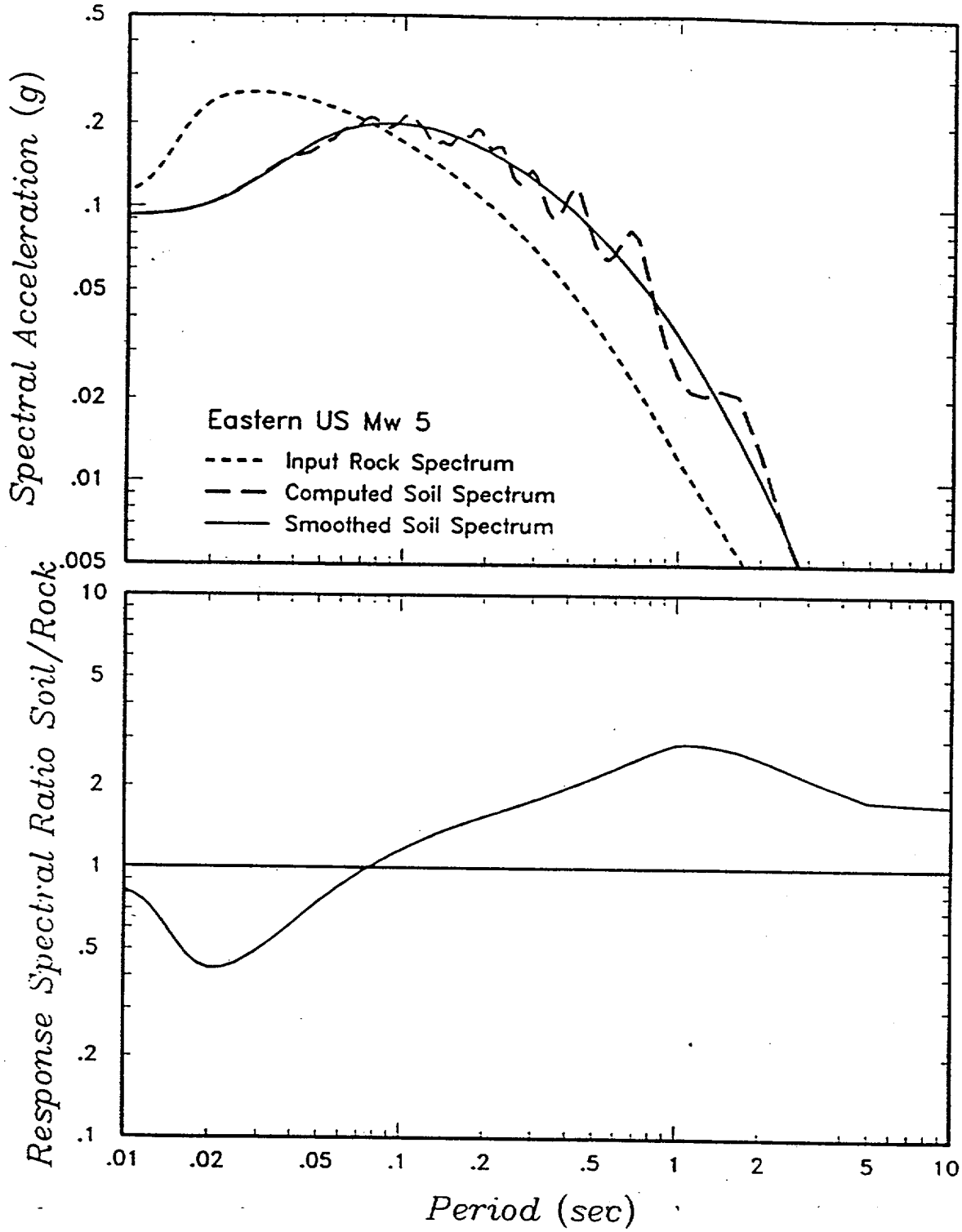

FIGURE 39. Computation of soil/rock response spectral ratios for eastern US motions. Shown in the top plot are the input rock motion spectrum, the computed soil spectrum, and a smoothed soil spectrum. Bottom plot shows ratio of smoothed soil spectrum to rock spectrum.

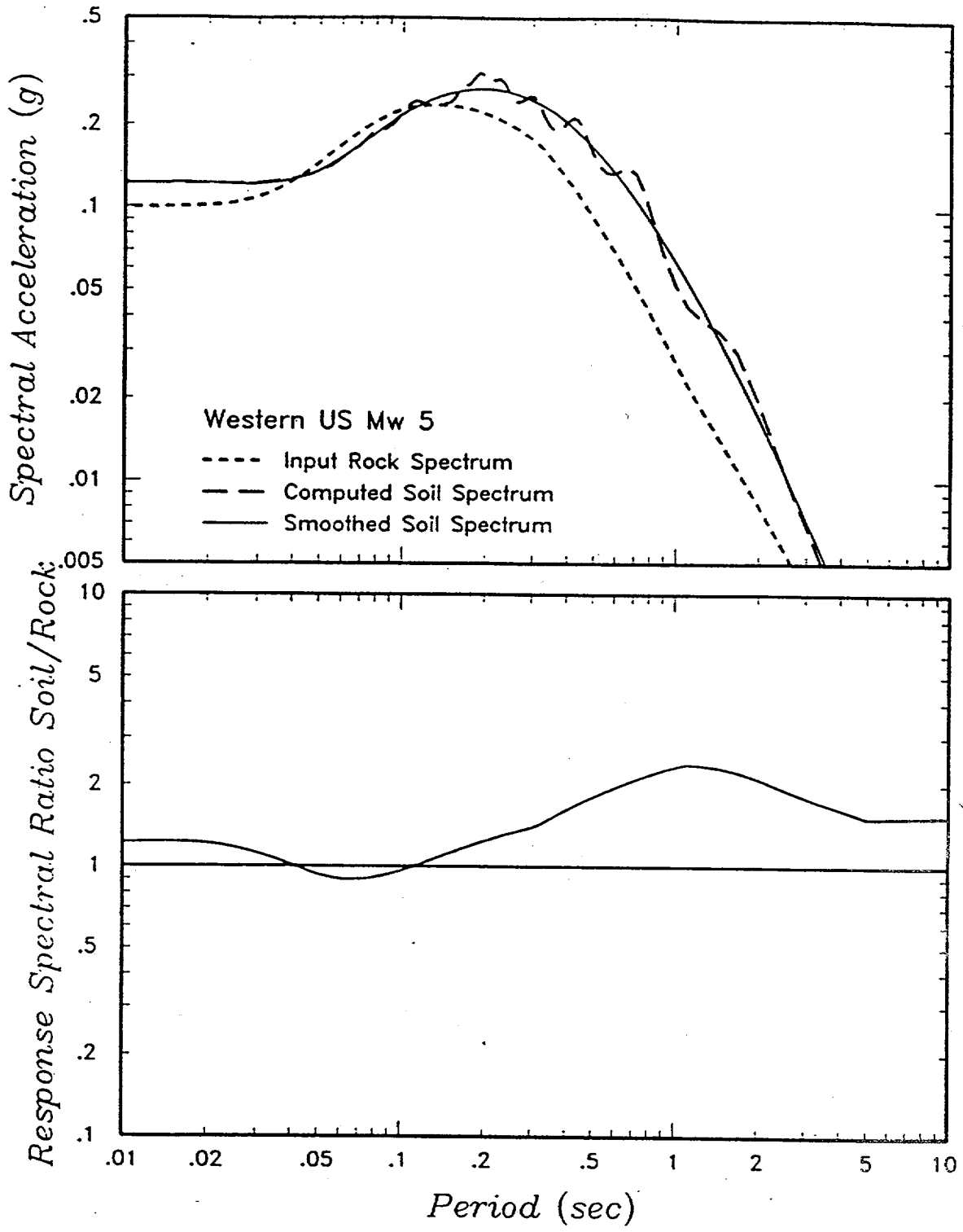

FIGURE 40. Computation of soil/rock response spectral ratios for western US motions. Shown in the top plot are the input rock motion spectrum, the computed soil spectrum, and a smoothed soil spectrum. Bottom plot shows ratio of smoothed soil spectrum to rock spectrum.

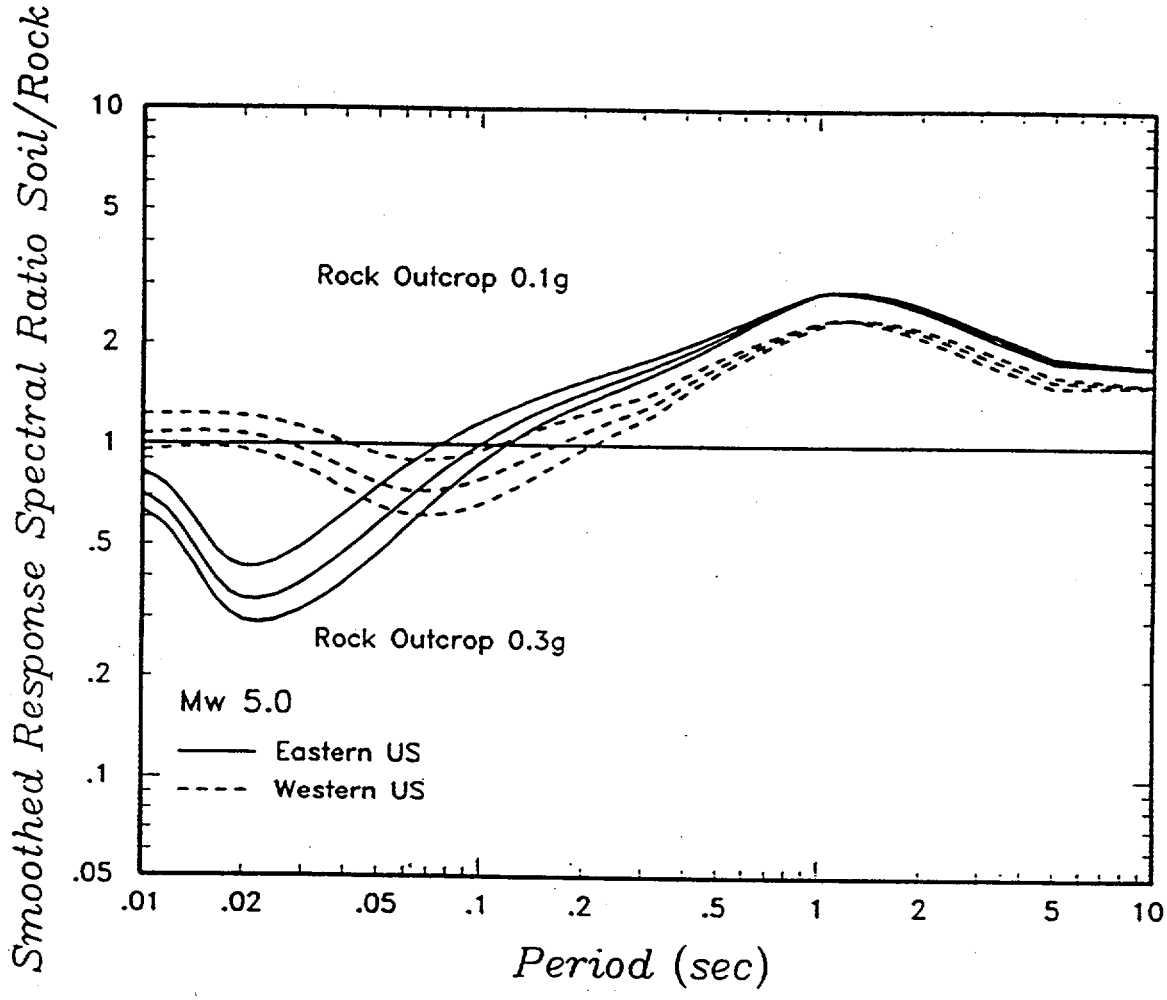

FIGURE 41. Smoothed soil/rock response spectral ratios for eastern and western US M 5 ground motions and corresponding eastern and western US rock velocities for K-Reactor soil profile. Input rock motion levels are 0.1, 0.2, and 0.3 g.

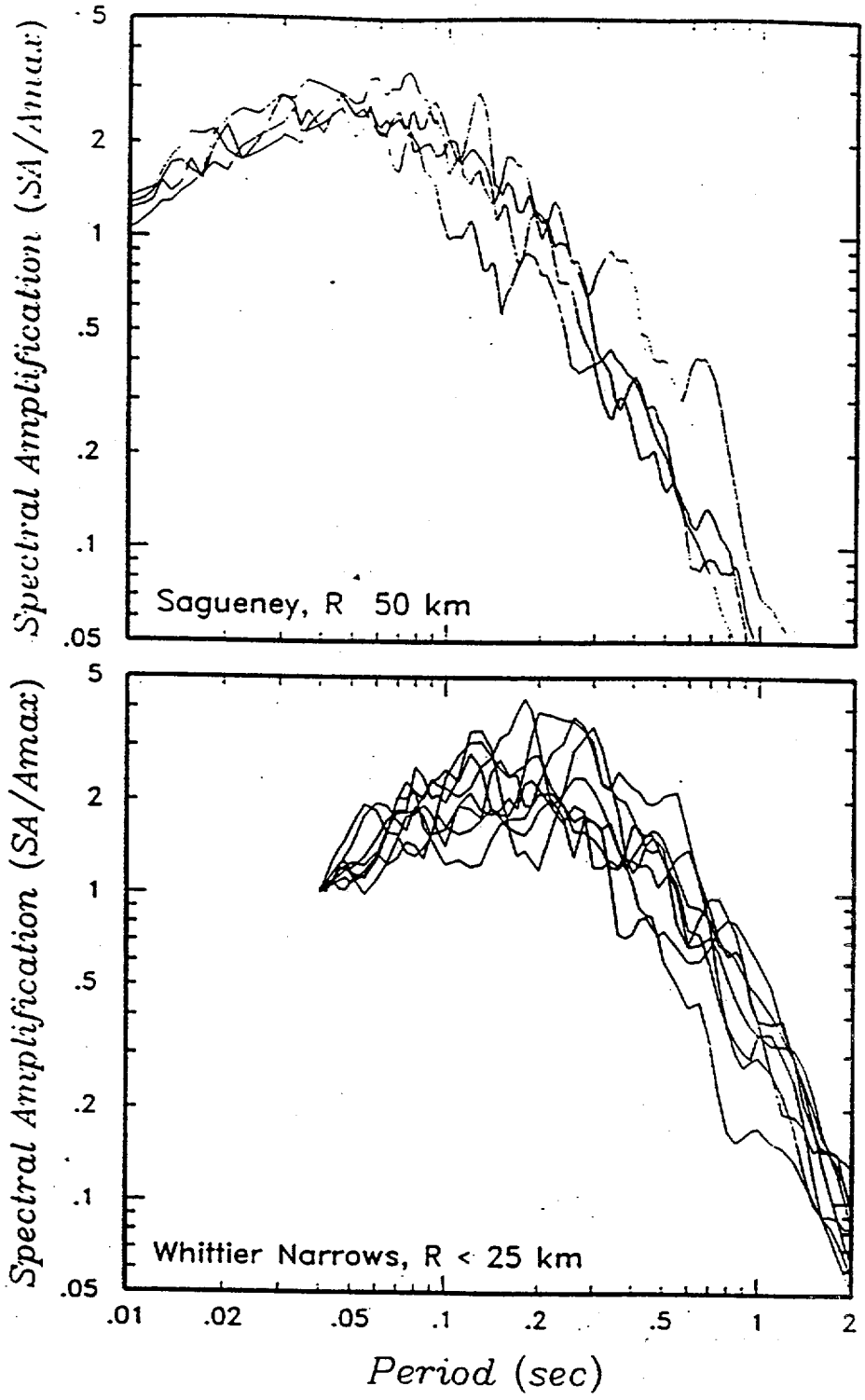

FIGURE 42. Comparison of eastern US and western US recorded rock motions for M ~ 6 events. Sagueney records are from Chicoutimi-Nord and St. Andre. Whittier Narrows records are from stations 289, 697, 709, and 5244.

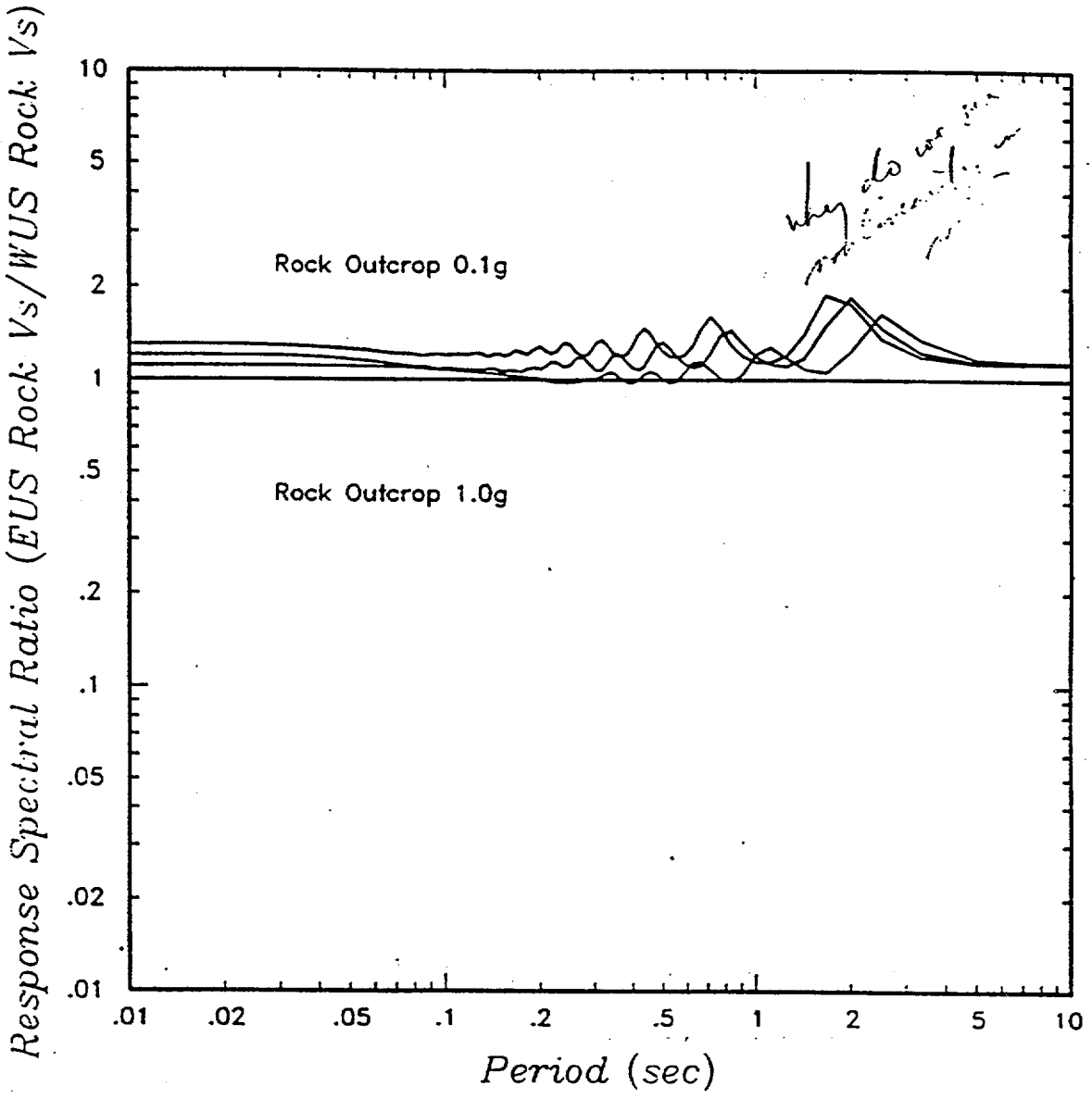

FIGURE 43. Effect of base rock velocity on soil/rock response spectral ratios. Eastern US rock has a shear wave velocity of 11,000 fps and western rock has a velocity of 4,000 fps. Input motion is based on eastern US parameters.

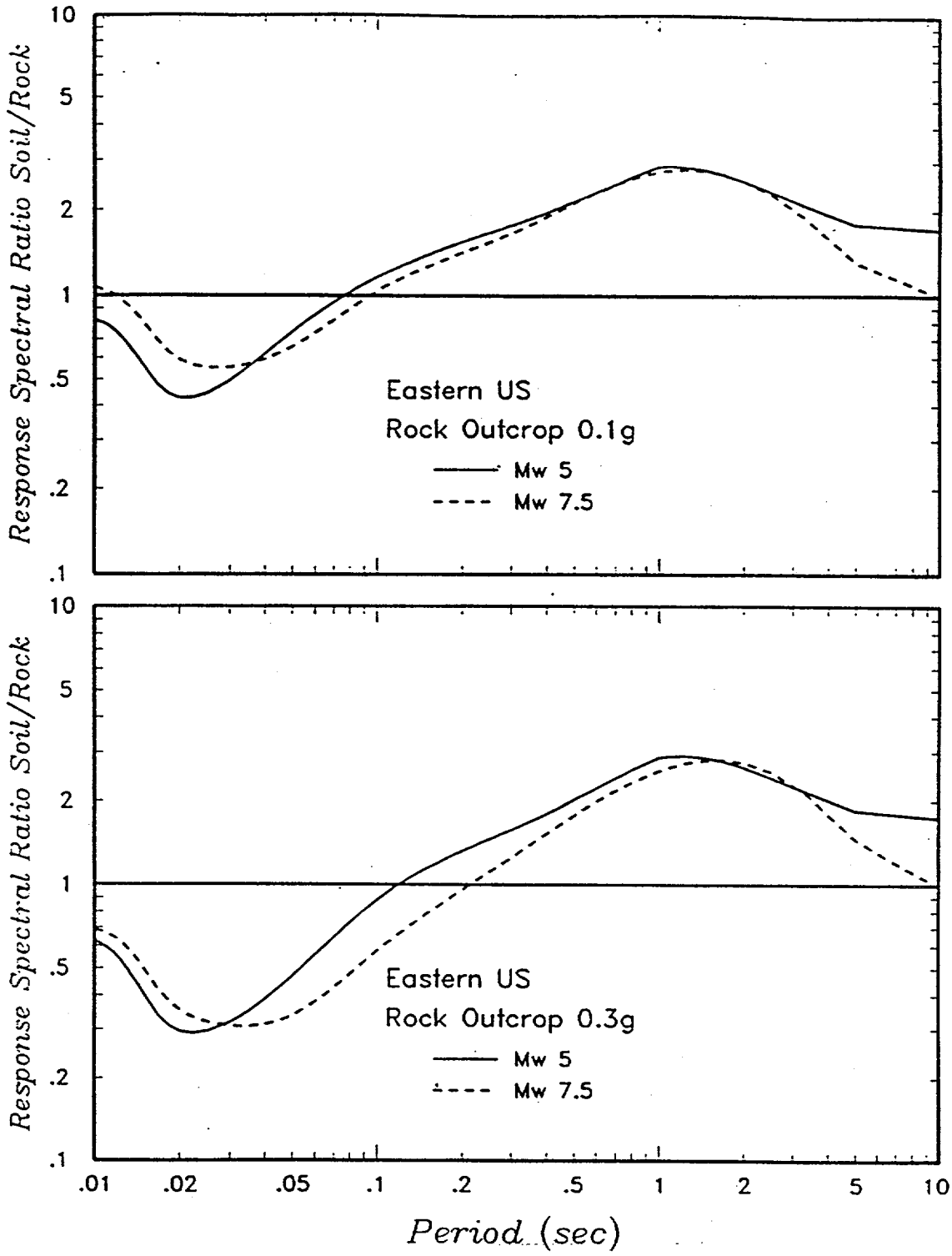

FIGURE 44. Effect of earthquake magnitude on computed soil/rock response spectral ratios.

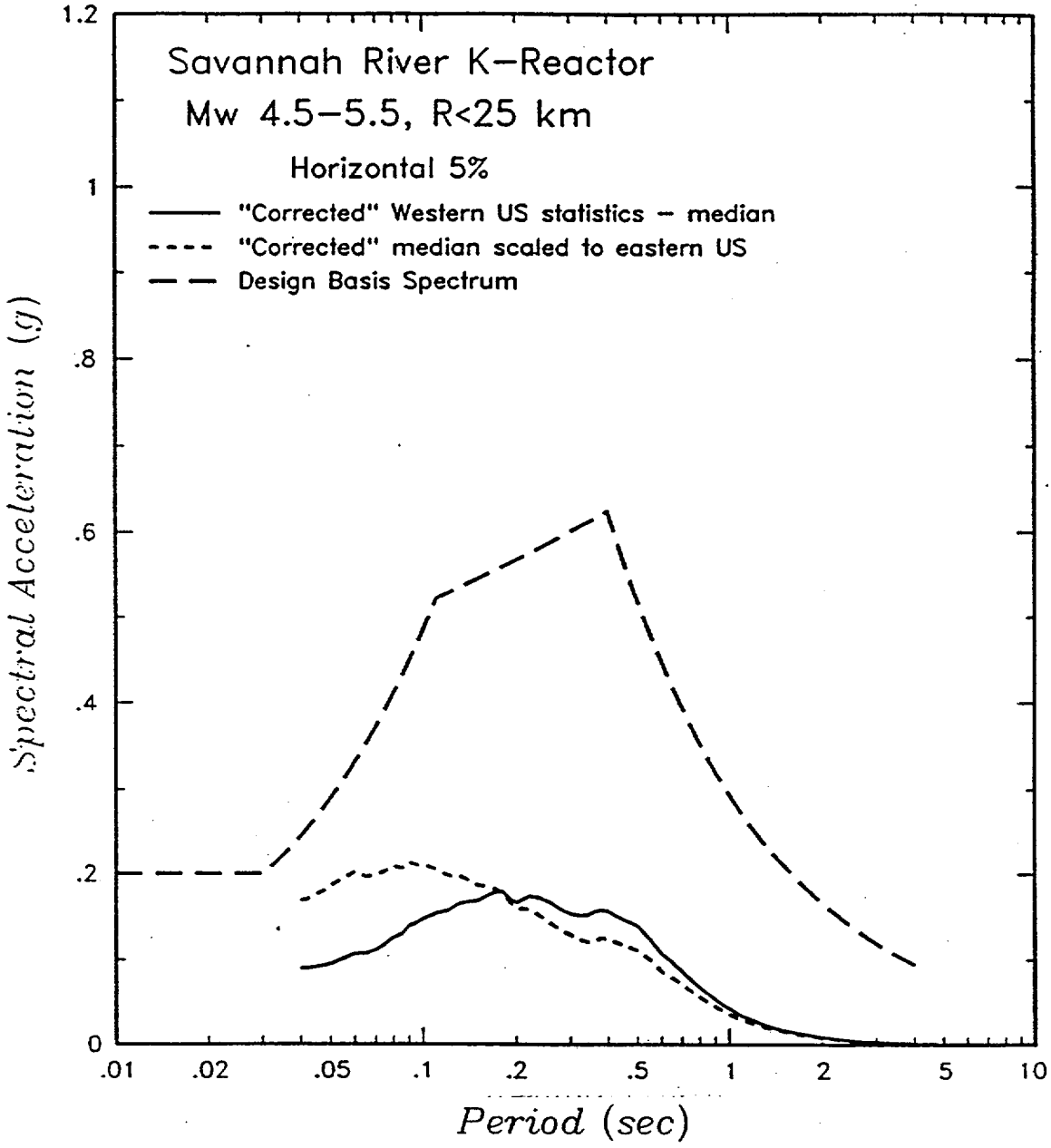

FIGURE 73. Comparison of estimates of random earthquake spectra with the design basis spectrum.

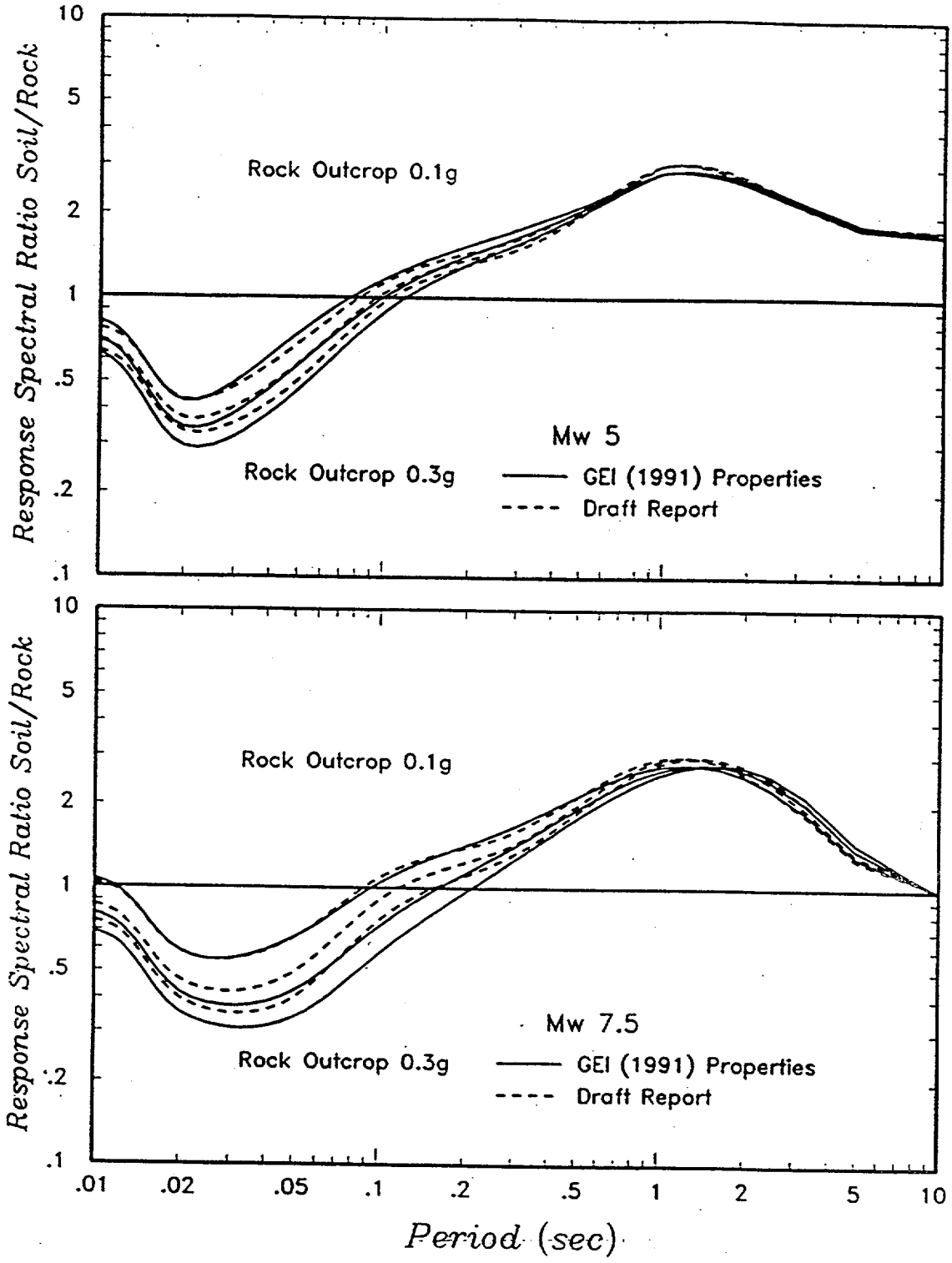

FIGURE 45. Comparison of soil/rock spectral ratios computed using site-specific soil properties (Figs. 33 and 34) with those computed using preliminary properties.

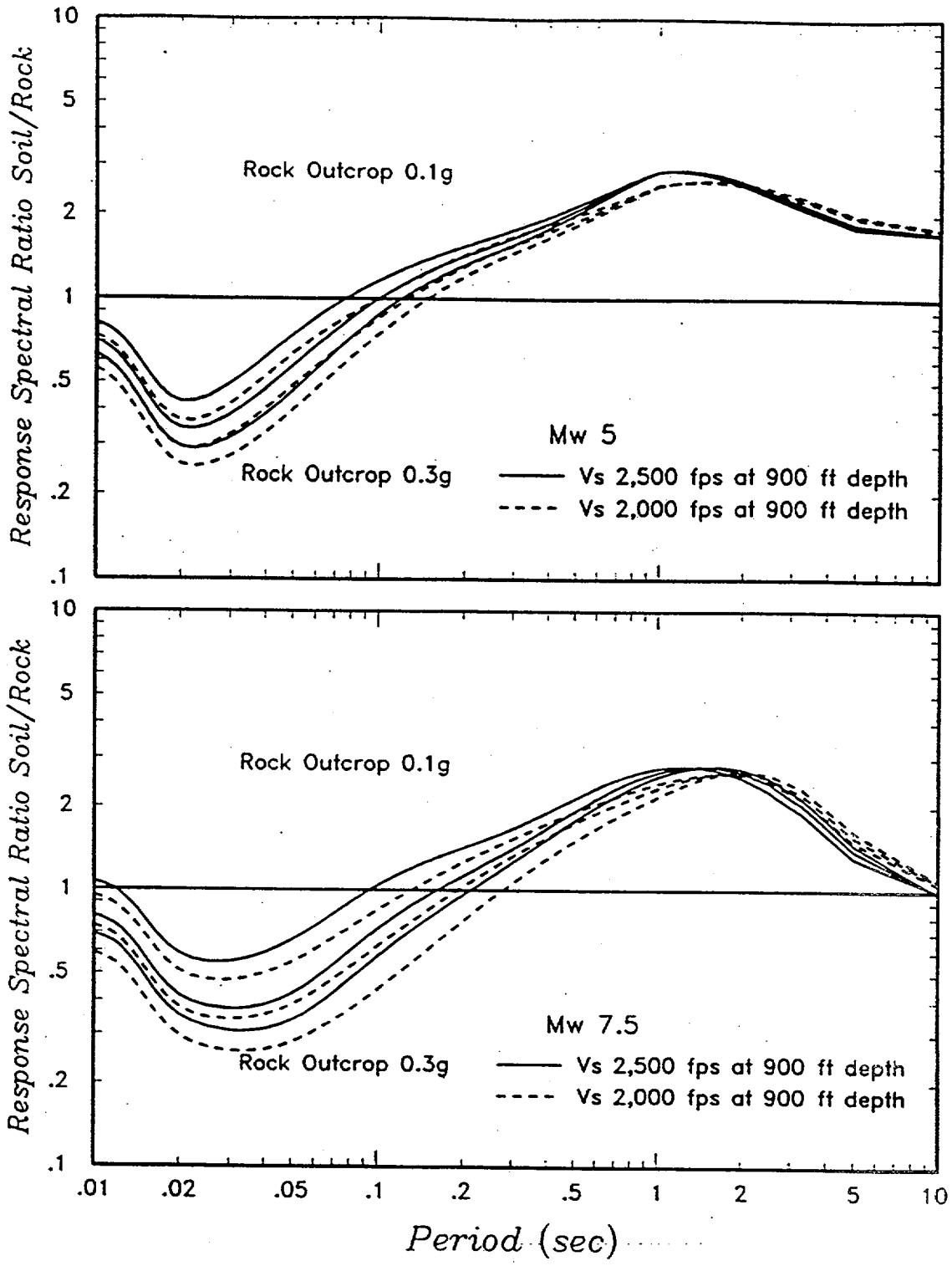

FIGURE 46. Sensitivity of soil/rock spectral ratios to variation in estimate of shear wave velocity with depth shown in Figure 33.

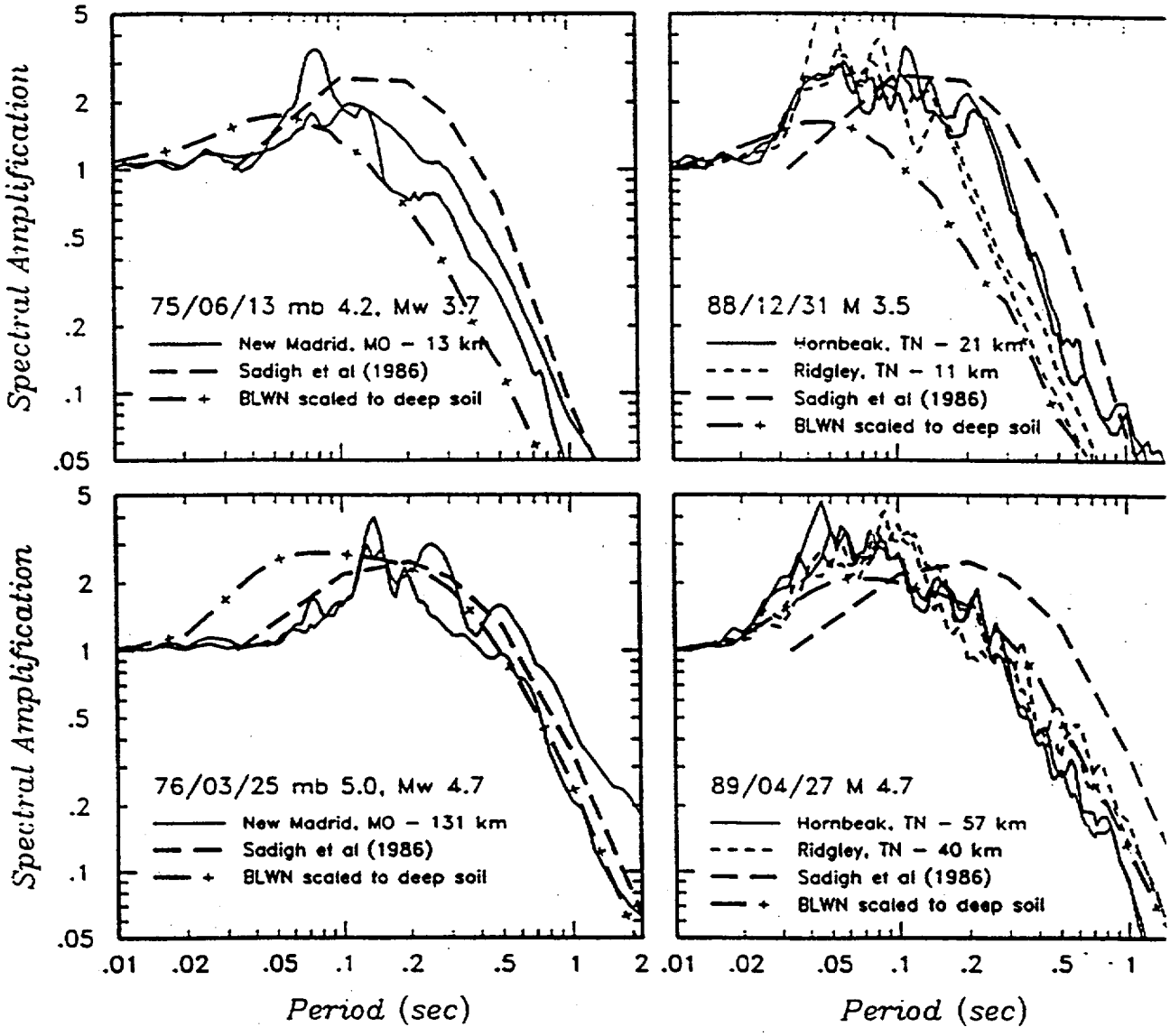

FIGURE 47. Comparison of eastern US response spectral shapes recorded on deep soil sites in the New Madrid region with western US response spectral shapes based on Sadigh et al (1986) and predicted eastern US response spectral shapes using BLWN/RVT rock motions and computed soil/rock spectral ratios.

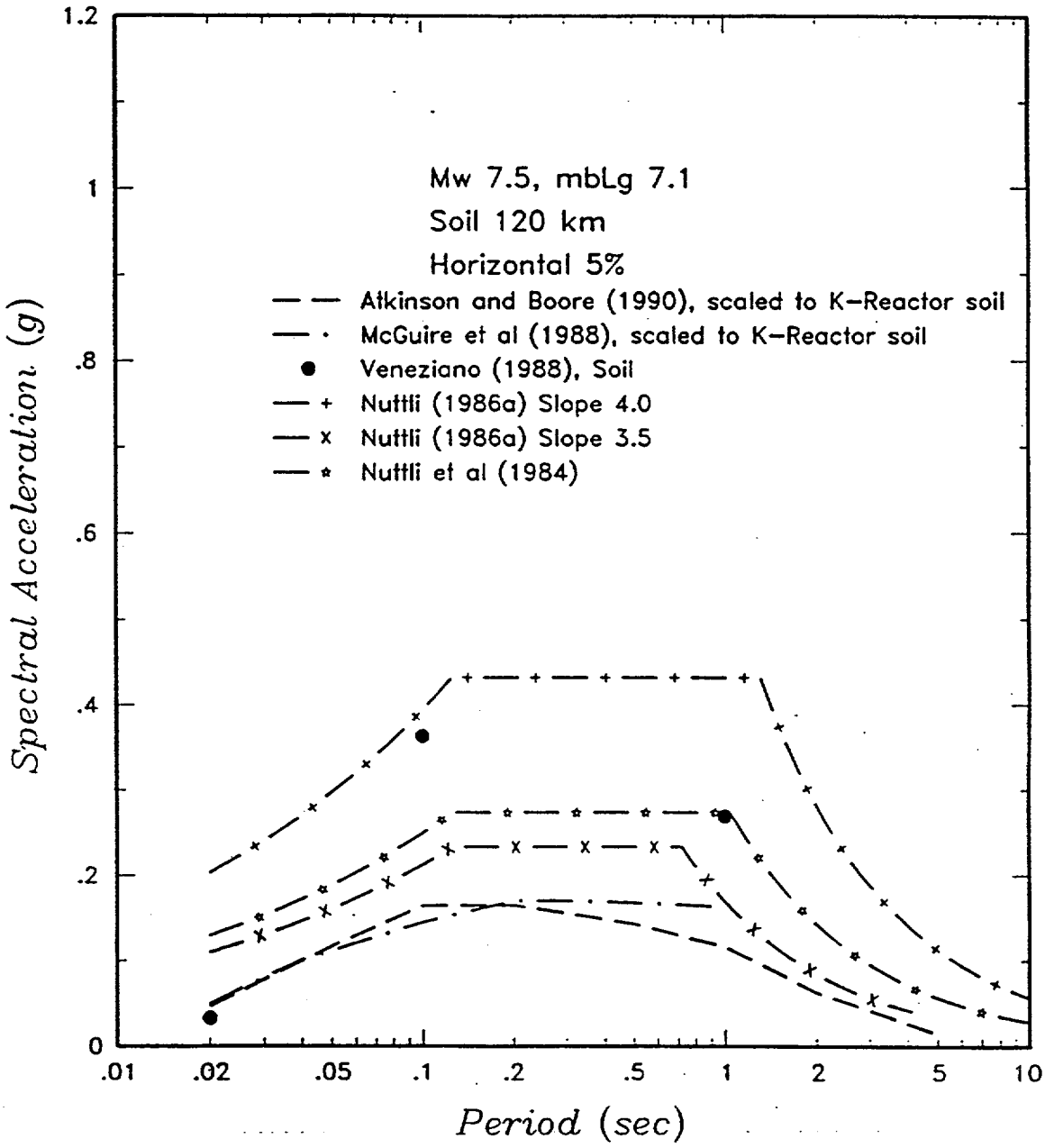

FIGURE 48. Predicted median response spectra on deep soil for M 7.5 Charleston earthquake at a distance of 120 km. Spectra labeled as scaled rock motions were scaled using spectral ratios computed for M 7.5 events.

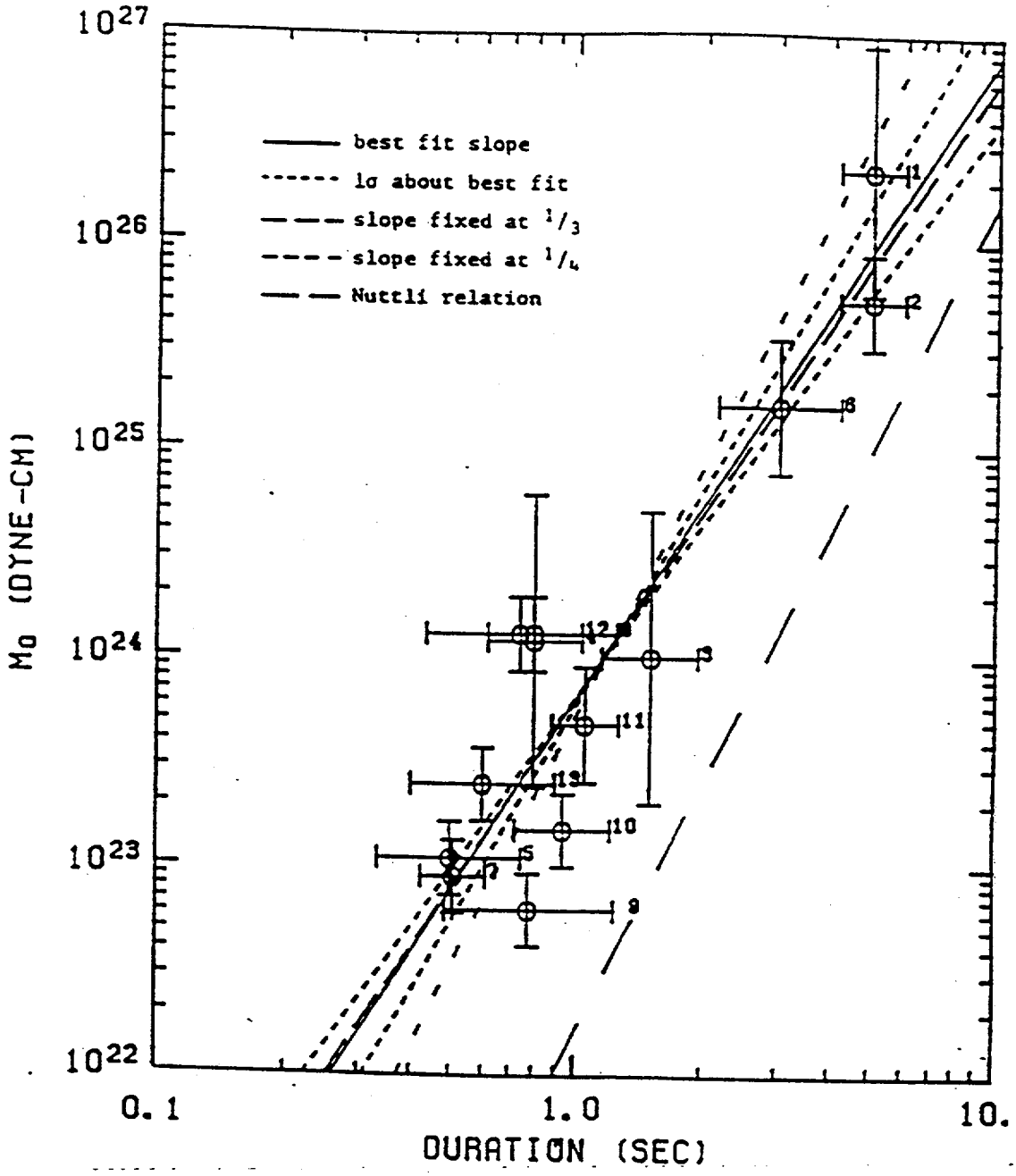

FIGURE 49. Source scaling relationships for eastern North America earthquakes (from Somerville et al, 1987).

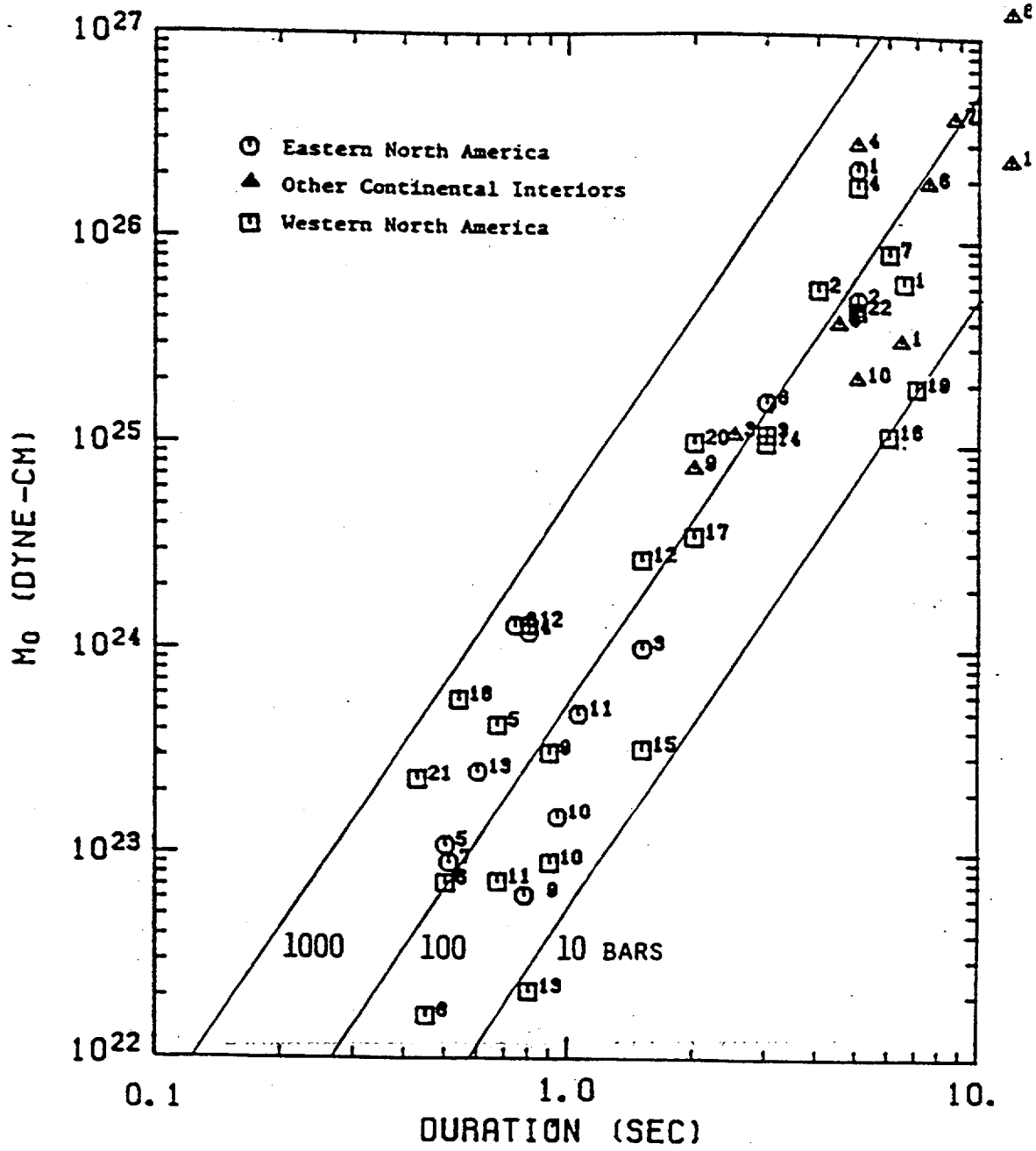

FIGURE 50. Seismic moments and source durations of earthquakes from various tectonic environments (from Somerville et al, 1987).

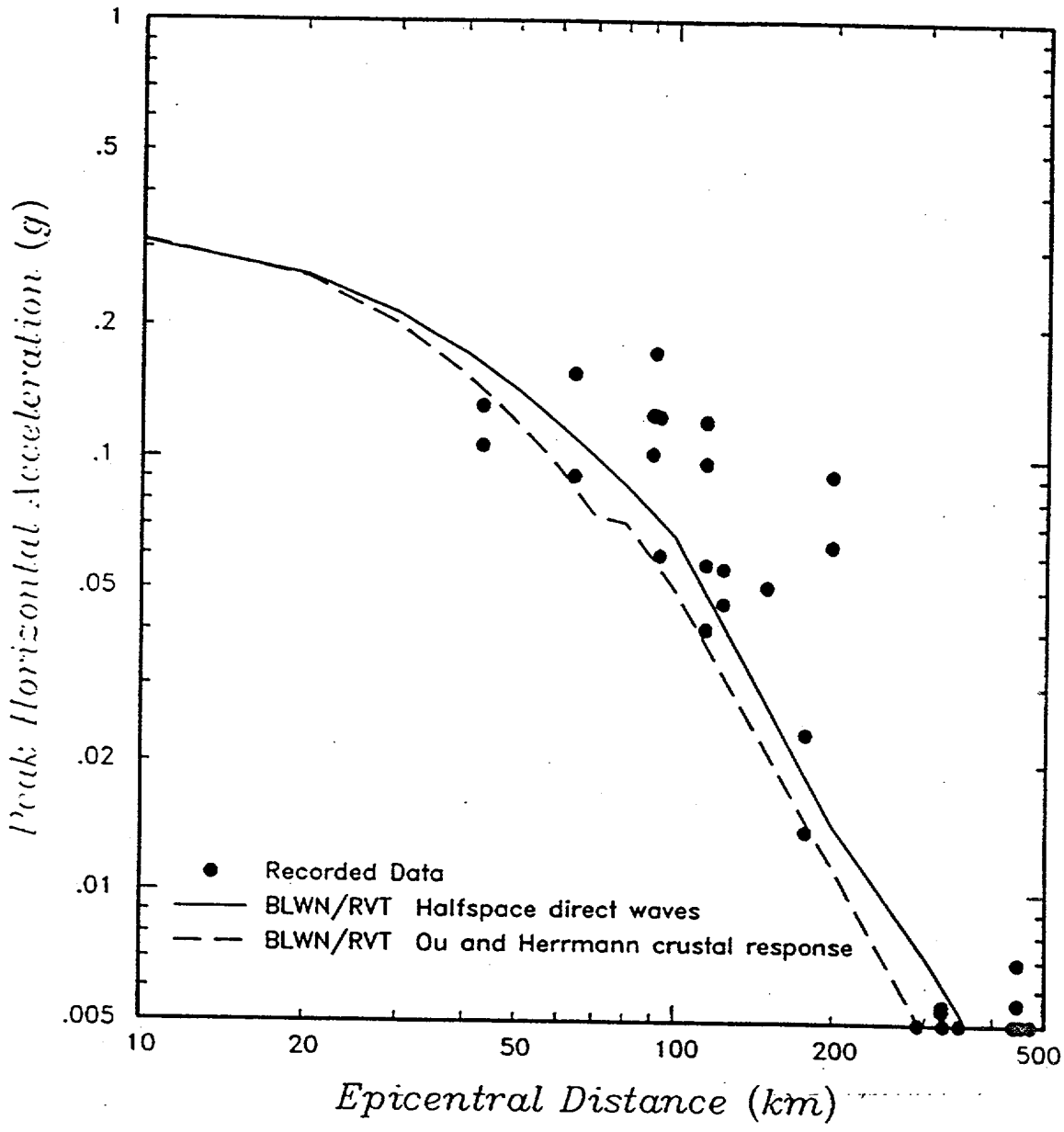

FIGURE 51. Prediction of attenuation of peak acceleration on rock for the 1988 Sagueney earthquake using the BLWN/RVT model with a stress drop of 300 bars. Predictions are made using direct waved in a halfspace (solid curve) and Ou and Herrmann's (in press) crustal response.

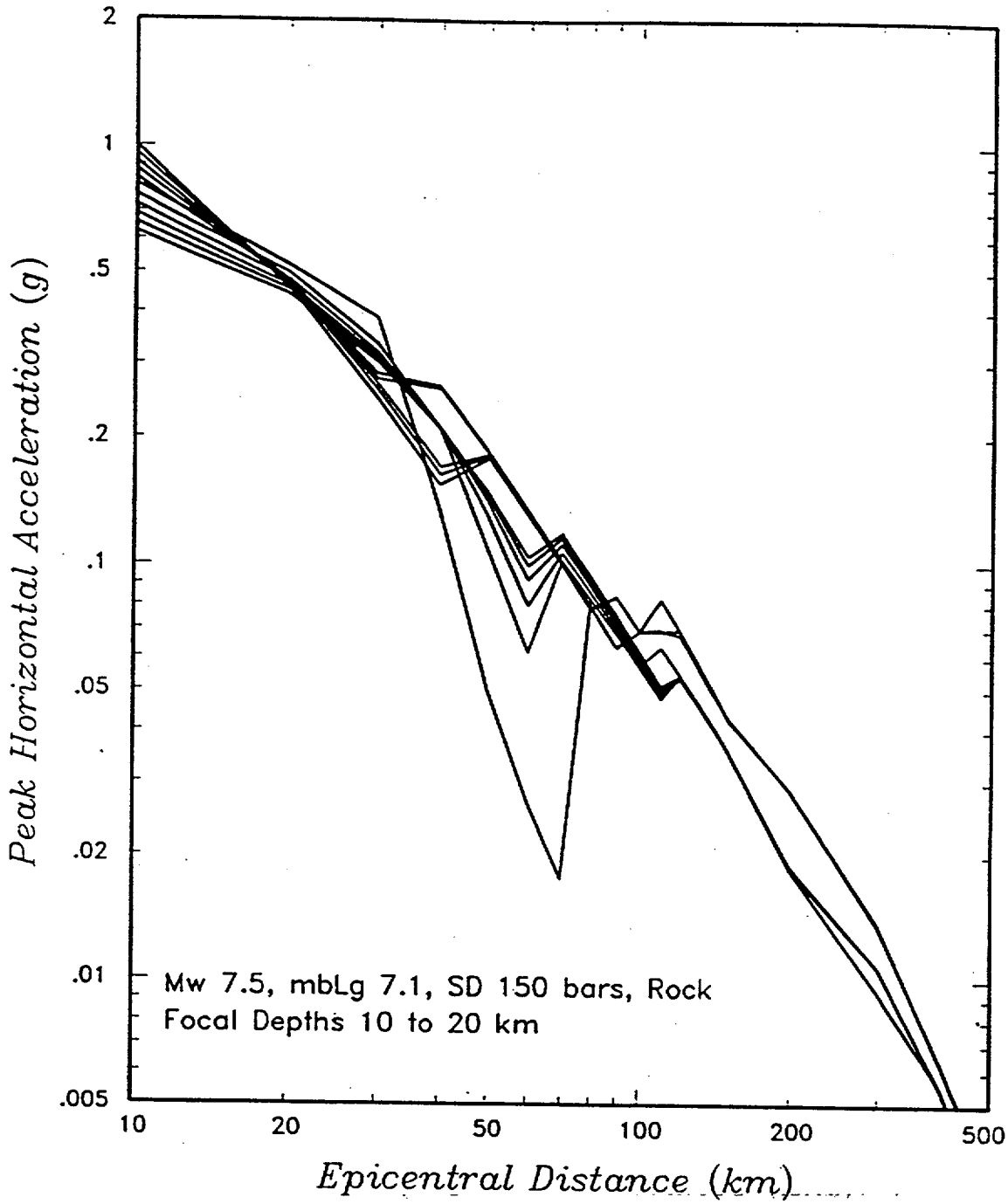

FIGURE 52. Predicted attenuation of M 7.5 Charleston earthquake peak accelerations for rock sites using the BLWN/RVT model, a stress drop of 150 bars, and $Q = 190f^{0.94}$. Results are shown for point source depths ranging from 10 to 20 km.

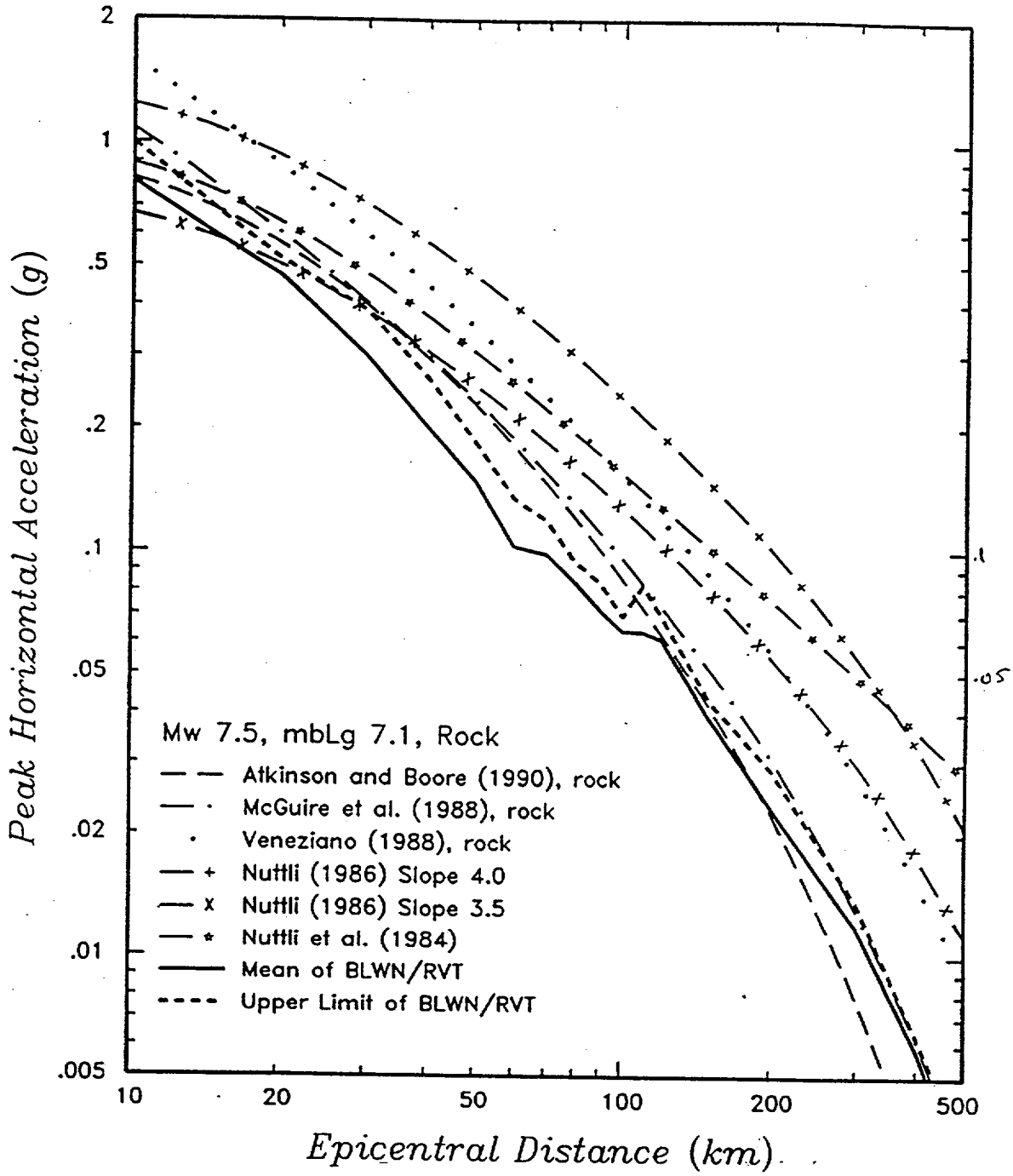

FIGURE 53. Comparison of average and upper limit peak accelerations on rock prediced by the BLWN/RVT model with attenuation relationships shown in Figure 37.

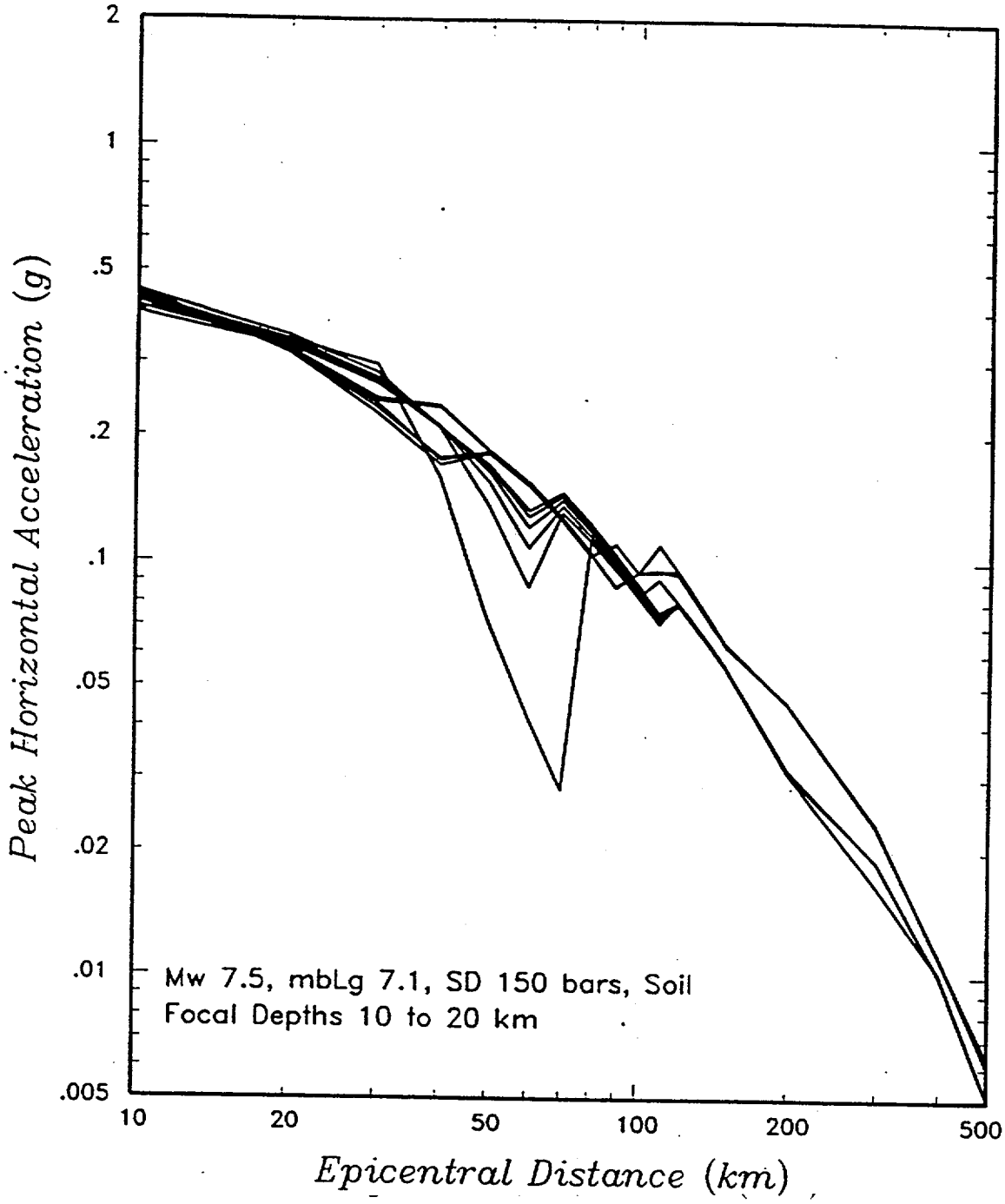

FIGURE 54. Predicted attenuation of M 7.5 Charleston earthquake peak accelerations for K-Reactor profile using the BLWN/RVT model (stress drop 150 bars) for point source depths of 10 to 20 km.

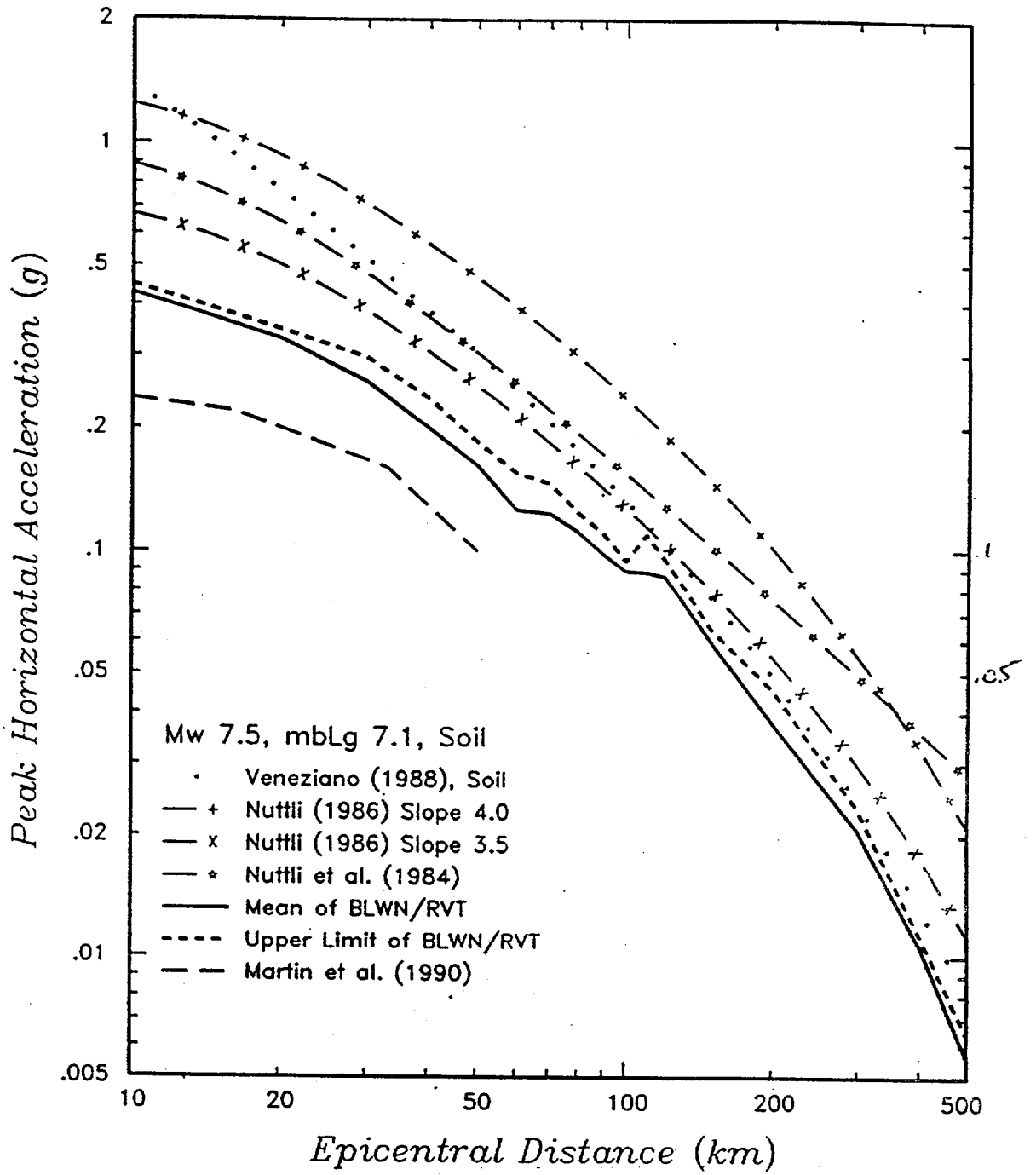

FIGURE 55. Comparison of predicted peak accelerations for M 7.5 Charleston earthquake for K-Reactor profile using the BLWN/RVT model (stress drop 150 bars) with published soil attenuation relationships.

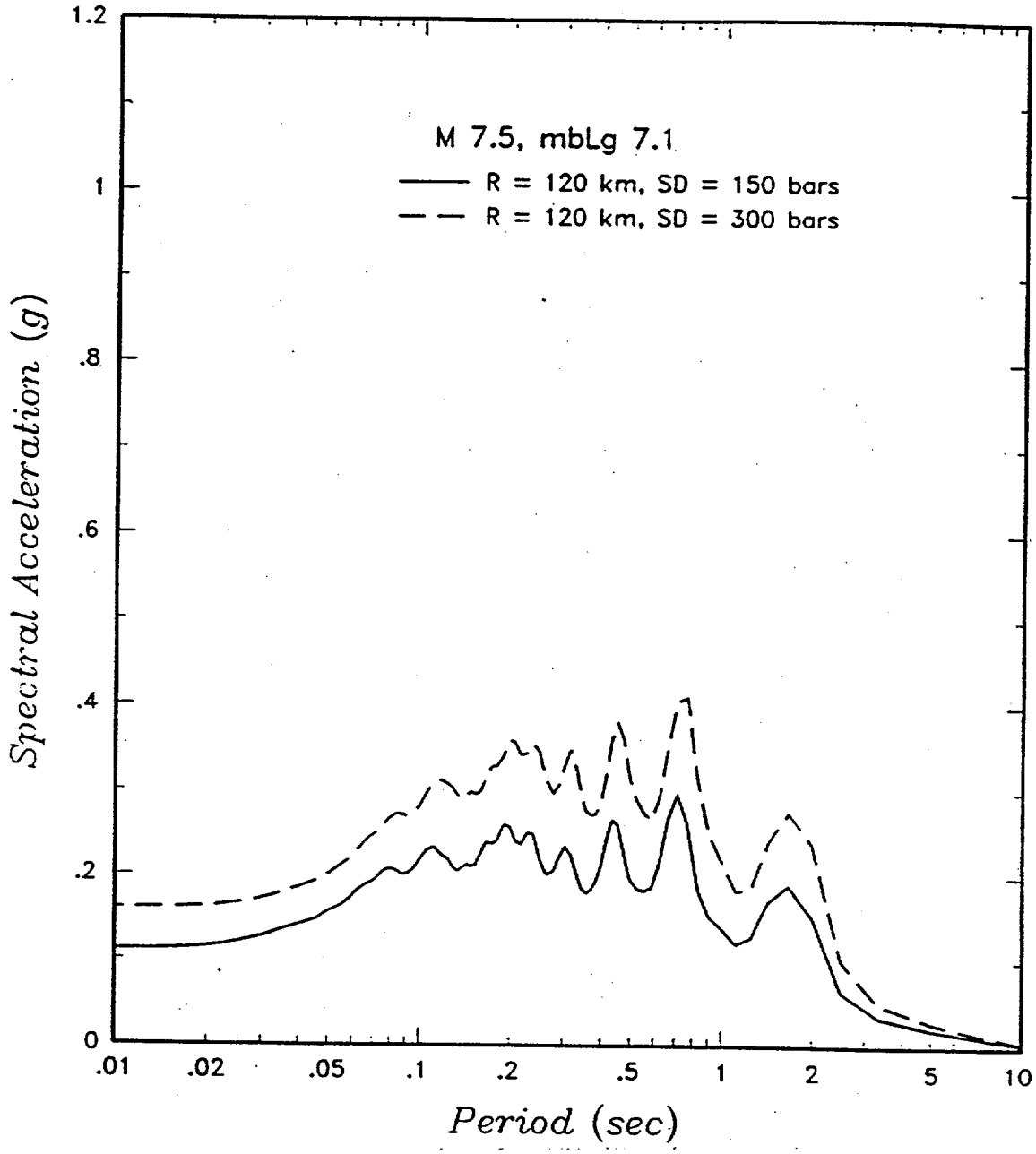

FIGURE 56. Prediction of K-Reactor soil site response spectra for Charleston source M 7.5 earthquake using the BLWN/RVT model. Shown is the effect of stress drop on predicted horizontal spectra.

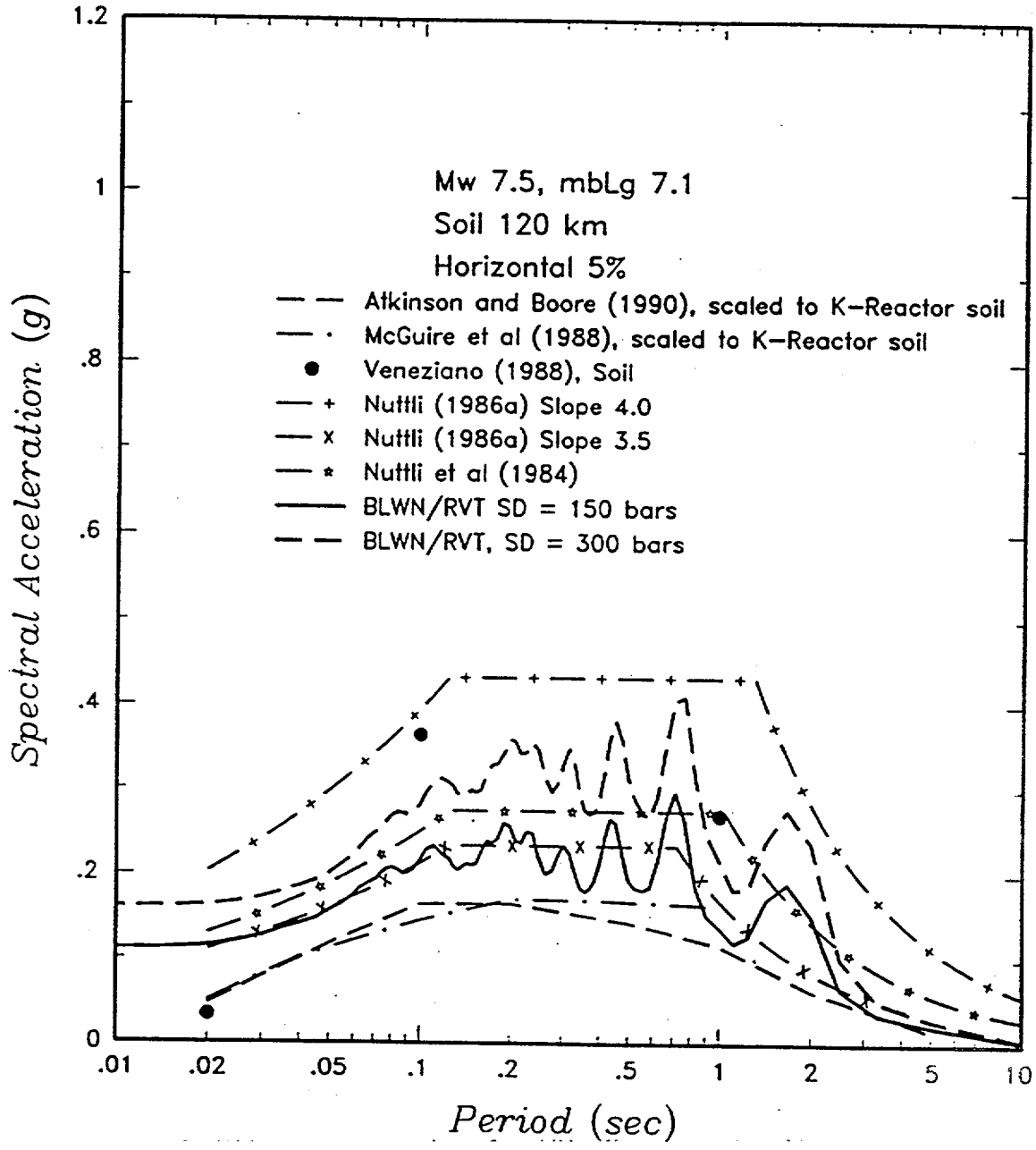

FIGURE 57. Comparison of estimates of median horizontal soil site response spectra for Savannah River K-Reactor site for M 7.5 Charleston event.

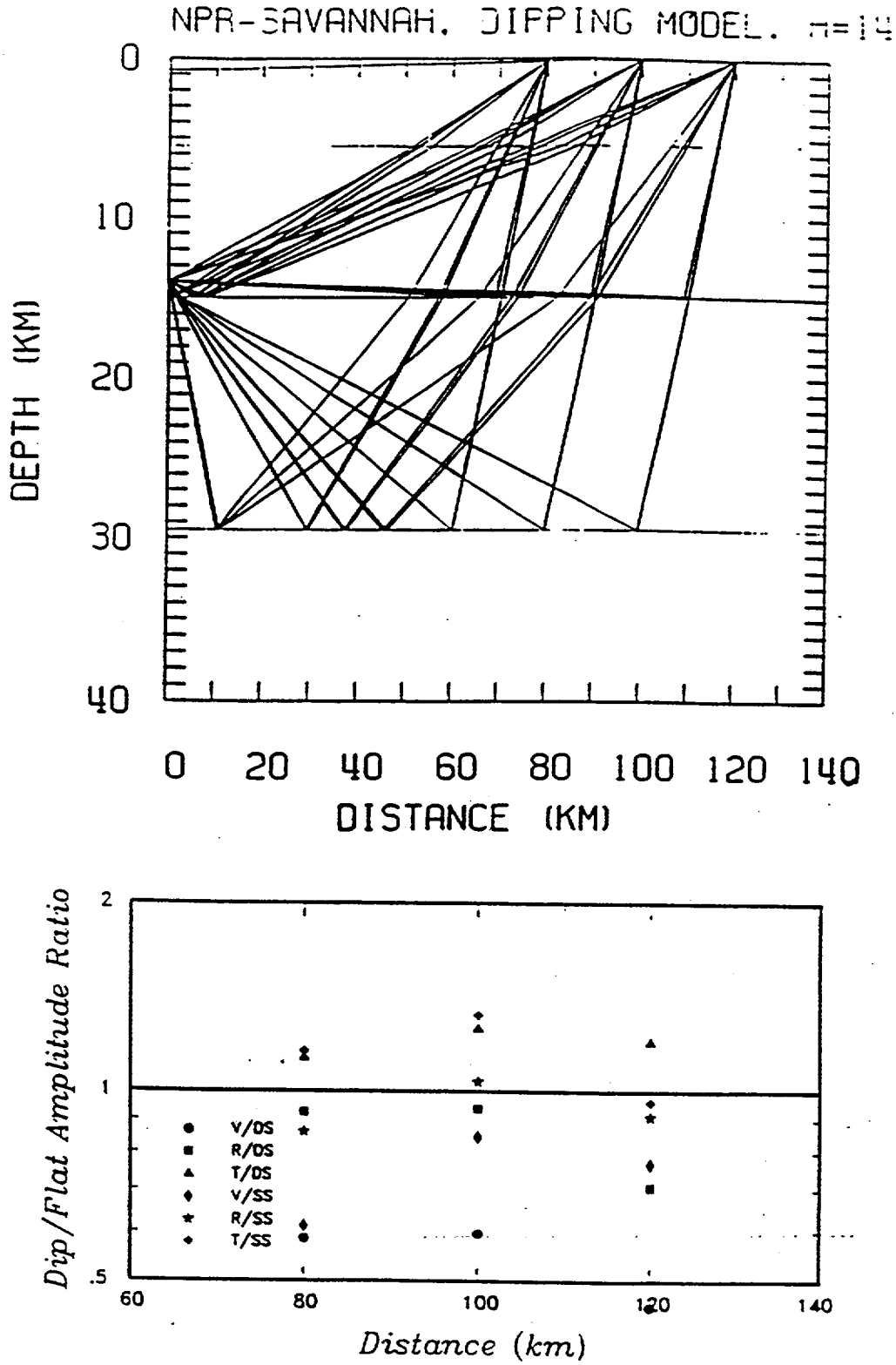

FIGURE 58. Ray tracing analysis of effect of dipping coastal plain sediments-base rock interface on ground motions at 3 distances from the Charleston source. Top figure shows ray tracing paths and crustal layers based on Talwani (1977). Bottom plot shows ratio of dipping layer to flat layer model amplitudes for canonical source functions.

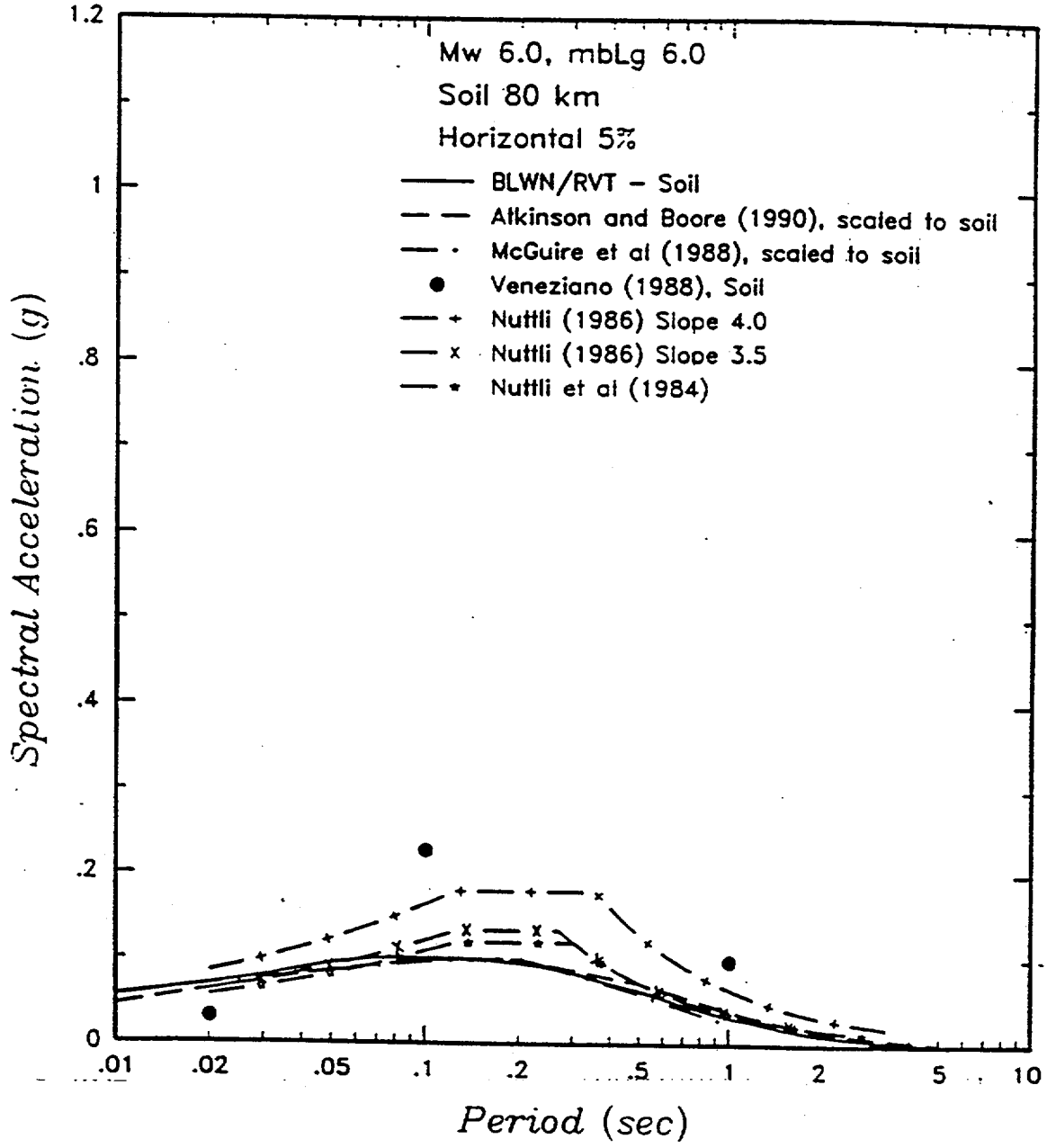

FIGURE 59. Predicted soil site median response spectra at K-Reactor site for Bowman source M 6.0 earthquake at a distance of 80 km. Shown are predictions based on both published relationships and BLWN/RVT model (stress drop 100 bars).

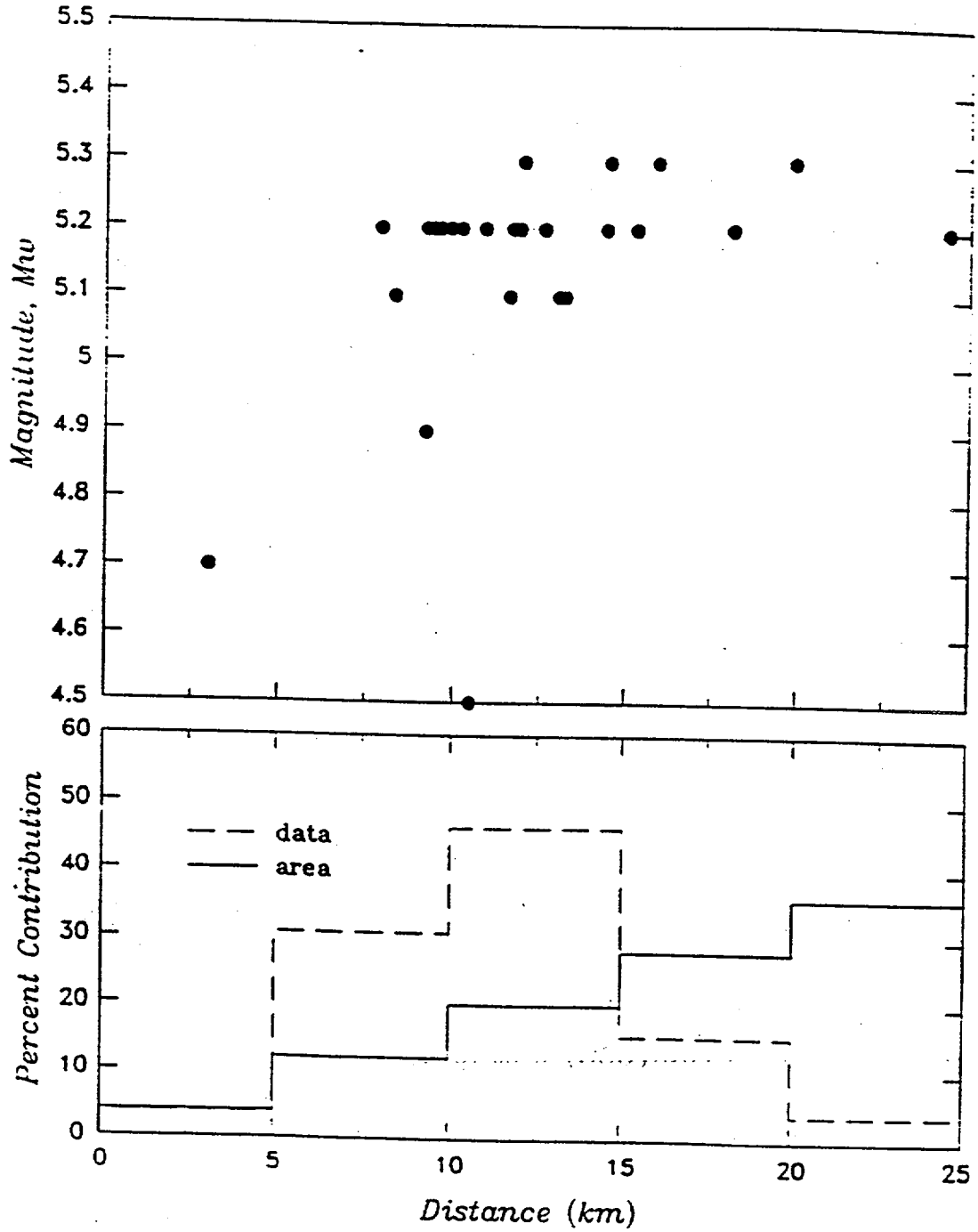

FIGURE 60. Distribution of available deep soil site recorded strong ground motions for a magnitude M 5.0 earthquake recorded within 25 km. Top figure is a magnitude-distance scattergram. Bottom plot shows a histogram of the distance distribution of the recorded data compared with that for the distance to a random location uniformly distributed in an area defined by a 25-km radius circle about the site.

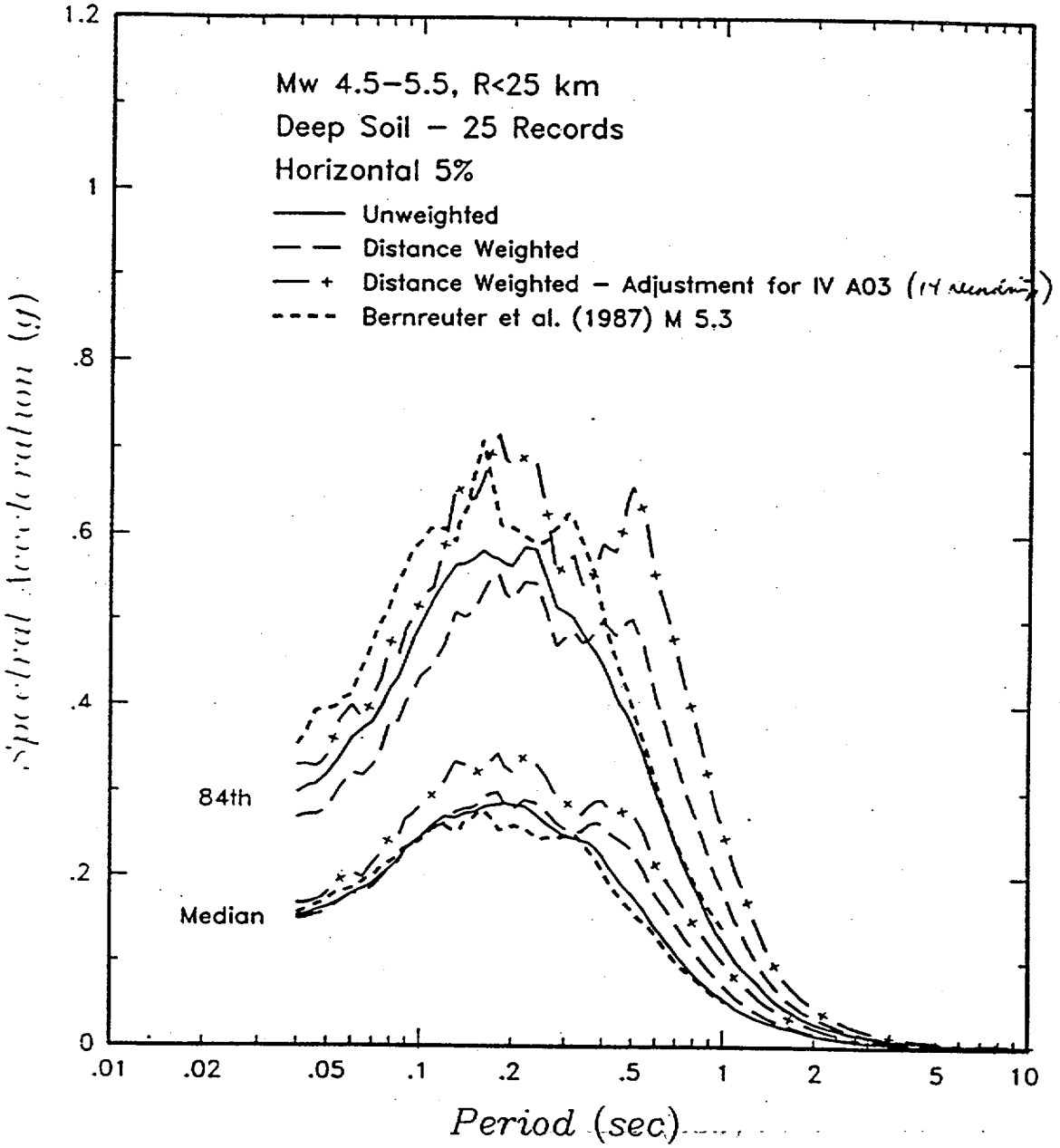

FIGURE 61. Median and 84th-percentile horizontal spectral ordinates computed from statistics of 25 deep soil recordings. Shown are the unweighted case and the effect of applying weights to obtain a uniform distribution in a 25-km radius circle about the site, and to adjust for the large number of recordings from a single aftershock.

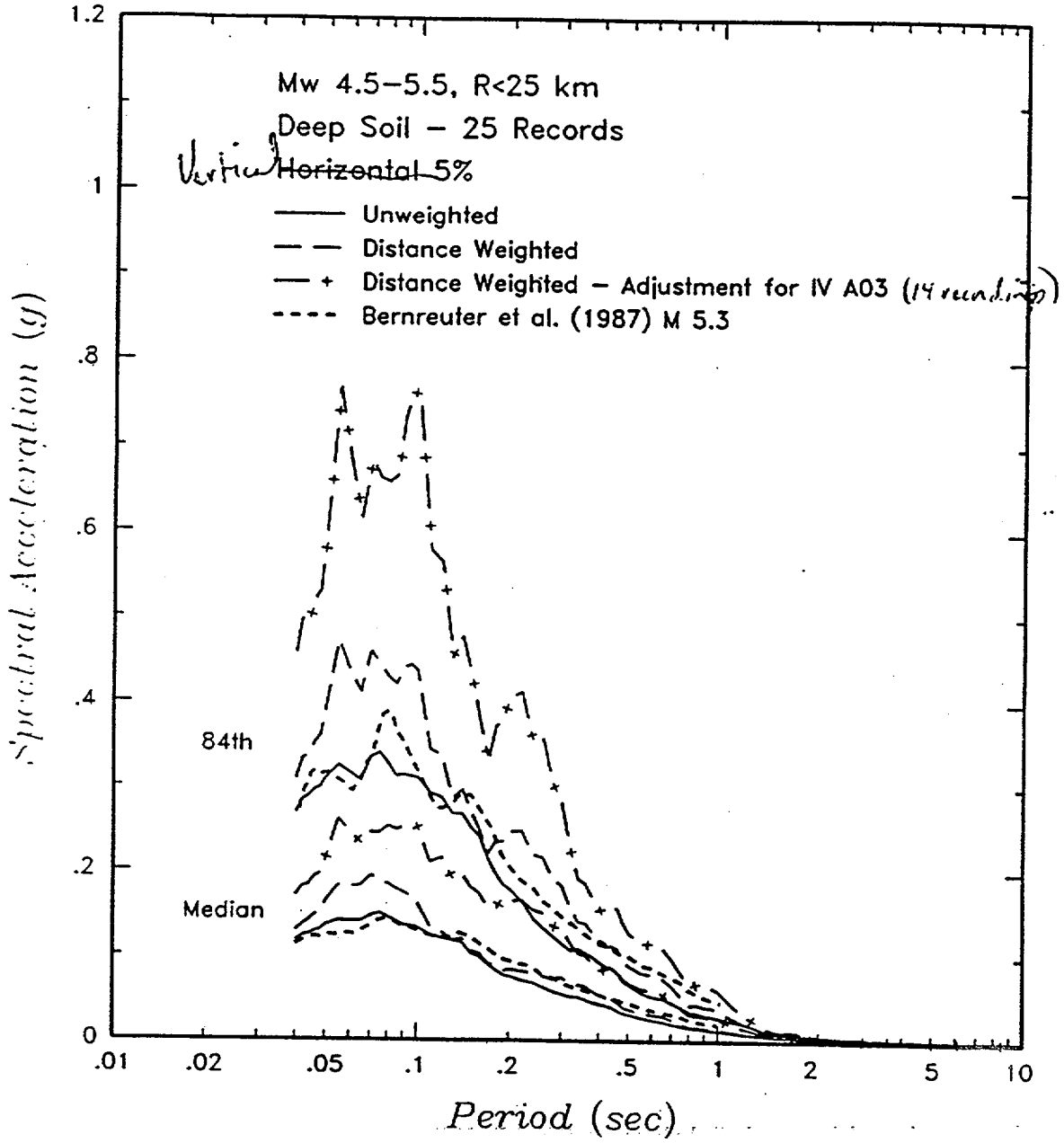

FIGURE 62. Median and 84th-percentile vertical spectral ordinates computed from statistics of 25 deep soil recordings. Shown are the unweighted case and the effect of applying weights to obtain a uniform distribution in a 25-km radius circle about the site, and to adjust for the large number of recordings from a single aftershock.

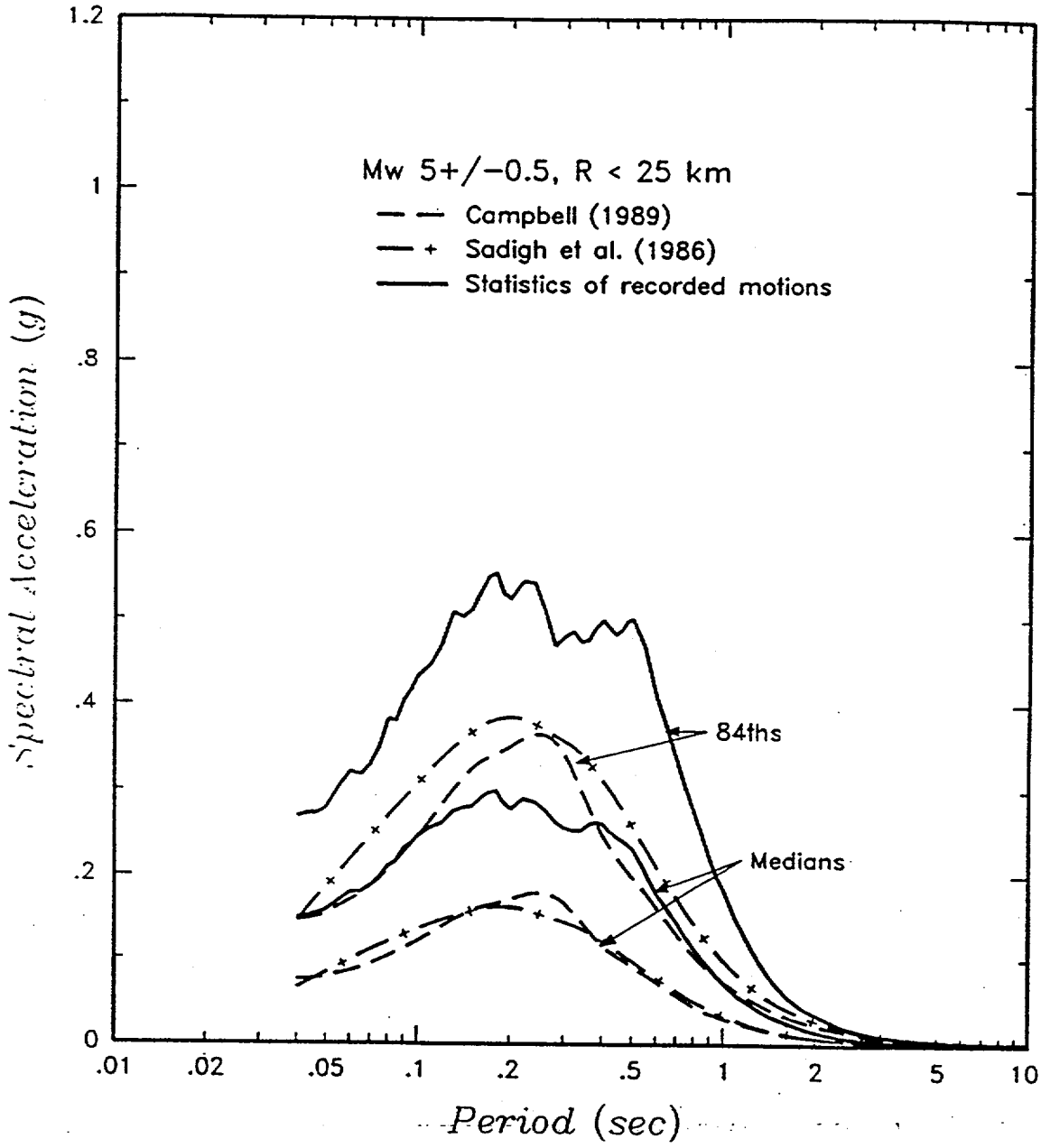

FIGURE 63. Comparison of median and 84th-percentile horizontal response spectra computed from statistics of recorded motions with spectra computed using western US deep soil attenuation relationships developed by Sadigh et al. (1986) and Campbell (1989).

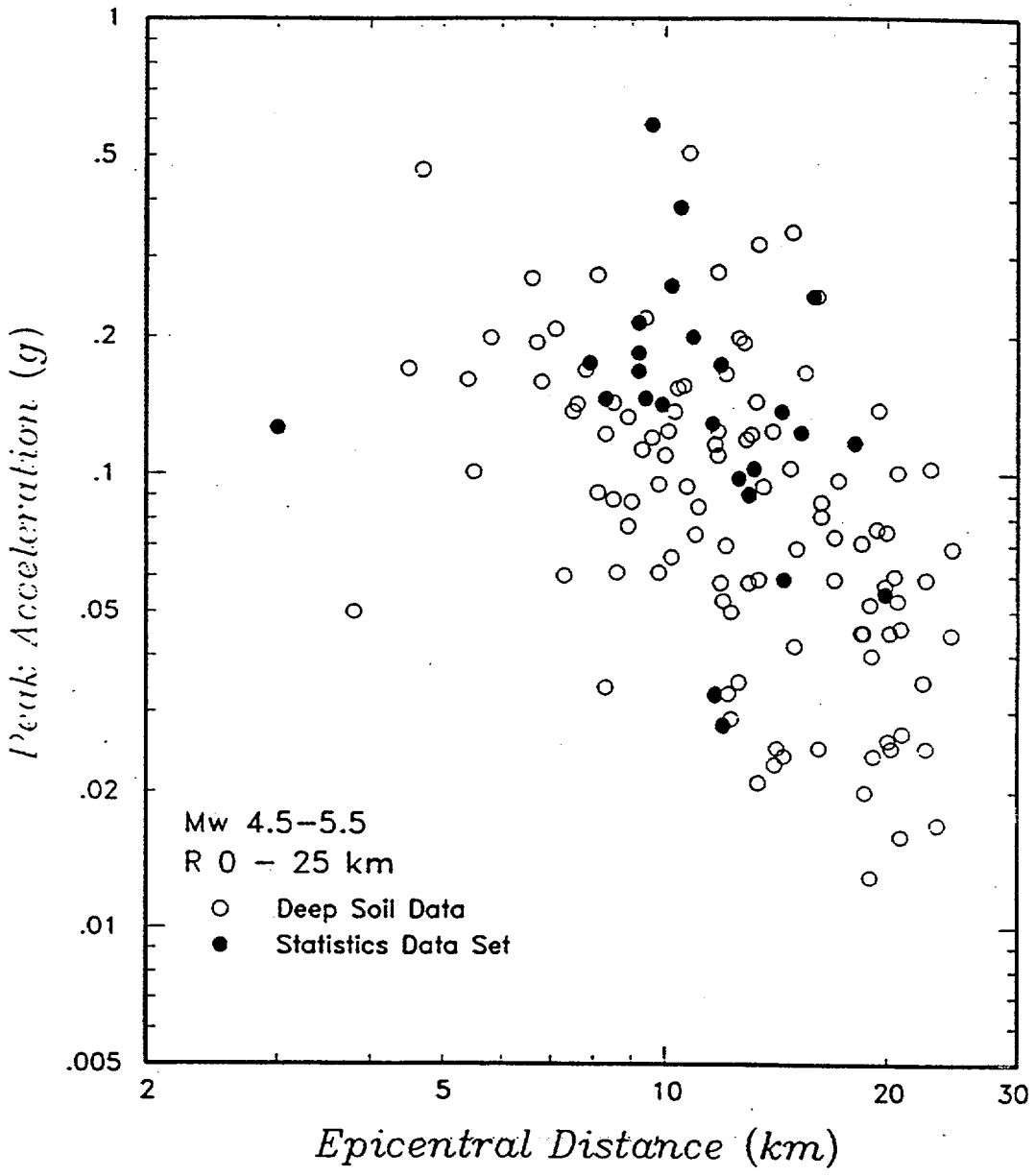

FIGURE 64. Comparison of data set for recorded peak acceleration on deep soil sites for M 4.5-5.5 earthquakes with 25 km of the site to the data set of processed accelerograms.

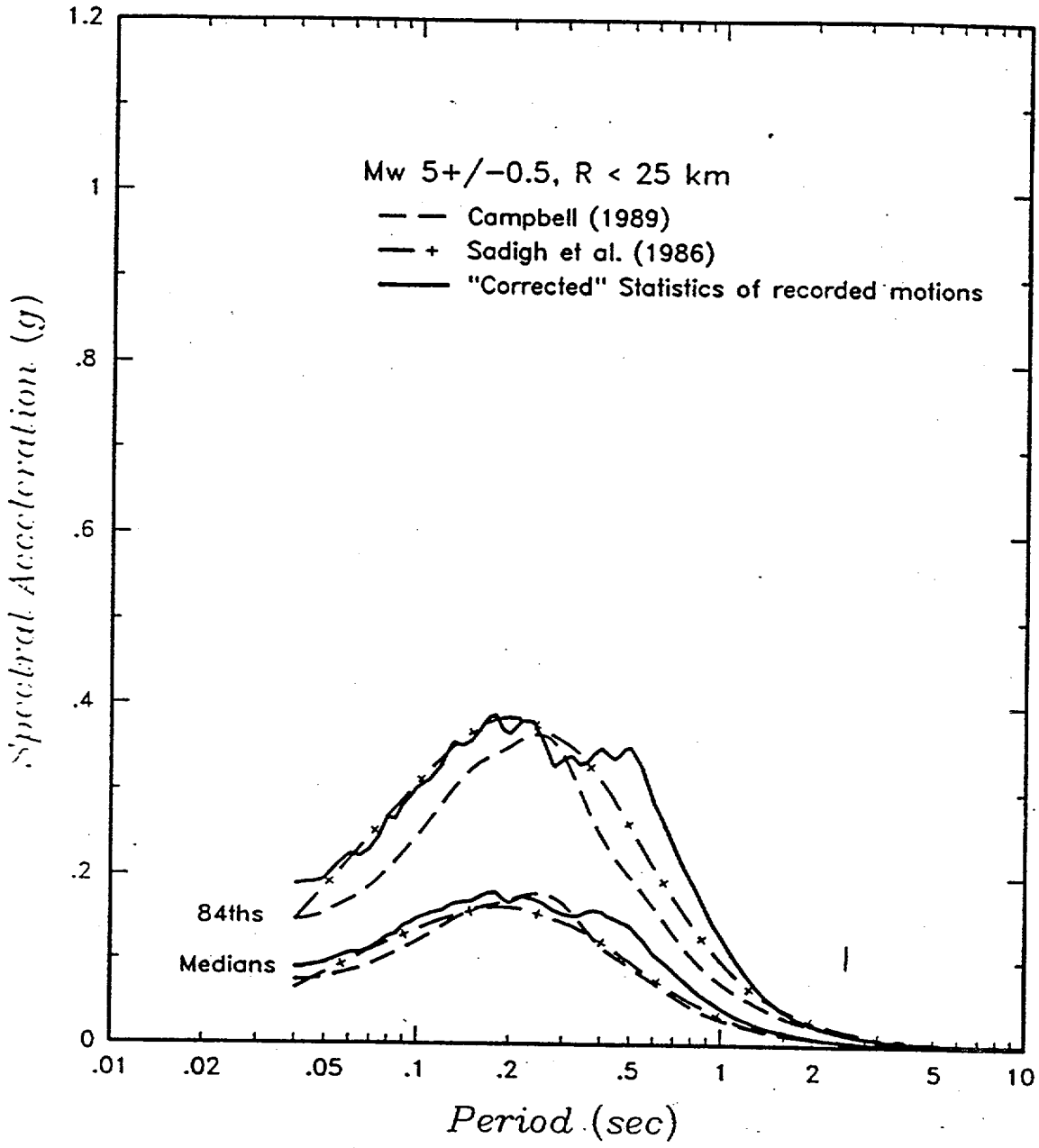

FIGURE 65. "Corrected" site-specific statistical spectra adjusted for bias in processed accelerogram data set. "Corrected" spectra are compared with empirical attenuation relationship based spectra from Figure 63.

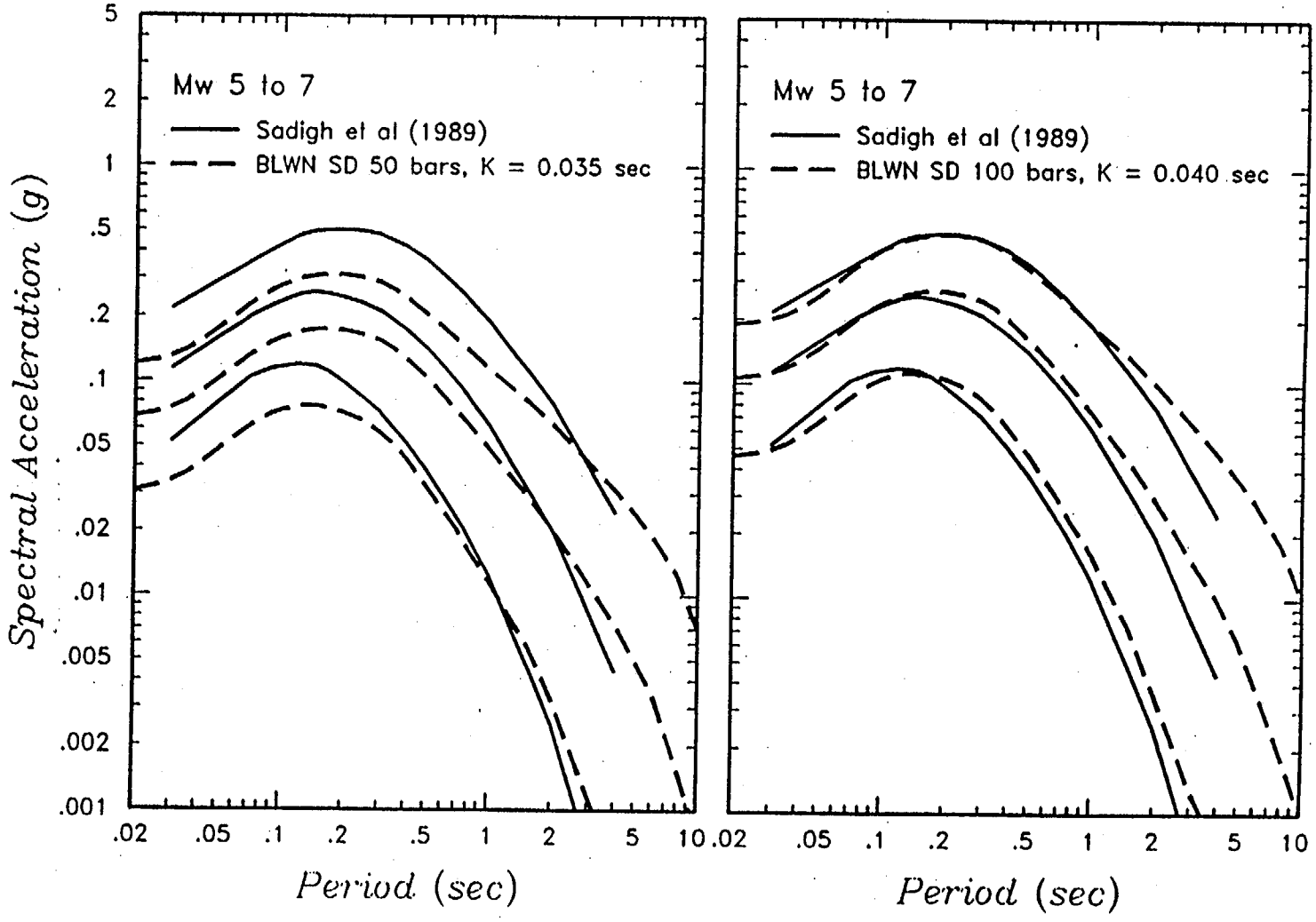

FIGURE 66. Comparison between horizontal rock site response spectra predicted by the empirical relationships developed by Sadigh et al. (1989) and the BLWN/RVT model for stress drops of 50 and 100 bars. Note that Kappa was increased from 0.035 to 0.04 seconds for the larger stress drop in order to better fit the response spectral shapes.

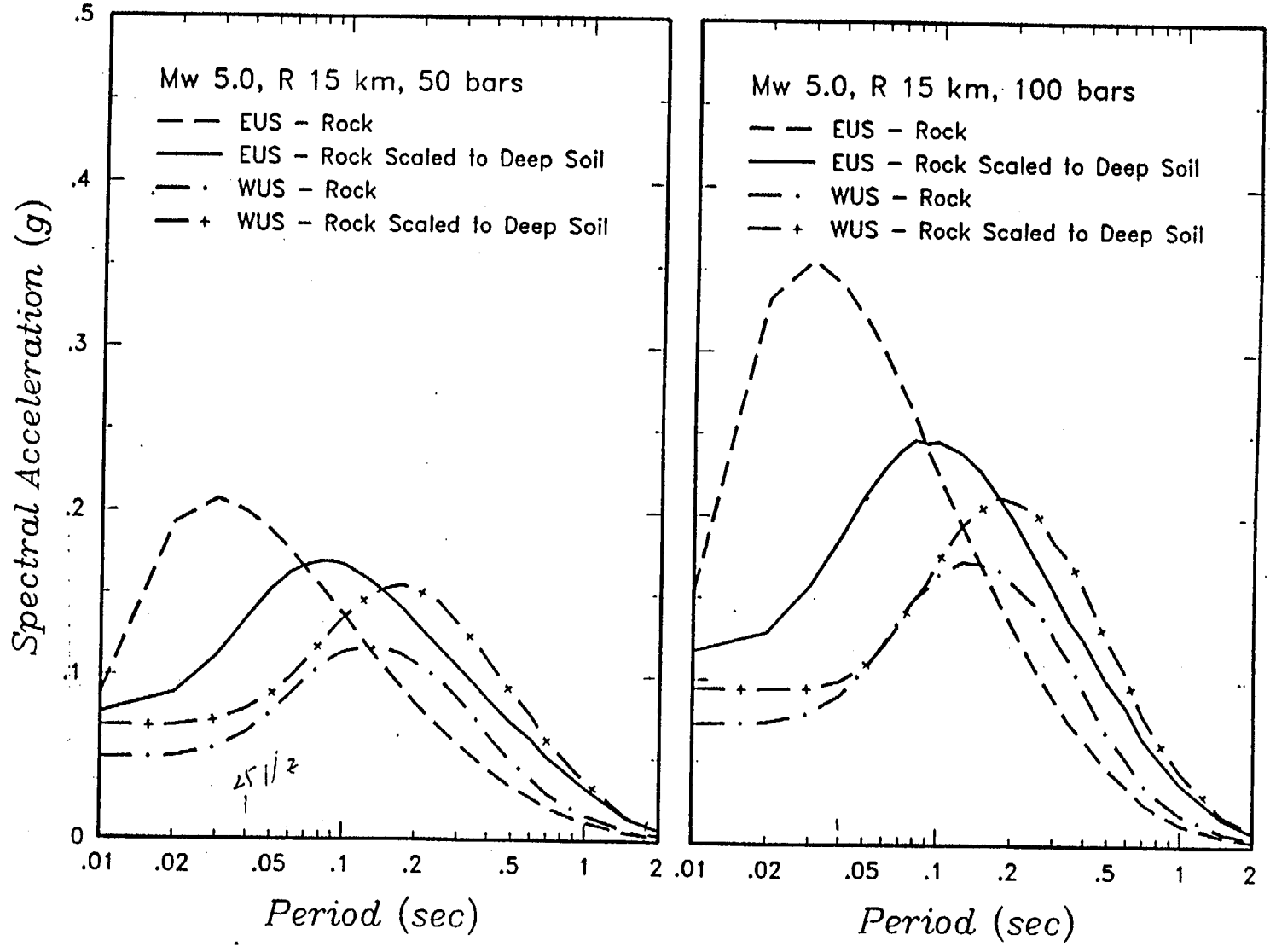

FIGURE 67. Predicted ground motions on deep soil and on rock for a M 5.0 earthquake at a distance of 15 km using the BLWN/RVT model and two values of stress drop. Shown are ground motions for eastern US and western US motions. Soil motions are obtained by scaling rock motions using soil/rock spectral ratios computed for M 5.0 events.

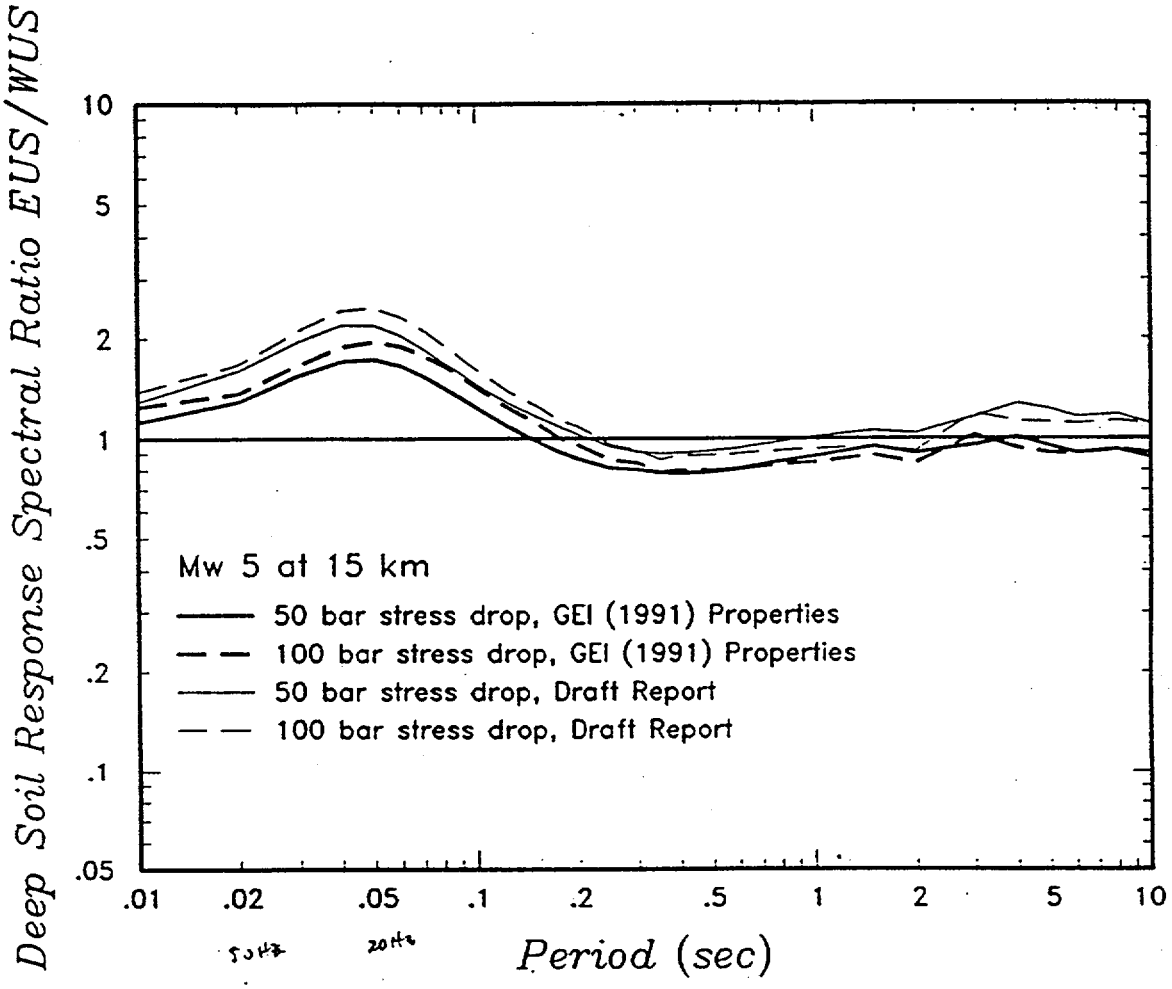

FIGURE 68. Response spectral ratio between eastern US and western US deep soil site spectra shown in Figure 67. Shown are the effects of the choice of site profile properties on the computed ratios.

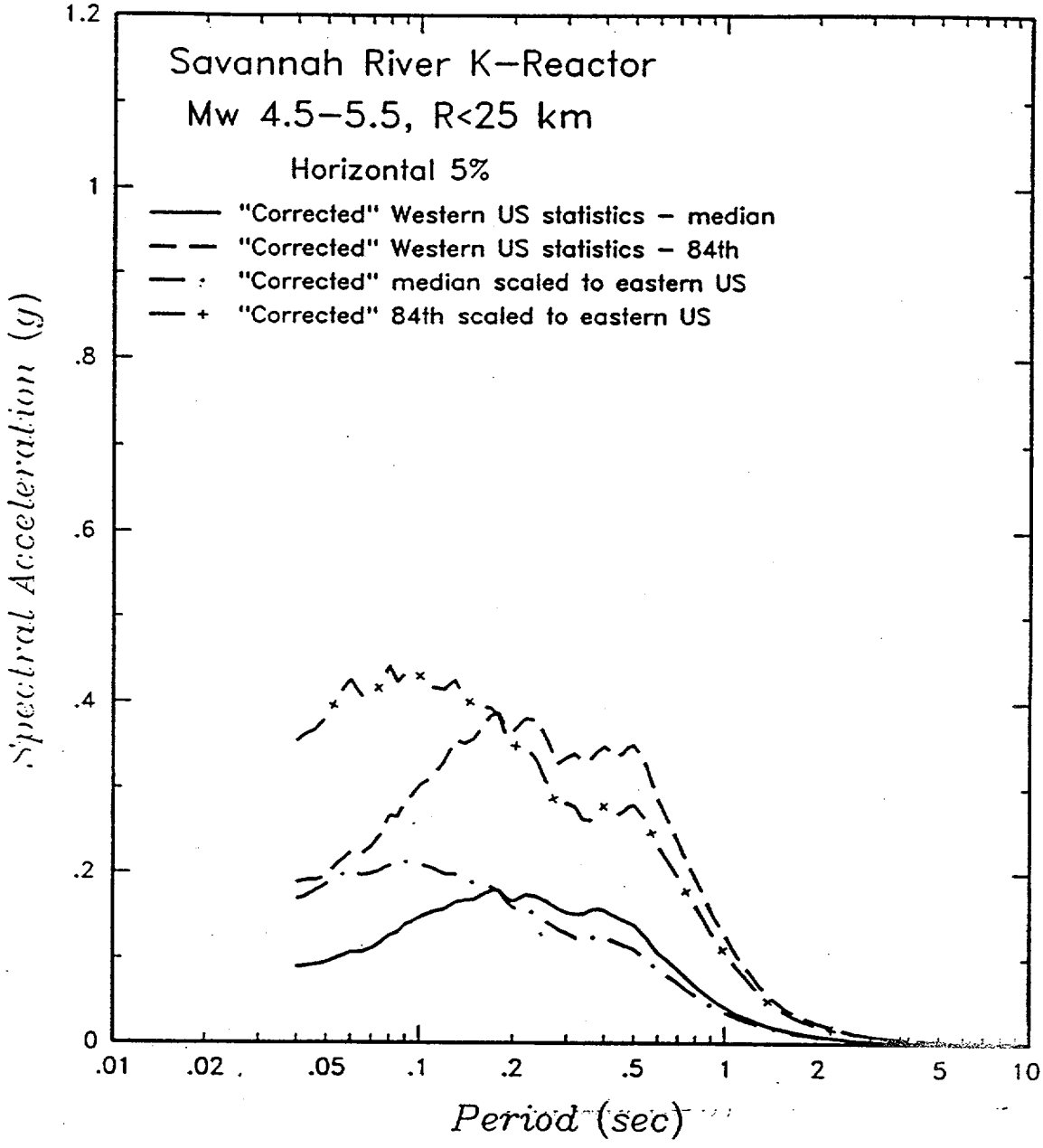

FIGURE 69. "Corrected" horizontal statistical spectra for western U.S. deep soil data set scaled using east/west spectral ratios of Figure 68.

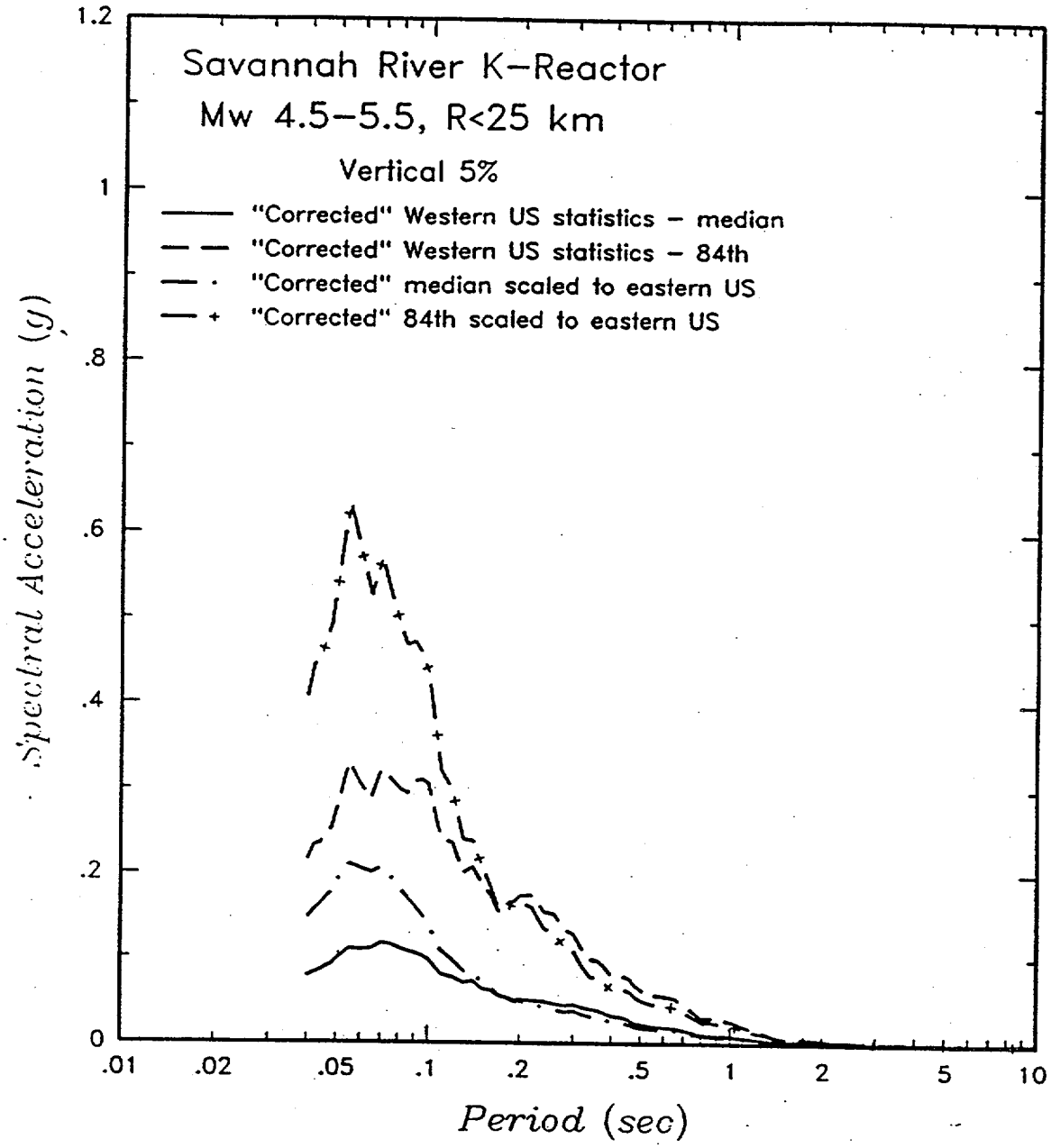

FIGURE 70. "Corrected" vertical spectra for western U.S. deep soil data set scaled using east/west spectral ratios of Figure 68.

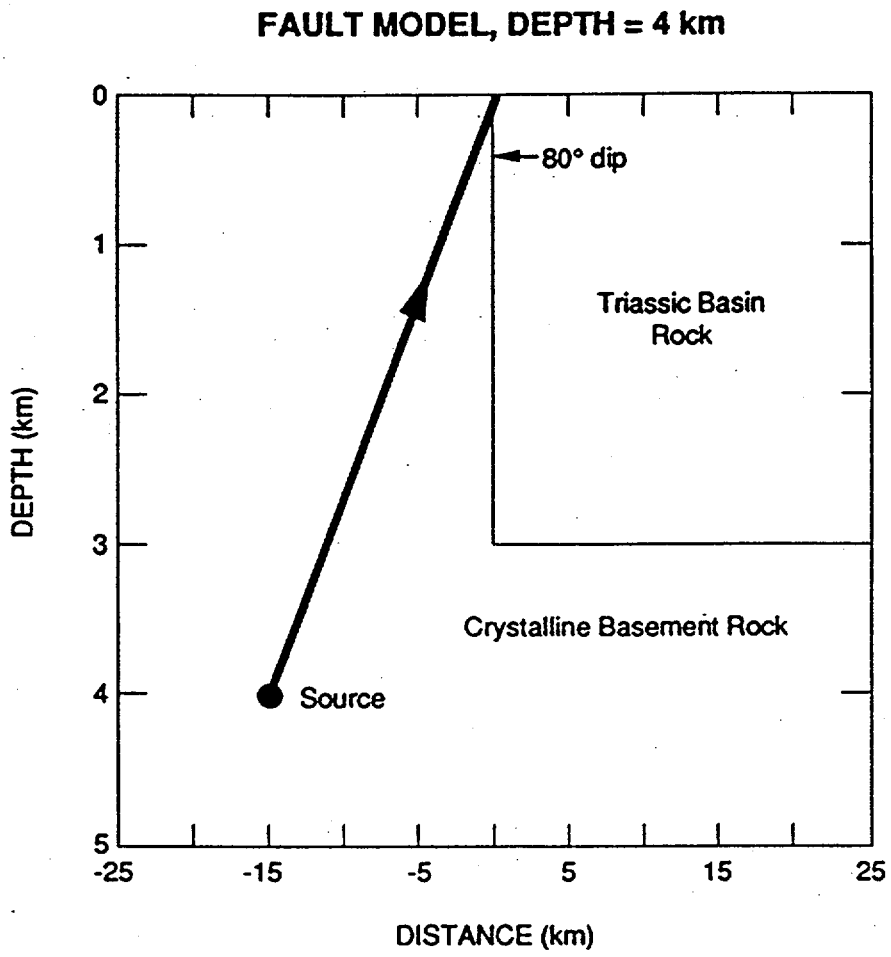

FIGURE 71. Comparison of median soil site response spectra (5% damping, horizontal motion) for Savannah River K-Reactor site for the Charleston source and local random events. Shown also is the Savannah River design basis earthquake.

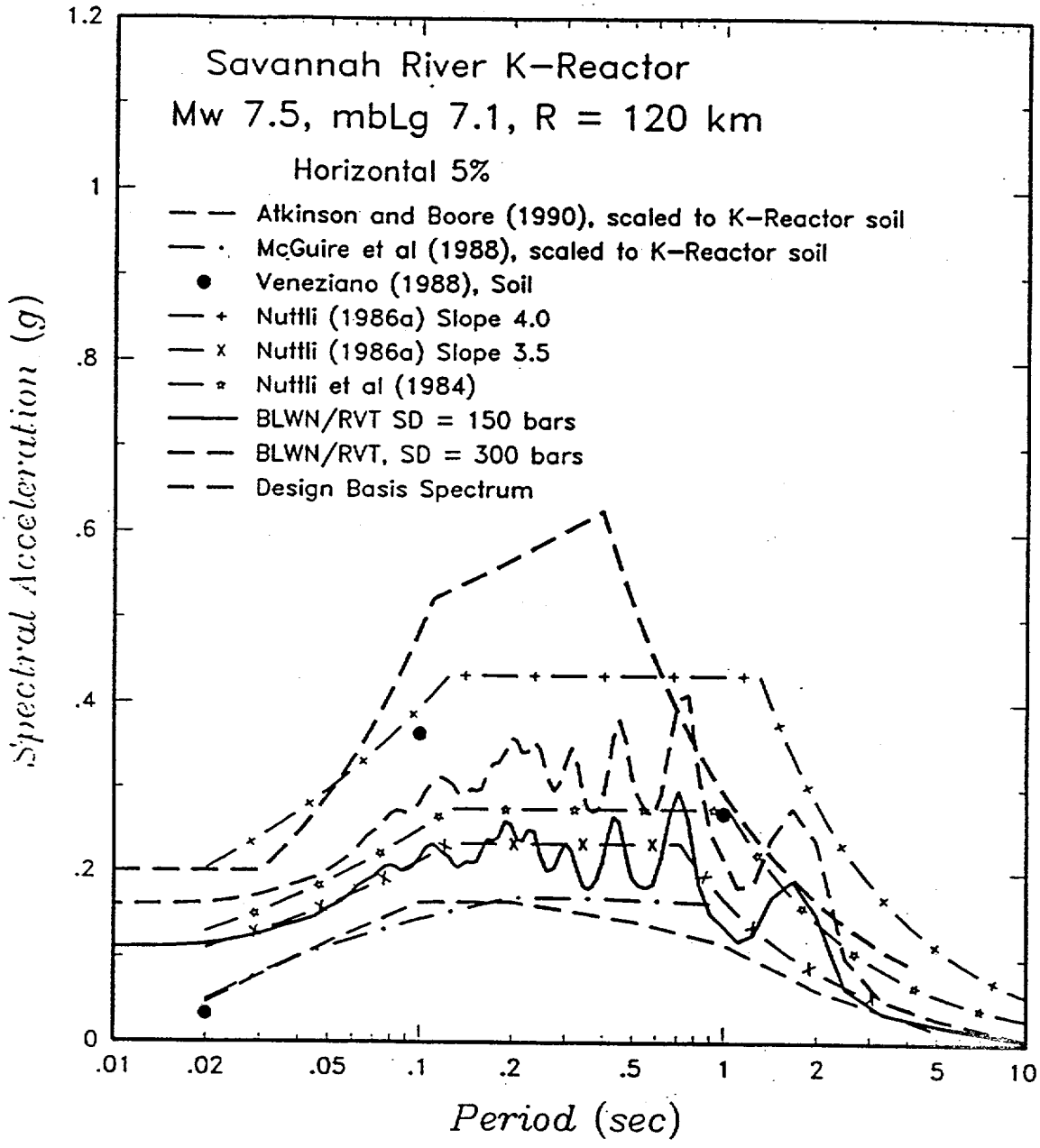

FIGURE 72. Comparison of various estimates of ground motions for the maximum Charleston source earthquake with the design basis spectrum.